AD NUMBER
AD869822
LIMITATION CHANGES
TO: **Approved for public release; distribution is unlimited.**
FROM: **Distribution authorized to U.S. Gov't. agencies and their contractors; Administrative/Operational Use; MAR 1970. Other requests shall be referred to Army Aviation Materiel Labs., Fort Eustis, VA.**
AUTHORITY
USAAVLABS ltr 23 Jun 1971

USAAVLABS TECHNICAL REPORT 70-12

PROGRAM FOR HELICOPTER GEARBOX NOISE PREDICTION AND REDUCTION

By

R. H. Badgley
I. Laskin

March 1970

U. S. ARMY AVIATION MATERIEL LABORATORIES
FORT EUSTIS, VIRGINIA

CONTRACT DAAJ02-68-C-0070

MECHANICAL TECHNOLOGY INCORPORATED
LATHAM, NEW YORK

This document is subject to special export controls, and each transmittal to foreign governments or foreign nationals may be made only with prior approval of US Army Aviation Materiel Laboratories, Fort Eustis, Virginia 23604.

U S ARMY MATERIEL COMMAND

Disclaimers

The findings in this report are not to be construed as an official Department of the Army position unless so designated by other authorized documents.

When Government drawings, specifications, or other data are used for any purpose other than in connection with a definitely related Government procurement operation, the United States Government thereby incurs no responsibility nor any obligation whatsoever; and the fact that the Government may have formulated, furnished, or in any way supplied the said drawings, specifications, or other data is not to be regarded by implication or otherwise as in any manner licensing the holder or any other person or corporation, or conveying any rights or permission, to manufacture, use, or sell any patented invention that may in any way be related thereto.

Disposition Instructions

Destroy this report when no longer needed. Do not return it to the originator.

DEPARTMENT OF THE ARMY
US ARMY AVIATION MATERIEL LABORATORIES
FORT EUSTIS, VIRGINIA 23604

This report presents a part of a continuing effort to understand and ultimately control the noise produced by helicopter power trains. The objective of this effort was to verify, refine, and extend the analysis techniques developed under Contract DA 44-177-AMC-416(T) and presented in USAAVLABS Technical Report 68-41. The model used for this study was the CH-47 helicopter power train.

This command concurs in the conclusions made by the contractor.

Task 1G162203D14414
Contract DAAJ02-68-C-0070
USAAVLABS Technical Report 70-12
March 1970

PROGRAM FOR HELICOPTER GEARBOX NOISE PREDICTION AND REDUCTION

By

R. H. Badgley
I. Laskin

Prepared by

Mechanical Technology Incorporated
Latham, New York

for

U. S. ARMY AVIATION MATERIEL LABORATORIES
FORT EUSTIS, VIRGINIA

ABSTRACT

This study is part of a continuing effort to understand and ultimately control the noise produced by helicopter power trains. As such, its aims are the extension of noise-prediction technology and the development of this technology into analytical tools which may be used to effect noise reduction, either in retrofit operations or in the design of future aircraft transmissions. The objectives of this study were as follows:

1. Application of the analytical tools developed under Contract DA 44-177-AMC-416(T) to the CH-47 helicopter power train.

2. Measurement of noise levels aboard operational CH-47 aircraft, and the comparison of these measured levels with the predicted levels developed under objective 1.

3. Measurement of gearbox casing resonant frequencies on the CH-47 forward rotor transmission to determine the existence of major housing structural resonances, if any, within the frequency spectrum of interest.

4. Investigation of the sensitivity of noise-level predictions for the CH-47 forward rotor transmission to changes in the following:

    a. Gear tooth profile manufacturing deviations on sun, planet, and ring gears in the upper planetary gear set.

    b. Upper planetary planet carrier torsional stiffness.

    c. Noise energy content, as a fraction of vibration energy, over the frequency spectrum of interest.

    d. Energy conversion and housing geometry and environment factors (Appendix VI of Reference 1).

5. Investigation of the utility of profile modification as a means of reducing gear tooth mesh excitation (and thereby noise levels) in the CH-47 forward rotor transmission upper planetary gears.

The analytical methods and computer programs developed under the previous referenced contract (UH-1D study) were applied to the CH-47 helicopter power train for both cruise and hover flight conditions. The empirical factors utilized for the UH-1D helicopter power train were modified to account for different gearbox materials in the CH-47 aircraft.

In-flight measurements were made on three CH-47 helicopters and included both acoustic and gearbox housing vibration data. These measurements were conducted under both cruise and hover flight conditions.

Comparison of predicted and measured noise results showed good correlation on a relative level basis, as had been found in the UH-1D study. On an

absolute basis, however, substantially less correlation was obtained. The conclusion may be drawn that the existing analytical procedure predicts adequately the distribution of acoustic energy with frequency at the transmission housing, but is not yet detailed enough to predict overall noise levels within the helicopter cabin itself.

Various physical properties of the CH-47 forward rotor transmission were investigated, with emphasis upon gear tooth profiles, in the attempt to effect a reduction in noise level. While certain tooth profiles were found which provide substantial reductions, present tooth machining accuracy limits appear to preclude use of this development as a design change for noise reduction.

FOREWORD

This report was prepared by Dr. Robert H. Badgley of Mechanical Technology Incorporated under Contract No. DAAJ02-68-C-0070 (Task 1G162203D14414). The contract was carried out under the technical cognizance of Mr. E. R. Givens, U.S. Army Aviation Materiel Laboratories, Fort Eustis, Virginia.

Contributions to the technical content of the report, particularly to the Task I studies, were made by Mr. I. Laskin, who was at MTI when the contract was initiated. He provided the general direction that the program followed and also served as a consultant during Task II investigations.

This program was carried out with the cooperation and assistance of many individuals. Special credit is due Mr. John Nobles of USAAVLABS and Mr. Robert Scribner of MTI, who were responsible for conducting the experimental measurements of Task I, and to Mr. Donald Wilson, also of MTI, who supervised the laboratory vibration and noise measurements.

TABLE OF CONTENTS

LIST OF ILLUSTRATIONS

Figure		Page

LIST OF TABLES

Table		Page

Table		Page
31	Tabulated One-Third-Octave Frequency Analysis of In-Flight Vibration Measurements for CH-47B, Cruise Operation, Aircraft No. 619109	134
32	Measured Casing Response	148
33	Measured Casing Response	150
34	Measured Casing Response	152
35	Conversion of Spiral Bevel Gears Into Equivalent Spur Gears for CH-47 Forward Rotor Transmission	160
36	Calculation of Modified Contact Ratio for CH-47 Forward Rotor Transmission Spiral Bevel Gears	161

INTRODUCTION

Helicopter cabin noise, particularly that originating in the transmissions, is well recognized as one of the important problems in the present and future use of helicopters. The nature and extent of the problem are seen when present noise levels are compared to existing and proposed noise specifications. Figure 1 gives such a comparison for the CH-47, in which cabin noise levels may exceed MIL-A-8806 by as much as about 35 db. These excessively high levels occur only in the higher frequency ranges, which include transmission tooth mesh frequencies (400-10,000 Hz), while the noise associated with the rotors is confined to the lower frequency range (below 400 Hz).

One approach to noise reduction has been the application of sound-absorbing materials. Although potential benefits have been demonstrated, these are sometimes accompanied by significant weight penalties. In addition, these materials may inhibit the removal of heat from the transmission, or they may be removed during operational use of the aircraft and not replaced, thereby destroying whatever noise reduction had been obtained. As was concluded by Reference 2, "Greater efficiency in noise control can be achieved by reduction at the source", and "Such achievement will require research into several basic mechanisms of aircraft noise". Since the most objectionable cabin noise appears to come from the gearbox, this component has received attention first.

The benefits of any new method of reducing noise from helicopter gearboxes will materialize only when the method is incorporated into technical specifications and applied to the design of new helicopter transmissions. An effort of this magnitude requires an overall technology development program containing a sequence of stages of engineering study and testing. Such a program is shown in the flow chart in Figure 2. It concentrates first on the development of analytical tools which can be used to predict noise levels from design data, and next upon the evaluation of an existing transmission to develop a theoretical noise prediction for an actual transmission. An experimental study of the same transmission is then required to prove the utility of the developed tools. Application of the analytical tools may then be used to identify physical quantities which are effective in reducing noise levels, and the suggested modifications may be verified by experiment. Feasible techniques may then be utilized in the design of new transmissions.

The results of studies undertaken under Contract DA 44-177-AMC-416(T) and reported in Reference 1 were directed toward the first three of these stages. Analytical methods were developed and used for theoretical noise predictions starting with transmission design data. In addition, experimental measurements were made on UH-1A and UH-1D helicopter aircraft, both to assist in the evaluation of empirical factors used to obtain the overall noise levels, and to provide for a direct comparison between predicted and measured noise spectrum shapes.

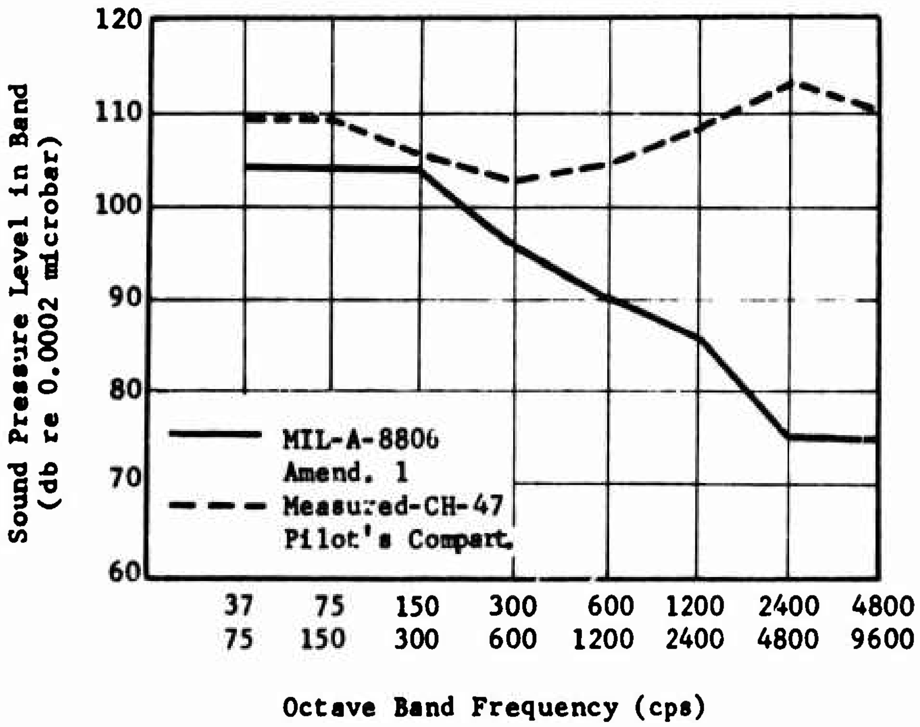

Figure 1. Comparison of Typical Measured Noise Levels in CH-47 Pilot's Compartment With Present Specifications.

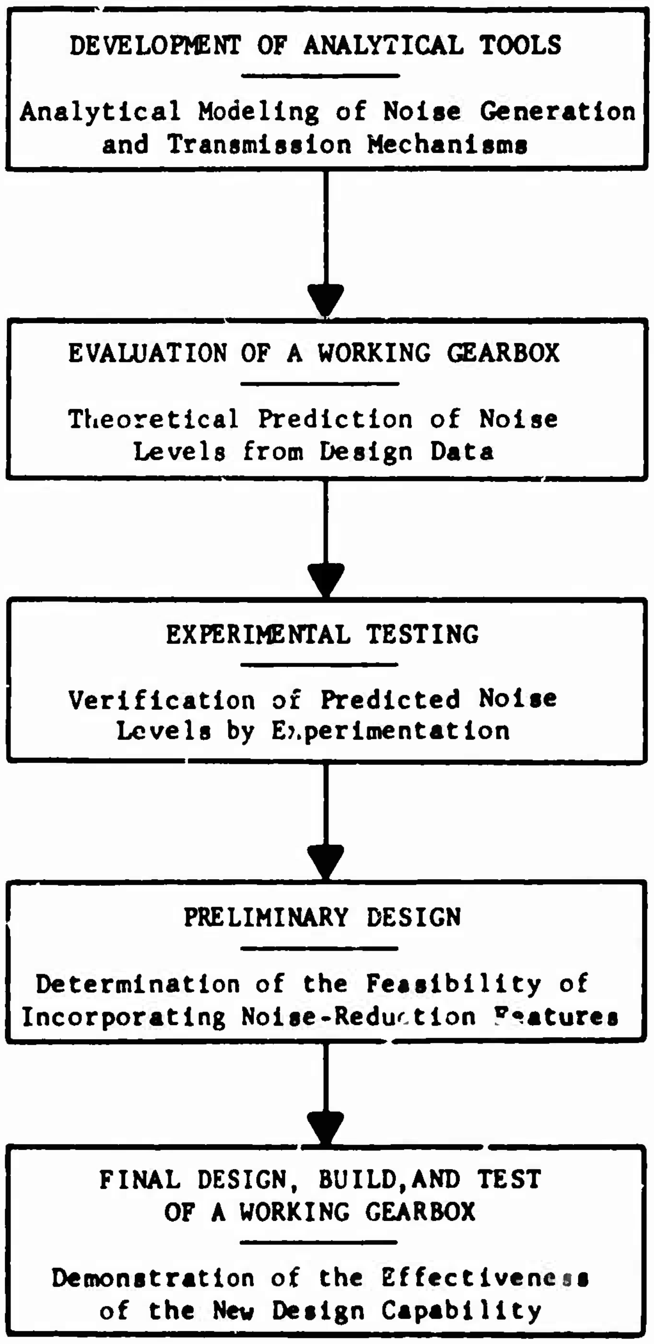

Figure 2. Overall Program for the Reduction of Noise Generated in Helicopter Gearboxes.

With regard to the shape of the noise spectrum, excellent comparisons were obtained. However, it was recognized that since this prediction procedure was still at the state-of-the-art level, more experience in the selection of the empirical overall noise-level factors would be required for good confidence in the predicted absolute noise levels. Consequently, the present CH-47 study was undertaken. This study was planned as a separate attempt to test the ability of the analysis to predict correctly the acoustic energy distribution with frequency while providing the opportunity to obtain better values of the empirical factors associated with the analysis. Most importantly, it was hoped that the Phase II portion of the study would yield a practical method of reducing the transmission gear noise of the CH-47 aircraft.

The objectives of this effort were as follows:

1. Application of the analytical tools developed under Contract DA 44-177-AMC-416(T) to the CH-47 helicopter power train.

2. Measurement of noise levels aboard operational CH-47 aircraft, and the comparison of these measured levels with the predicted levels.

3. Measurement of gearbox casing resonant frequencies on the CH-47 forward rotor transmission to determine the existence of major housing structural resonances, if any, within the frequency spectrum of interest.

4. Investigation of the sensitivity of noise-level predictions for the CH-47 forward rotor transmission to changes in the following:

   a. Gear tooth profile manufacturing deviations on sun, planet, and ring gears in the upper planetary gear set.

   b. Upper planetary planet carrier torsional stiffness.

   c. Noise energy content, as a fraction of vibration energy, over the frequency spectrum of interest.

   d. Energy conversion and housing geometry and environment factors (Appendix VI of Reference 1).

5. Investigation of the utility of profile modification as a means of reducing gear tooth mesh excitation (and thereby noise levels) in the CH-47 forward rotor transmission upper planetary gears.

DESCRIPTION OF PROGRAM

This study of helicopter transmission gear noise was conducted in two tasks, the individual efforts of which are summarized below. Detailed descriptions and explanations may be found under Discussion of Results and in the appropriate appendixes.

PHASE I - FURTHER VALIDATION OF ANALYTICAL TOOLS

For the first portion of Phase I, detail and assembly drawings of the CH-47 power train were provided by Boeing-Vertol. From the drawings pertaining to the drive train gears, tooth profiles were selected as representative of those expected to be encountered in actual operation, and excitation analyses were performed. Using the drawings of the drive train mechanical components, an analytical model was prepared for the torsional dynamics analysis. Using the excitation and torsional dynamics results, and the newly computerized noise calculation sequence, noise predictions for various operating conditions were calculated for the CH-47.

In the second part of this phase, experimental measurements were made at Fort Eustis, Virginia, in two CH-47A and one CH-47B helicopter aircraft. Acoustic measurements at several locations within the aircraft and vibration measurements at several points on the transmission and transmission mounts were made. All measurements were made with the aircraft in both cruise and hover flight conditions. Experimental data gathered in this study was reduced and displayed for direct comparison with calculated noise data.

In the third portion of Phase I, laboratory vibration experiments were performed at MTI. A CH-47 forward rotor transmission was instrumented with accelerometers at several key points. While suspended by overhead cables and without shaft rotation, the transmission was subjected to constant force vibrations at acoustic frequencies at the various accelerometer locations. Accelerometer readings and acoustic levels were recorded.

PHASE II - INVESTIGATION AND VERIFICATION

Based upon the comparisons of the theoretical and measured noise levels obtained in Task 1 studies, work was undertaken in which the analytical tools were first used in the design mode.

In the first part of this phase, investigations were made into the spectral shape differences between calculated and measured results at frequencies corresponding to the second and third harmonics of the upper planetary tooth mesh frequency. Consideration was given to possible effect upon excitation levels of profile deviations which fell within the manufacturing tolerances. Also, the effect of variations in upper planetary planet carrier torsional stiffness upon tooth dynamic forces was studied. Next, the noise energy content as a fraction of vibration energy was examined.

Finally, the sensitivity of the entire analysis to the empirical conversion factor and the housing geometry and environmental factor was studied.

In the second portion of this phase, the utility of profile modification as a means of reducing gear tooth mesh excitation (and thereby noise levels) was studied using as a model the forward rotor transmission. Variations in tooth mesh excitation as a function of transmitted tangential force were a part of this study.

DISCUSSION OF RESULTS - PHASE 1

INTRODUCTION

In this program, many of the factors which are important in the generation of helicopter gearbox noise and its transmittal to the cabin area have been studied. The factors and their relationships are pictured in flow chart form in Figure 3. The first factor is the tooth mesh excitation which sets up torsional vibrations in the drive system. Depending on the response of the system, dynamic forces are developed at the gear teeth, superimposed on the steady forces transmitting power from engine to rotor. These dynamic forces act through the shafts and bearings to set up lateral vibrations in the gearbox housing, with the magnitude of vibration being influenced by any natural resonances in the housing. One result of this vibration is the transfer of vibratory motion from the large areas of the housing to the air, thus generating noise. At the same time, some of the vibration of the housing is transferred through its mounting into the aircraft structure. At this point, the direct role of the gearbox in influencing cabin noise has ceased. The intensive study of the program was confined to those noise factors directly related to the gearbox. However, when in-flight measurements were being made, and because of the convenience of doing so, the investigation was to a limited extent carried over to some of the factors associated with the aircraft proper. Figure 3 shows these factors which relate to the transmittal of noise to the pilot after it leaves the gearbox. The upper path in the chart shows, in highly simplified fashion, how the noise in the air surrounding the gearbox housing passes through the gearbox compartment bulkhead and continues through the air until it reaches the pilot. Since this mode of noise transmittal originated and continued with the vibration in the form of noise, or air pressure pulsations, the noise using this path is referred to as airborne noise. The lower path in the chart shows, again in highly simplified fashion, that the gearbox vibration transmitted to the structure is carried by the structure to the cabin bulkheads, where it is for the first time transformed into the noise reaching the pilot. Since the structure played a pronounced role in this mode of noise transmittal, the noise at the end of the path is referred to as structure-borne noise.

The earlier work performed under Contract DA 44-177-AMC-416(T) confirmed the concepts discussed in the foregoing paragraph. In particular, it showed that the concepts of gear mesh excitation and the resulting torsional vibrations formed a valid basis for the calculation of the shape of the noise spectrum, and that with proper selection of the empirical housing and geometry factors for the aircraft involved, good predictions of overall noise level could be obtained.

This section of the report describes how each of these factors has been investigated in the program, gives some representative results, and discusses their interpretation leading to the conclusions. The comprehensive data collected, the instrumentation and methods used, and the derivation and justification of the analyses have been reserved for the various appendixes.

NOISE PREDICTION

The predicted noise calculation is described by the flow chart shown in Figure 4. The three categories of input data used in the calculations were developed as follows:

1. The gearbox and drive system design data were taken mostly from Boeing-Vertol drawings of the CH-47 (A and B) transmissions, their components, and their connecting members. These data were supplemented by calculated rotor inertias and other system data taken from Boeing-Vertol report number 77272. A schematic drawing of the drive system is shown in Figure 5, including the numbers of gear teeth and the speed-reduction ratios.

2. The operating conditions of horsepower and speed were taken from the contract work statement, with the division of power between forward and aft rotor transmissions based on estimates supplied by Boeing-Vertol. These data were reduced to static tooth forces, given in Table 1, and to gear tooth meshing frequencies and their harmonics, given in Table 2.

3. Since no provision was made in the contract for obtaining actual or typical profile measurements, the spur gear tooth profiles were taken from the gear part drawings as the profile falling halfway between the profile tolerance limits, as shown in Figure 6.

The first step in the noise prediction calculation is finding the excitation components. The specific items of input data used for this are the gear data of category 1, the static tooth forces of category 2, and the spur gear profiles of category 3.

In the case of the spur gear excitation components, this information was entered into the computer program described in Appendix IV of Reference 1. The resulting values are listed in Tables 3 and 4.

Since the computer program is directly applicable to spur gears only, and since there is no equivalent means for calculating the spiral bevel gear excitation components, a computation procedure was improvised. This procedure is based on several major simplifying assumptions which make the results very approximate. Some of these assumptions are:

1. The spiral bevel gear excitation results only from variation in tooth deflection with no direct influence from actual or design gear profile or lead deviations.

2. The variation in tooth deflection results only from the changes in the number of teeth sharing load, taking the tooth compliance as constant regardless of load distribution on the tooth. Furthermore, the spiral bevel gear tooth compliance is found by calculating an "equivalent" set of meshing spur gear teeth and using the compliance portion of the spur gear excitation computer program.

3. The variation of the number of teeth sharing load during rotation of one tooth spacing is determined by the "modified contact ratio" calculated according to published Gleason Works procedures.

4. The magnitude of the fundamental and second harmonic of the spiral bevel gear excitation is derived from the "square wave" pulsation which results from the above assumptions, except that these magnitudes cannot fall below a fixed percentage of the square wave amplitude, as would result when the contact ratios fall close to, or at, integer or half-integer values.

The spiral bevel gear excitation values found from this procedure are given in Tables 5 and 6.

The second step in the noise-prediction calculation is finding the dynamic gear tooth forces generated by the computed excitations. The original input data required for this are the drive system torsional vibration parameters and the excitation frequencies derived from the operating speed.

The basis for this calculation step was the set of two computer programs described in Appendix V of Reference 1. The auxiliary computer program in its original form was used to calculate the forces for the first and second excitation harmonics of the upper planetary gears. In this gear set, relationship between the number of planets and the number of teeth in the sun gear was such that the planet-to-planet phasing was not synchronized. Under these conditions, the remainder of the dynamic system did not enter into the calculations and the simple auxiliary program was the appropriate one to use. In all the other planetary excitations, the planet-to-planet phasing was synchronous and the main program was required. However, the main program in its original form could not handle the rather complex, five-transmission drive system of the CH-47. It was therefore modified to extend its capability to treat the more complex system. The program was further extended to permit the introduction of torsional damping between adjacent portions of the dynamic system. However, this added provision was not used in the actual force calculations because meaningful values of damping for vibrations at acoustic frequencies were not available.

The computations of gear forces were made with two different treatments of the drive system. In one treatment, the entire system of five transmissions was considered. In the second, the forward rotor transmission and the cluster of the remaining four transmissions were considered as two separate systems. The computed results were almost completely identical, indicating that dynamically the long forward rotor drive shaft effectively isolates the forward transmission from the balance of the drive system, at least for acoustic frequencies.

The calculated results for the spur gear sets for both flight conditions are listed in Tables 7 and 8, while those for the spiral bevel sets are presented in Tables 9 and 10.

The third and final step in the noise-prediction calculation combines the excitation and dynamic forces for each of the noise components with suitable factors describing the role of the casing and its acoustic environment.

The calculation procedure followed was that described in Appendix VI of Reference 1. However, instead of using manual calculations, the entire procedure was incorporated in a new computer program. This program not only gives the levels of the individual noise components, but also combines them into both a one-third-octave band spectrum and a full-octave band spectrum. The program, however, has no direct provision for introducing the background or "white" noise, nor has any method been developed for evaluating the levels of this noise. The computer values for the peaks of the one-third-octave band spectrum are not strongly affected by this "white" noise, and may therefore be used as suitable indicators of predicted noise. The valleys of the one-third-octave band spectrum, however, are directly influenced by the "white" noise, and the values computed from this program (which omits their influence) should not be used as predicted noise indicators. This same restriction should be applied to the computed full-octave band spectra. Such spectra normally do not have sharp peaks, and the error due to the omission of the "white" noise is reflected throughout the entire spectrum.

In performing this noise-level calculation for the CH-47, tentative values for the casing and environmental factors were used. These values were taken as the same as those used in the UH-1D study, except that an adjustment was introduced for the difference in casing material, aluminum for the CH-47 versus magnesium for the UH-1D. This adjustment was in the form of a reduction of the energy conversion factor from $3. \times 10^{-9}$ to $2. \times 10^{-9}$ in accordance with the explanation in Appendix VI of Reference 1. (This adjustment is equivalent to decreasing predicted noise levels by about 2 db.) The factors used did not reflect any attempt to introduce the probable influence of the changed manner of transmission mounting to the aircraft structure, hard mounting in the CH-47 versus mostly soft mounting in the UH-1D.

The predicted noise levels for the four different transmissions under the two flight conditions are given in Tables 11 and 12. The levels tabulated are the one-third-octave band levels for those bands containing a gear meshing excitation frequency.

IN-FLIGHT NOISE AND VIBRATION MEASUREMENTS

The in-flight measurements were made on three CH-47 aircraft, two of type A and the other of type B. There was apparently no difference in the drive systems of these two types, and no consistent acoustic differences were observed between the two aircraft. The collection of noise level data for comparison with predicted noise levels was only one of the objectives of these measurements. It was felt that with limited additional effort, data could be obtained which would contribute to the overall picture of the internal acoustics of the CH-47 aircraft. Thus, while measurements at only one location, near the forward rotor transmission, were needed for validation of the analytical noise-level prediction, measurements were also made at two or three additional locations within the aircraft. Similarly, instead of considering only the data related to the gear meshing frequencies, the entire noise spectrum was analyzed.

Before an analysis of these results is undertaken, it will be useful to review briefly some of the pertinent basic information about complex sound and its measurement. More detailed background information may be found in Reference 3.

Typical noise, such as that measured in the helicopter, may be considered a blend of two kinds of sounds. In one, the sound is distributed continuously in frequency (meaning that all frequencies are present) and is fairly constant in sound pressure level over a wide frequency range. This kind of sound is often referred to as "white noise". The other kind consists of discrete frequencies (meaning a limited number of isolated frequencies), which are greater in sound pressure level than the "white noise" of adjacent frequencies. Instrumentation used to measure sound cannot measure the sound pressure level of each individual frequency; instead, by using adjustable band-pass filters, it measures the combined effect of all the frequencies within each selected band. Because the filters cannot be made with perfectly sharp cutoff limits, an actual measurement is affected by noise in adjoining bands. The band width is referred to as a "narrow band" if its width is small, perhaps one-thirtieth of an octave. The term "wide band" is used for band widths of one-third, one-half, and full octave. If the instrument measures the entire sound frequency range as one band, the measurement is an "overall" sound pressure level. The indication of the sound pressure level instrument is not based on a linear measurement; instead, the unit used is the decibel (db), which is based on a logarithmic scale. The sound pressure is indicated as proportional to the logarithm of its ratio to a very small standard pressure. The significance of the decibel is such that a sound having 10 times the pressure level of another will be indicated as measuring 20 db higher.

The selection of the band width depends on the purpose for which the measurements are to be used. A narrow-band plot is useful to pinpoint the exact values of the discrete frequencies, especially when these are crowded. The full-octave band width, on the contrary, obscures the individual frequency values and instead shows the manner in which the general noise level varies over the full frequency range.

The information derived from the measurements made on board the CH-47 aircraft pertains to the following subjects, which will be discussed below:

1. General character of the internal noise-level spectrum.

2. Similarities and differences among the three aircraft studied.

3. Comparison between noise levels at the two flight conditions, cruise and hover.

4. Relationships between noise level and microphone locations, and their implications concerning noise sources and modes of noise propagation within the aircraft.

5. Specific role of the gear mesh excitations of the forward rotor transmission in defining the upper frequency portion of the noise spectrum.

All the reduced data is contained in Appendix I. Representative portions of the data, used to illustrate the above subjects, are presented in this section of the report. In presenting the results, both full-octave band and one-third-octave band spectra are used, according to whether the overall spectrum characteristics are of interest or whether the underlying specific frequencies are to be illustrated. These spectrum plots are not in the conventional format, characterized by a broken line connecting points at the band midpoints, but rather are in a format which utilizes horizontal line segments in each band. This modified format more closely resembles the chart developed during the actual analysis of recorded noise, and also conveys the idea that the level shown applies to a band of frequencies rather than to individual frequencies. Another departure from common practice in several of the figures is a slight shift in the exact limits of each of the full-octave bands in comparison to standard band limits. For example, the band 175 to 350 Hz may be used instead of the standard 150 to 300 Hz. The change makes each full-octave band correspond exactly with three adjacent standard one-third-octave bands.

The operating power and speed during the CH-47 test flights are tabulated in Table 13. The table also shows for comparison the anticipated flight conditions which were used as the basis of the noise-prediction measurements. The comparison shows that the actual power was about 10 percent lower than the anticipated power for the cruise flight condition and about 30 percent lower for the hover flight condition.

The general character of the helicopter internal noise is best illustrated in Figure 7. The noise levels shown were recorded at the pilot's location and provide an indication of how the aircraft sounds to the pilot. The noise in the pilot's compartment under these conditions has a typical spectrum with very high levels at the lowest frequencies. The levels drop off with increasing frequencies to reach a low at not quite midrange. They rise again to a peak but fall off sharply at the very end of the complete range. The two frequency zones with the highest noise levels are associated with two different noise-producing effects. As will be shown below, the noise at the very low frequency peak comes from the rotor blades, while the high frequency noise is predominantly due to the gear mesh excitation in the nearest gearbox, that driving the forward rotor.

As an aid toward relating the different portions of the frequency spectrum to the likely noise sources, one set of narrow-band noise measurements is given in Table 14. The measurements describe the "peaks" that appeared in the narrow-band analysis of the same noise recording from which one of the plotted full-octave band spectrums was made. The same table contains those excitation frequencies, calculated from the main drive members, which are closest to the noted narrow-band peaks. Most corresponding pairs of frequencies agree closely. Greater discrepancies may be due to the difficulty of correctly locating "peaks" on the recording, or may possibly be due to the omission of other excitations whose frequencies more closely match those of the peaks.

The general shape of the CH-47 pilot's compartment noise level spectrum differs from that of the UH-1D studied in the prior program. The UH-1D noise spectrum had the high level at the low frequencies extend into the intermediate frequency range because of the noise associated with the faster rotating tail rotor blades. The UH-1D results show another difference: noise at the rotor transmission gear mesh frequencies has levels well below the level from the rotor blades. As Figure 7 shows, the CH-47 results indicate little or no such change in level. This difference between the two curve shapes will be noted again in the discussion of noise attenuation within the aircraft.

The information in Figure 7 also permits a comparison of the noise spectra of the three aircraft studied. For each of the flight conditions, the three plots are quite close, generally separated by less than 5 db. In general, the differences are greatest in the gear mesh frequency range, and are greatest between aircraft No. 12409 and No. 58012. However, even though these two aircraft show the greatest difference in noise level, their two spectra have essentially the same shape. It is the remaining aircraft, No. 619109, which has a noise-level spectrum whose shape differs somewhat from the other two. Instead of a continuing increase in noise level with increasing gear mesh frequency, the plot for this aircraft shows a leveling off, so that in three adjacent full-octave bands, the noise level is practically unchanged. This uniqueness of the latter aircraft is also revealed in Figures 8 and 10. These figures compare the noise levels adjacent to the forward rotor gearbox in the three aircraft. While these two plots are in one-third-octave bands and are limited to the gear mesh frequency range, they too show that aircraft No. 619109 differs from the other two in the uppermost portion of the noise spectrum.

No reason for this difference is apparent. The only formal difference among these aircraft is that No. 619109 is of type CH-47B while the other two are of type CH-47A. It might prove instructive to identify any differences in construction or outfitting between the two types which could have influenced the measured noise levels.

With one of the aircraft presenting a noise spectrum noticeably different from the other two, the question arose as to which sets of data should be used for the comparison of the calculated predicted noise levels. Because the difference was more in spectrum shape than in overall spectrum level, it was decided that the data from the two type CH-47A aircraft should form the basis for the comparison.

It was the original intention in planning the test program that two significantly different flight conditions be encountered, one at cruise with 2750 hp transmitted through the drive system and the second at hover with 3750 hp. However, the practical conditions under which the in-flight measurements were made did not permit a hover condition with sufficient load to give the higher horsepower figure. Instead, the hover flight condition was carried out with just about the same engine power as the cruise condition, as shown in Table 13. Returning to Figure 7, the two sets of curves show nearly identical noise spectra for the two flight conditions. The similarity is even more strikingly shown in Figure 9, which contains superimposed plots for the two flight conditions in both type CH-47A aircraft. These plots, in one-third-octave bands, show that the gear mesh frequency portion of the noise spectra as measured adjacent to the forward rotor gearbox is almost identical for the cruise and hover flight conditions.

The various locations for the microphones while making the in-flight noise measurements are identified in Figure 65. Each position was used for each of the aircraft and in each of the flight conditions, except that the measurement at the rear of the cargo compartment was limited to aircraft No. 12409 for the cruise condition.

The primary noise measurements (with respect to comparison with analytical results) were those made adjacent to a transmission because they record the noise closest to its source and are least affected by the noise transmissibility of the aircraft. These measurements were made at only the forward rotor transmission, since it is the noise from this source which is most likely to affect the pilot. Measurements at this location for the cruise flight condition are given in Figure 8. This one-third-octave band plot is shown in both the conventional and modified format for the purposes of comparison. The plot shows that the noise level peaks appear primarily in those bands which contain the gear meshing excitation frequencies in the particular gearbox. The one exception is the peak in the 630 Hz band in aircraft 3. The source of this peak is unknown and could possibly be outside the gearbox itself.

As the microphone location is moved, the noise spectrum varies. The lower plot of Figure 10 illustrates the changes. The noise level drops about 10 db from a point near the forward transmission to the pilot's compartment and another 10 db or so to the point inside the cargo compartment. However, when the microphone is located in the rear of the cargo compartment, or closer to the aft rotor transmission, the noise spectrum goes up. Figure 11 shows the same relationships for the hover flight condition, except that the measurement at the rear of the cargo compartment was not made.

A comparison of the noise spectra for the four measurement locations is shown in full-octave form in Figure 12, which presents the noise levels over the entire frequency range. It is most instructive to consider first the plots for the three locations in the forward half of the aircraft. In the low frequency range, the three plots for the locations, alongside the forward rotor gearbox, in the pilot's compartment, and at the center of the cargo compartment, are all very closely matched. However, when the upper frequency range is examined, there are significant differences between the noise levels. It is clear that the further the microphone is from the forward rotor gearbox, the lower the noise level is in this frequency range. This comparison further emphasizes the difference between the manner in which the rotor blade noise is transmitted throughout the aircraft and the nature of the gear mesh noise propagation. If the forward rotor blade noise is in large part transmitted by the outside air through the walls of the aircraft, its noise level could easily be similar throughout the aircraft. If, on the other hand, the noise generated by the forward rotor gearbox is transmitted by the structure, and especially by air within the aircraft, its intensity would readily fall off with increased distance. The remaining plot of noise level, for the microphone located at the rear of the cargo compartment, does not fit the pattern described above. First, it lies above the other plots at the two lowest full-octave bands. The higher noise level may well be attributed to its location close to the aft rotor transmission, which generates the same noise frequencies as the forward rotor gear. The proximity to the aft rotor transmission also is indicated by the relatively higher gear mesh frequency noise components.

The rear location is also close to the two engine transmissions and the engine combining transmission. It is therefore likely that the noise spectrum will include the influences of the three. This appears in two ways. Within the 175 to 350 Hz band, which contains the frequencies of rotation of the gears in these transmissions, the rear measurement location has recorded a higher noise level. Then, at the very highest band, 5600 to 11200 Hz, which contains the gear mesh frequencies of the same transmissions, the noise level is again higher in a manner different from that of the other plotted spectra.

It is interesting to note that apparently no discernible portion of the engine transmission and engine combining transmission noise has reached the more forward microphone locations, apparently even that of the center of the cargo compartment. This again indicates airborne gear noise propagation. The noise may also be structureborne with sharply increasing attenuation to the more remote areas of the aircraft structure.

The lower portion of Figure 12 shows the difference of noise level as a noise attenuation between the forward rotor transmission location and the pilot's compartment, and between the transmission and the center of the cargo compartment. There is no real attenuation in the lowest frequencies, as explained above. At the higher frequencies, however, both curves step up sharply, with perhaps about 15 db attenuation from the transmission source to the pilot's compartment and about 7.5 db attenuation from the transmission to the center of the cargo compartment. These curves effectively demonstrate the different effect of the aircraft structure on the two noise sources.

When this last information is compared to the corresponding results in the UH-1D study, a significant difference emerges. In the latter, the degree of attenuation between the source, i.e., the transmission and the pilot's compartment, was much higher, about 28 db for the UH-1D compared to about 15 db for the CH-47. This higher attenuation is enough to further explain why the general shape of the pilot's noise spectra is different between the UH-1D and the CH-47. As pointed out above, the gear noise appears quieter than the rotor blade noise to the UH-1D pilot, whereas the CH-47 pilot hears no real difference. It is suggested that the greater noise attenuation at the higher frequency is a major cause of the UH-1 advantage.

This naturally brings up the question of why the noise attenuation is lower in the CH-47. One obvious difference of construction is the type of mounting used at the rotor transmissions. The CH-47 mounting is rigid, while that of the UH-1D is soft. Hence, more of the transmission noise reaches the nearby pilot's compartment.

On each of the one-third-octave sound pressure level plots referred to previously in Figures 8, 9, and 10, the one-third-octave bands with the highest levels contain one or more of the excitation frequencies of the forward rotor transmission. Most of the bands with less pronounced peak levels also contain these excitation frequencies. This direct correspondence between the high noise levels and the gear mesh excitation frequencies is also demonstrated by the data in Table 14 as well as by the other narrow-band data collected. All this tends to confirm the validity of a transmission noise-level prediction method based on the gear mesh excitations.

The in-flight vibration measurements were made on three aircraft in the cruise flight condition. Pickups were located at four locations, three on the casing itself and the fourth on the aircraft supporting structure near one of the support arms. The results are shown in Figures 13 and 14. The locations of the peak vibrations are found to generally reflect the excitation frequencies. One significant item is the very high peak in the lower casing vibration in the 3150 Hz band. Also of special significance is the relationship between the vibrations on both sides of one mounting point, given in the lower plots of Figures 13 and 14. As shown in Figure 15, there is relatively little attenuation (reduction in vibration) between the support arm on the casing and the aircraft structure. Only in the highest frequencies does this attenuation reach about 10 db. This is to be contrasted with the attenuation across the soft mounts of the UH-1D transmission, which was found to be as high as 30 db.

The comparison between predicted and measured noise levels must necessarily be limited to the cruise flight condition. For the hover flight condition, the actual static loads are substantially different from those specified for noise-prediction purposes. A further restriction in the measured data to be used results from the difference in noise levels between the type CH-47B and the type CH-47A, as discussed above. Until this difference is accounted for, it would be wise to compare the predicted levels to those measured for the type-A aircraft only.

The comparison is made in Figure 16. The measured noise levels are represented by a zone defined by the larger and smaller values recorded for the two type-A aircraft. The calculated predictions are represented by two broken plots. The predictions are limited to the noise levels of those one-third-octave bands which contain a gear excitation frequency and, in some cases, bands immediately adjacent to these. In the other bands, the actual noise levels are due to secondary noise effects or noise from sources outside the gearbox. (There is no procedure for predicting this noise. Until the primary noise components can be reduced appreciably, there will be no practical benefits from the study of the secondary noise.) The lower prediction curve is based on the assumption that the empirical factors which suited the UH-1D helicopter studies previously also apply to the CH-47. The upper curve shows the fit between calculated and predicted levels if the factor of general spectrum level is ignored. This comparison shows excellent agreement, within 3 db, for six of the eight bands directly influenced by the gear-induced noise. The two remaining bands are those containing the excitation frequencies of the second and third harmonics of the tooth-meshing frequencies at the upper planetary gear set. The differences between measured and adjusted predicted levels in these bands are further discussed in Phase II.

The difference in spectrum levels deserves further discussion. In this procedure the general level is directly determined by empirical factors reflecting the construction of the casing and the nature of the acoustic environment. The factors used in the noise-level calculations were, as explained above, essentially those which proved satisfactory for the UH-1D study. These were, in turn, derived from factors which applied to marine gear casings in a test environment. The casing resonance measurements which were part of this program were not planned to give definitive comparisons between the UH-1D and CH-47 casings, and examination of these data have not revealed the kind of differences which would explain the difference in spectrum levels.

A more likely explanation of this difference lies in the comparison between the acoustical environments surrounding the two casings. The UH-1D was largely soft mounted with little transfer of mechanical excitations into the structure and bulkheads surrounding the casing. The CH-47, on the other hand, was hard mounted with considerable excitation transfer. In effect, the CH-47 surrounding structure is an extension of the gearbox casing, adding appreciably to the conversion of cyclic mechanical energy into acoustic energy. Beyond pointing up the low vibration attenuation at the casing mounts, any further consideration of the acoustic environment is beyond the planned scope of this study.

TRANSMISSION HOUSING NOISE AND RESONANCE MEASUREMENTS

These measurements were made in a manner very similar to that used in the UH-1D investigation reported in Reference 1. Figure 17 shows a typical set of these vibration measurements. The vibrations at the excited surfaces show a large number of resonances that are local in two senses. First, there is very little frequency difference between adjacent peaks. Second, there is no similarity between the resonances at one pickup location and those at others. All this suggests that the casing vibrates at acoustic frequencies with relatively small areas on the casing undergoing independent motions. The exact location on the frequency scale at which a particular response valley or peak appears is determined by the exact location of the pickup. Very likely, if a second pickup had been placed a slight distance from the first, it would have shown its own resonance peaks. However, the actual levels measured by this adjacent pickup would be quite similar to those of the first. In other words, a proper composite response curve, reflecting the entire casing rather than just the one point at which the pickup happened to be located, would consist of many more peaks, even more closely packed than shown on the single pickup curves. Therefore, to better interpret the casing resonance measurements, a smooth curve, skimming the peaks, should be used. Such curves are shown in Figure 18.

The upper curve showing the vibration at the driving point shows the fundamental way in which the casing responds to the excitation force. The other response curves generally follow the shape of the upper curve, showing that the rest of the casing merely reflects the motion at the drive point.

It is of interest to compare this CH-47 casing resonance data with those of the UH-1D. If Figure 18 is compared to Figure 23 in Reference 1, the similarity is obvious. The response levels for the two curves are both in db, but the db levels were based on two different reference values. Also, the driving forces in the two tests were somewhat different. If allowance is made for these differences, the drive point response curves are still remarkably similar.

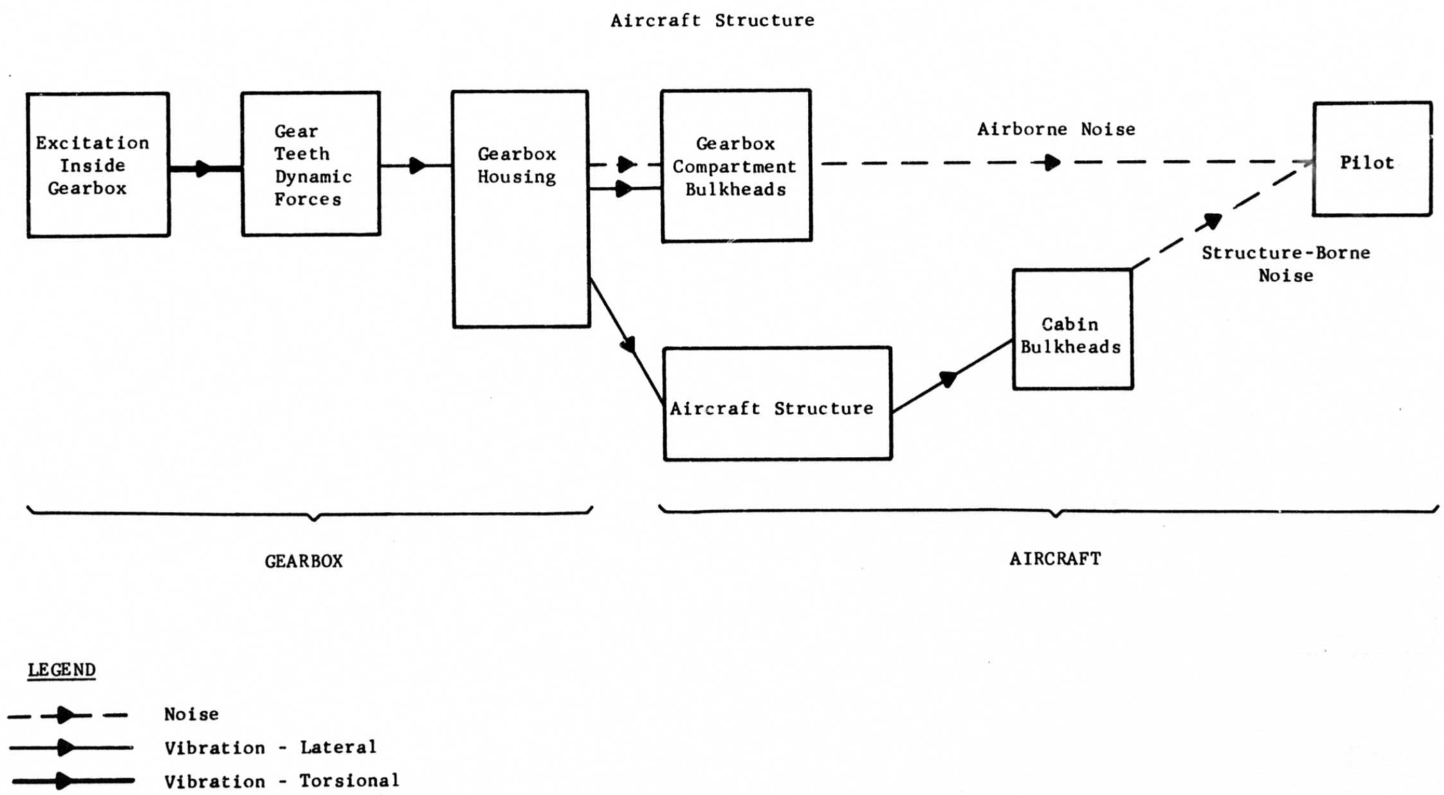

Figure 3. Transmission of Helicopter Gearbox Noise.

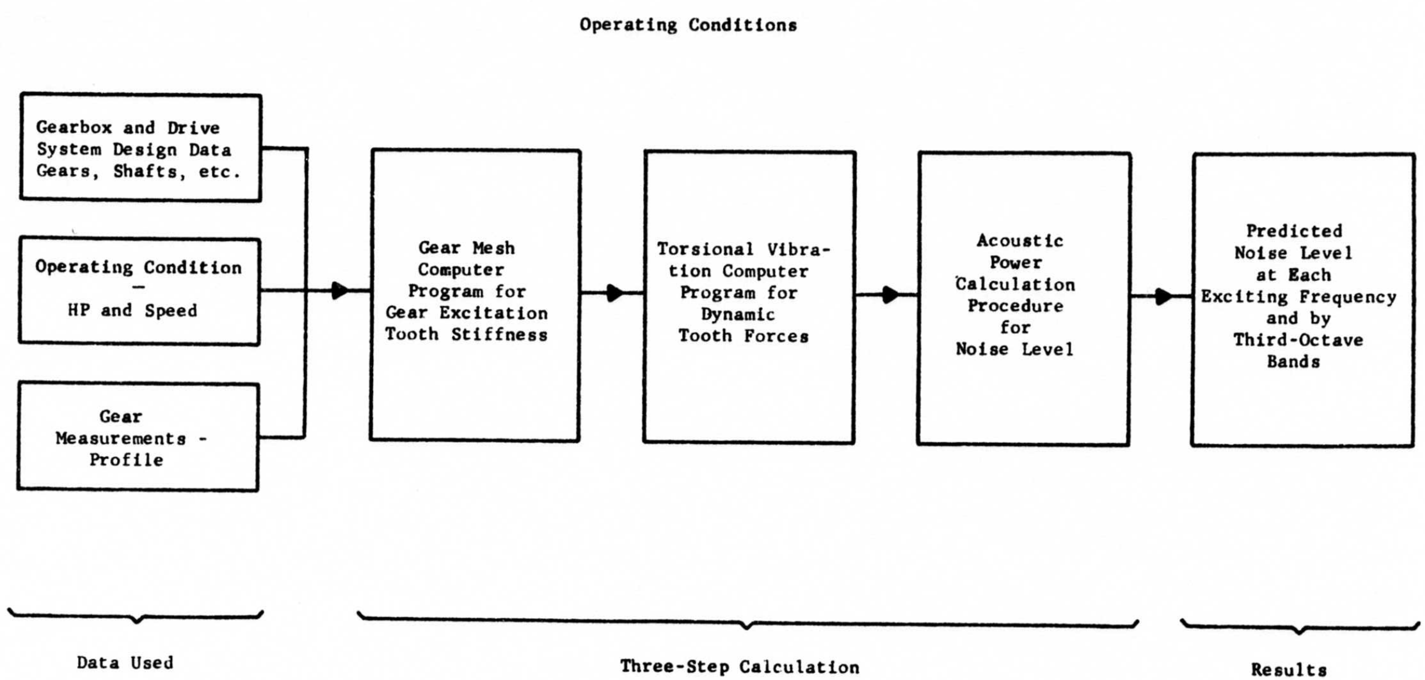

Figure 4. Flow Chart Description of Predicted Noise Calculation.

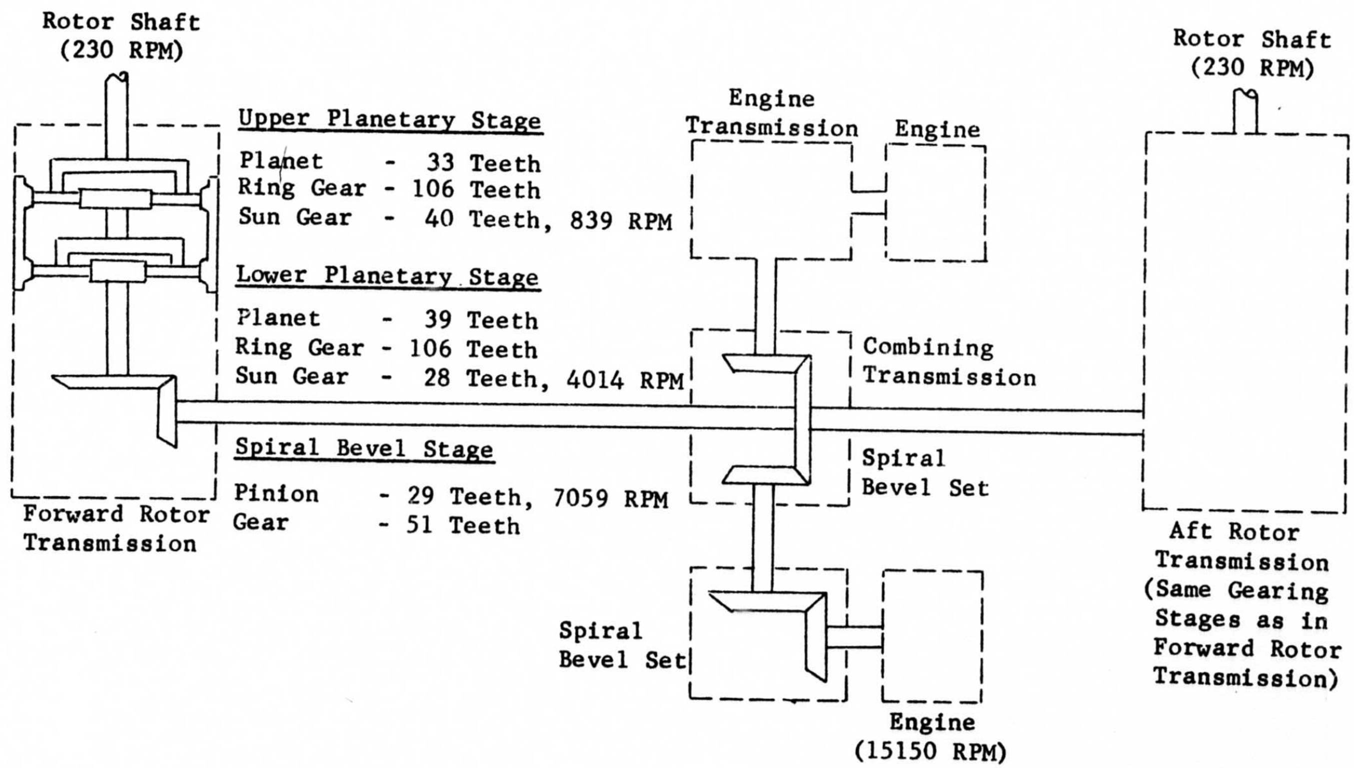

Figure 5. Schematic Diagram of CH-47 Drive System.

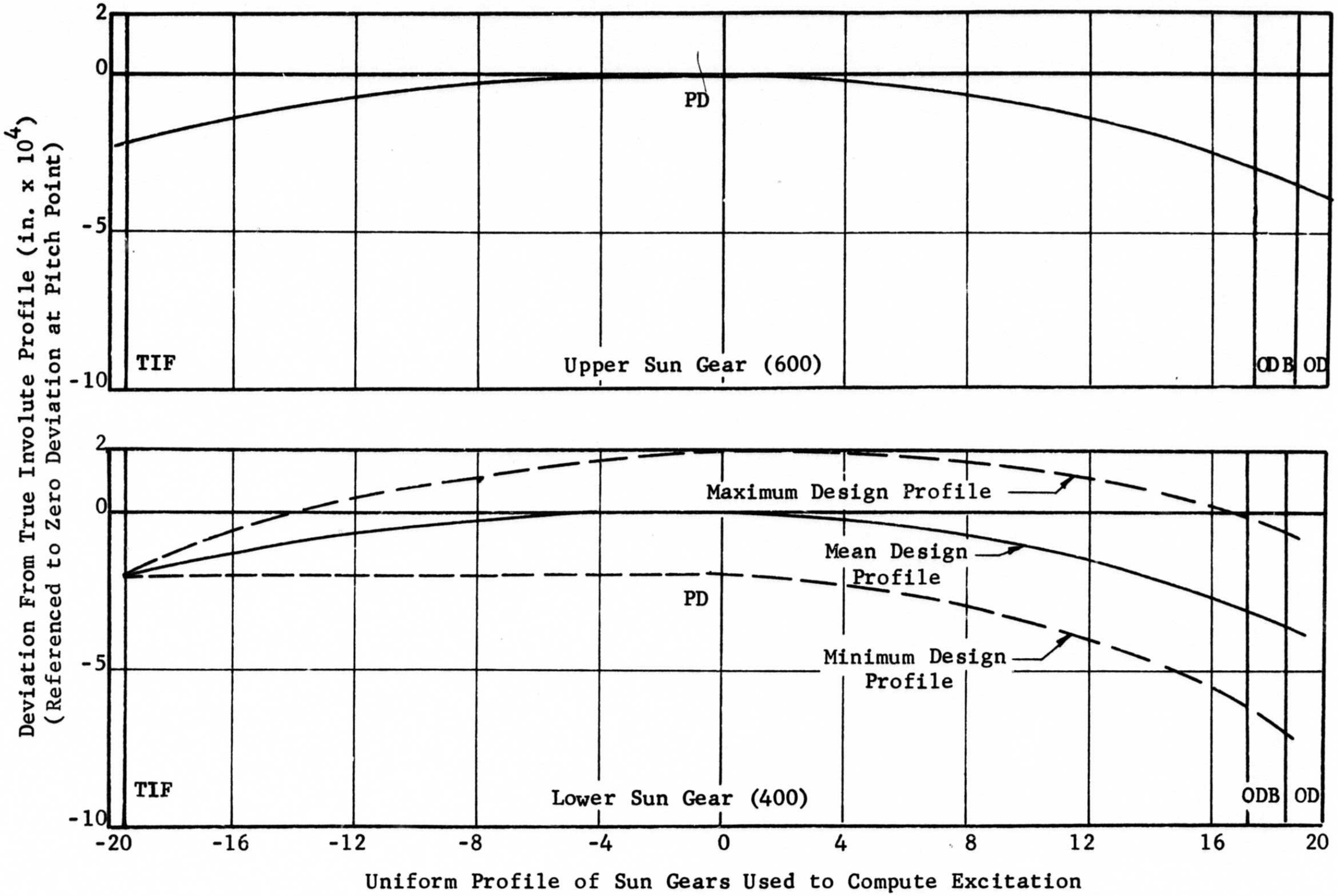

Figure 6. Design Profile of Sun Gears Used to Compute Excitation.

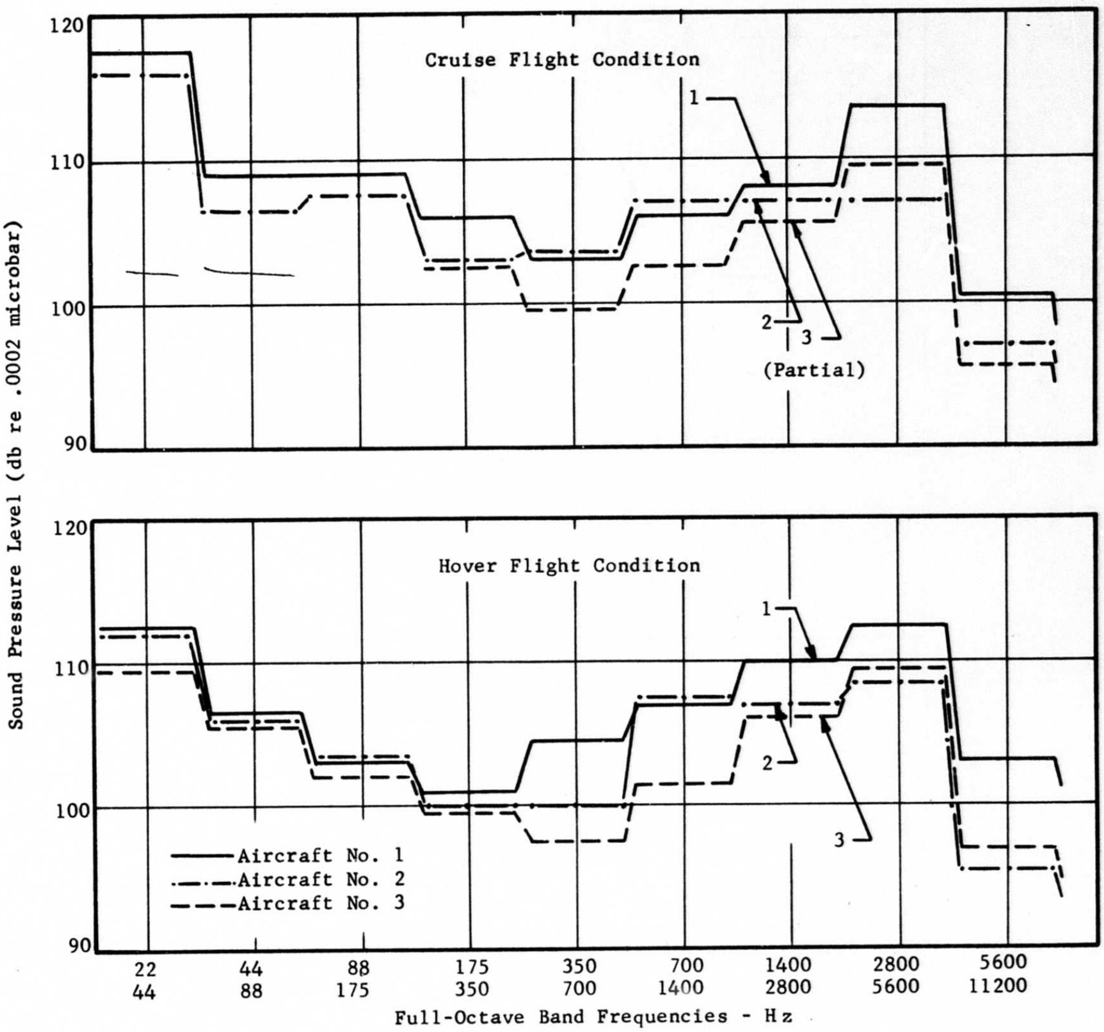

Figure 7. Noise Measurement in Full-Octave Bands at the Pilot's Location for Three Aircraft at Cruise and Hover Flight Conditions.

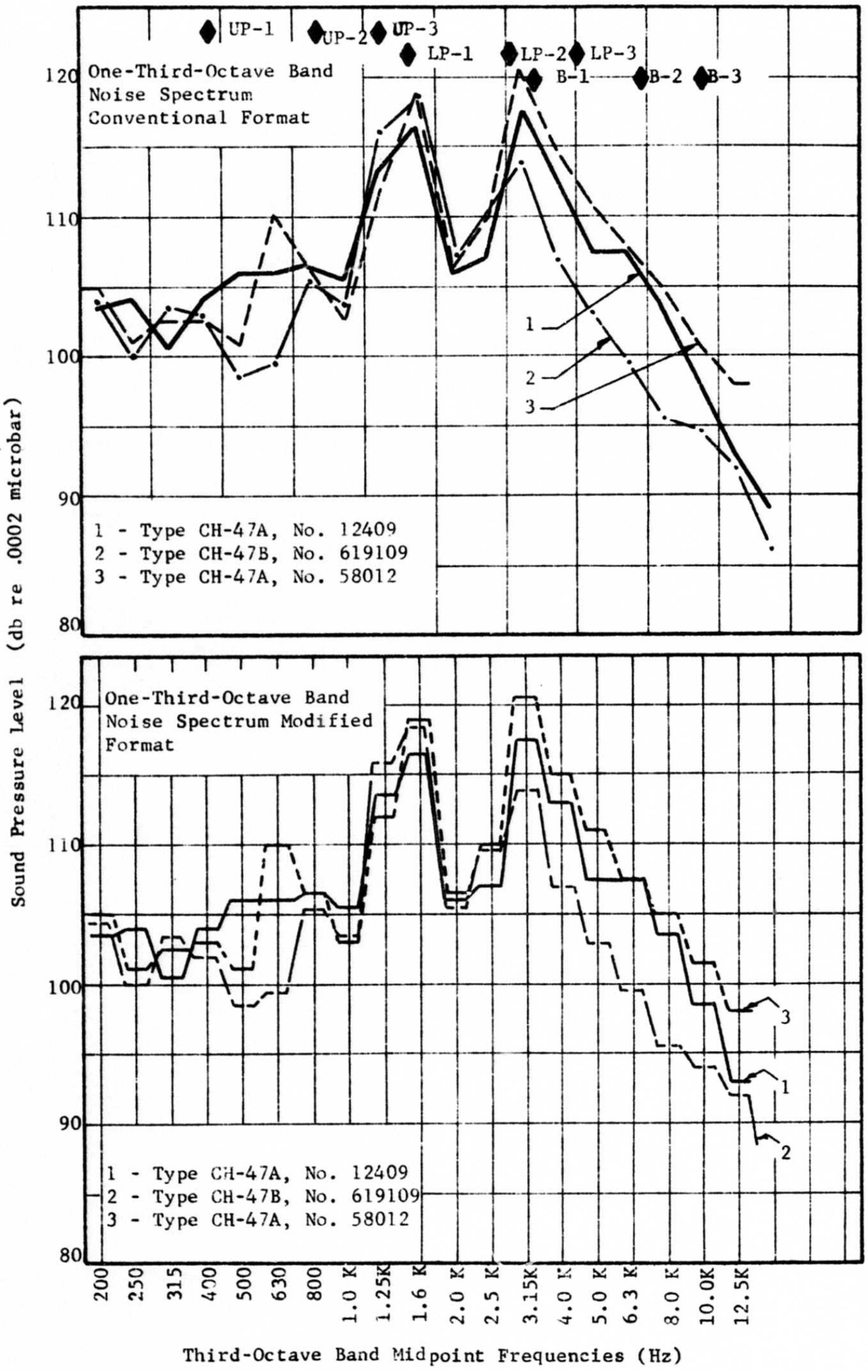

Figure 8. Comparative Noise Levels in Three Aircraft for Cruise Flight Condition With Microphone Located Adjacent to Forward Rotor Gearbox.

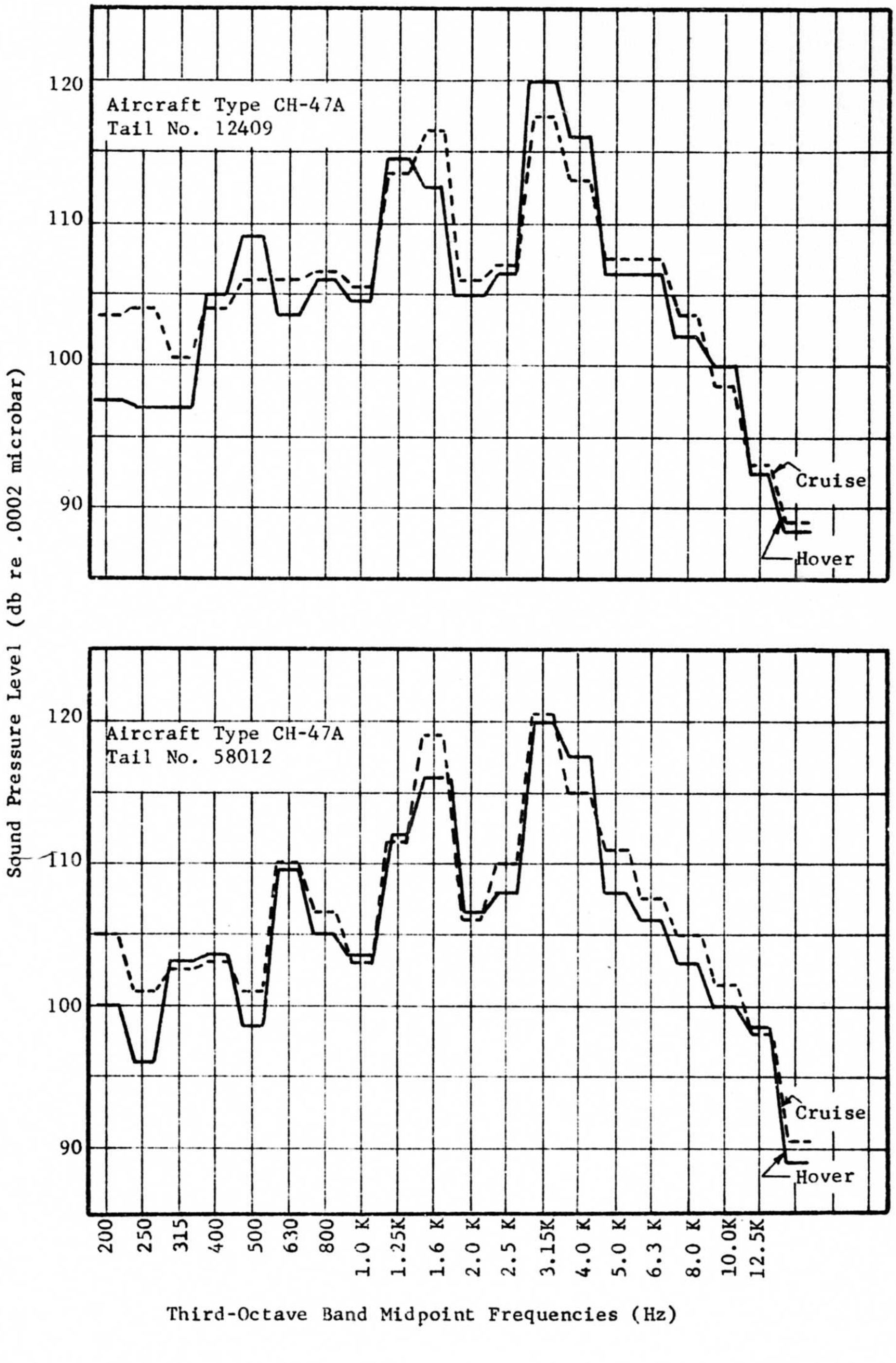

Figure 9. Comparative Noise Levels in Two Aircraft for Cruise and Hover Flight Conditions With Microphone Located Adjacent to Forward Rotor Gearbox.

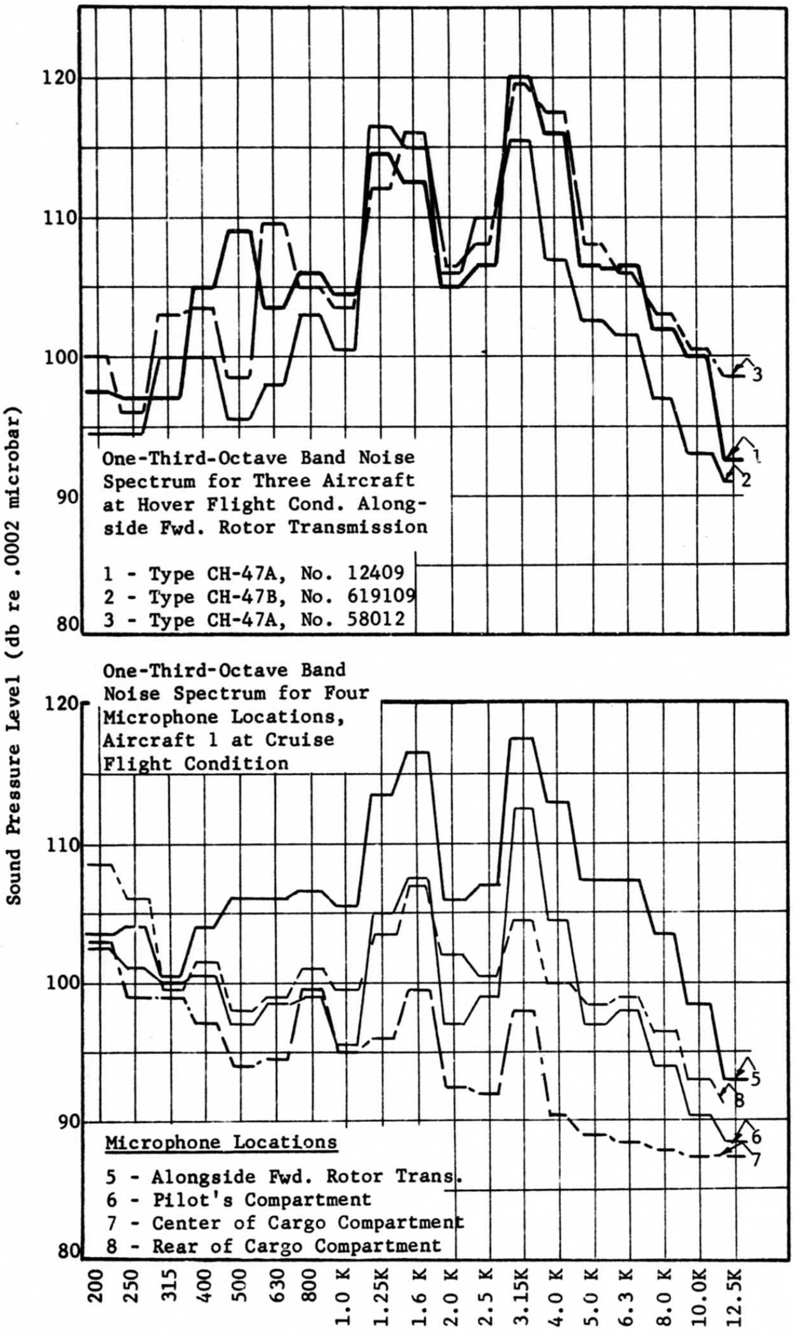

Figure 10. Comparative Noise Levels in Three Aircraft for Cruise and Hover Flight Conditions With Microphones Located as Indicated.

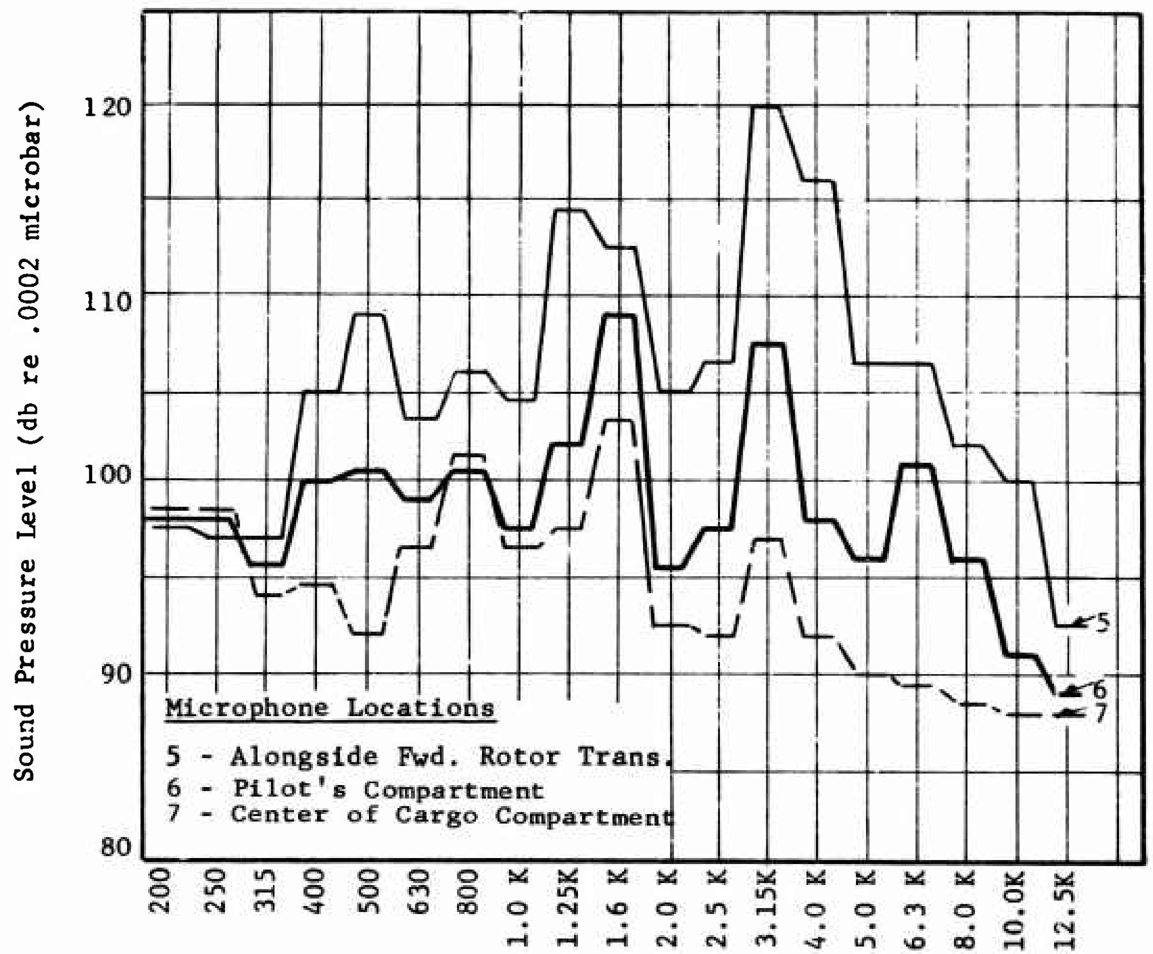

Third-Octave Band Midpoint Frequencies (Hz)

Figure 11. Comparative Noise Levels for Three Microphone Locations - Aircraft 1 at Hover Flight Condition.

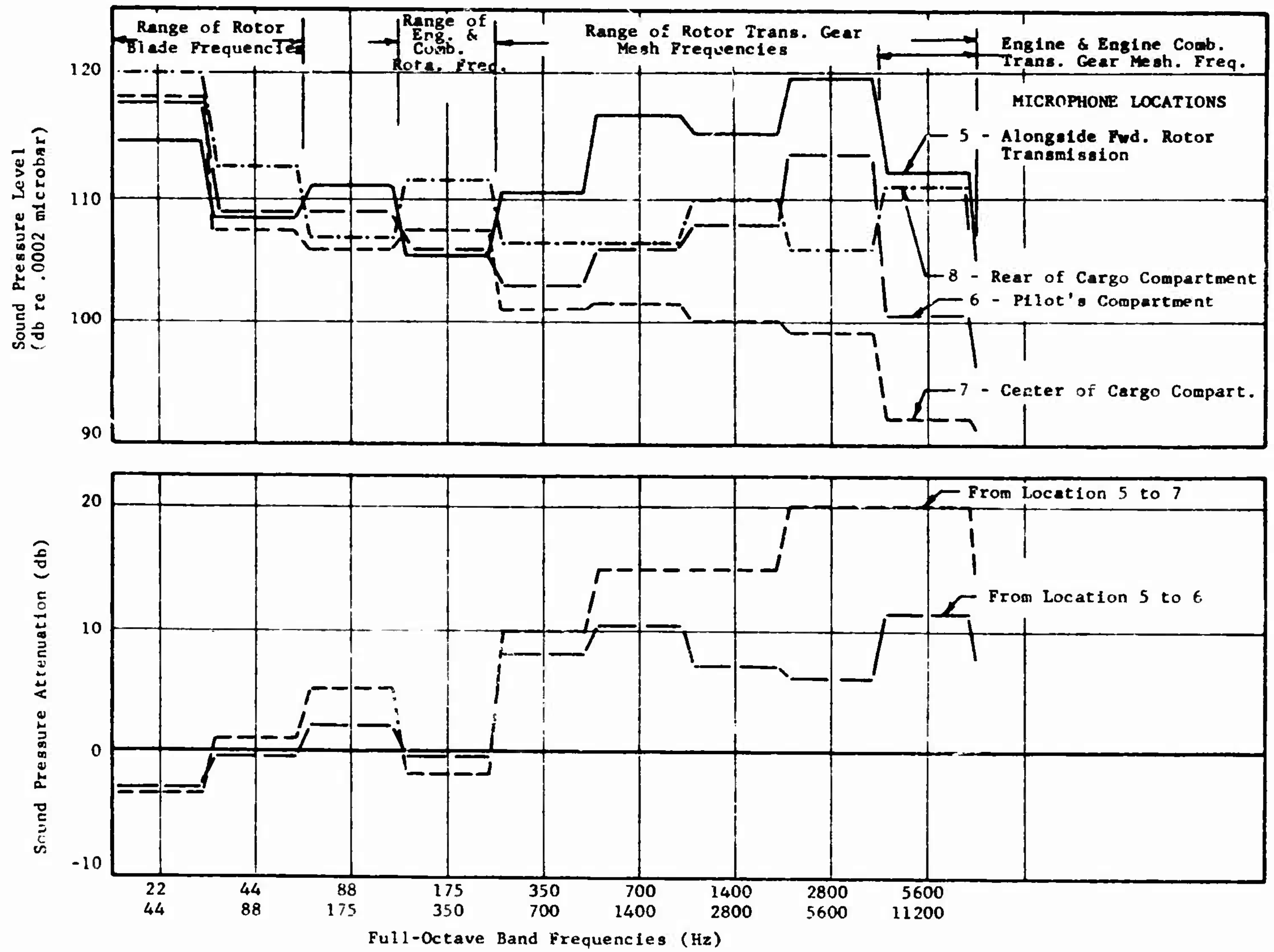

Figure 12. Comparative Noise Levels at Four Locations, Aircraft Cruise Condition.

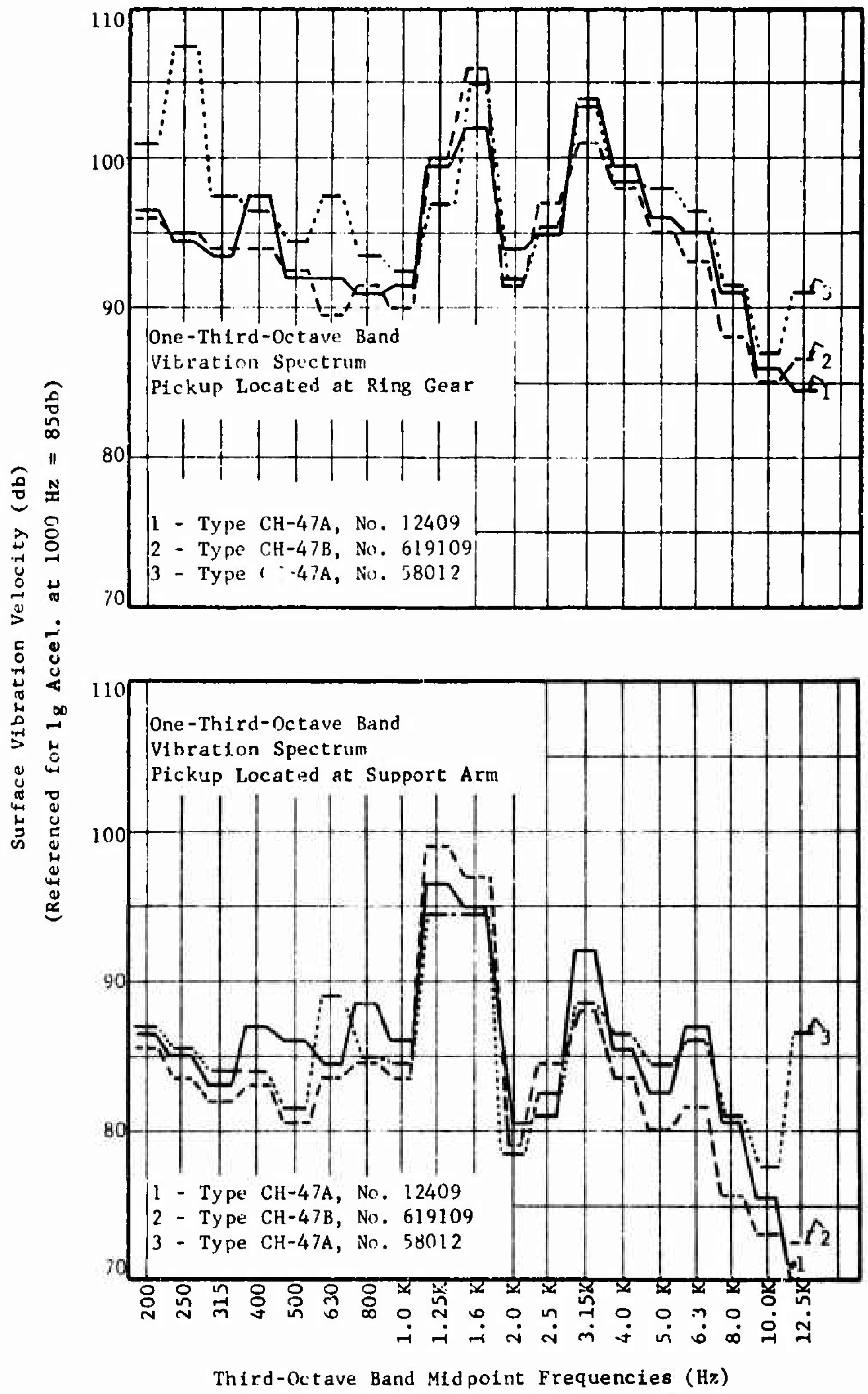

Figure 13. Casing Vibration Measurements in Three Aircraft for Cruise Flight Condition With Microphones Located at Ring Gear and Support Arm.

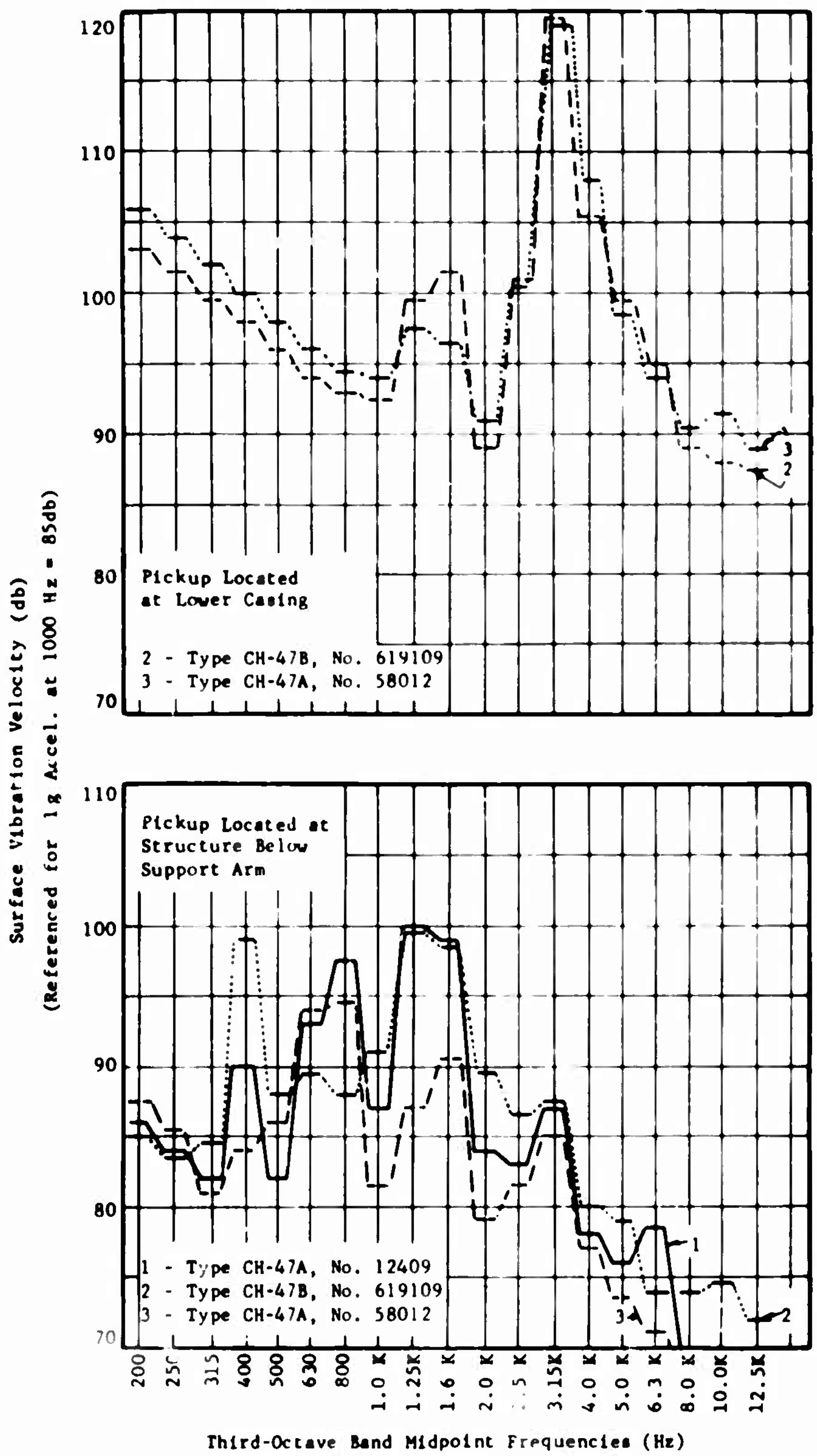

Figure 14. Casing Vibration Measurements in Three Aircraft for Cruise Flight Condition With Microphones Located at Lower Casing and Structure.

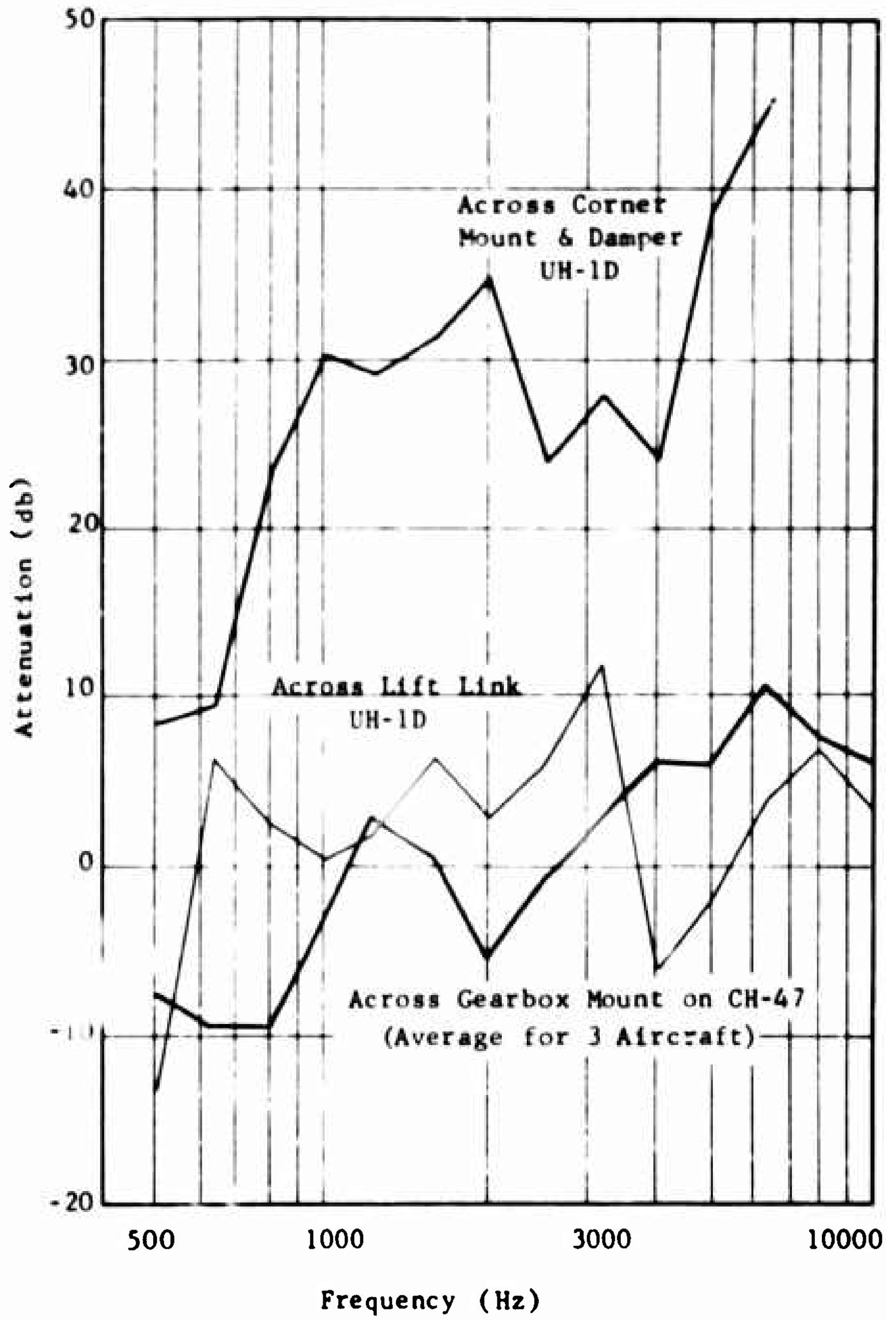

Figure 15. Vibration Attenuation Across Gearbox Lift Link and Mounts on UH-1D and Across Gearbox Mounts on CH-47.

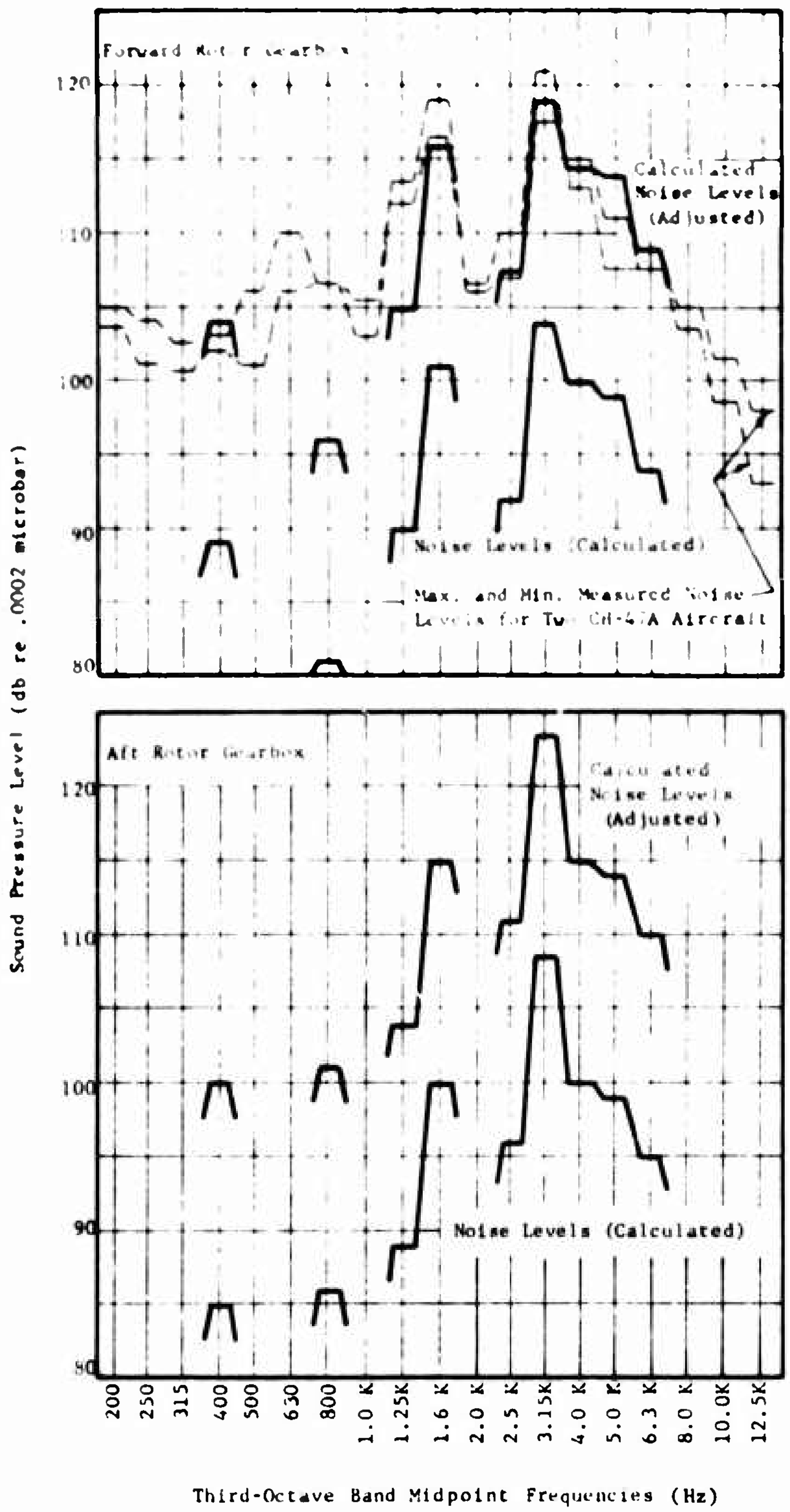

Figure 16. Calculated Noise Levels for Cruise Flight Conditions, Above for Forward Rotor Gearbox With Comparison to Measured Noise Levels, Below for Aft Rotor Gearbox.

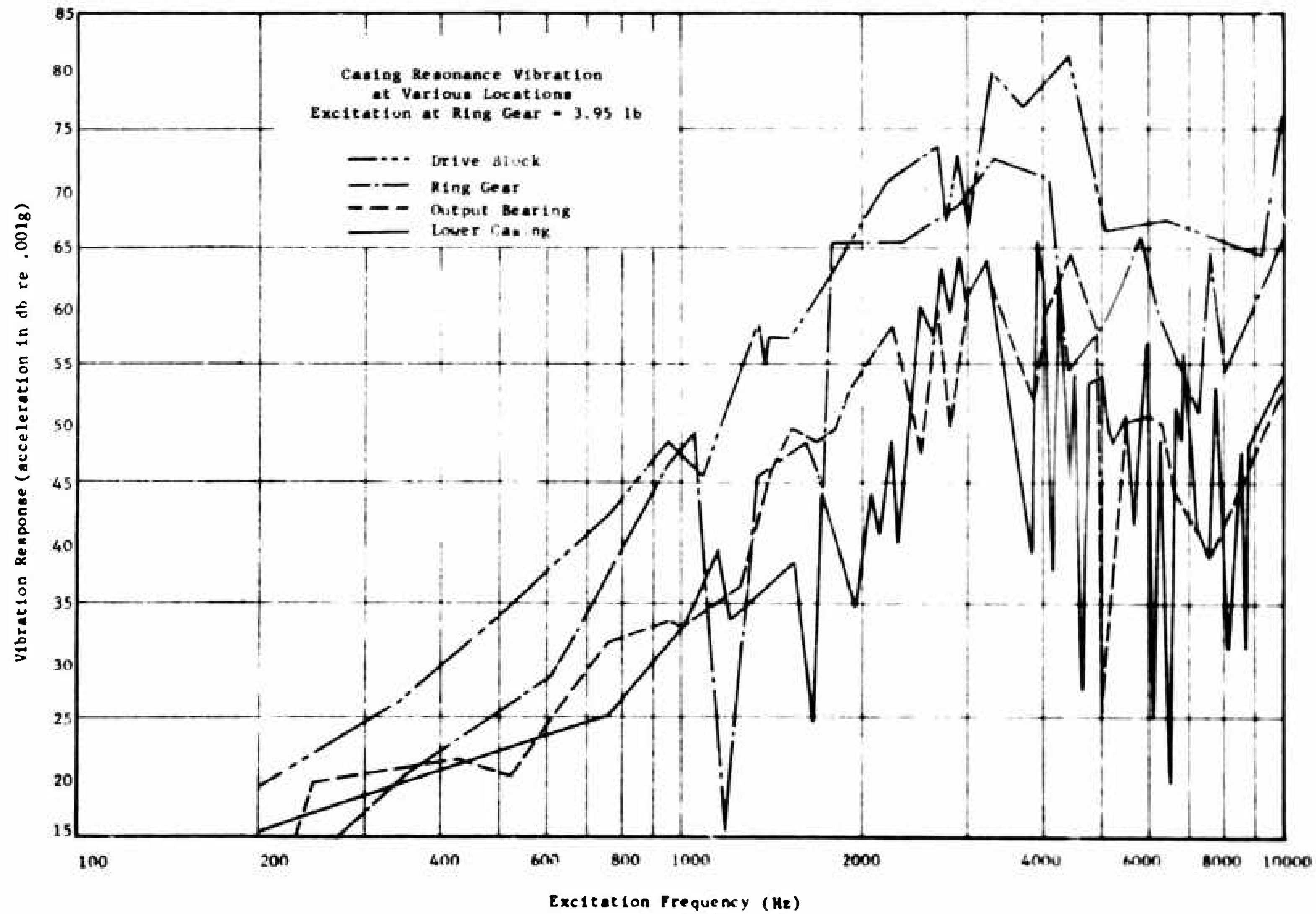

Figure 17. Casing Resonance Vibrations - Excitation at Ring Gear.

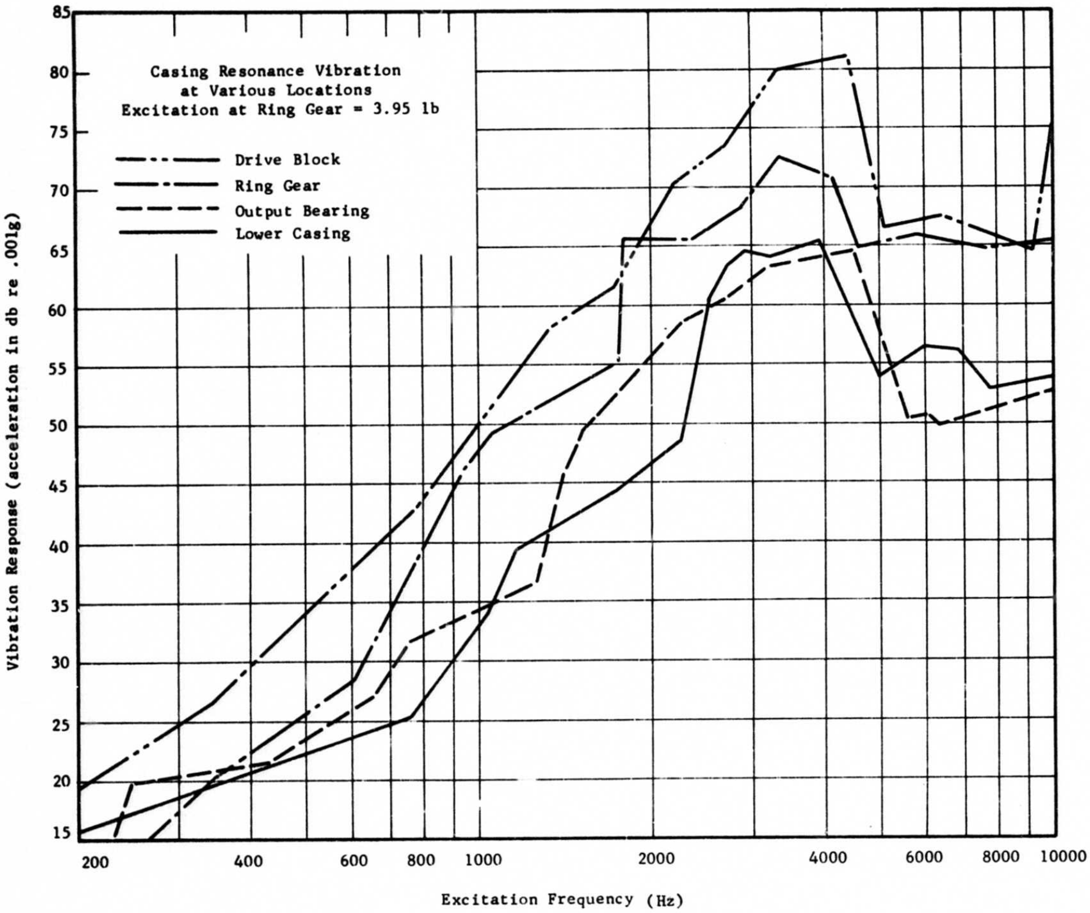

Figure 18. Casing Resonance Vibrations - Excitation at Ring Gear, Showing Smoothing of Curves.

TABLE 1. STATIC TOOTH FORCE TRANSMITTED BY DRIVE SYSTEM GEARS

Cruise Condition, 2750 hp; Hover Condition, 3750 hp.
Power supplied equally by the two engines. Power to rotors divided with 60 percent to the aft rotor and 40 percent to the forward rotor. Power to auxiliary drives is neglected.

		Static Tooth Force (lb) Tangential to Mean Pitch Circle	
Transmission	Gear Set	Cruise	Hover
Rotor-forward	Upper Plan	3445	4698
	Lower Plan	1542	2103
	Bevel	2760	3764
Rotor-aft	Upper Plan	5167	7046
	Lower Plan	2313	3154
	Bevel	4140	5646
Engine-comb	Bevel	2895	3948
Engine	Bevel	2256	3077

TABLE 2. CALCULATED EXCITATION FREQUENCIES - GEAR TOOTH MESHING FREQUENCIES AND THEIR HARMONICS

Third-Octave Band Midpoints (Hz)	Forward and Aft Transmission			Engine Combining Trans-mission (Hz)	Engine Trans-mission (Hz)
	Upper Stage Planetary (Hz)	Lower Stage Planetary (Hz)	Bevel Set (Hz)		
400	406				
500					
640					
800	816(2)				
1,000					
1,250	1,220(3)				
		1,482			
1,600					
2,000					
2,500					
		2,964(2)			
3,200			3,412		
4,000					
		4,446(3)			
5,000					
6,400			6,824(2)	6,588	
8,000					8,585
10,000			10,236(3)		
12,500				13,176(2)	

*Figures in parentheses show order of harmonic.

TABLE 3. COMPUTED SPUR GEAR EXCITATION COMPONENTS - HOVER FLIGHT CONDITION

Trans-mission	Stage	Mesh	Pro-file	Tangential Load (lb)	Amplitudes - Zero to Peak - (μin.) Fundamental			Second Harmonic			Third Harmonic		
					A*	B*	C*	A	B	C	A	B	C
Rotor Forward	Upper Planetary	Sun Planet	601FH Design	4698	+ 64.0	-- 30.1	70.7	+ 20.3	+ 14.9	25.2	− 17.8	− 5.7	14.0
		Planet Ring	701FH Design	4698	+ 37.1	+ 24.5	44.5	6.2	− 43.5	44.0	+ 15.4	+ 17.5	23.3
	Lower Planetary	Sun Planet	401FH Design	2103	+ 103.4	− 23.6	106.1	+ 6.8	+ 9.6	11.8	− 13.3	− 11.9	17.9
		Planet Ring	501FH Design	2103	+ 82.3	+ 31.9	88.3	− 20.1	− 37.3	42.4	+ 29.8	+ 7.4	30.7
Rotor Aft	Upper Planetary	Sun Planet	601AH Design	7046	+ 9.2	− 36.6	37.7	+ 43.2	+ 14.1	47.4	− 3.5	− 2.6	4.3
		Planet Ring	701AH Design	7046	− 13.5	+ 53.3	55.0	+ 30.9	− 58.0	65.7	+ 16.2	+ 9.3	18.6
	Lower Planetary	Sun Planet	401AH Design	3154	+ +63.9	− 31.3	71.1	+ +36.7	+ 10.8	38.3	− -19.9	− 10.2	22.3
		Planet Ring	501AH Design	3154	+ 44.9	+ 69.1	82.4	+ 2.6	− 60.5	60.6	+ 23.0	+ 7.4	24.2

*A Refers to Cosine or Real Component
B Refers to Sine or Imaginary Component
C Refers to Resultant of A and B

TABLE 4. COMPUTED SPUR GEAR EXCITATION COMPONENTS - CRUISE FLIGHT CONDITION

Trans-mission	Stage	Mesh	Profile	Tangential Load (lb)	Amplitudes - Zero to Peak - (μ in.) Fundamental A*	B*	C*	Second Harmonic A	B	C	Third Harmonic A	B	C
Rotor Forward	Upper Planetary	Sun Planet	601 FC (Design)	3445	+ 90.2	- 20.7	92.5	+ 3.7	+ 9.3	10.0	- 11.5	- 6.9	13.4
		Planet Ring	701 FC (Design)	3445	+ 55.9	+ 2.6	56.0	- 4.2	- 25.8	26.1	+ 18.2	+ 12.8	22.3
	Lower Planetary	Sun Planet	401 FC (Design)	1542	+ 121.3	- 15.7	122.3	- 9.6	+ 3.9	10.4	- 6.1	- 9.5	11.3
		Planet Ring	501 FC (Design)	1542	+ 94.2	+ 7.9	94.5	- 26.5	- 17.7	31.8	+ 31.0	- 1.3	31.1
Rotor Aft	Upper Planetary	Sun Planet	601 AC (Design)	5167	+ 53.5	- 32.7	62.7	+ 26.2	+ 15.9	30.6	- 12.3	- 4.8	13.2
		Planet Ring	701 AC (Design)	5167	+ 27.9	+ 31.4	42.0	+ 11.1	- 47.9	49.2	+ 14.6	+ 16.8	22.3
	Lower Planetary	Sun Planet	401 AC (Design)	2313	+ 96.3	- 26.2	99.8	+ 13.0	+ 11.2	17.2	- 15.8	- 12.2	20.0
		Planet Ring	501 AC (Design)	2313	+ 75.5	+ 40.0	85.5	- 15.9	- 42.9	45.7	+ 28.1	+ 8.3	29.3

*A Refers to Cosine or Real Component
B Refers to Sine or Imaginary Component
C Refers to Resultant of A and B

TABLE 5. COMPUTED SPIRAL BEVEL GEAR EXCITATION COMPONENTS - HOVER FLIGHT CONDITION

Transmission	Minimum Combined Tooth Compliance (μ in./lb)	Effective Contact Ratio	Tangential Load (lb)	Resultant Amplitudes - Zero to Peak (μ in.)	
				Fundamental	Second Harmonic
Engine	.231	1.950	3077	23.9	--
Combining	.194	2.244	3948	63.8	--
Aft Rotor	.164	2.016	5646	29.4	29.4
Forward Rotor	.156	1.936	3764	23.2	21.7

TABLE 6. COMPUTED SPIRAL BEVEL GEAR EXCITATION COMPONENTS - CRUISE FLIGHT CONDITION

Transmission	Minimum Combined Tooth Compliance (μin./lb)	Effective Contact Ratio	Tangential Load (lb)	Resultant Amplitudes - Zero to Peak (μ in.)	
				Fundamental	Second Harmonic
Engine	.231	1.950	2256	17.5	--
Combining	.194	2.244	2895	46.7	--
Aft Rotor	.164	2.016	4140	21.5	21.5
Forward Rotor	156	1.936	2760	17.0	16.6

TABLE 7. COMPUTED SPUR GEAR DYNAMIC TOOTH FORCES - HOVER FLIGHT CONDITION

Trans-mission	Stage	Mesh	Profile	Tang. Load (lb)	Fundamental (lb)			Second Harmonic (lb)			Third Harmonic (lb)		
					A*	B*	C*	A	B	C	A	B	C
Rotor Forward	Upper Planetary	Sun Planet	601FH (Design)	4698	+ 17.3	+ 1.5	17.4	− 2.5	− 11.3	11.6	+ 4.5	+ 3.7	5.9
		Planet Ring	701FH (Design)	4698	+ 19.8	− 3.5	20.1	+ 2.9	+ 10.9	11.3	− 10.3	− 11.2	15.2
	Lower Planetary	Sun Planet	401FH (Design)	2103	− 110.3	+ 31.7	114.8	− 110.2	− 181.7	212.5	− 15.3	− 23.6	28.1
		Planet Ring	501FH (Design)	2103	− 72.2	− 33.5	79.6	+ 480.8	+ 939.3	1055.2	+ 300.3	+ 80.1	310.8
Rotor Aft	Upper Planetary	Sun Planet	601AH (Design)	7046	− 1.5	+ 6.0	6.2	− 6.1	− 10.8	12.4	+ 2.9	+ 1.9	3.5
		Planet Ring	701AH (Design)	7046	+ 0.4	− 1.7	1.7	− 1.0	+ 14.8	14.8	− 10.4	− 6.1	12.1
	Lower Planetary	Sun Planet	401AH (Design)	3154	− 92.1	+ 48.6	104.1	+ 80.3	− 231.0	244.5	− 47.8	− 9.5	48.8
		Planet Ring	501AH (Design)	3154	− 36.8	− 71.0	80.0	+ 74.6	+ 1655.6	1657.3	+ 241.8	+ 76.2	253.5

* A Refers to Cosine or Real Component
B Refers to Sine or Imaginary Component
C Refers to Resultant of A and B

TABLE 8. COMPUTED SPUR GEAR DYNAMIC TOOTH FORCES - CRUISE FLIGHT CONDITION

Transmission	Stage	Mesh	Profile	Tangential Load (lb)	Fundamental (lb)			Second Harmonic (lb)			Third Harmonic (lb)		
					A*	B*	C*	A	B	C	A	B	C
Rotor Forward	Upper Planetary	Sun Planet	601FC (Design)	3445	−15.6	+2.8	15.6	−4.5	−8.7	9.8	+0.7	+3.6	3.7
		Planet Ring	701FC (Design)	3445	−12.0	+0.7	12.0	−2.0	+9.7	9.9	+10.3	−8.5	13.4
	Lower Planetary	Sun Planet	401FC (Design)	1542	−131.1	+19.9	132.6	−189.9	−88.0	209.3	−3.7	−15.5	15.9
		Planet Ring	501FC (Design)	1542	−82.3	−9.2	82.8	+541.6	+442.1	699.1	+309.0	−8.6	309.1
Rotor Aft	Upper Planetary	Sun Planet	601AC (Design)	5167	+448.0	−4.2	448.1	+203.0	−188.8	277.2	+8.0	−4.6	9.2
		Planet Ring	701AC (Design)	5167	+450.4	−10.1	450.5	+208.7	−164.5	265.8	−3.8	−4.1	5.6
	Lower Planetary	Sun Planet	401AC (Design)	2313	−132.2	+38.9	137.8	+88.07	−156.6	179.7	−45.7	−11.2	47.1
		Planet Ring	501AC (Design)	2313	−63.6	−41.9	76.2	−378.4	+1188.8	1247.6	+291.9	−86.0	304.3

*A Refers to Cosine or Real Component
B Refers to Sine or Imaginary Component
C Refers to Resultant of A and B

TABLE 9. COMPUTED BEVEL GEAR DYNAMIC TOOTH FORCES - HOVER FLIGHT CONDITION

Transmission	Tangential Load (lb)	Forces - Zero to Peak (lb)	
		Fundamental	Second Harmonic
Engine	3077	256	
Combining	3948	780	
Aft Rotor	5646	199	292
Forward Rotor	3764	431	288

TABLE 10. COMPUTED BEVEL GEAR DYNAMIC TOOTH FORCES - CRUISE FLIGHT CONDITION

Transmission	Tangential Load (lb)	Forces - Zero to Peak (lb)	
		Fundamental	Second Harmonic
Engine	2256	188	
Combining	2895	571	
Aft Rotor	4140	146	214
Forward Rotor	2760	326	220

TABLE 11. PREDICTED NOISE LEVELS - HOVER FLIGHT CONDITION, ONE-THIRD-OCTAVE BAND LEVELS FOR THOSE BANDS CONTAINING AN EXCITATION FREQUENCY

One-Third-Octave Band Midpoint Frequencies (Hz)	Noise Level (db) (1db = .0002 microbar)			
	Forward Rotor Transmission	Aft Rotor Transmission	Combining Transmission	Engine Transmission
400	87.2	79.3		
500				
630				
800	85.9	88.7		
1,000				
1,250	89.9	88.5		
1,600	100.6	99.3		
2,000				
2,500				
3,150	107.8	111.3		
4,000				
5,000				
6,300	96.4	97.8	108.2	
8,000				97.3

TABLE 12. PREDICTED NOISE LEVELS - CRUISE FLIGHT CONDITION, ONE-THIRD-OCTAVE BAND LEVELS FOR THOSE BANDS CONTAINING AN EXCITATION FREQUENCY				
One-Third-Octave Band Midpoint Frequencies (Hz)	Noise Level (db) (1db = .0002 microbar)			
	Forward Rotor Transmission	Aft Rotor Transmission	Combining Transmission	Engine Trans-mission
400	89.9	85.9		
500				
630				
800	80.9	87.0		
1,000				
1,250	90.3	89.4		
1,600	101.6	100.9		
2,000				
2,500				
3,150	105.0	108.7		
4,000				
5,000				
6,300	94.1	95.1	102.5	
8,000				94.6

TABLE 13. HELICOPTER POWER TRAIN LOADS DURING IN-FLIGHT NOISE MEASUREMENTS

	During In-Flight Measurements			Predicted
Aircraft Type Tail No.	CH-47A 12409	CH-47B 619109	CH-47A 58012	CH-47A or B
Hover				
Rotor Speed	230 rpm	225 rpm	230 rpm	230 rpm
Engine Speed	15150 rpm	14800 rpm	15150 rpm	15150 rpm
Engine Torque	480 ft-lb	450 ft-lb	450 ft-lb	
Engine Horsepower	1385 hp	1270 hp	1300 hp	
Combined Engine Horsepower	2770 hp	2540 hp	2600 hp	3750 hp
Cruise				
Rotor Speed	230 rpm	225 rpm	230 rpm	230 rpm
Engine Speed	15150 rpm	14800 rpm	15150 rpm	15150 rpm
Engine Torque	420 ft-lb	450 ft-lb	430 ft-lb	
Engine Horsepower	1210 hp	1270 hp	1240 hp	
Combined Engine Horsepower	2420 hp	2540 hp	2480 hp	2750 hp

TABLE 14. NOISE LEVEL PEAKS IN THE NARROW-BAND ANALYSIS, MICROPHONE LOCATED IN THE PILOT'S COMPARTMENT, AIRCRAFT NO. 12409, CRUISE FLIGHT CONDITION

Narrow-Band Peaks		Full-Octave Band Limits (Hz)	Excitation (Hz)	Associated Main Drive Members
Freq (Hz)	Level (db)			
		22		
24	98.5		23 (2)	Forward Rotor Transmission - Rotor Blades
31.8	83		34.5 (3)	Forward Rotor Transmission - Rotor Blades
		44		
48	82		46 (4)	Forward Rotor Transmission - Rotor Blades
69	83		69 (6)	Forward Rotor Transmission - Rotor Blades
69	83		67	Forward Rotor Transmission - Bevel Gear Rotation
84	88		84	Forward Rotor Transmission - Upper Planet Passing
		88		
94	87		92 (8)	
126	85		118	Forward Rotor Transmission - Bevel Gear Pinion Rotat.
144	89			
		175		
190	83		200	Gear Rotations - Engine Combining Pinion
240	82.5		253	Gear Rotations - Engine Pinion
		350		
360	78			
410	82			
560	76		400	Transmission Gear Meshing - Fwd. & Aft Rotor - Upper Planetary
		700		
825	80		816 (2)	Transmission Gear Meshing - Fwd. & Aft Rotor - Upper Planetary
1250	80		1220 (3)	Transmission Gear Meshing - Fwd. & Aft Rotor - Upper Planetary
		1400		

TABLE 14 - Continued

Narrow-Band Peaks Freq (Hz)	Narrow-Band Peaks Level (db)	Full-Octave Band Limits (Hz)	Excitation (Hz)	Associated Main Drive Members
1480	87.5		1482	Transmission Gear Meshing - Fwd. & Aft Rotor - Lower Planetary
1560	86			Transmission Gear Meshing - Fwd. & Aft Rotor - Lower Planetary
		2800		
3020			2964 (2)	Transmission Gear Meshing - Fwd. & Aft Rotor - Lower Planetary
3560				
4450			3412	Transmission Gear Meshing - Fwd. & Aft Rotor - Bevel Gear
5400			4446 (3)	Transmission Gear Meshing - Fwd. & Aft Rotor - Lower Planetary
		5600		
6600	70		6588	Transmission Gear Meshing - Engine - Combining
6800	80		6824 (2)	Transmission Gear Meshing - Fwd. & Aft Rotor - Bevel Gear
7200	76			
8600*	78**		8585	Transmission Gear Meshing - Engine
10000*	78**		10236 (3)	Transmission Gear Meshing - Fwd. & Aft Rotor - Bevel Gear
		11200		
13000*	78**		13176 (2)	Transmission Gear Meshing - Engine - Combining

* Figures Show Multiple of Original Frequency
** No Individual Peaks

DISCUSSION OF RESULTS - PHASE II

INTRODUCTION

As originally formulated, the Phase II studies were to be directed toward analytical comparisons between several specified transmission design modifications with the objective of reducing overall gear noise levels. Following evaluation of the results of Phase I, the remaining contract efforts were revised to include consideration of the following Phase I results:

1. Differences between calculated and measured noise levels at frequencies corresponding to the second and third harmonics of tooth meshing frequencies for the upper planetary gear set.

2. The possibility that while significant noise-reduction benefits may result from tooth-profile modifications, the accuracy required to ensure the consistent achievement of such reductions may not be realistic by present manufacturing standards.

In addition, the difference in overall level between the calculated and measured noise spectra required further examination. An analysis of the sensitivity of the entire calculation procedure to variations in the energy conversion factor, the housing geometry and environmental factor, and the distance factor was deemed appropriate.

The original objective of performing analytical comparisons between several possible design modifications would most nearly be achieved by considering design-type variations in transmission physical properties which are also the most likely contributors to the observed differences between calculated and measured results discussed above. Consequently, profile variations, variations in the torsional stiffness of the upper planetary planet carrier, and noise energy fraction were selected as quantities for study. In a more direct attempt to effect noise reduction, the double-ramp profile proposed in the UH-1D study was considered. This analysis also included the effect of variations in tooth loading.

GEAR TOOTH PROFILE MANUFACTURING DEVIATIONS

Information relative to involute profile tolerances for the upper planetary gears was obtained from the following Boeing-Vertol design drawings:

Print No.	Identification
J-114D2077-M	Gear-Sun, 2nd Stage Planet, Rotor Transmission
J-114D2084-K	Gear-Planet, 2nd Stage, Rotor Transmission
J-114D2086-M	Gear-Stationary Ring Planetary, Rotor Transmission

The profile tolerance information contained on these drawings was plotted with enlarged scales to show pitch diameter (PD) and outer diameter (OD) limits, referenced to zero at the beginning of the true involute form (BIF). Fullness limits relative to PD were plotted as indicated on the Vertol drawings.

Five profiles were selected for each of the three gears. These profiles were considered to represent the extremes which might be encountered within the allowed tolerances. The following identifying labels were assigned to these profiles:

1. True Involute
2. Minimum Fullness
3. Maximum Fullness
4. "Crossover" Profile - Minimum to Maximum
5. "Crossover" Profile - Maximum to Minimum

These profiles thus identified are shown in Figures 19, 20 and 21 for the sun gear, the planet gear, and the ring gear, respectively.

The following selected profile combinations were run on Program GEARO (Appendix IV of Reference 1) to calculate pitch-line excitations:

Sun/Planet Series No.	Planet/Ring Series No.	Profile Identification (Driver/Driven)
601	701	Average/Average (Repeat of Phase I Calculation)
602	702	True Involute/True Involute
603	703	Minimum/Minimum
604	704	Maximum/Maximum
605	705	Minimum/Maximum
606	706	Maximum/Minimum
607	707	Minimum to Maximum/Minimum to Maximum
608	708	Maximum to Minimum/Maximum to Minimum
609	709	Minimum to Maximum/Maximum to Minimum
610	710	Maximum to Minimum/Minimum to Maximum

The resulting pitch-line excitations, in microinches, were converted to db by means of the relationship

$$db = 20 \log_{10} \left(\frac{\text{new excitation}}{\text{original excitation}} \right)$$

In all cases, the original excitation value used as a basis of comparison was that value obtained in series 601 (701 for the planet-to-ring mesh) for the particular harmonic under consideration. Excitation values in db were thus obtained for the two meshes at loads corresponding to cruise and hover conditions. These results are presented in Figures 22 and 23 for the sun-to-planet mesh and in Figures 24 and 25 for the planet-to-ring mesh. The connecting lines between different series numbers serve only to provide continuity so that variations for any single harmonic may be compared between different cases. It should be noted that the results shown in Figures 22 through 25 are excitation results. Therefore, the effect of profile differences upon predicted noise levels is only approximately indicated by plotting the results as db levels. The effects of profile variations, if any, on the shape of the noise spectrum depend upon both the magnitude and proximity of other noise components.

Examination of Figures 22 through 25 yields certain positive information which is of definite importance to the designer who seeks noise reduction through the design process:

1. Profile variations are increasingly less important as a means of modifying excitation amounts as transmitted load increases. This is evidenced by the relatively narrower band of results for the hover condition compared to the lower power cruise condition.

2. Relatively large variations in calculated pitch-line excitation appear between the various profile combinations considered for the upper planetary gear set. This indicates that while modifications to tooth profiles are able to change the amount of torsional excitation produced (and thus the noise level), the amount of modification required to achieve a specified change is apparently smaller than the manufacturing and measuring capabilities available at the present time.

3. Comparison of the AVERAGE/AVERAGE (601 and 701 curves) with the corresponding TRUE INVOLUTE/TRUE INVOLUTE (602 and 702 curves) in Figures 22 through 25 indicates that the use of the relieved tip and base tooth profiles (AVERAGE/AVERAGE) yields significantly lower levels of torsional excitation than does the use of the true involute profiles.

PLANET CARRIER TORSIONAL STIFFNESS VARIATIONS

Calculations were made to determine the effect upon dynamic force levels of variations in the upper planetary planet carrier compliance. The transmission model used is that reported in the results of the Phase I study. Excitations introduced into the program are those obtained with the "AVERAGE" sun, planet, and ring gear tooth profiles (601 and 701 series) reported in detail in Phase I. Thus, these calculations were designed to show clearly the effect of variations in a single system design parameter, with all other quantities held constant.

The significance of variations in dynamic tooth force as a function of planet carrier compliance should be pointed out at this time. If relatively large percentage changes occur as a result of reasonably small variations in carrier torsional compliance, then carrier compliance may be identified as a "high sensitivity" parameter with respect to noise. This serves principally to focus attention upon the method by which the compliance is calculated and the limiting assumptions upon which the calculations are based. It further indicates the approximate accuracy within which carrier compliance must be calculated for good confidence in the predicted noise levels.

Order of magnitude (0.1 and 10.0 times) as well as smaller variations in the planet carrier compliance were selected for the calculations. The original Phase I planet carrier compliance, measured tangentially along the circumference of the circle passing through the planet mounting points, was 1.33×10^{-6} in./lb. Thus, values between 1.33×10^{-7} and 1.33×10^{-5} in./lb were selected for this study. These variations were applied, in turn, in calculations in which the appropriate amount of excitation was applied at the proper frequency at each gear mesh point. These calculations were done first with excitation at the spiral bevel gear set at 3412 Hz; with excitation at the lower planetary at 1482, 2964, and 4446 Hz; and finally with excitation at the upper planetary at 406, 816, and 1220 Hz.

The results of these calculations are presented in Figures 26 through 28. When excitation is specified at the spiral bevel gear at the fundamental tooth mesh frequency of 3412 Hz, little, if any, variation in the dynamic tooth force level is observed at the spiral bevel gear mesh point when variations are made in the upper planetary planet carrier compliance. The same results are observed with excitation at the lower planetary at the second and third harmonics of lower planetary tooth mesh frequency (2964 and 4446 Hz, respectively).

However, with fundamental frequency excitation (at 1482 Hz) applied at the lower planetary location, variations as great as 40 percent appear in dynamic force le s over the range of compliance considered. In addition, with excitations at the upper planetary location, particularly at frequencies corresponding to the first and third harmonics of tooth meshing frequency, extremely large variations in dynamic forces, on the order of 100 to 1, appear for compliances in the neighborhood of the design value. The appearance of such large variations in the upper planetary dynamic tooth forces leads to the following conclusions:

1. The drive train appears to be sensitive to variations in the compliance of the upper planetary planet carrier with excitation at frequencies corresponding to the fundamental and second and third harmonics of upper planetary gear mesh frequency (406, 816, and 1220 Hz, respectively), and at the fundamental mesh frequency of the lower planetary gear set (1482 Hz). It appears to be particularly sensitive at 406 and 1220 Hz.

2. Variations on the order of 2 to 1 in the compliance of the upper planetary planet carrier can result in very large increases (100 to 1) in dynamic tooth forces in the upper planetary gear

set at a frequency of 1220 Hz (third harmonic) if the actual compliance is half the calculated value. On the other hand, if the actual torsional compliance is approximately twice that calculated, the dynamic force component at 406 Hz will be about 100 percent.

3. The adjusted predictions from Phase I indicate that the noise level predicted at 406 Hz is very close to that measured. Since relatively large variations in the tooth dynamic force component at 406 Hz would appear to accompany any deviations from the proper planet carrier compliance, it must be concluded that the calculated value of compliance is relatively near the actual value. It is possible that should the actual compliance be higher, the effect of the lower planet-ring dynamic force would be cancelled by the higher sun-planet force. Even so, the relative flatness of the respective dynamic force component curves at 816 and 1220 Hz removes the torsional planet carrier compliance as a possible source of the difference between predicted and measured values for the second and third harmonics.

ANALYSIS OF NOISE - ENERGY FRACTION

During laboratory measurements made under Phase I, Part C studies, extensive transmission casing acceleration measurements were taken at various locations with constant force vibration applied to several other locations. Acoustic measurements were also made for the particular case in which mechanical excitation was applied to the input bearing drive block (nearest the spiral bevel drive shaft input). Results of these measurements for two microphone orientations relative to the transmission are shown in Figure 29.

Mechanical vibration (acceleration) data recorded at the same drive block has been reduced to velocity data in db form (basis: 42.5 db at 1000 H) for comparison on a relative basis with the sound pressure level data. The three curves are shown in Figure 30. The relative separation between the surface velocity and acoustic curves (not the absolute separation) provides an indication of the amount of change of the ratio of acoustic to mechanical energy. These relative separations for the two microphone orientations are shown in Figure 31.

Variations from a mean value of the difference are found to be about 3-4 db with the microphone in the vertical orientation and on the order of 8-10 db for the horizontal orientation. These results appear to suggest that whatever variability exists is due to the manner in which the sump walls vibrate. The magnitude of the variations (about 20 db peak to peak) appears to indicate that the ratio of acoustic to mechanical energy dissipation is not constant over the frequency range 200-10,000 Hz.

SENSITIVITY OF CALCULATIONS TO VARIATIONS IN EMPIRICAL FACTORS

The sensitivity of calculated noise levels to variations in the empirically obtained energy conversion factor α and housing geometry and environment factor β, as well as in the radial distance r, was studied by means of Program GENOC (Appendix V). This program was developed in Phase I to automate the calculations shown in Appendix VI of Reference 1 which were previously done manually.

Such an analysis was deemed necessary because of the limitied amount of information available concerning the transfer of mechanical to acoustic energy for this particular transmission (factor α). Further, very little data has been obtained relating the intensity of noise measured within the actual helicopter to those noise levels which would be observed with nonreflective and nonvibrating surroundings. This noise would be most nearly comparable to that which is calculated by the computer program. Phase I results were obtained with the housing geometry and environment factor β set equal to 1.0, which was intended to represent nonreflective, nonvibrating surroundings.

The radius r separating the center of noise generation from the measuring point was also included in the sensitivity study. This was considered appropriate because of the very general nature of the model used for the calculations. While quantity r is intended to be the radial distance from the center of a noise-generating sphere to the recording device, and while the microphone was in fact positioned approximately 1 foot from the center of the spiral bevel gear mesh point during in-flight testing, it is recognized that the shape of the transmission casing is far from a sphere and also that many other vibrating parts are in close proximity to it. Consequently, it was felt that for this particular transmission, a more representative distance might be the distance from the transmission casing itself to the microphone (approximately 3 inches), and that some measure of variability of noise level with respect to this distance should be obtained.

The results of the Phase I calculations shown in Figure 16 were used as a basis for the sensitivity calculations. In those results, radius r was equal to 1.0 ft, energy conversion factor α was equal to 2.06×10^{-9}, and the environment factor β was 1.0. In this study, each of these quantities was varied systematically with all others held constant. Values considered were as follows:

r (ft) : 0.5, 1.0, 1.5, 2.0, 3.0
α : 2.06×10^{-10}, 1.03×10^{-9}, 4.12×10^{-9}, 2.06×10^{-8}
β : 0.01, 0.1, 10.0

The resulting noise spectra were plotted on the same axes as Figure 16. Examination of the results revealed that little or no variation in spectrum shape was introduced by the variations considered. Thus, variations in the overall level of the spectrum can be presented by plotting the calculated noise levels of a single third-octave band versus each of the variables. This has been done in Figure 32, where the selected third-octave band is that one having 3150 Hz as its midpoint. These results indicate that probably the major part of the differences between the calculated and measured values shown in Figure 16 may be resolved by improved knowledge about the vibration characteristics of the transmission and its mounting within the aircraft.

In the attempt to verify the calculated variations in noise level with distance from the transmission, further noise measurements were made aboard two CH-47 aircraft at Fort Eustis. Under flight-idle conditions, noise transverses were made as follows:

1. CH-47A Aircraft. The microphone was positioned beside the transmission and then vertically below the bottom center of the forward transmission at preset distances. The following results were obtained.

Position	Noise Level db (3150 Hz - third octave)
Beside Forward Transmission	107
3 in.	108
6 in.	103
9 in.	108.5
12 in.	109
24 in.	102

2. CH-47B Aircraft. The microphone was again positioned beside the transmission and then below the bottom center of the forward transmission and aft along a line 30° to the vertical, extending backward into the cargo compartment with increased distance from the transmission. The following results were obtained:

Position	Noise Level db (3150 Hz - third octave)
Beside Forward Transmission	118
3 in.	113.5
6 in.	114
9 in.	108
12 in.	113.5
24 in.	114

The results of these additional measurements are plotted in Figure 32. At distances on the order of 3 to 9 inches, the measured noise levels appear to follow the theoretical prediction. This indicates that at distances less than about 1 foot from the transmission casing, the acoustic vibration of the transmission is the predominant noise source.

At greater distances, however, the measured data depart drastically from the predicted data. The noise levels at these distances are not due primarily to noise radiated from the transmission, but are apparently strongly influenced by the induced vibrations of the aircraft structure itself. In these particular measurements, the structure panels between the pilot and cargo compartments are very likely the chief noise source. It is interesting to note that in the CH-47B measurements the noise level remained nearly constant during the traverse downward and aft into the cargo compartment, whereas the noise levels measured in the CH-47A vertical traverse dropped slightly as the microphone was moved vertically downward. It would appear that vibration of the structure associated with the cargo compartment itself might be responsible for a significant portion of the noise measured within it.

In summary, strong indications exist that structural vibrations are responsible for a significant portion of the noise within the CH-47 helicopter. It is felt that probably the majority of the vibration energy in the structure is received across the transmission mounts, with a lesser proportion received by airborne noise impinging upon the vibration surfaces. The measurements of vibration attenuation across the gearbox mounts shown in Figure 15 appear to support this conclusion.

RELIEVED TIP AND BASE TOOTH PROFILE MODIFICATIONS

Tooth profile variations for the sun, planet, and ring gears in the CH-47 forward transmission upper planetary gear set were discussed earlier in this chapter. Typical combinations of these profiles were examined for predicted excitation at tangential tooth forces corresponding to cruise and hover conditions. These combinations were identified by the series numbers 601-610 for the sun/planet mesh and 701-710 for the planet/ring mesh. Resulting excitation values were presented as db levels so that they could be compared on the basis of noise. For these same profile combinations, additional tangential tooth loads were selected, and further excitation calculations were performed.

In order to study the effect of tangential tooth loading, forces corresponding to 75% of cruise load and 125% of hover load were assumed. The resulting pitch-line excitations, in microinches, have been plotted vs. load, and appear in Figures 33 through 50. The information contained in these figures is essentially a cross-plot of portions of that data contained in Figures 22 through 25 with additional data for higher and lower loads. For convenience, the profile series numbers and labels are repeated here.

Sun/Planet Series No.	Planet/Ring Series No.	Profile Identification (Driver/Driven)
601	701	Average/Average (repeat of Phase I Calculations)
602	702	True Involute/True Involute
603	703	Minimum/Minimum

Sun/Planet Series No.	Planet/Ring Series No.	Profile Identification (Driver/Driven)
604	704	Maximum/Maximum
605	705	Minimum/Maximum
606	706	Maximum/Minimum
607	707	Minimum-Maximum/Minimum-Maximum
608	708	Maximum-Minimum/Maximum-Minimum
609	709	Minimum-Maximum/Maximum-Minimum
610	710	Maximum-Minimum/Minimum-Maximum

Several immediate trends may be observed from Figures 33 through 50. First, the results for the relieved tip and base type profiles show a decrease in fundamental excitation magnitudes with an increase in load for all but three cases (705, 705, 707). This is in contrast to uniformly increasing fundamentals for the true involute profiles (601, 701).

Second, the results for many of the relieved tip and base profiles (604, 606, 607, 608, 609, 610, 703, 704, 707, 708, 710) show distinct minimum values of second harmonic excitation, in contrast to the uniformly increasing second harmonics for the true involute profiles. The occurrence of a minimum point in the second harmonic would appear to be very important if the location of the minimum can be changed by design modifications. In view of the decrease of fundamental excitation with increase of load, it would appear most desirable to have the second harmonic minimum point occur at as high a load as possible. The ultimate effect of such modifications upon noise level, however, is not as easily predicted since system dynamic forces may not be constant over the range of loads involved.

Finally, the third harmonic results appear to be largely insensitive to tangential tooth force level, although excitation changes may be as large as 50 to 60 percent over the range of forces involved. From the noise-reduction standpoint, it would appear that modifications involving the fundamental and second harmonic excitations show more promise.

RAMP-MODIFIED TOOTH PROFILE MODIFICATIONS

Based upon the studies described in the foregoing discussion of relieved tip and base tooth profiles, five profiles have been selected for each of the sun, planet, and ring gears in the forward transmission upper planetary gear set. These profiles were selected in an attempt to combine into single profiles those portions of profiles which appeared to give the lowest excitations in the profile-variation study. These profiles, shown in Figure 51 are identified as RM-1 through RM-5, respectively. Combinations of these profiles were selected as follows:

Sun/Planet Series No.	Planet/Ring Series No.	Profile Identification (Driver/Driven)
650	750	RM-1/RM-1
651	751	RM-2/RM-2
652	752	RM-3/RM-3
653	753	RM-4/RM-4
654	754	RM-5/RM-5

Excitation calculations were made for these several profile combinations, and the results are presented in Figures 52 through 61. Again, several trends may be observed. First, the calculated fundamental excitation magnitudes increase with increase in tangential tooth load, in a manner similar to the true involute results but in contrast to the majority of the cases considered in the relieved tip and base profile analysis.

Second, minimum values are apparent in the second harmonic results only for series numbers 653 and 753, and decreases in second harmonic excitation are found in series numbers 653, 654, 753, and 754.

Third, at tooth load conditions corresponding to hover flight, the excitation magnitudes are substantially the same as those found for the relieved tip and base profiles. This indicates that, overall, the ramp-modified profiles considered are not substantially superior to the relieved tip and base profiles for noise reduction at hover conditions. At cruise conditions, however, the ramp-modified profiles all yield values of pitch-line excitation substantially lower than all tip and base profiles except those of series 706.

While the results of the above analysis are encouraging, it is at once apparent that the profiles yielding the lowest amounts of excitation are those which are also the most difficult to produce because of the extremely small differences between them and the true involute. Their utility as an effective method of noise reduction must therefore await more accurate manufacturing and measurement techniques.

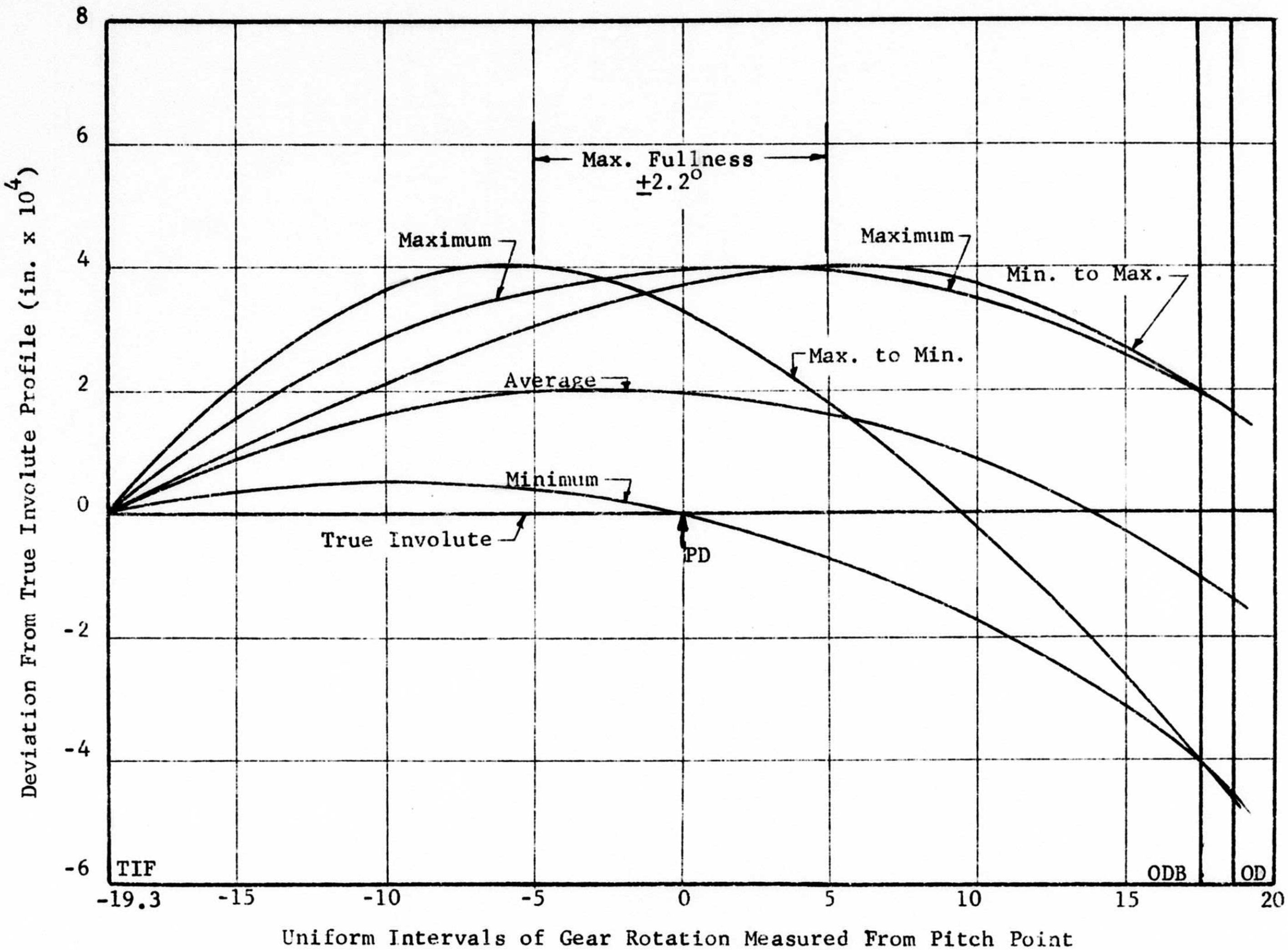

Figure 19. Profile Tolerances and Extremes, Sun Gear - Boeing-Vertol Print No. J-114D2077-M.

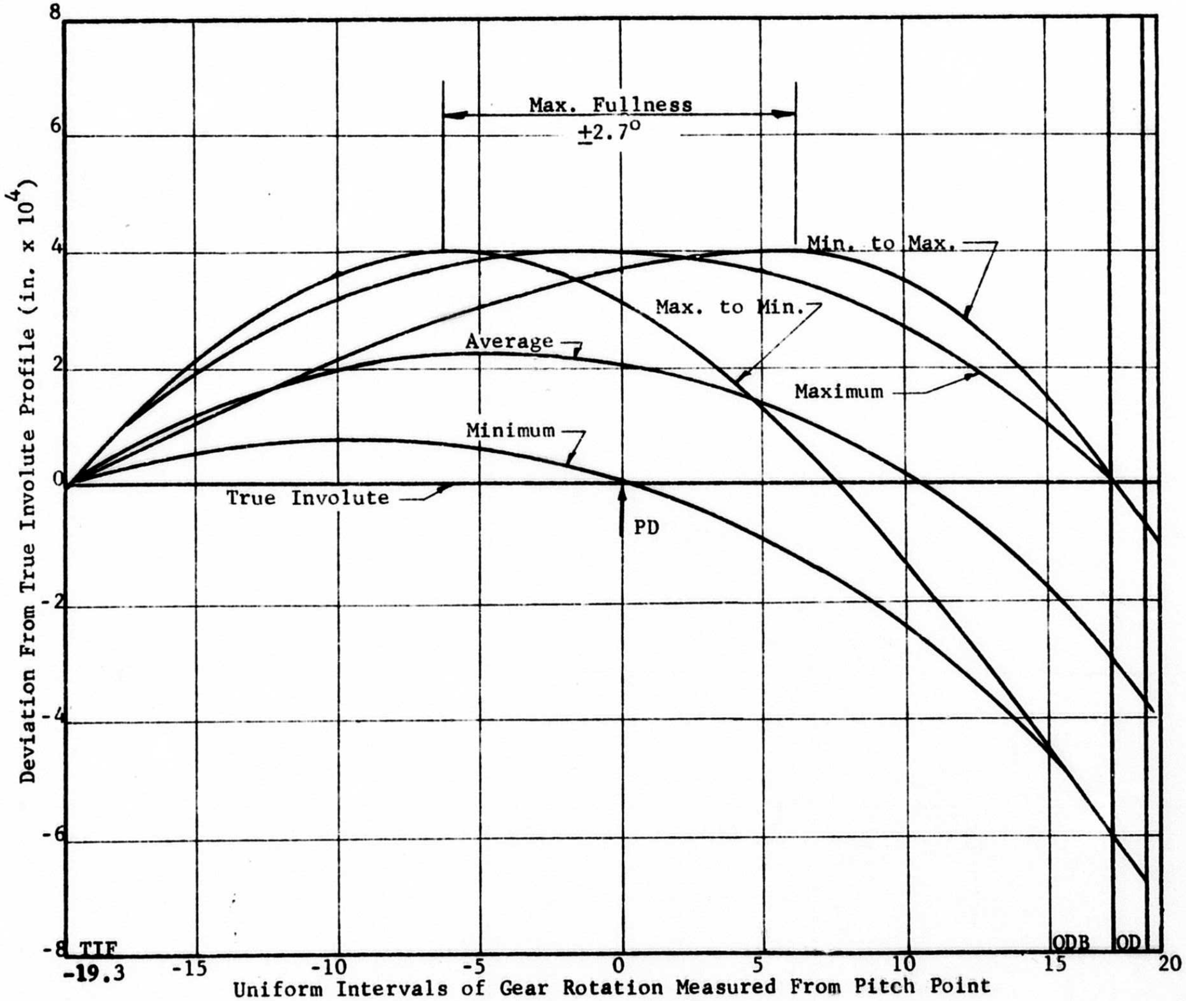

Figure 20. Profile Tolerances and Extremes, Planet Gear - Boeing-Vertol Print No. J-114D-2084-K.

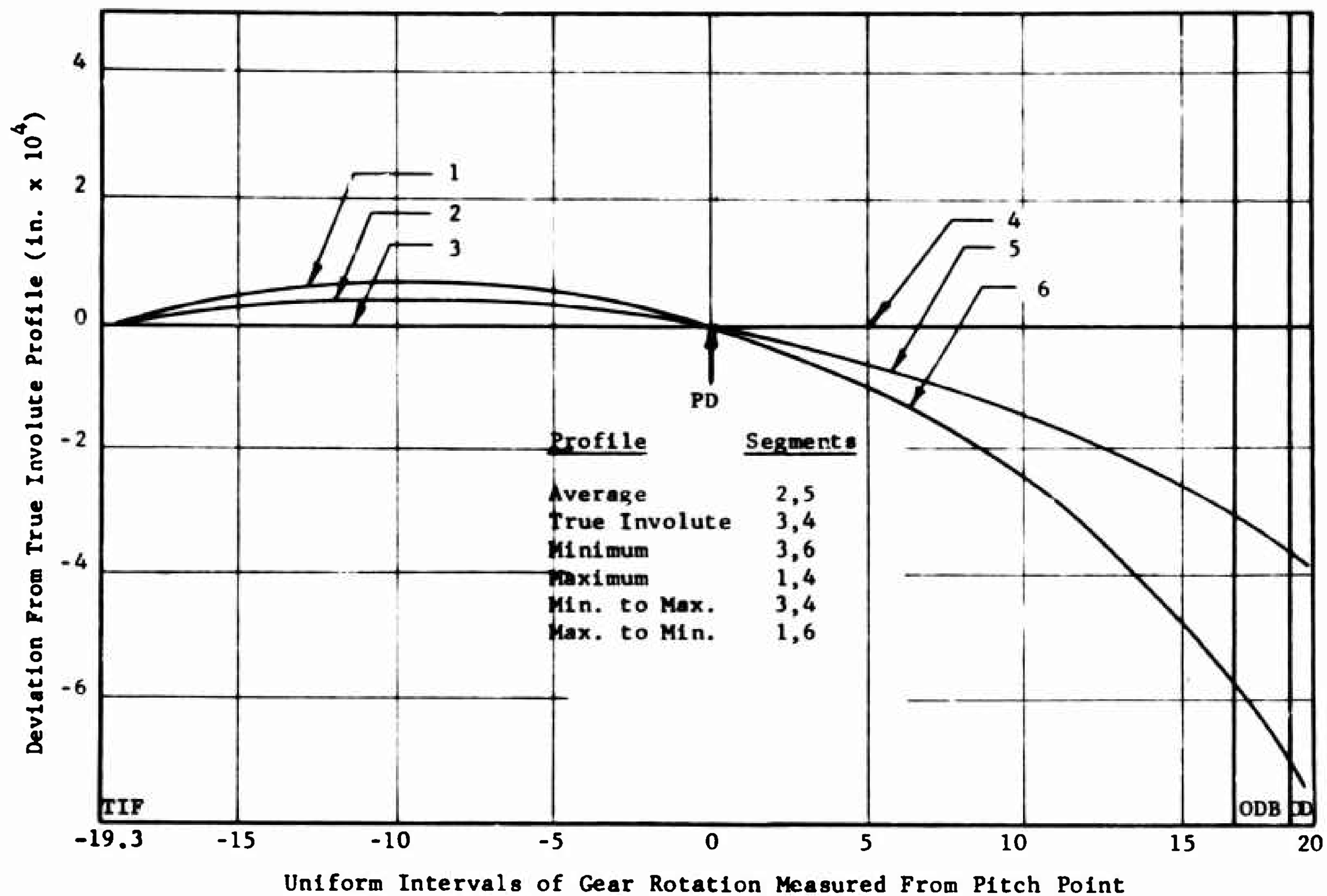

Figure 21. Profile Tolerances and Extremes, Stationary Ring Planetary Gear - Boeing-Vertol Print No. J-114D2086-M.

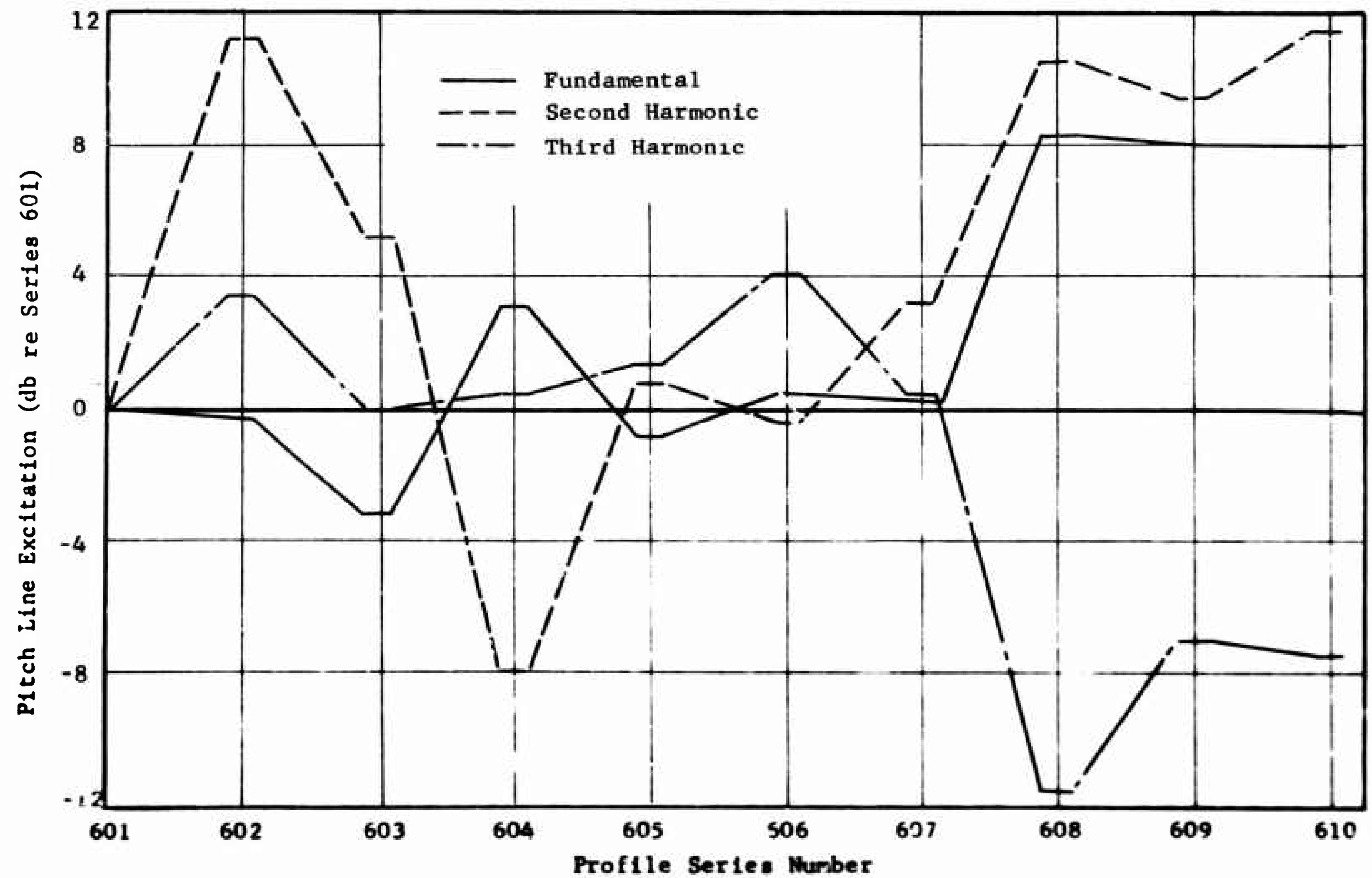

Figure 22. Profile Variations for Forward Cruise - Sun to Planet.

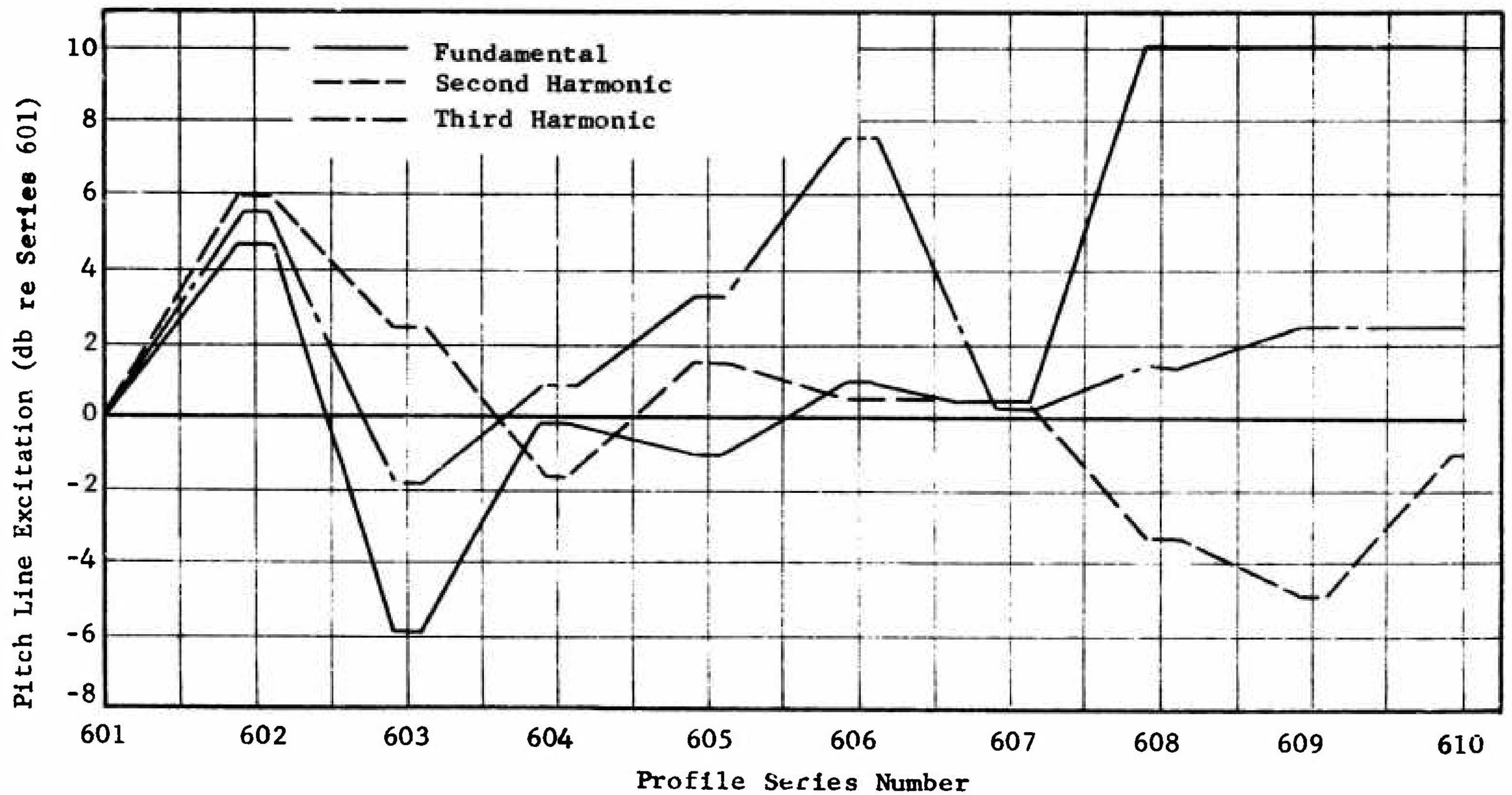

Figure 23. Profile Variations for Forward Hover - Sun to Planet.

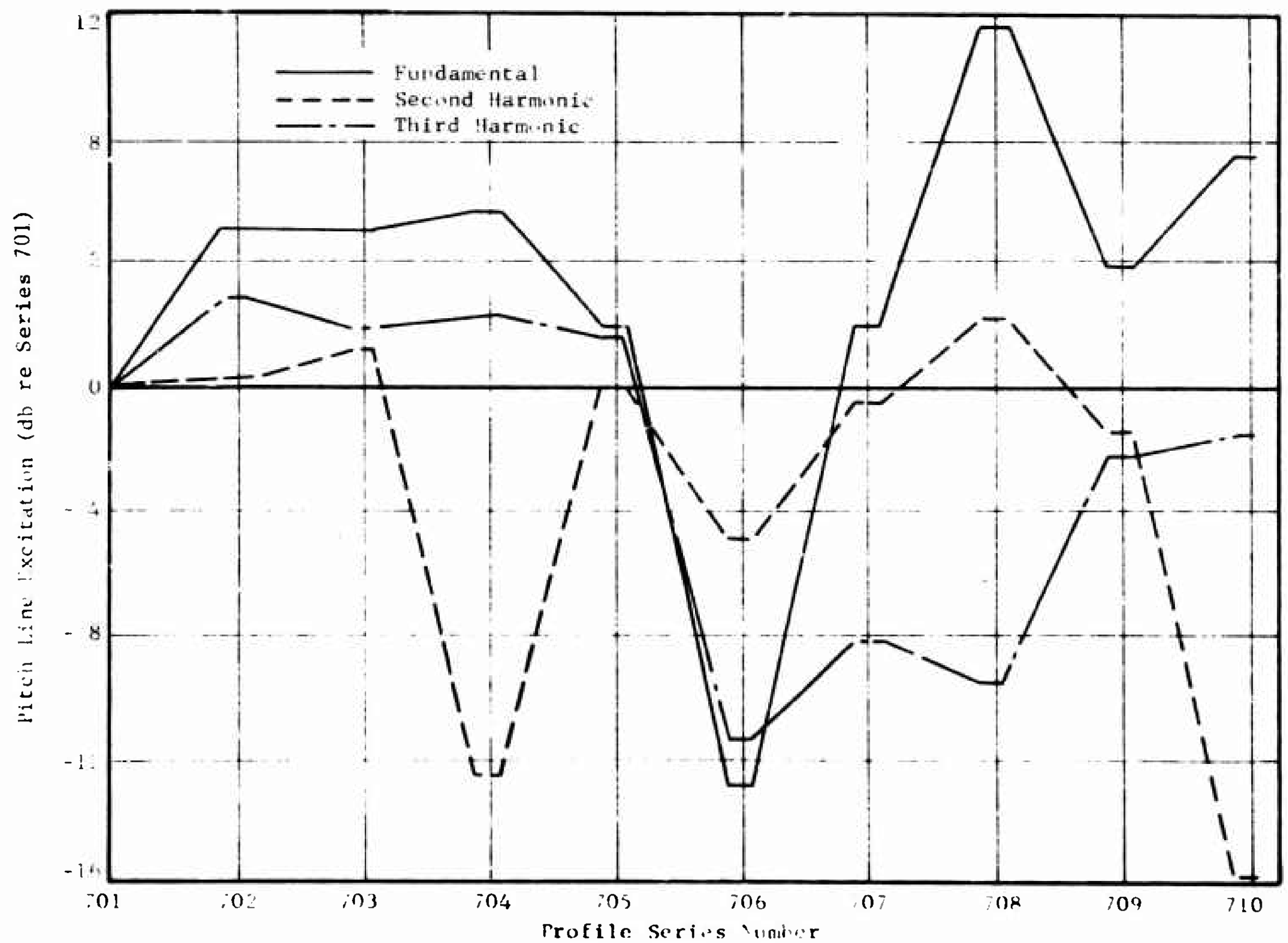

Figure 24. Profile Variations for Forward Cruise - Planet to Ring.

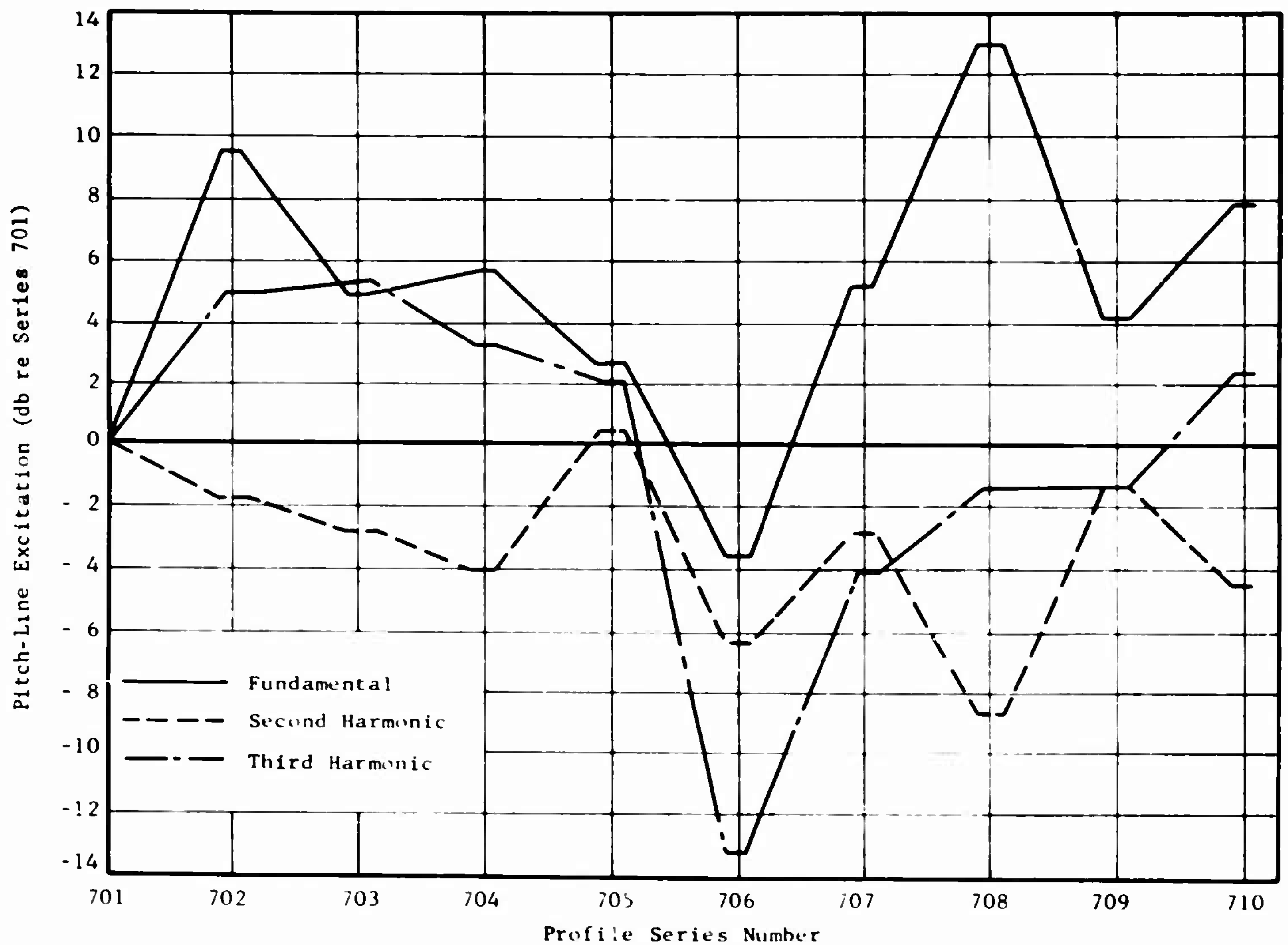

Figure 25. Profile Variations for Forward Hover - Planet to Ring.

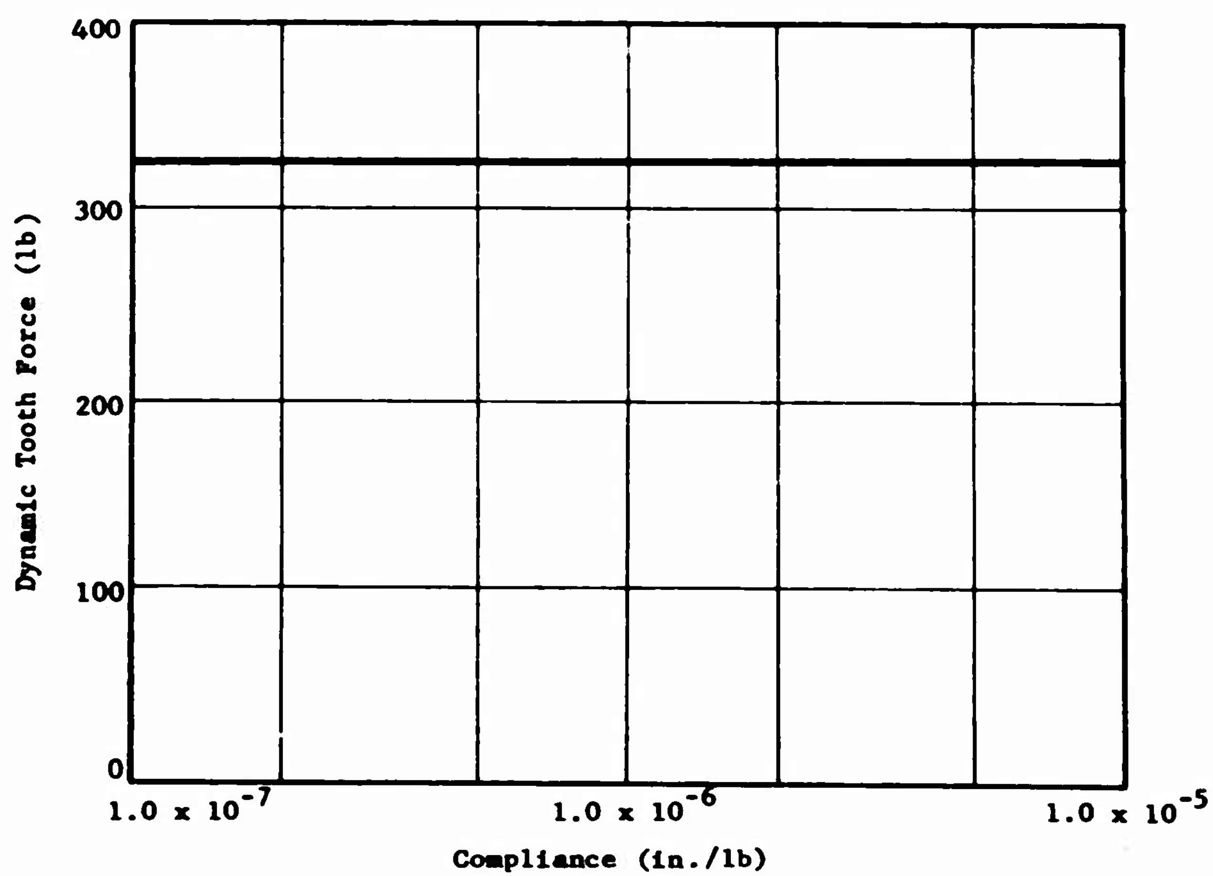

Figure 26. Spiral Bevel Gear Dynamic Tooth Force vs. Upper Planetary Planet Carrier Compliance - Excitation at Spiral Bevel Gear Mesh at 3412 Hz.

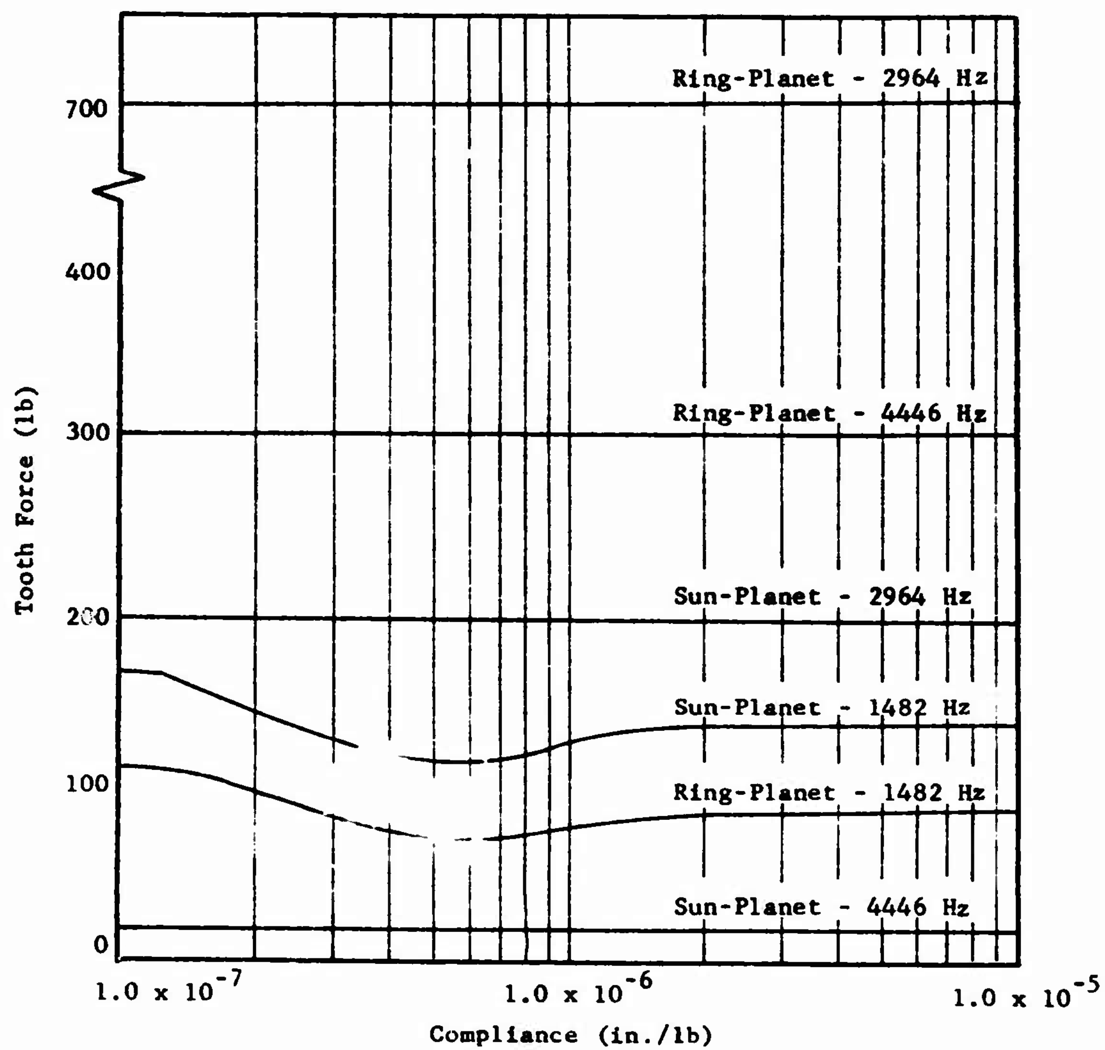

Figure 27. Upper Planetary Dynamic Tooth Forces vs. Upper Planetary Planet Carrier Compliance - Excitation at Indicated Places and Frequencies.

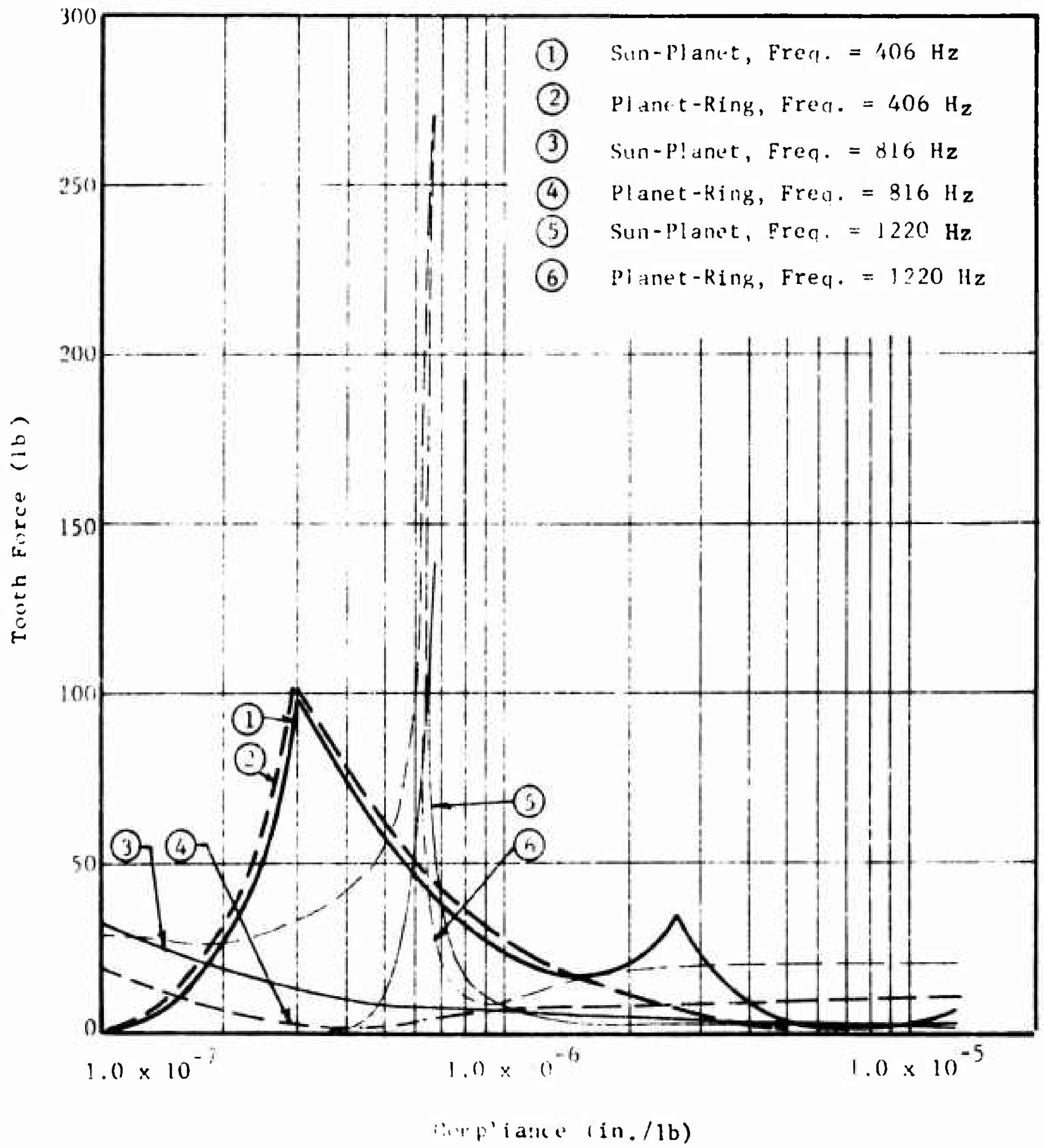

Figure 28. Upper Planetary Dynamic Tooth Forces vs. Upper Planetary Planet Carrier Compliance With Various Frequencies at Indicated Locations.

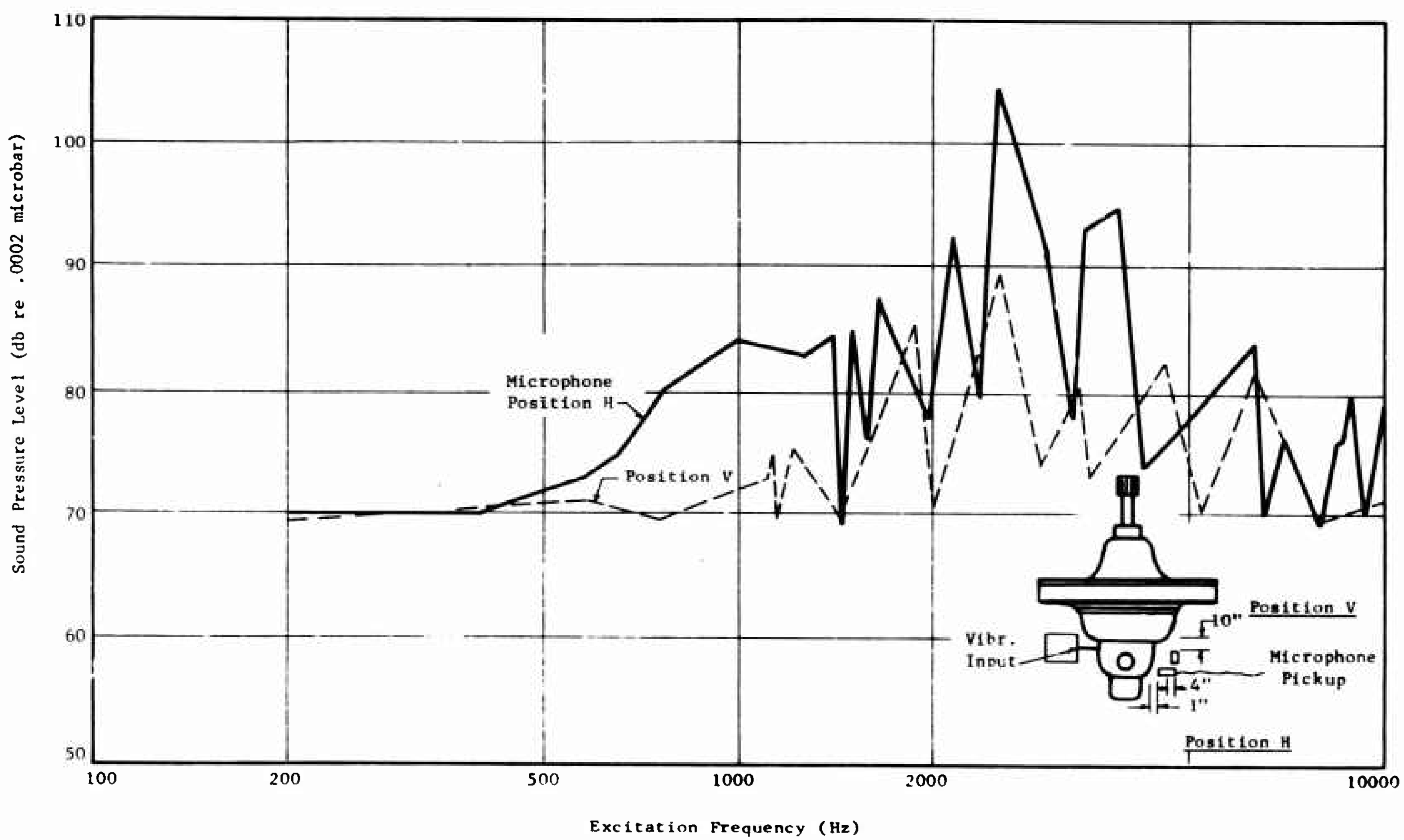

Figure 29. Acoustic Response vs. Excitation Frequency for Two Microphone Locations With Vertol Transmission S/N A7 - 4.

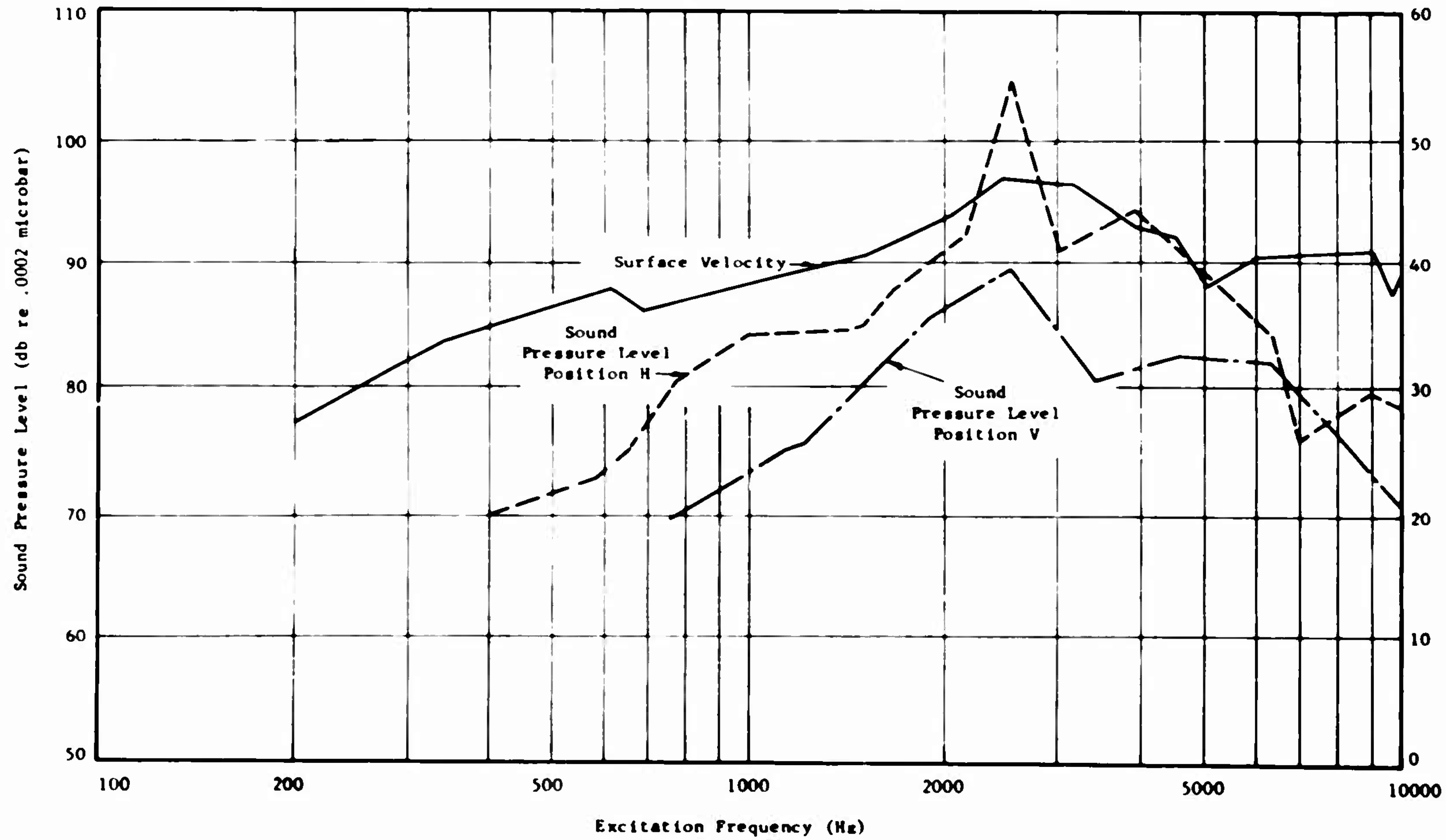

Figure 30. Mechanical Velocity at Drive Block With Drive at Input Bearing - Sound Pressure Level vs. Frequency.

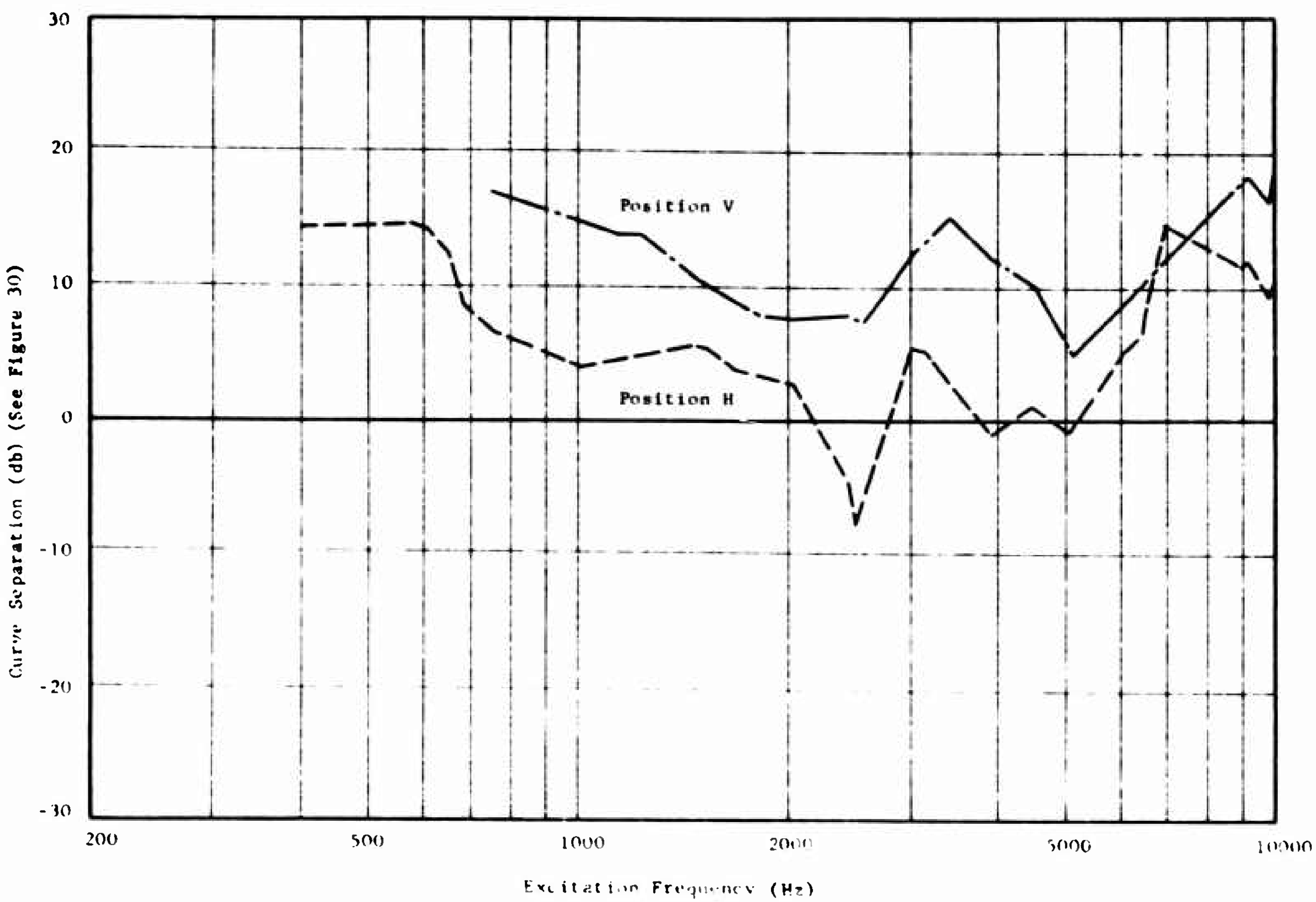

Figure 31. Velocity and Sound Pressure Level Curve Separation vs. Excitation Frequency for Two Microphone Positions.

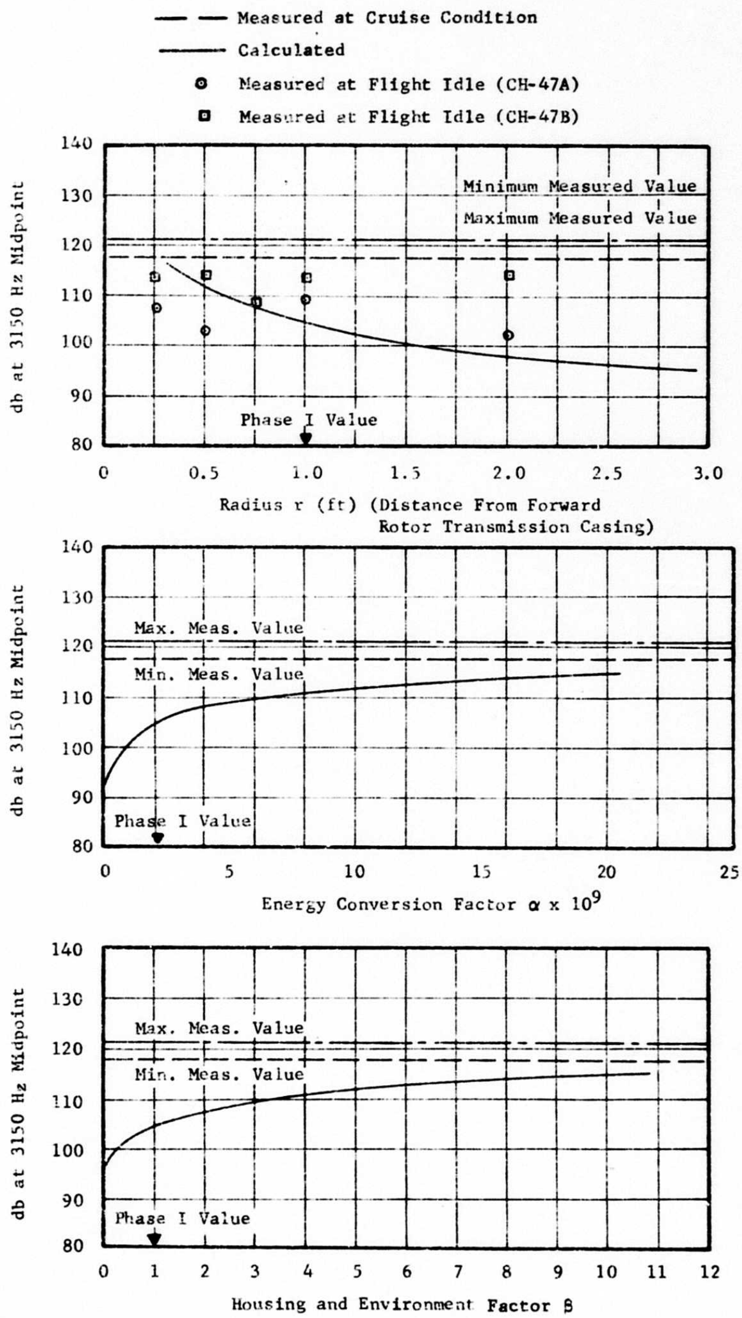

Figure 32. Effect of Radius and Empirical Factors α and β Upon Calculated Noise Levels at 3150 Hz.

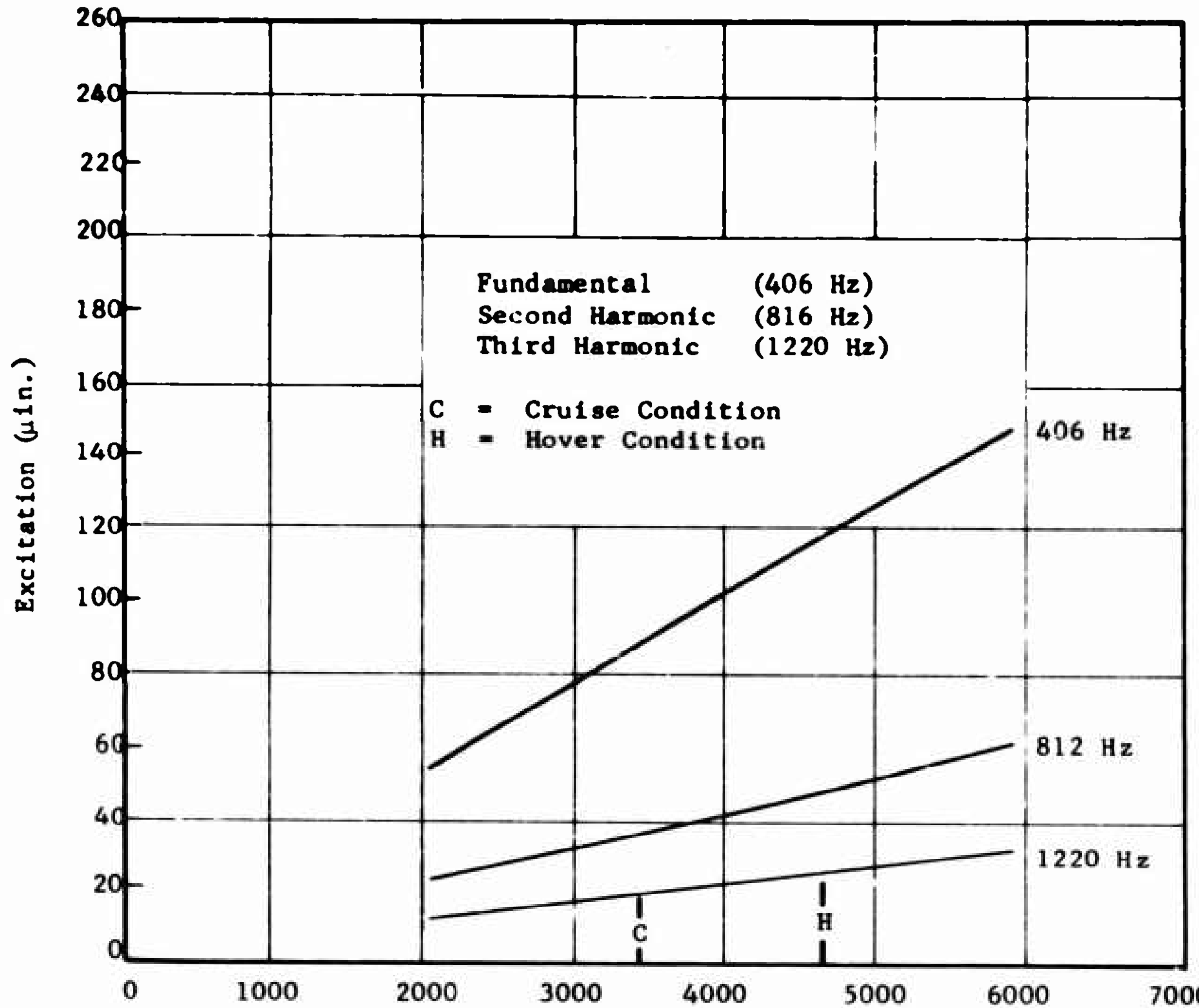

Figure 33. Excitation vs. Tooth Load in CH-47 Forward Transmission Upper Planetary Gear Set - Mesh Series 602.

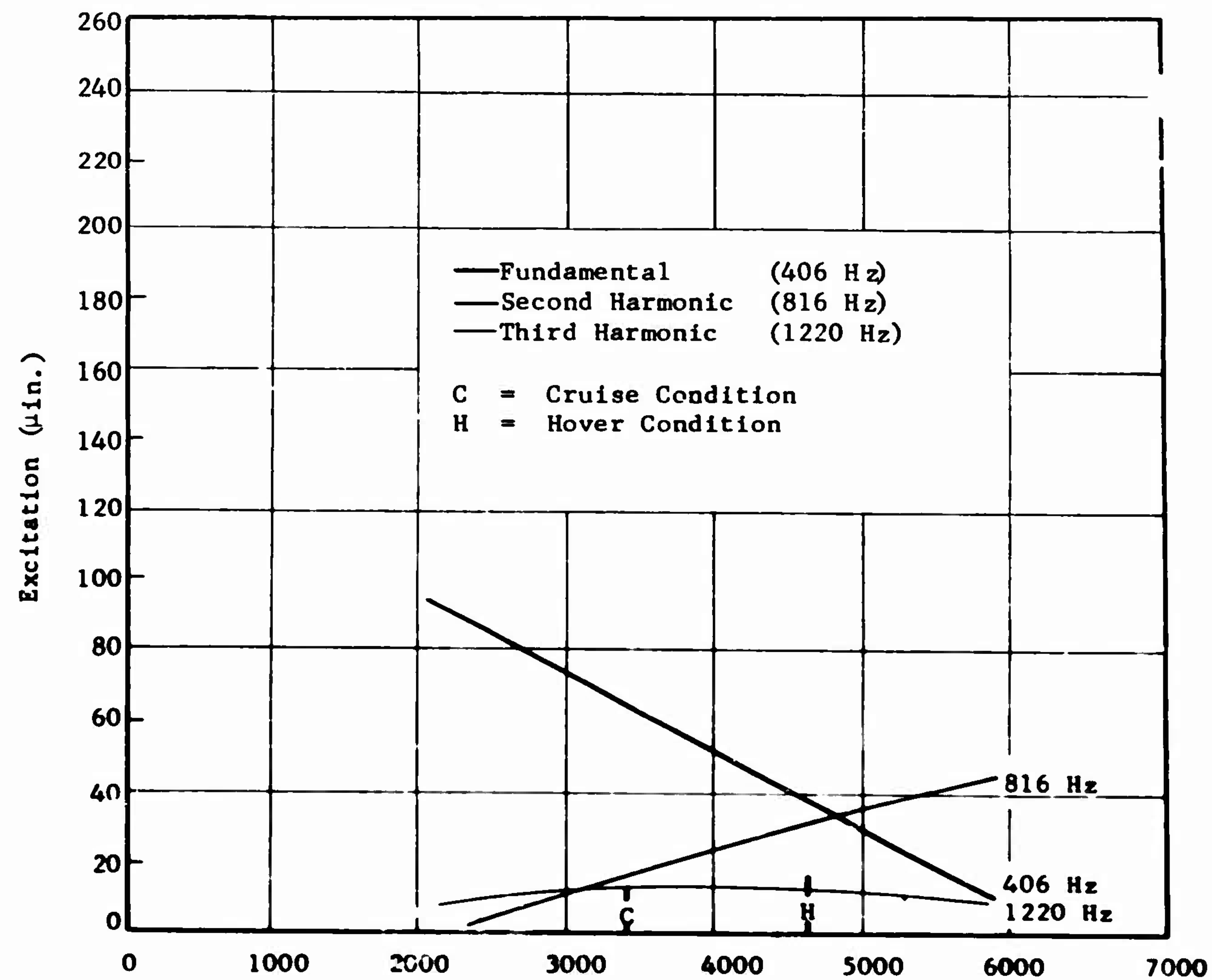

Figure 34. Excitation vs. Tooth Load in CH-47 Forward Transmission Upper Planetary Gear Set - Mesh Series 603.

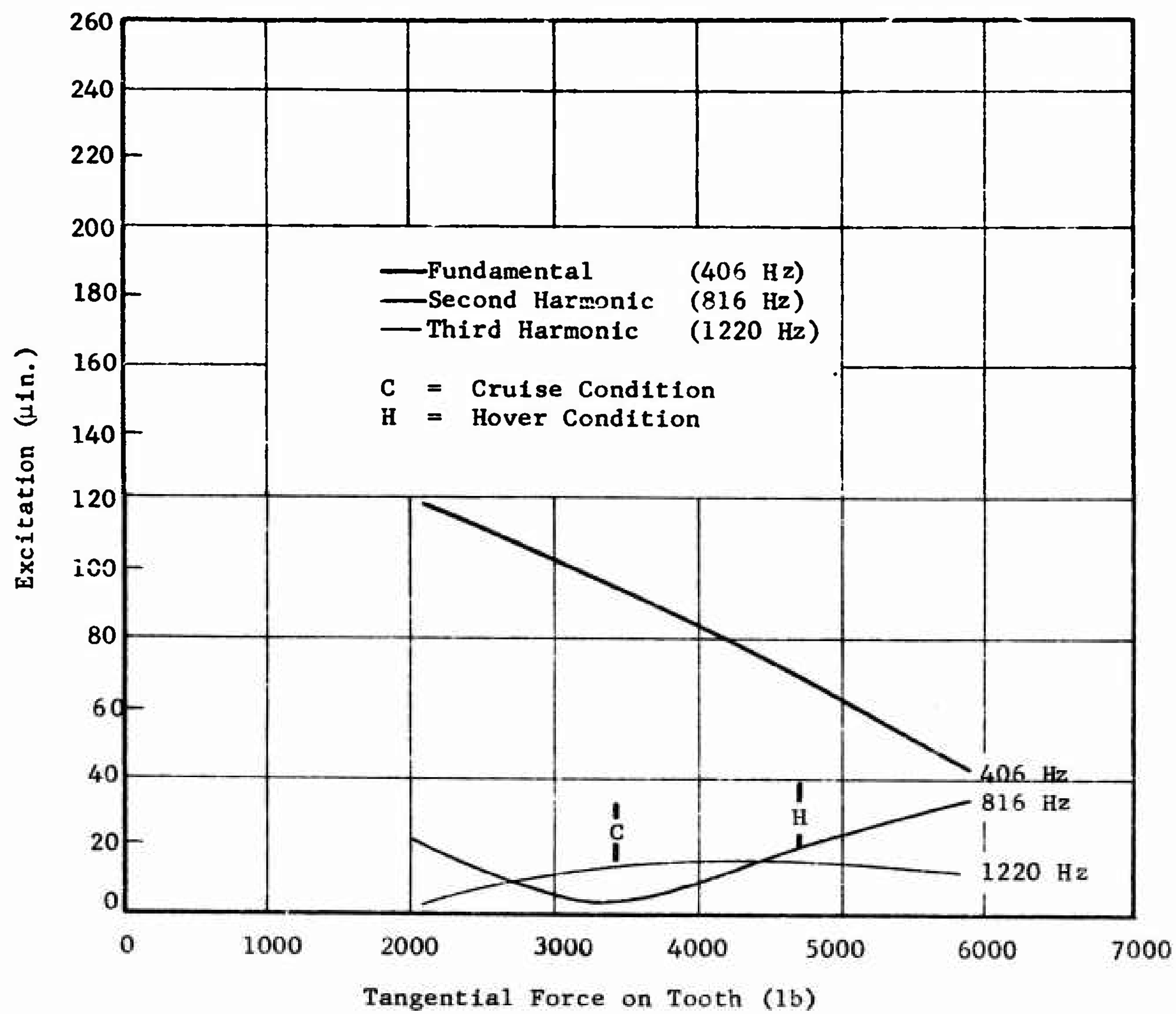

Figure 35. Excitation vs. Tooth Load in CH-47 Forward Transmission Upper Planetary Gear Set - Mesh Series 604.

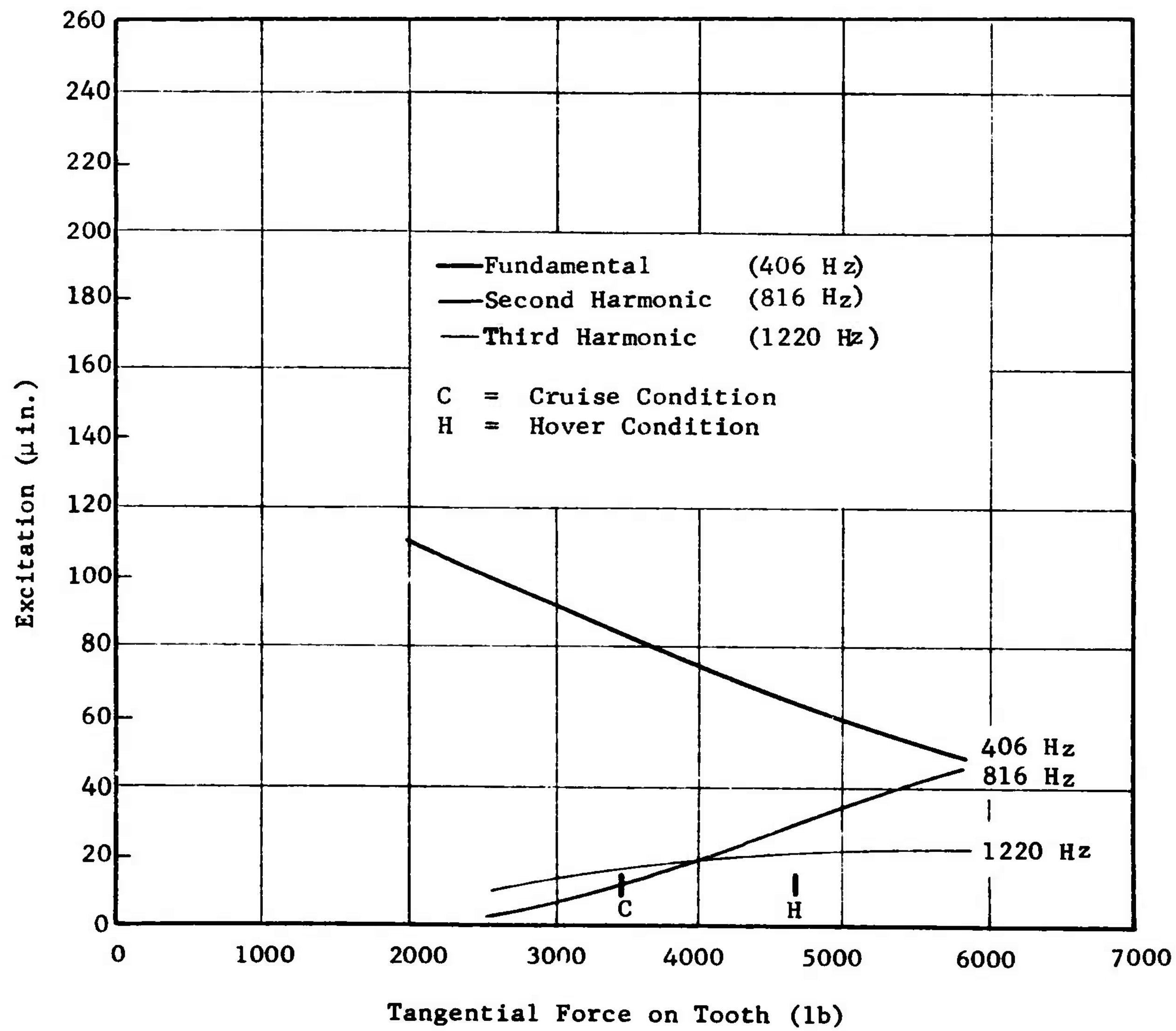

Figure 36. Excitation vs. Tooth Load in CH-47 Forward Transmission Upper Planetary Gear Set - Mesh Series 605.

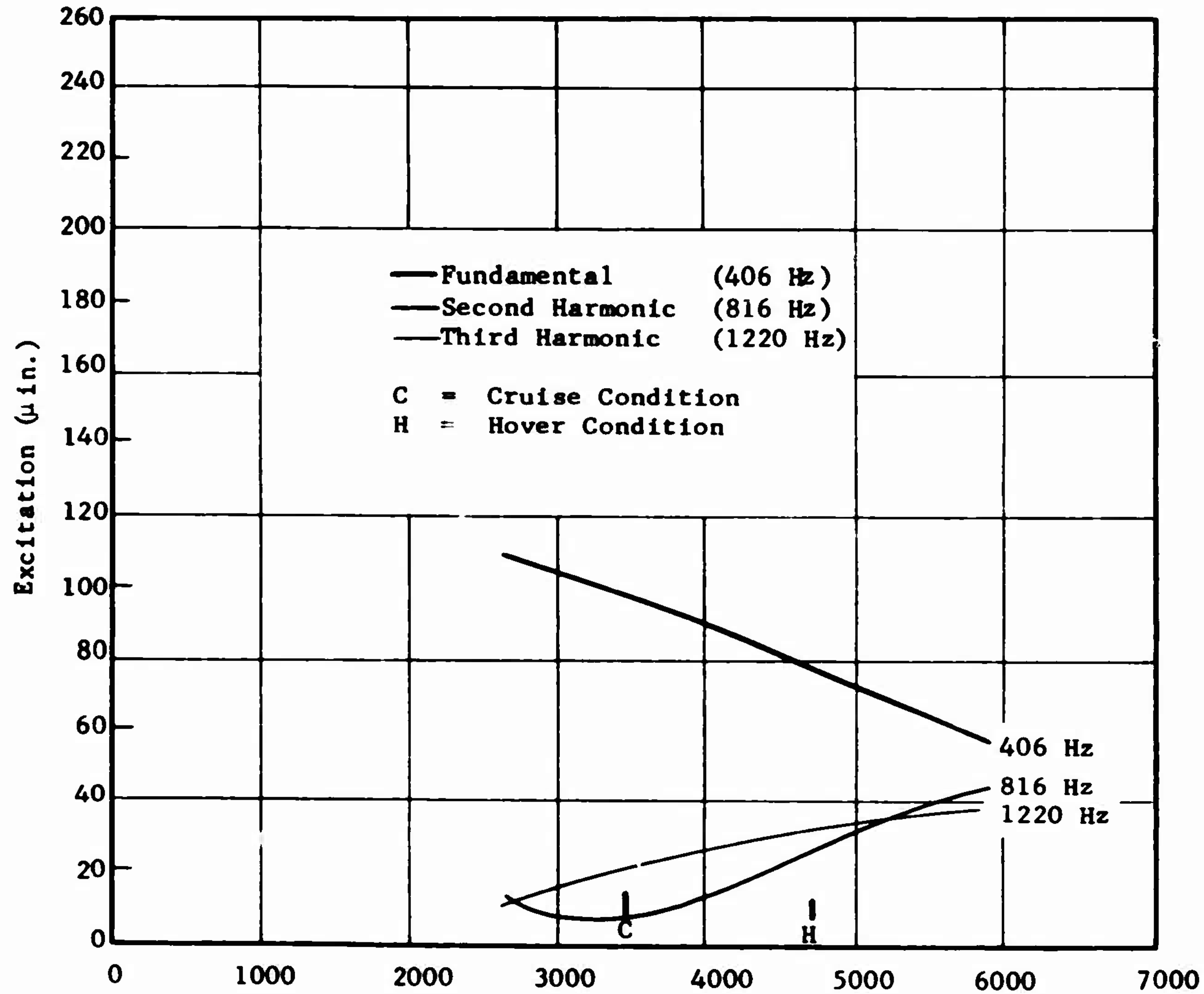

Figure 37. Excitation vs. Tooth Load in CH-47 Forward Transmission Upper Planetary Gear Set - Mesh Series 606.

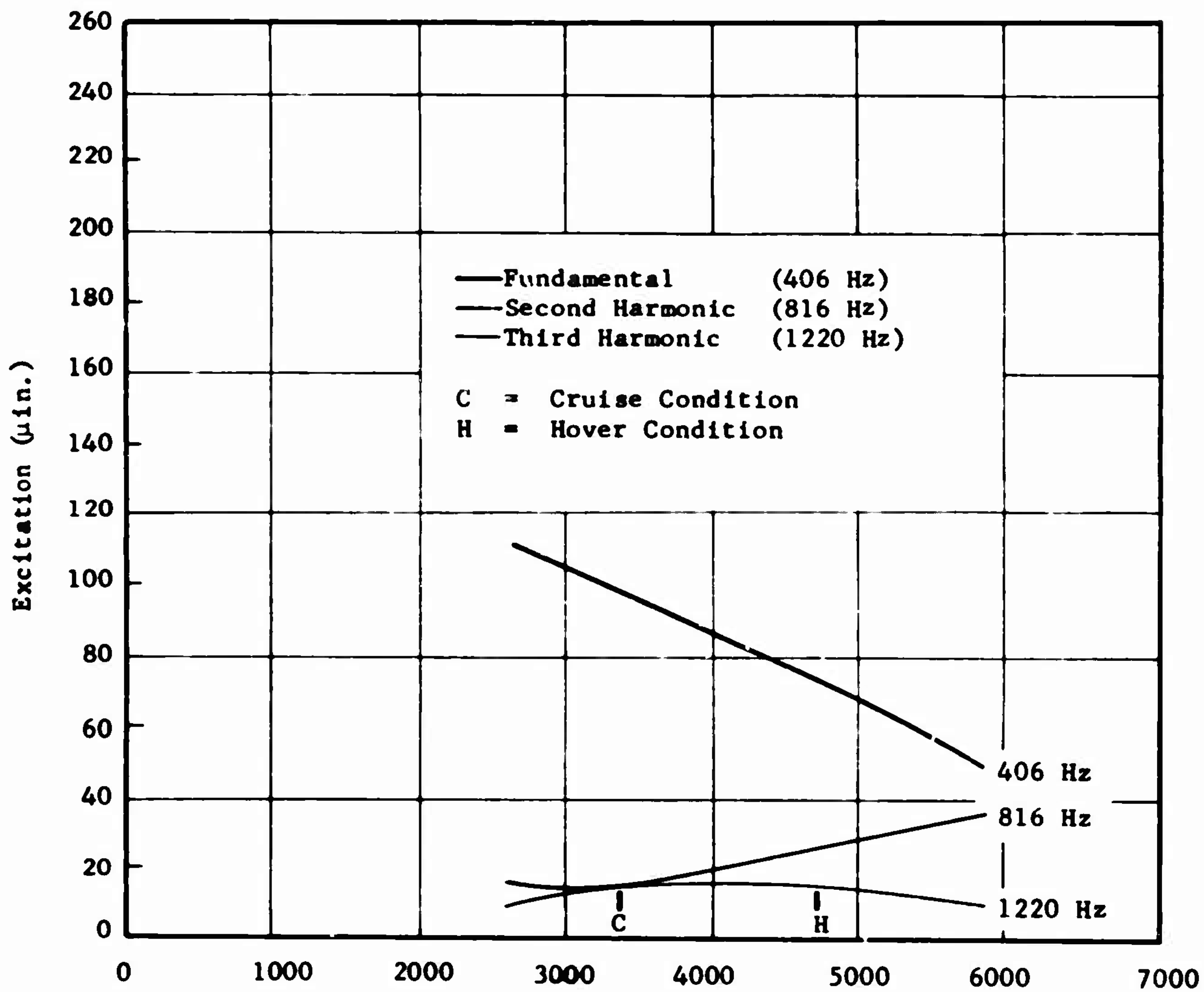

Figure 38. Excitation vs. Tooth Load in CH-47 Forward Transmission Upper Planetary Gear Set - Mesh Series 607.

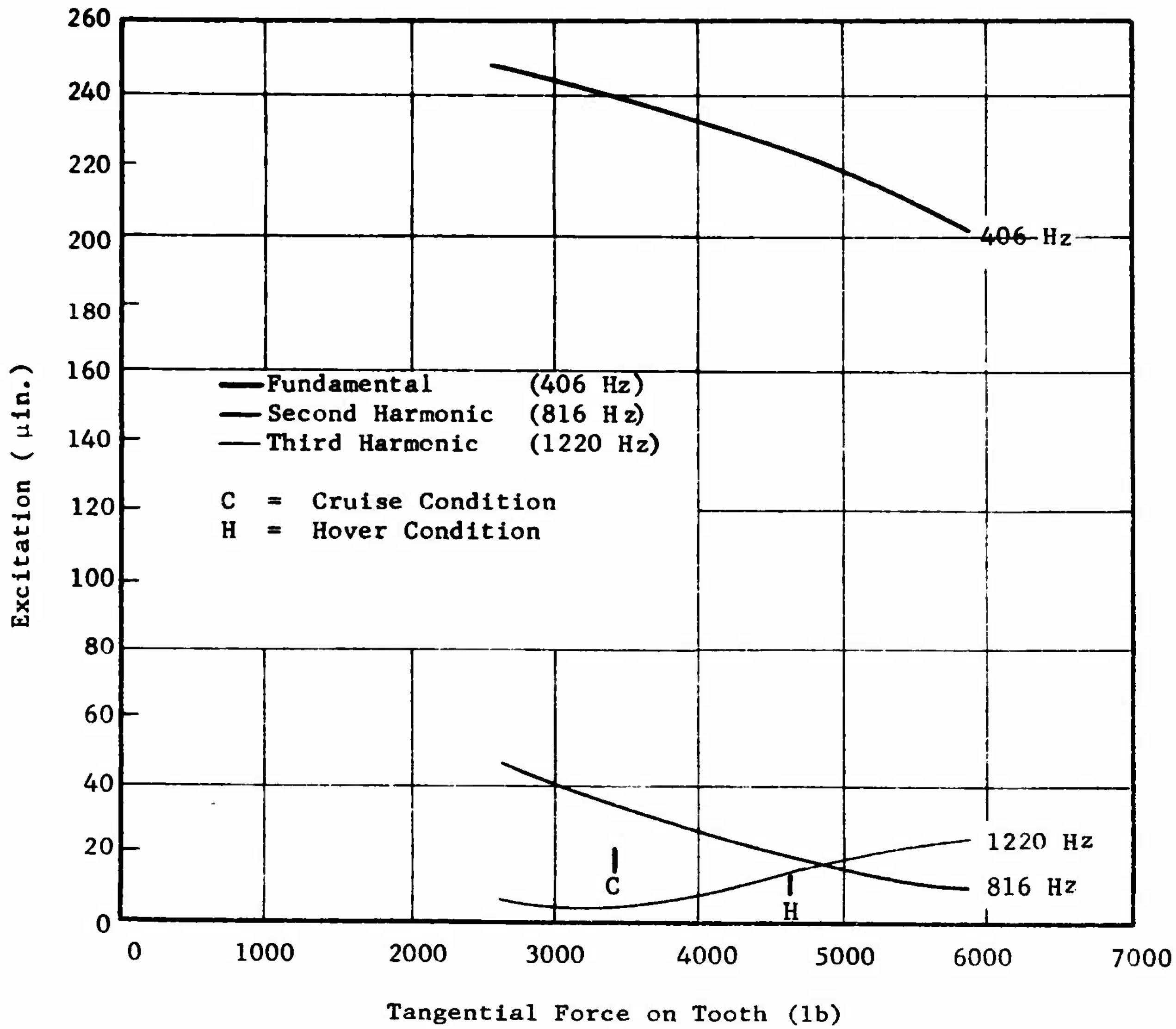

Figure 39. Excitation vs. Tooth Load in CH-47 Forward Transmission Upper Planetary Gear Set - Mesh Series 608.

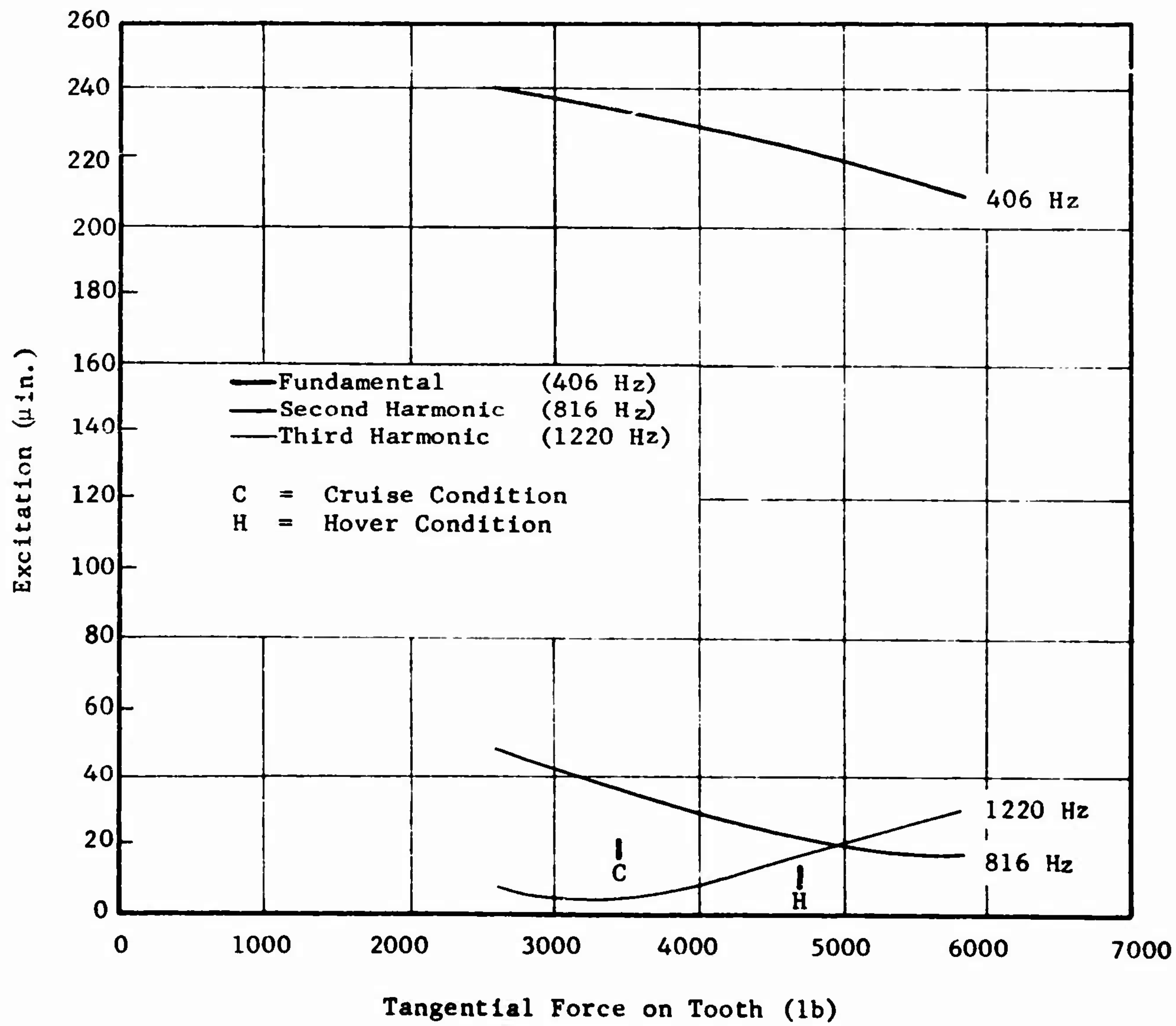

Figure 40. Excitation vs. Tooth Load in CH-47 Forward Transmission Upper Planetary Gear Set - Mesh Series 609.

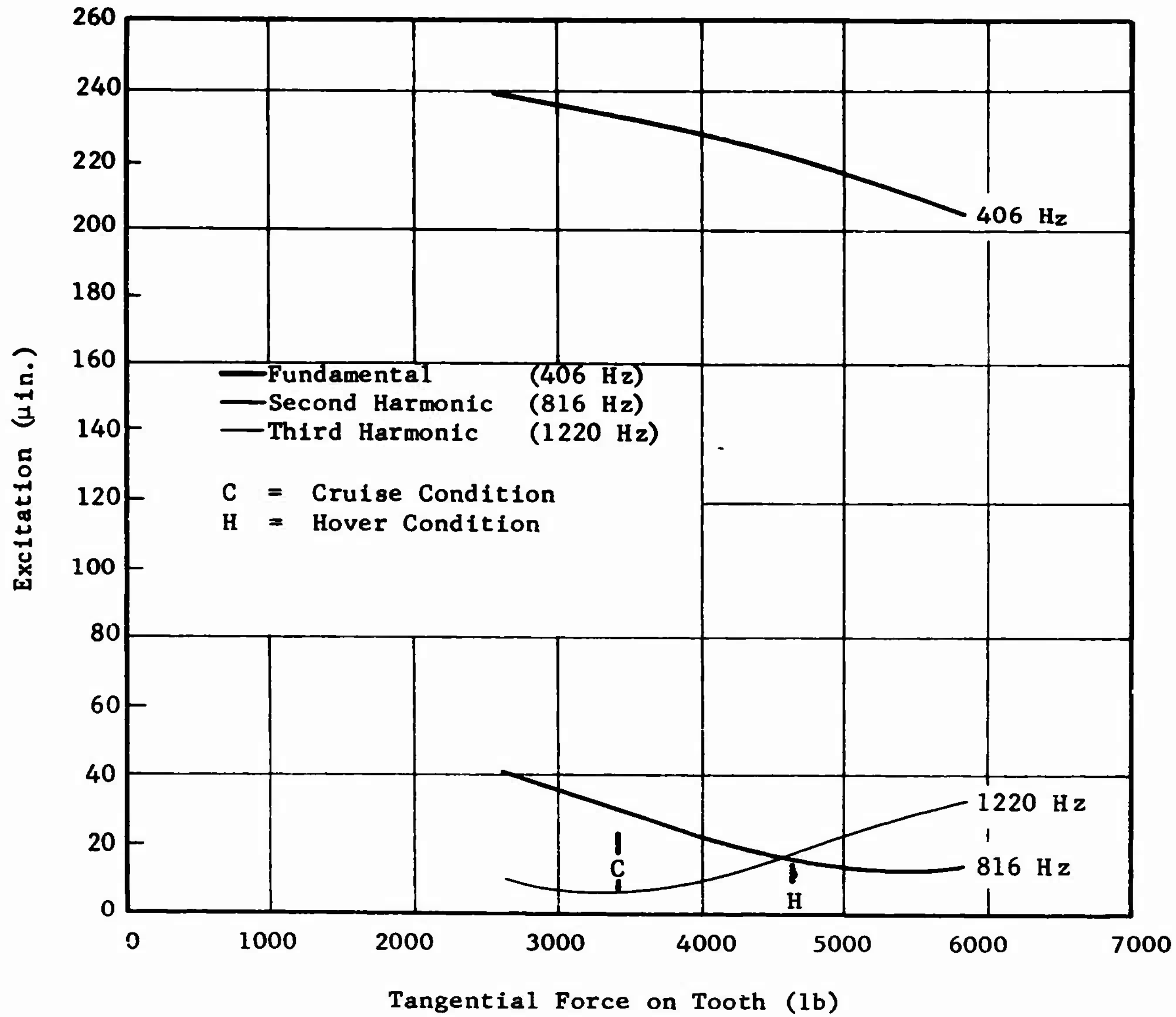

Figure 41. Excitation vs. Tooth Load in CH-47 Forward Transmission Upper Planetary Gear Set - Mesh Series 610.

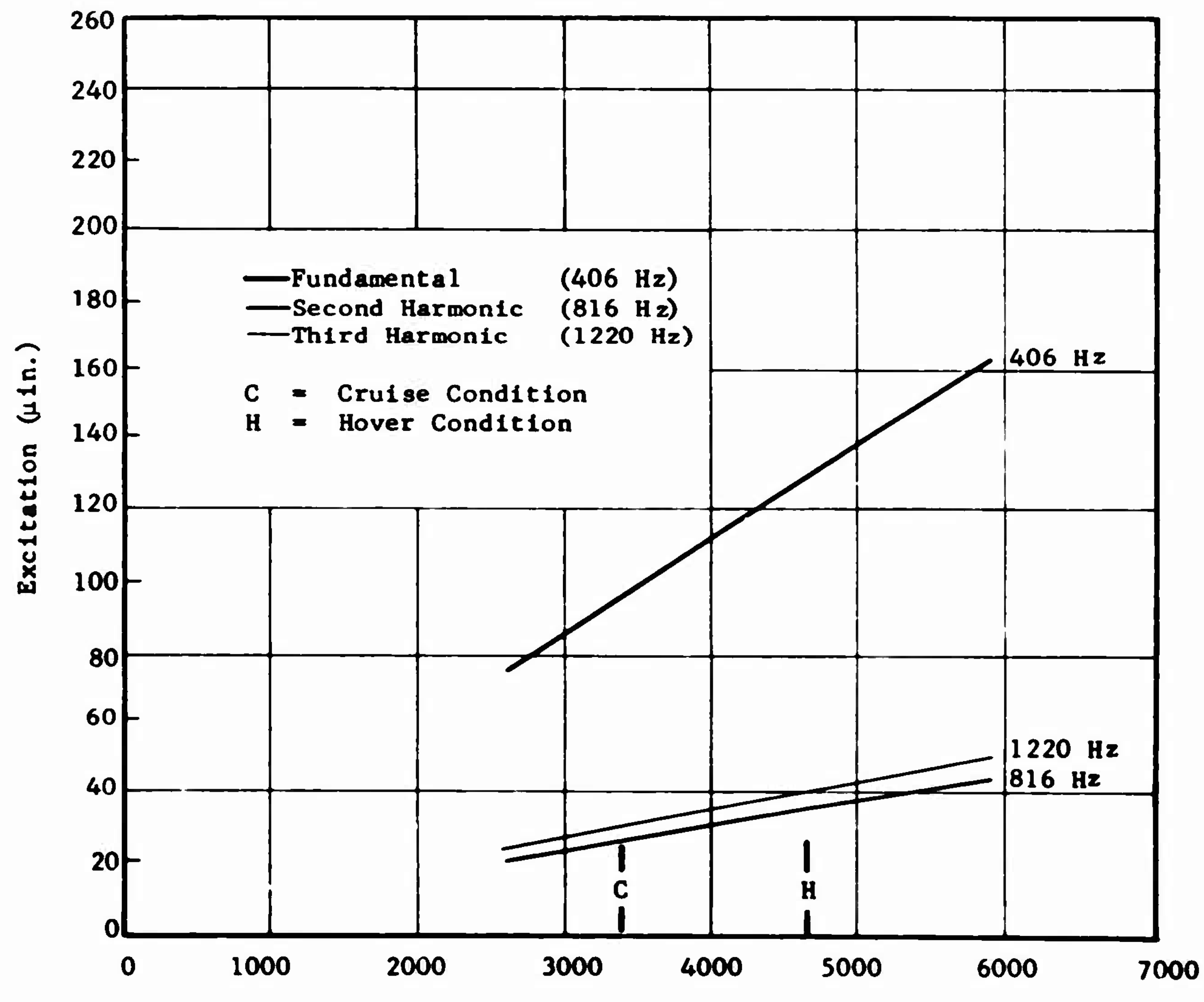

Figure 42. Excitation vs. Tooth Load in CH-47 Forward Transmission Upper Planetary Gear Set - Mesh Series 702.

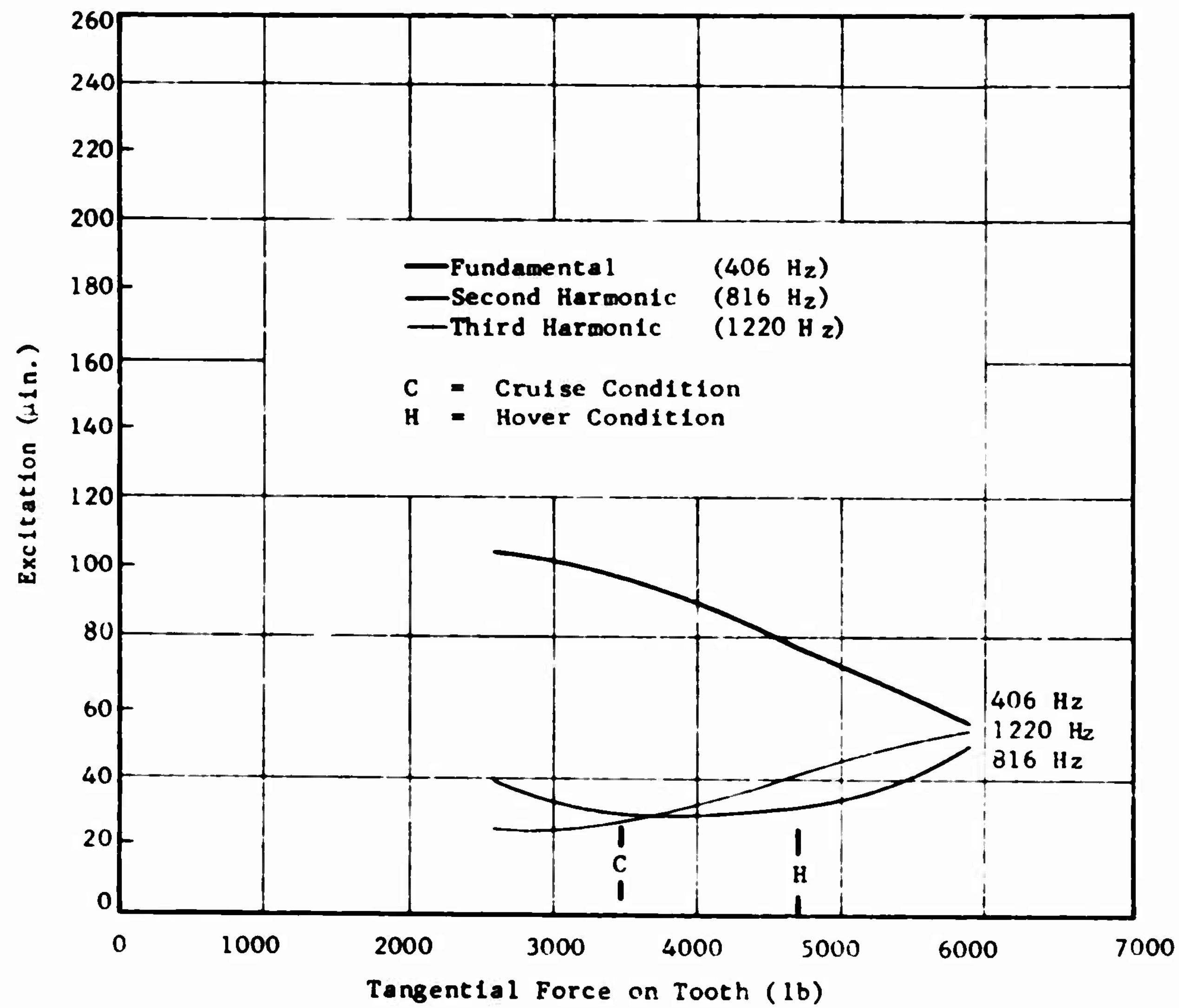

Figure 43. Excitation vs. Tooth Load in CH-47 Forward Transmission Upper Planetary Gear Set - Mesh Series 703.

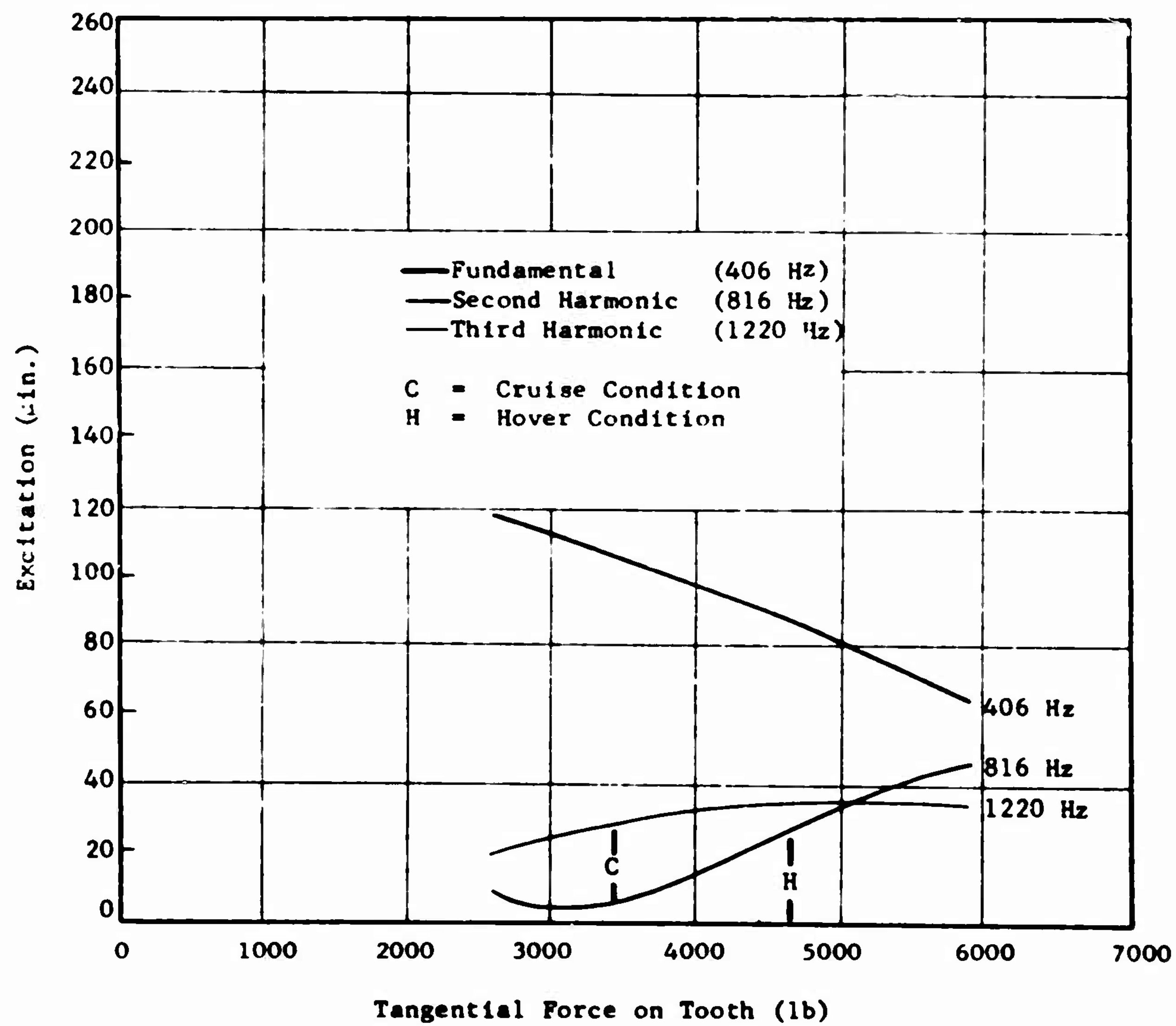

Figure 44. Excitation vs. Tooth Load in CH-47 Forward Transmission Upper Planetary Gear Set - Mesh Series 704.

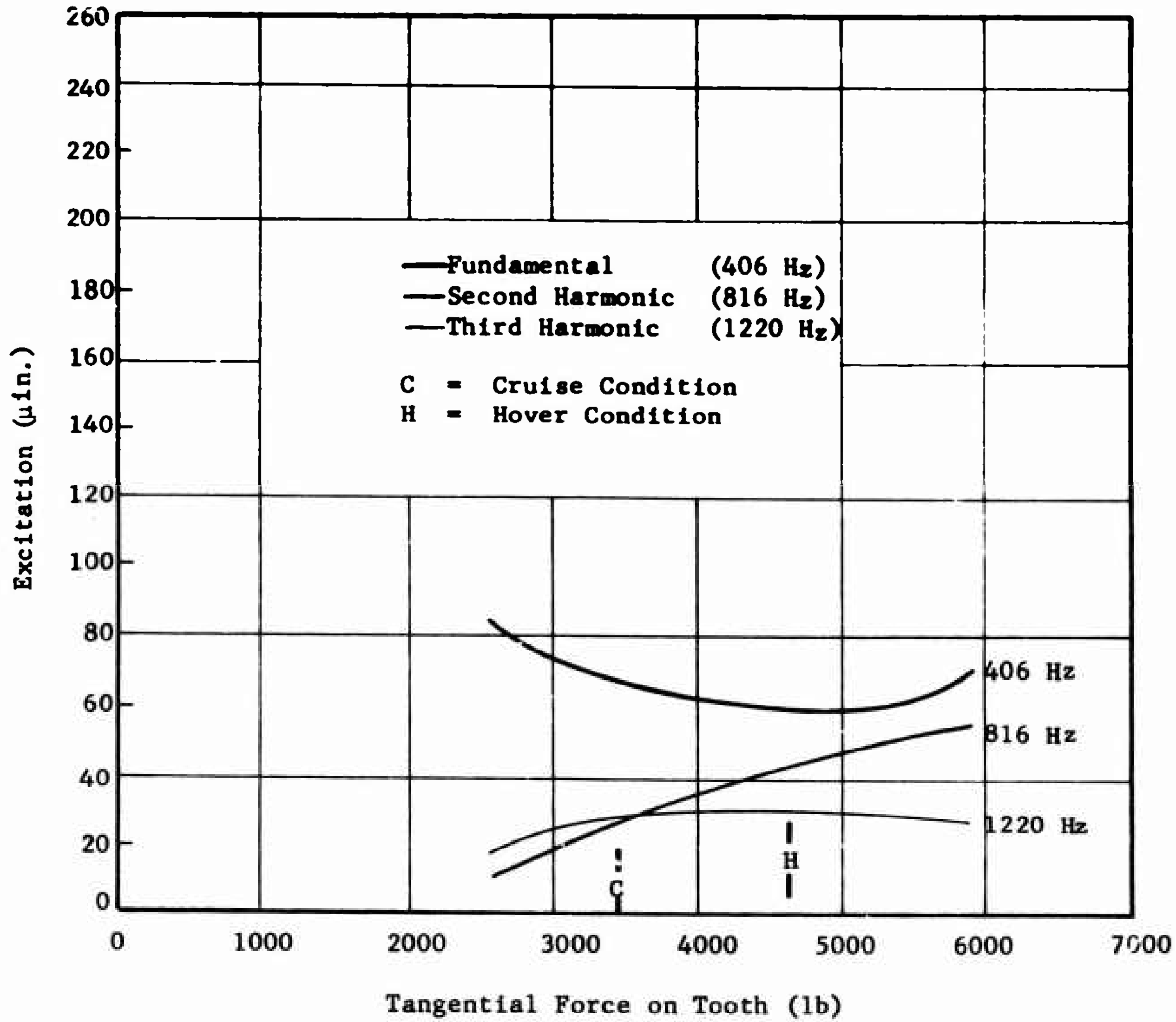

Figure 45. Excitation vs. Tooth Load in CH-47 Forward Transmission Upper Planetary Gear Set - Mesh Series 705.

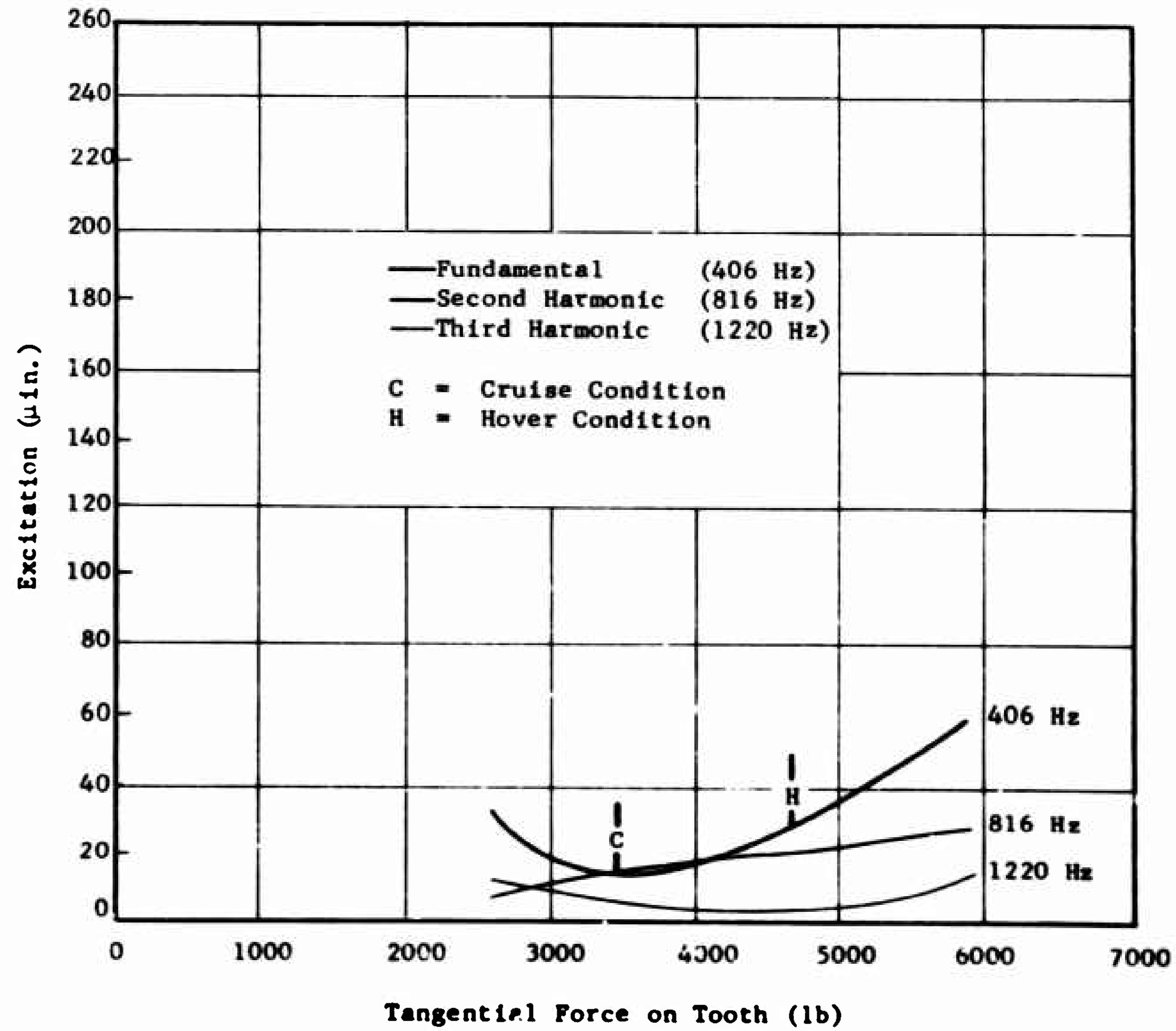

Figure 46. Excitation vs. Tooth Load in CH-47 Forward Transmission Upper Planetary Gear Set - Mesh Series 706.

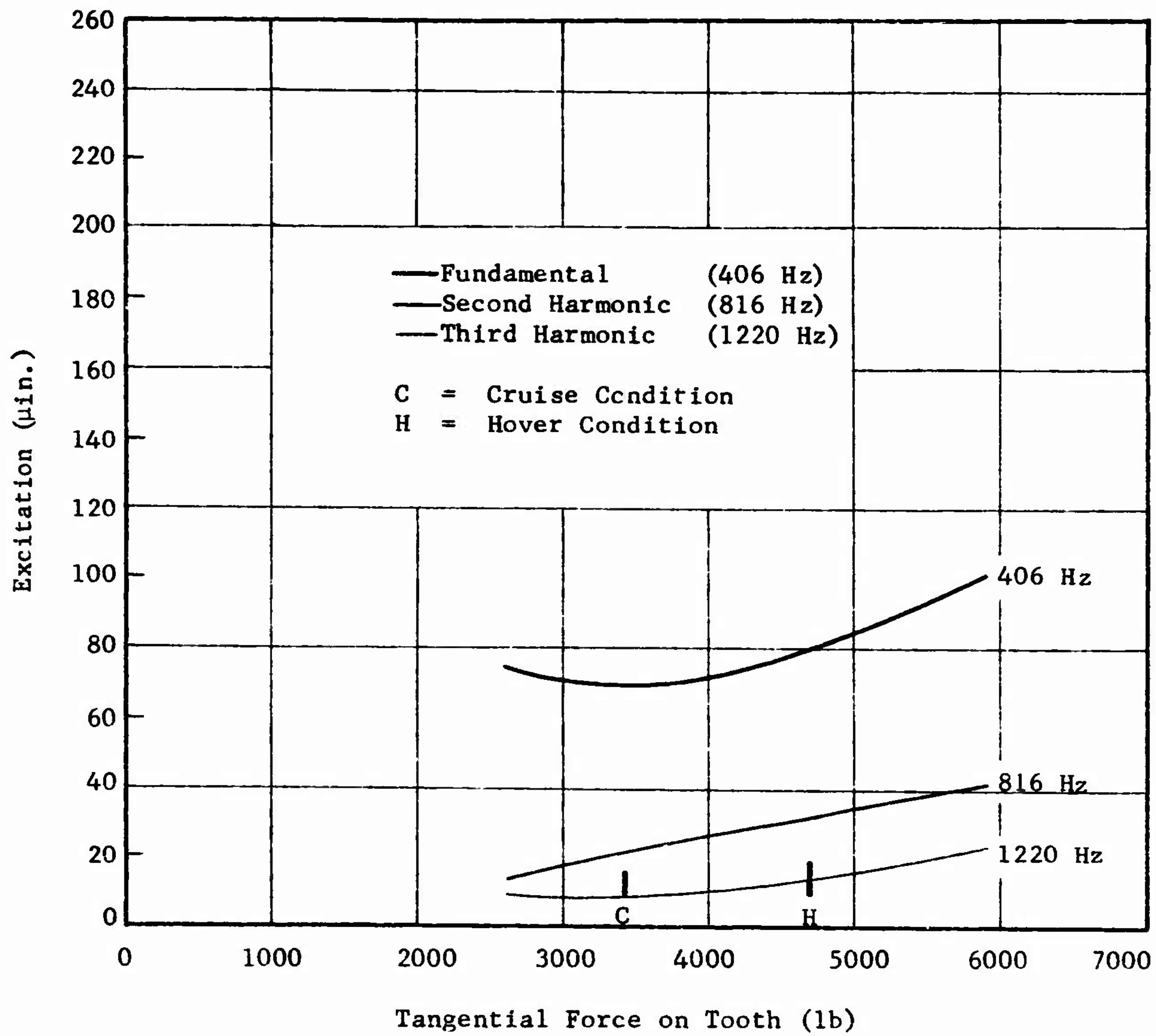

Figure 47. Excitation vs. Tooth Load in CH-47 Forward Transmission Upper Planetary Gear Set - Mesh Series 707.

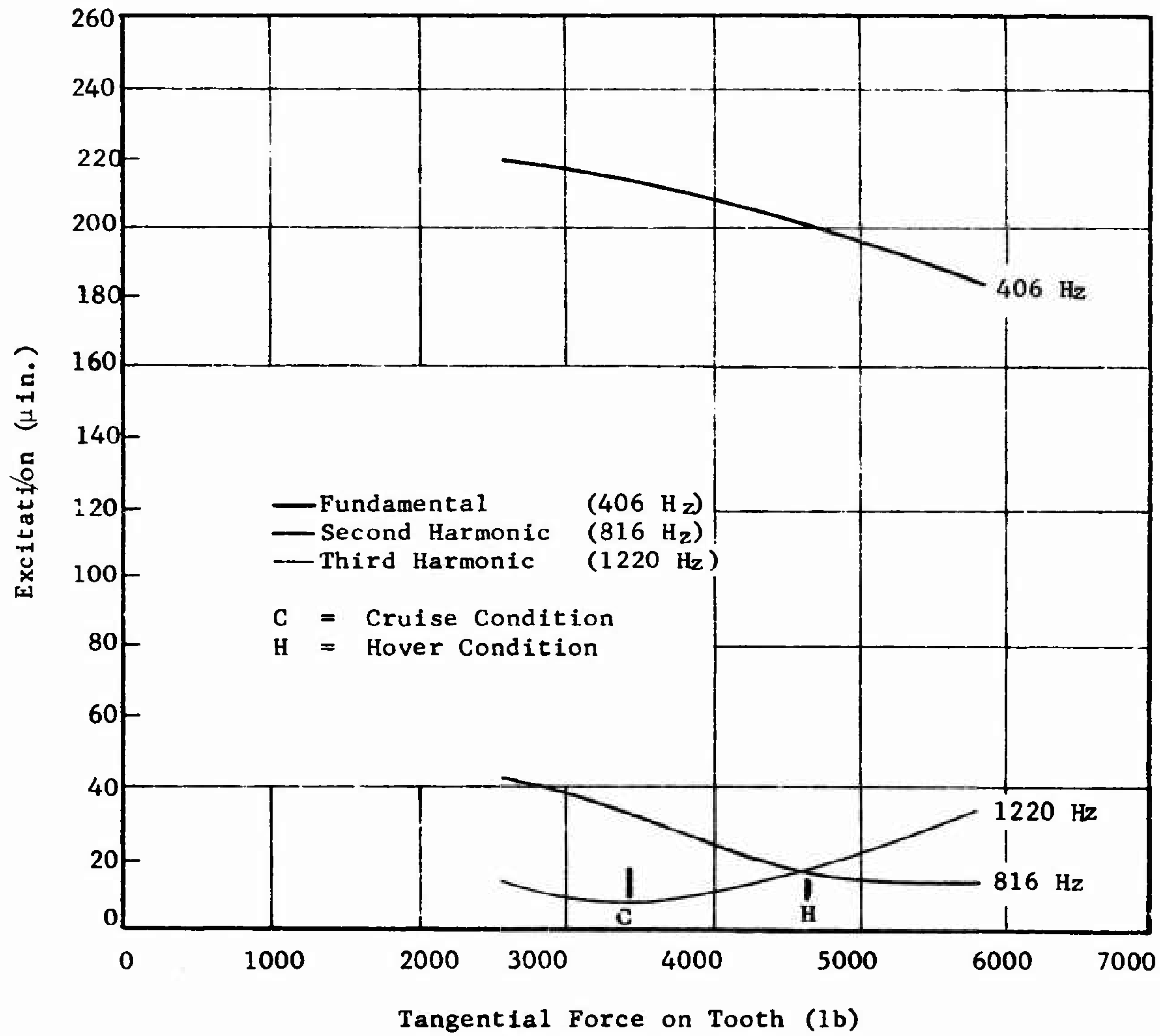

Figure 48. Excitation vs. Tooth Load in CH-47 Forward Transmission Upper Planetary Gear Set - Mesh Series 708.

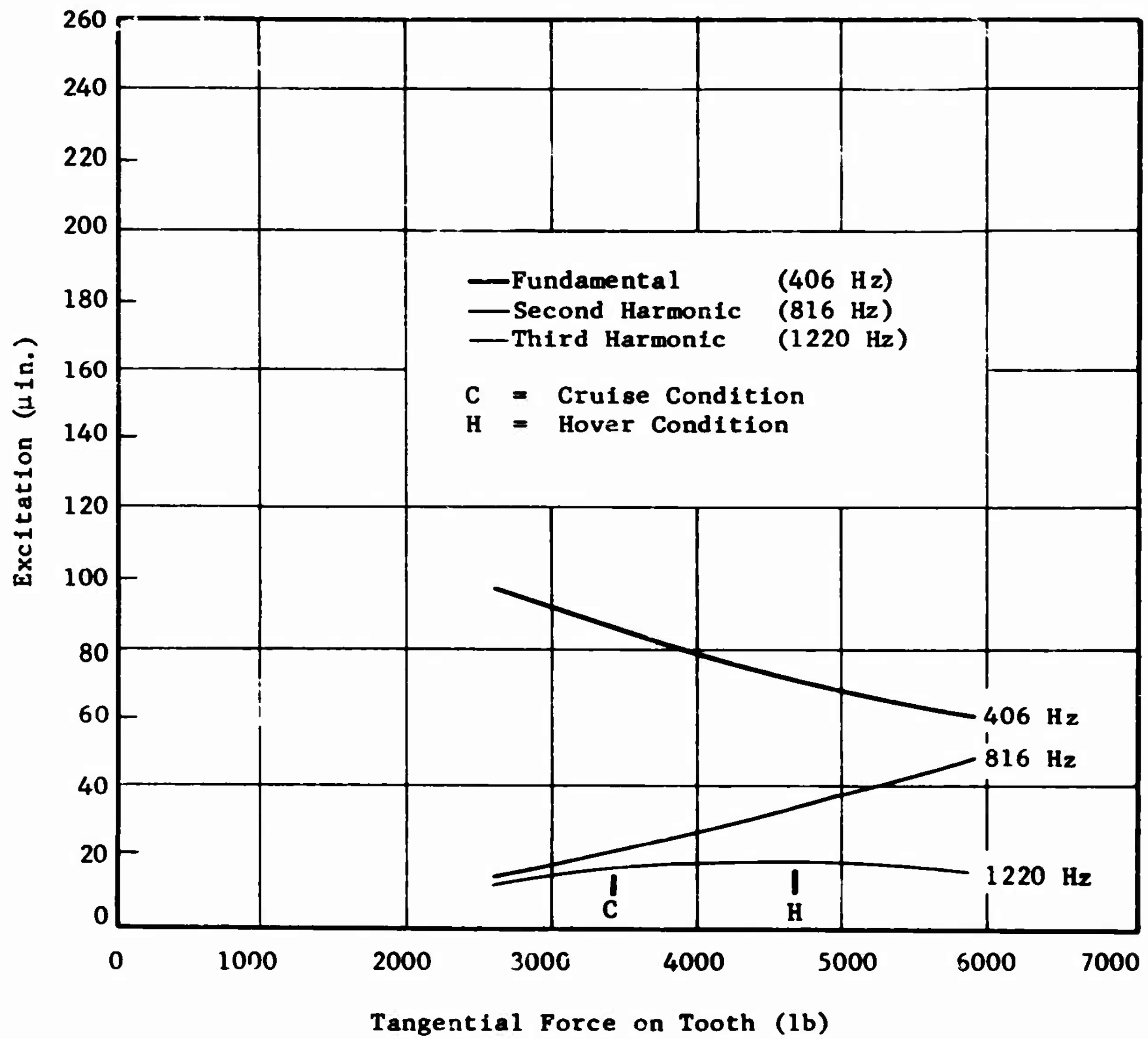

Figure 49. Excitation vs. Tooth Load in CH-47 Forward Transmission Upper Planetary Gear Set - Mesh Series 709.

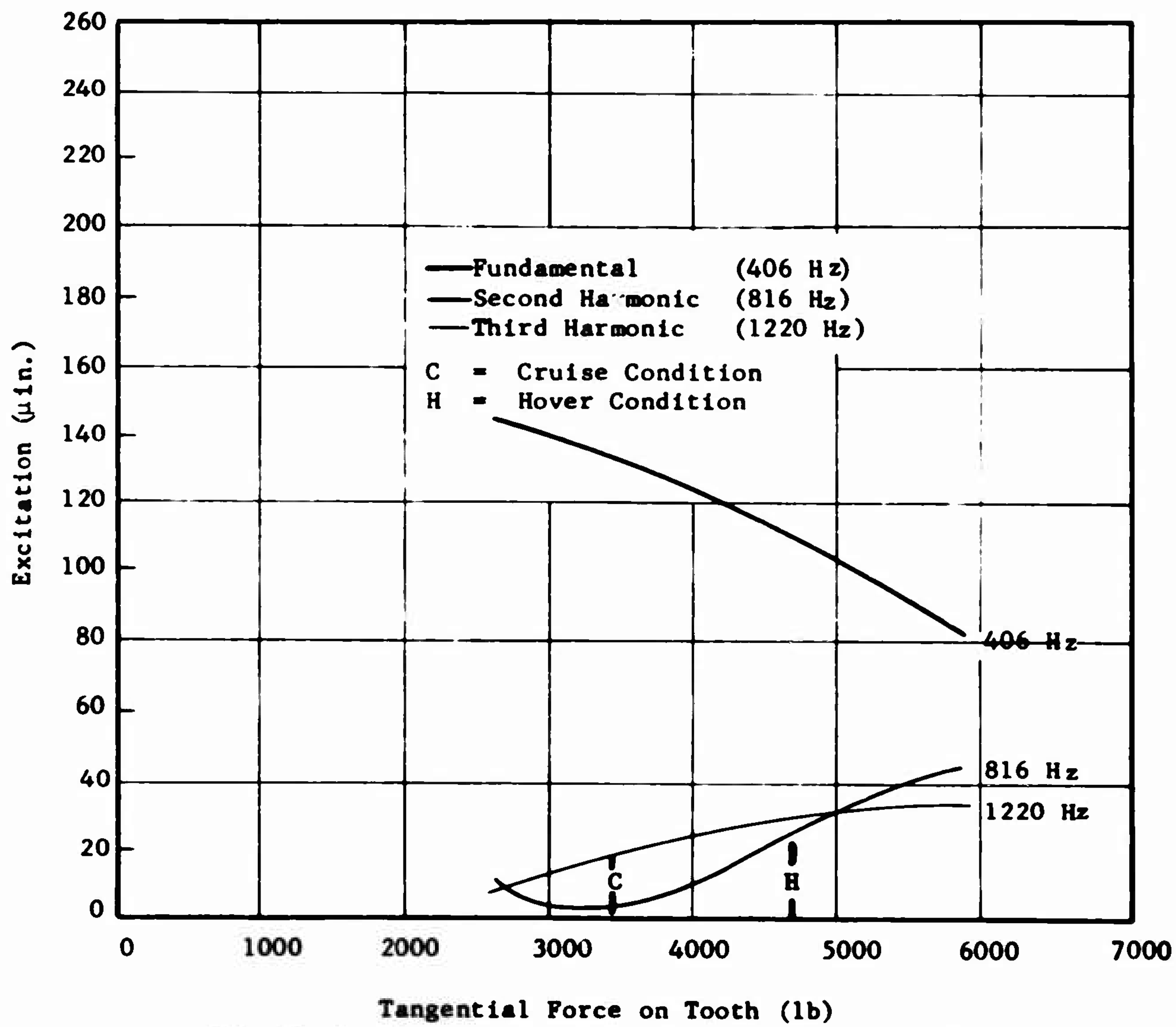

Figure 50. Excitation vs. Tooth Load in CH-47 Forward Transmission Upper Planetary Gear Set - Mesh Series 710.

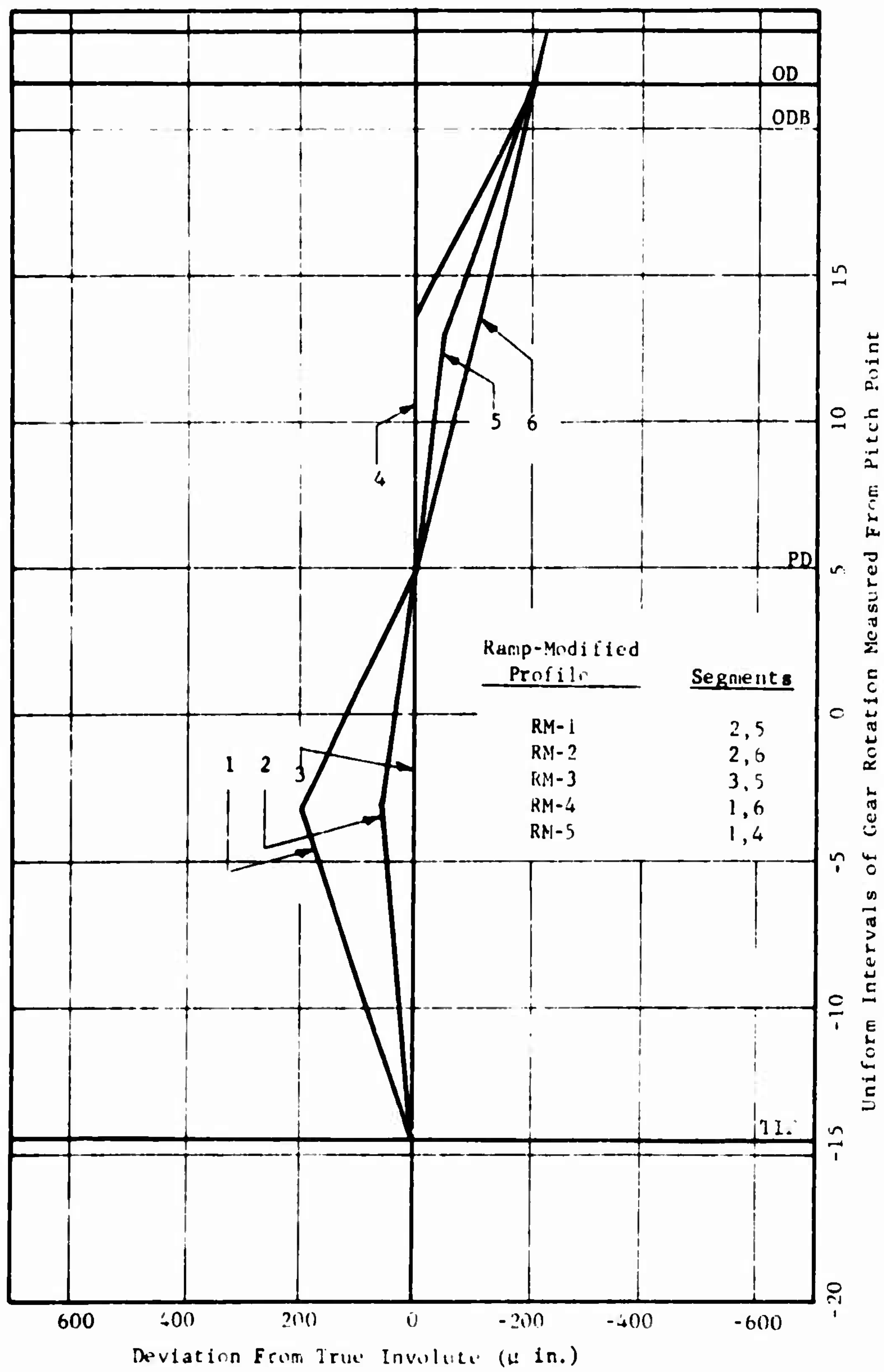

Figure 51. Ramp-Modified Tooth Profile Variations for Forward Transmission Upper Planetary Gear Set.

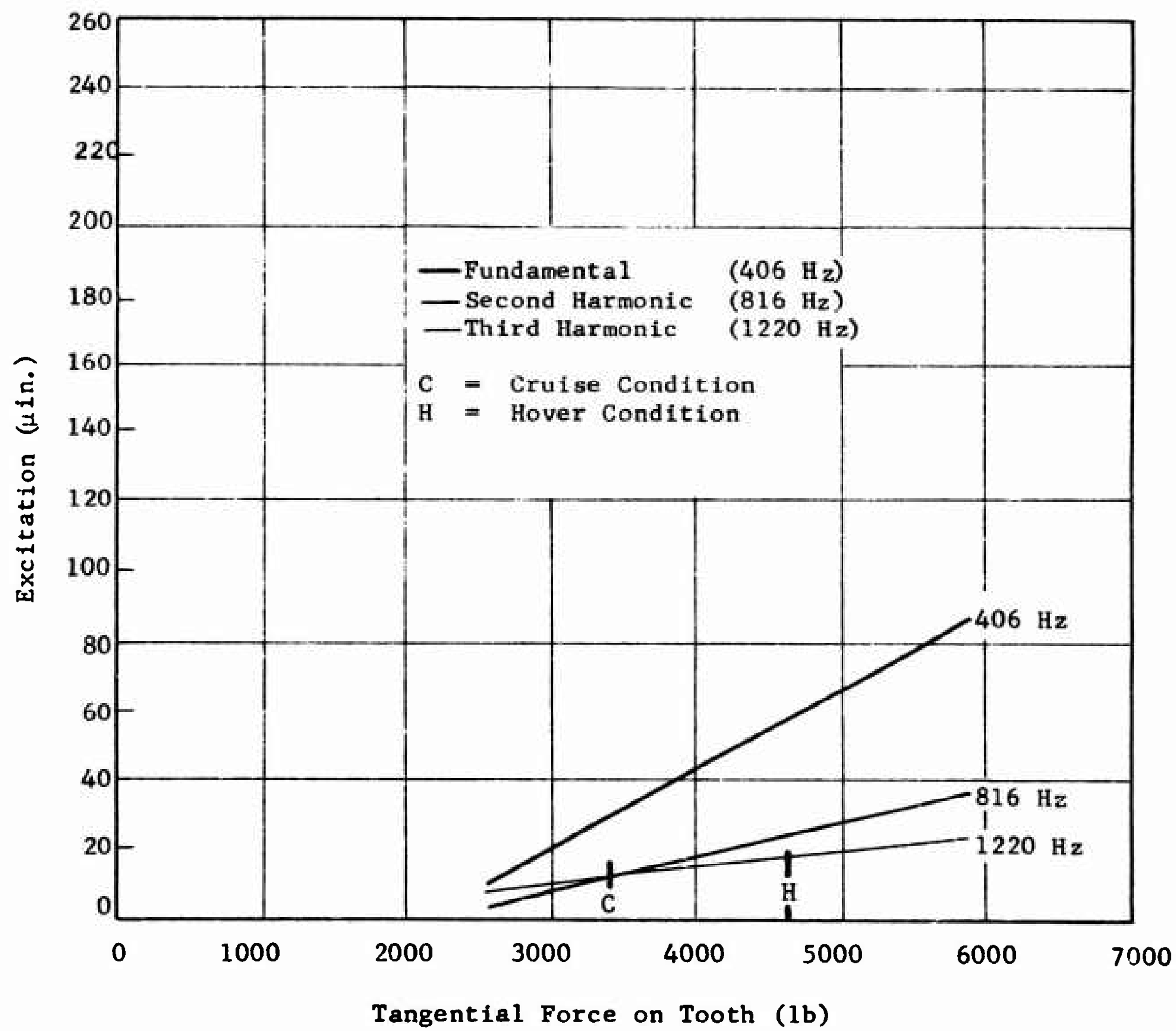

Figure 52. Excitation vs. Tooth Load in CH-47 Forward Transmission Upper Planetary Gear Set - Mesh Series 650.

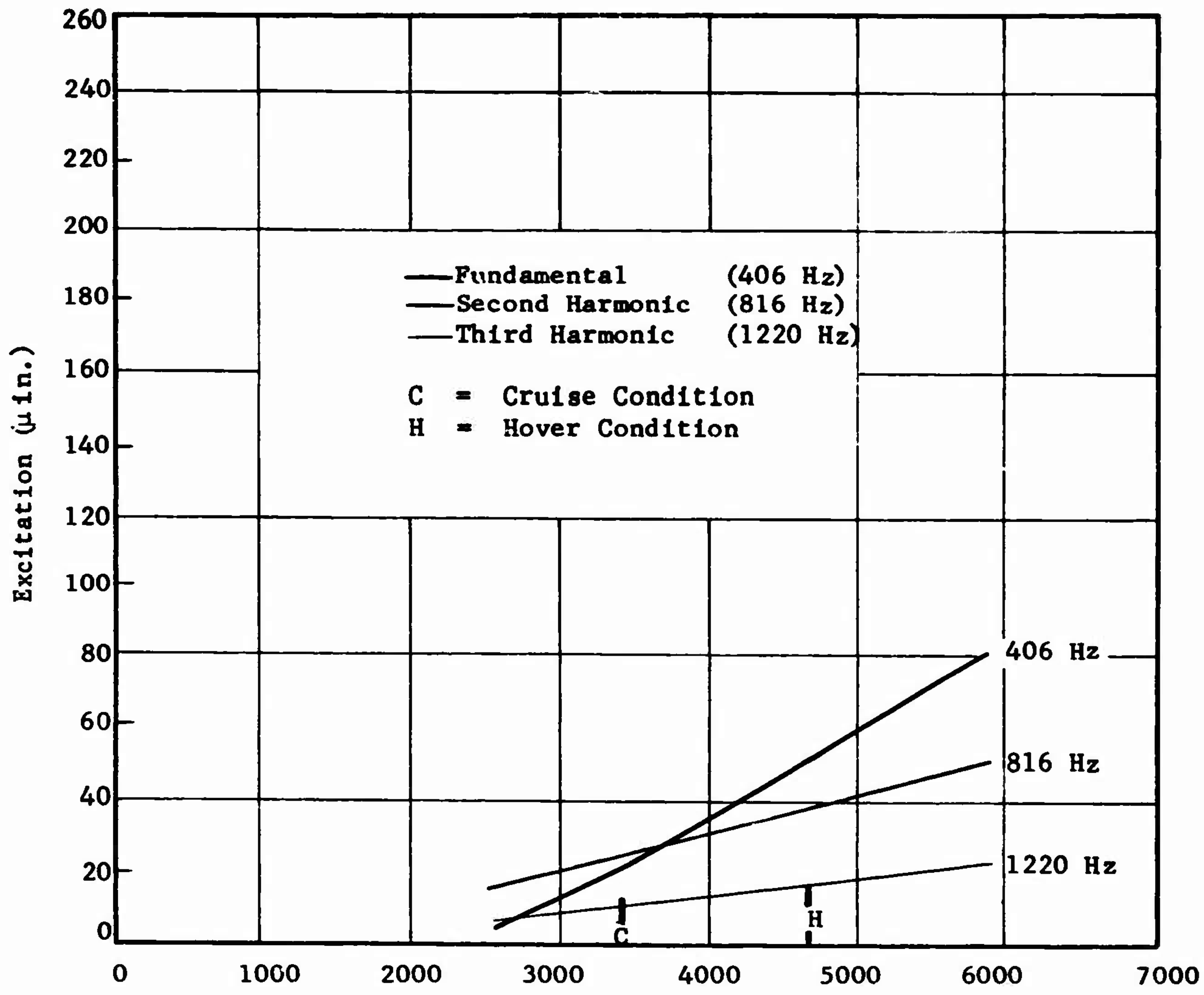

Figure 53. Excitation vs. Tooth Load in CH-47 Forward Transmission Upper Planetary Gear Set - Mesh Series 651.

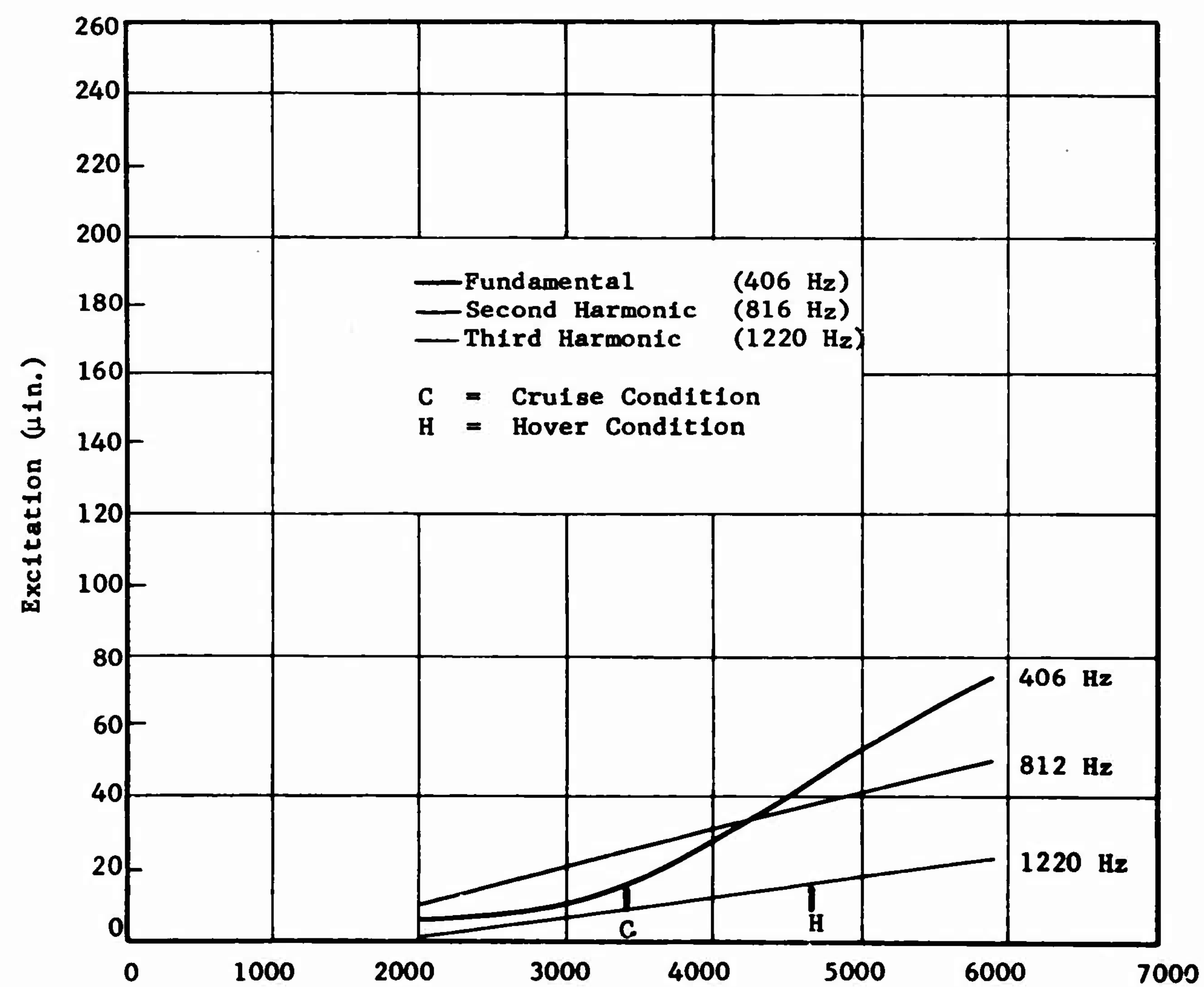

Tangential Force on Tooth (lb)

Figure 54. Excitation vs. Tooth Load in CH-47 Forward Transmission Upper Planetary Gear Set - Mesh Series 652.

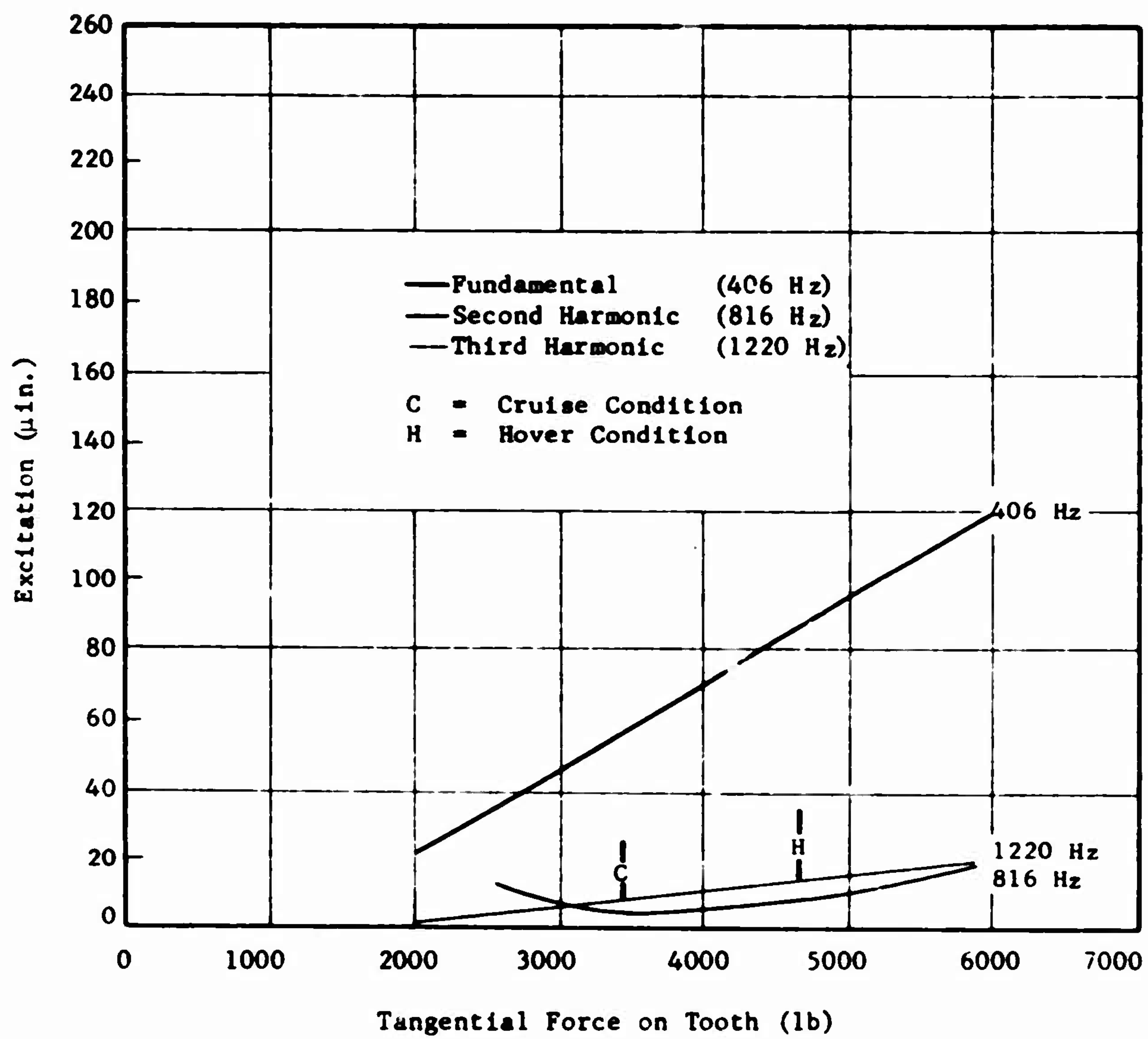

Figure 55. Excitation vs. Tooth Load in CH-47 Forward Transmission Upper Planetary Gear Set - Mesh Series 653.

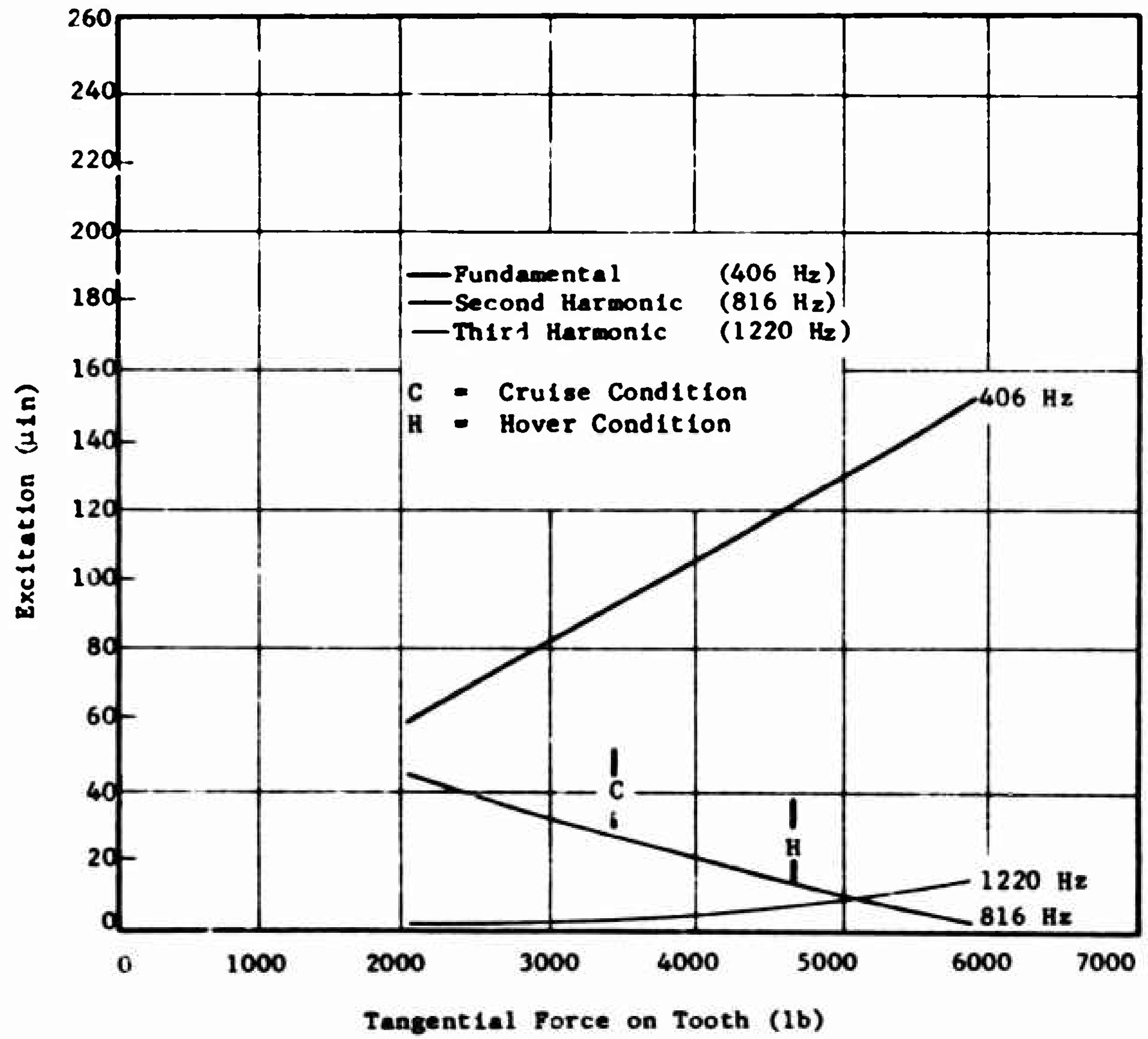

Figure 56. Excitation vs. Tooth Load in CH-47 Forward Transmission Upper Planetary Gear Set - Mesh Series 654.

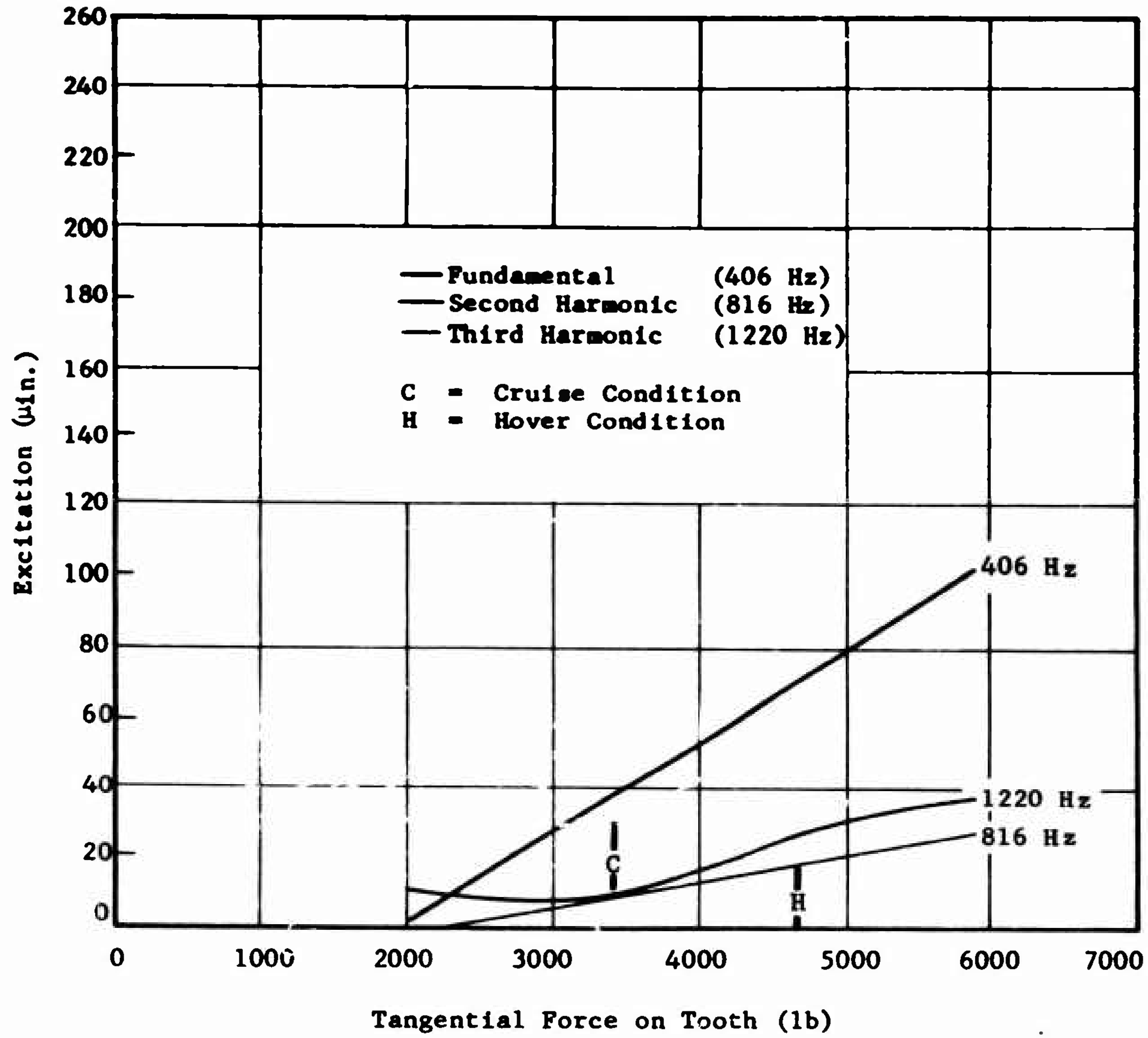

Figure 57. Excitation vs. Tooth Load in CH-47 Forward Transmission Upper Planetary Gear Set - Mesh Series 750.

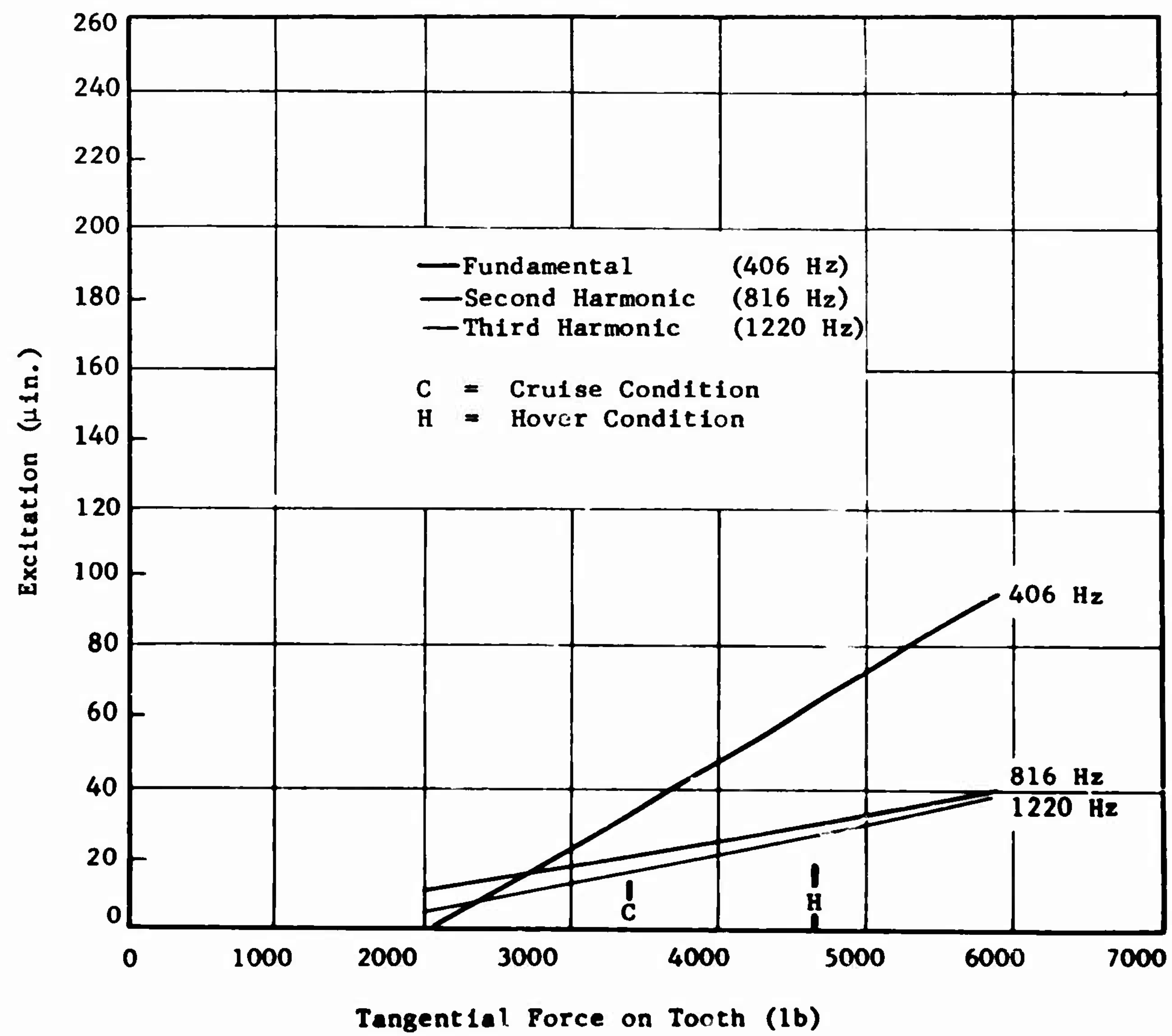

Figure 58. Excitation vs. Tooth Load in CH-47 Forward Transmission Upper Planetary Gear Set - Mesh Series 751.

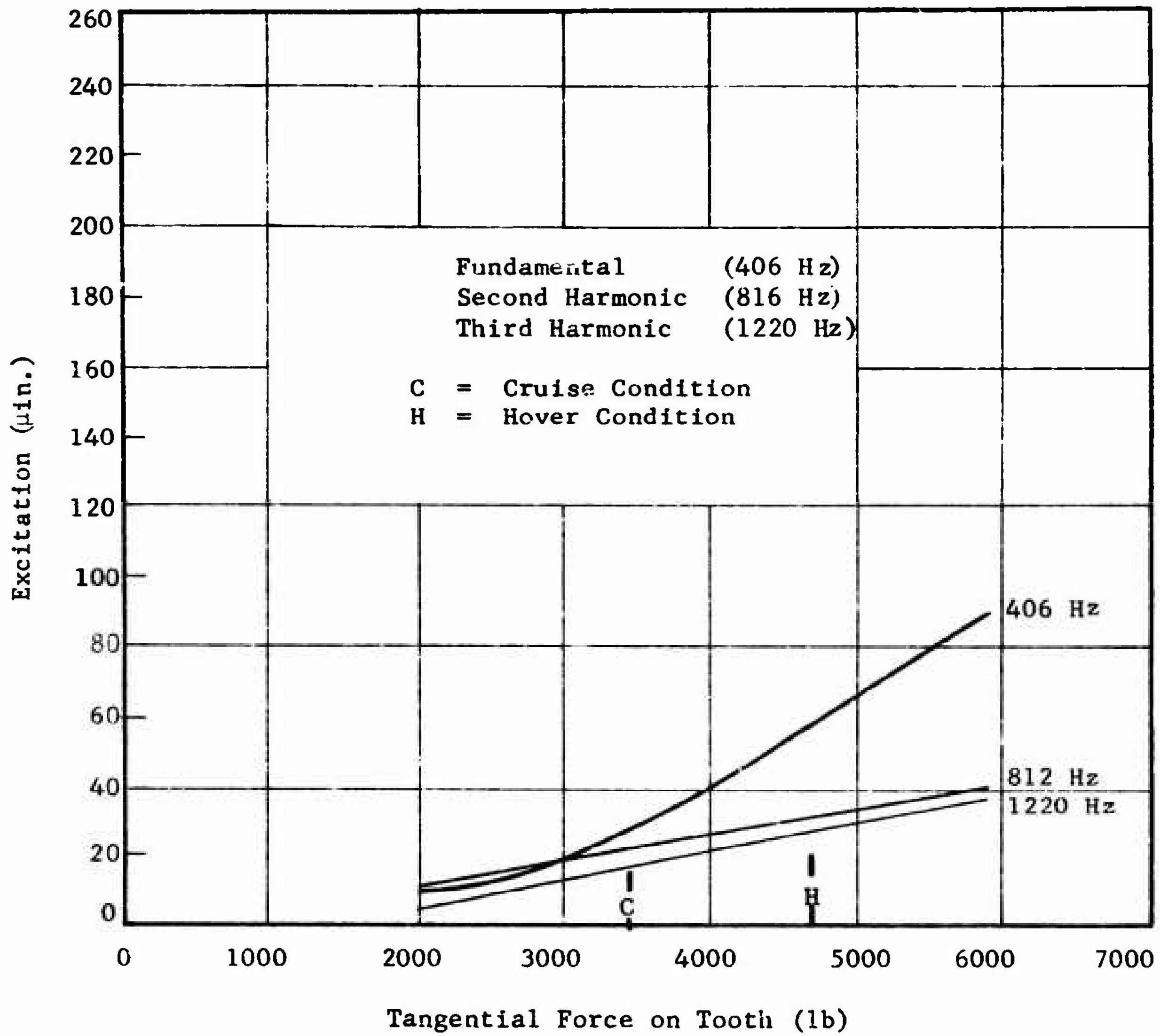

Figure 59. Excitation vs. Tooth Load in CH-47 Forward Transmission Upper Planetary Gear Set - Mesh Series 752.

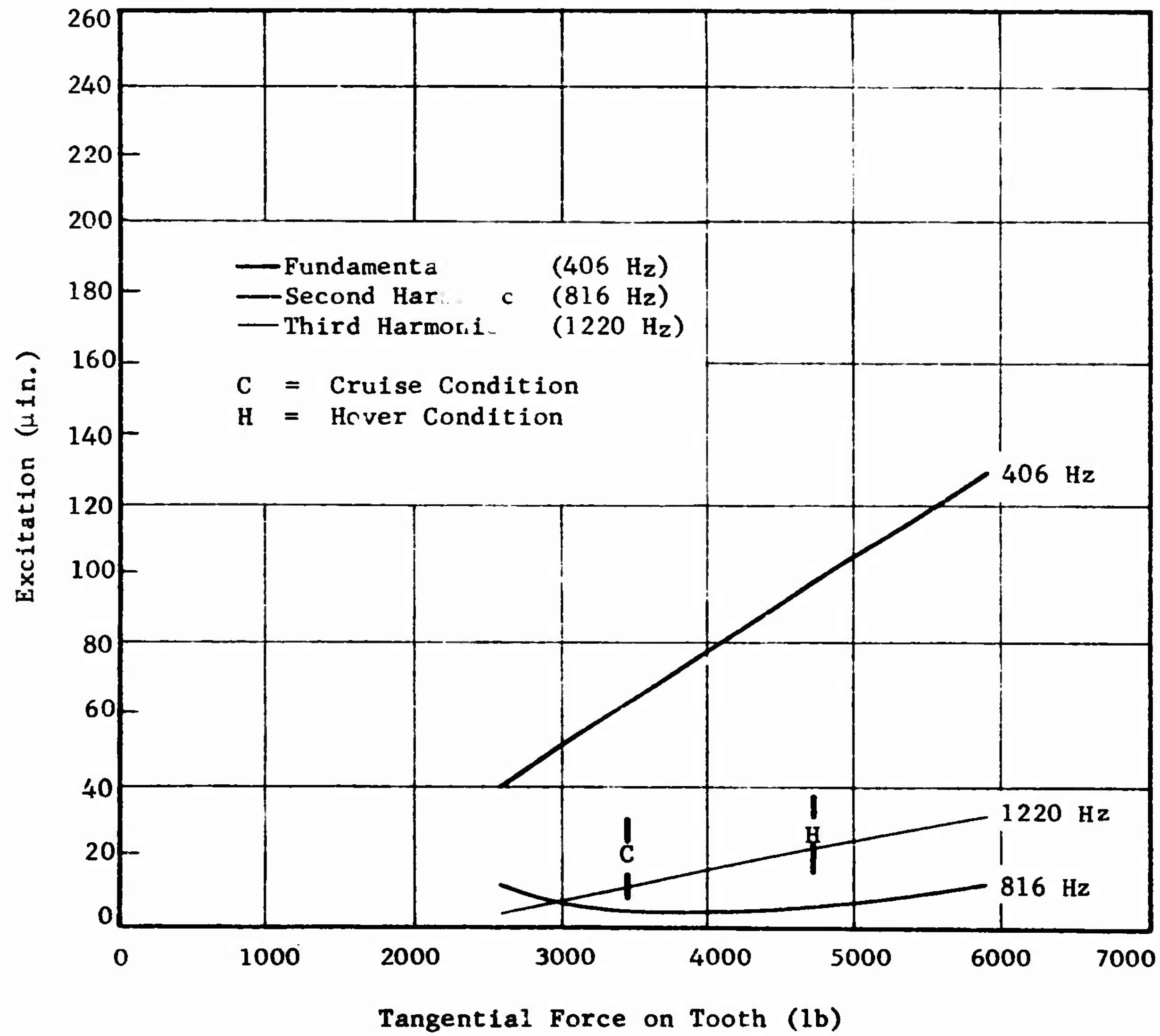

Figure 60. Excitation vs. Tooth Load in CH-47 Forward Transmission Upper Planetary Gear Set - Mesh Series 753.

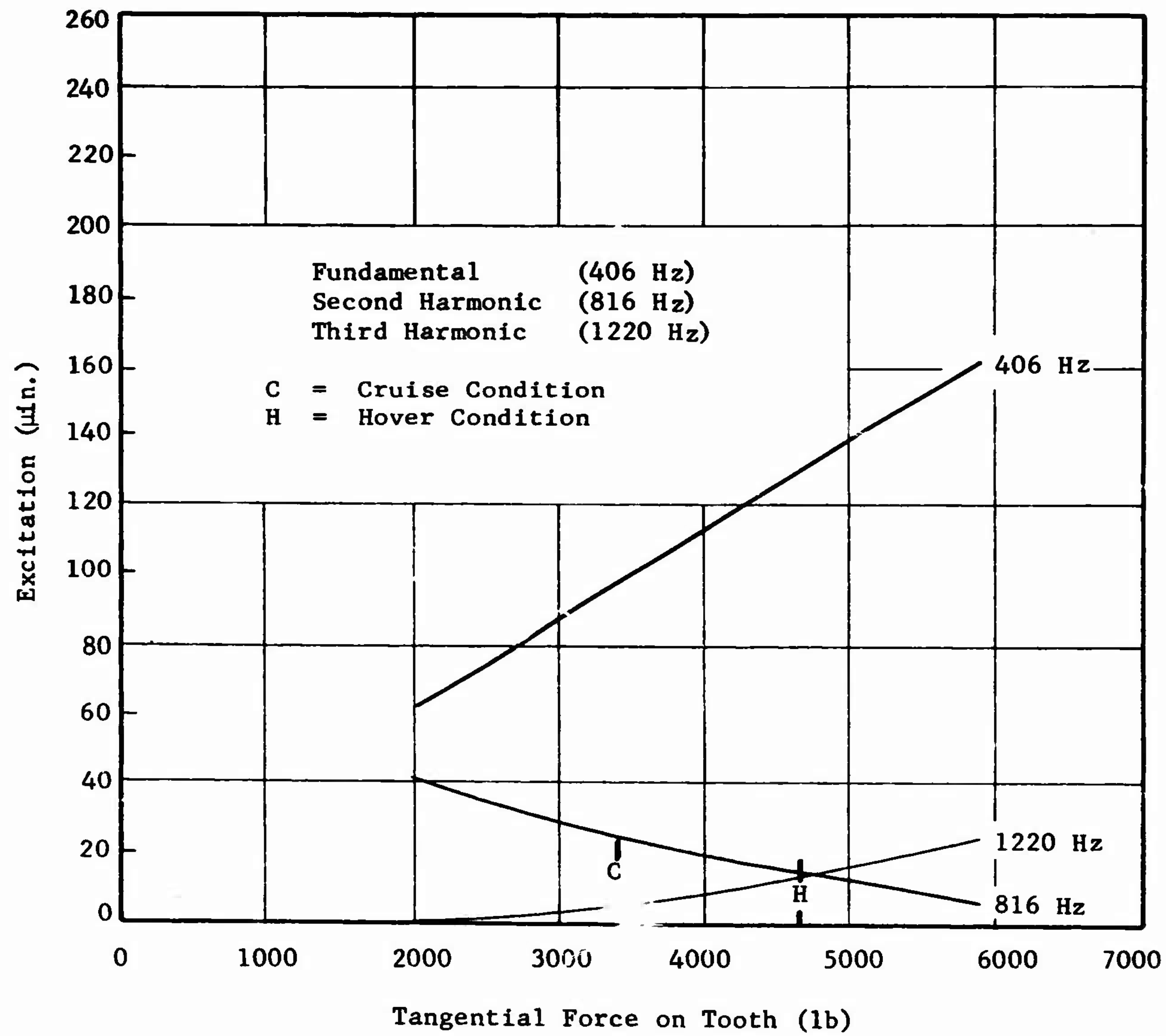

Figure 61. Excitation vs. Tooth Load in CH-47 Forward Transmission Upper Planetary Gear Set - Mesh Series 754.

CONCLUSIONS

GENERAL

The prime objective of this study has been achieved. The analytical tools developed under Contract DA 44-177-AMC-416(T) have been verified and refined through application to the CH-47 power train. Positive identification of the source and mechanism of gearbox noise energy has been made. Analytical methods for predicting the exciting force harmonics due to gear meshing have been developed. Positive correlation has been established between the theoretically predicted distribution of acoustic energy over the gear mesh frequency range and the distribution obtained experimentally in operating aircraft.

The further objective of investigating several potential gearbox mechanical design modifications for noise reduction has also been achieved. The relative abilities of the modifications to reduce torsional excitation and gear tooth dynamic force levels have been demonstrated. More importantly, however, a technique has been demonstrated by which similar studies may be performed on any or all of the drive train design parameters considered in the analysis. The analytical tools thus are ready to be utilized in a systematic study of transmission gear noise reduction.

While good agreement was obtained between the predicted and measured gearbox noise spectrum shapes, a significant difference was noted between the absolute db noise levels. This difference is believed to be due to the fact that attention was restricted to the gearbox itself, while the gearbox mounting and helicopter frame were not considered. Empirical factors were used to represent the complex manner in which energy is transmitted through and emitted from the gearbox. (This process is illustrated in Figure 3, in which the empirical factors represent all system elements except those in the leftmost two boxes.) While this use of empirical factors to represent these large system segments leads to an inability to predict exact noise levels, it is perfectly justified when the study objective is to predict changes in gearbox noise levels which might be achieved by power train design modifications imposed prior to the introduction of the empirical factors. This was the case in this study. The observed noise level differences thus serve to focus attention in precisely the proper area: those portions of the system which are at present the least well understood.

PHASE I

Comparison of the calculated and measured spectrum shapes confirms the validity of the analytical noise-prediction techniques. The use of these techniques for the prediction of the absolute level of noise spectrum, however, requires data beyond those presently available and pertinent to the scope of this program. These data involve the vibration characteristics of the aircraft structure and the transmission casing mounts. The very low attenuation of vibration across the mounts during in-flight tests indicates a relatively high level of vibration energy transfer from the transmission casing to the aircraft structure through the transmission mounts.

The transmission housing resonance measurements indicate that the CH-47 transmission is essentially similar to that of the UH-1D, and that no major change is required in the analytical procedures derived from the earlier UH-1D study.

The spiral bevel gear excitation calculation procedure utilized for this study is not yet considered to be a fully developed analytical tool. While the noise predictions obtained with it appear to be acceptable, the procedure is dependent upon a number of highly limiting assumptions and approximations.

PHASE II

Consideration of various gear tooth profile combinations for the forward transmission upper planetary gear set leads to the conclusion that calculated pitch-line excitations are strongly dependent upon tooth profile, apparently to such an extent that profile variations smaller than the manufacturing and measurement tolerances are able to effect gross changes in the computed excitation levels.

These changes are apparently great enough to explain the observed differences between the predicted and measured noise levels at the second and third harmonics of upper planetary tooth mesh frequency. It may also be observed that the relieved tip and base tooth profiles exhibit significantly lower levels of torsional excitation than do the true involute tooth profiles. In addition, tooth profile variations appear to be less important as a means for reducing excitation as transmitted tooth load increases. This is because of the increased amount of tooth bending with increased loading.

Variations in planet carrier torsional stiffness in the upper planetary gear reduction are potential contributors to high noise levels, particularly near frequencies of 406 and 1220 Hz. In the forward rotor drive train, this is particularly likely at values of planet carrier torsional (pitch-line) compliance on the order of 0.65×10^{-6} in./lb, or about half of the present calculated design compliance of 1.33×10^{-6} in./lb.

Comparison of acoustic and mechanical vibration data recorded during casing resonance studies indicates that the ratio of acoustic to mechanical energy levels is not constant over the frequency range 200-10,000 Hz. The relative variations are apparently low enough, however, so that the energy conversion factor may be taken as constant over this range of frequencies.

The overall predicted noise spectrum level is affected not only by variations in the distance from the noise source to the detecting instrument, but also by variations in the energy conversion factor σ, and by variations in the housing geometry and environment factor. With regard to the effect of distance upon noise level, a separation of 3 inches between the theoretical noise source and the microphone results in an increase of 15 db in the overall calculated noise spectrum level above that calculated at a distance of 1 foot.

Variations in spectrum level of plus or minus about 5 db may be produced by 2 to 1 changes in the energy conversion factor, while 5 to 1 changes in the housing geometry and environment factor are required for the same noise variation. Experimental confirmation of the effect of distance was obtained for distances of less than about 1 foot from the transmission, while at greater distances, noise emanating from other sources is apparently predominant.

Examination of the effects of tangential tooth load on pitch-line excitation for the relieved tip and base tooth profile combinations indicates that excitation magnitude is strongly dependent upon tooth load. While with true involute profile, the fundamental excitation increases with increase in tooth load, the reverse is observed for the relieved tip and base profiles. At the same time, the excitation second harmonics for certain profiles are observed to pass through minimum values and the third harmonics are relatively insensitive to variations in tooth loading.

The ramp-modified profile variations considered all exhibit the characteristic of increasing excitation with increase in tooth loading. While excitation magnitudes for these profile combinations are not significantly lower at hover conditions than those of the relieved tip and base profiles, the magnitudes at cruise conditions are considerably reduced compared to the corresponding values for relieved tip and base profiles. This fact is significant when the percentage of operating time at given tooth loadings may be predicted in advance, as in the operation of a helicopter.

LITERATURE CITED

1. Laskin, I., Orcutt, F. K., and Shipley, E. E., ANALYSIS OF NOISE GENERATED BY UH-1 HELICOPTER TRANSMISSION, Technical Report 68-41, U. S. Army Aviation Materiel Laboratories, Fort Eustis, Virginia, June 1968, AD 675457.

2. Sternfeld, H., Jr., Spencer, R. H., and Schaeffer, E. G., STUDY TO ESTABLISH REALISTIC ACOUSTIC DESIGN CRITERIA FOR FUTURE ARMY AIRCRAFT, TREC Technical Report 61-72, U. S. Army Aviation Materiel Laboratories, Fort Eustis, Virginia, June 1961.

3. Harris, C. M., HANDBOOK OF NOISE CONTROL, Chapter 2, McGraw-Hill Book Company, Inc., 1957.

4. Dudley, Darle W., PRINCIPLES OF ACOUSTICAL ENGINEERING OF GEAR TRANSMISSIONS, presented at the American Institute of Aeronautics and Astronautics, Torpedo Propulsion Conference, U. S. Naval Underwater Ordnance Station, Newport, R.I., July 25, 1963.

SELECTED BIBLIOGRAPHY

Bell Helicopter Co., TORSIONAL VIBRATION ANALYSIS OF THE AH-1G HELICOPTER DRIVE SYSTEM, Report No. 209-099-043, 6 January 1967.

Bell Helicopter Co., UH-1A INTERNAL NOISE SURVEY, Report No. 204-099-278, 21 August 1961.

Harris, C. M., HANDBOOK OF NOISE CONTROL, Chapter 23, McGraw-Hill Book Company, Inc., 1957.

O'Donnel, W. J., STRESS AND REFLECTION IN BUILT-IN BEAMS, ASME Paper No. 62-WA-16, 1962.

Palmgren, Arvid, BALL AND ROLLER BEARING ENGINEERING, 3rd Edition, SKF Industries, Inc., p. 46.

Scanlan, R. H., NOISE IN ROLLING ELEMENT BEARINGS, ASME Paper No. 65-WA/MD-6, 1965.

Schlegel, Ronald G., and Mard, Kenneth C., TRANSMISSION NOISE CONTROL - APPROACHES IN HELICOPTER DESIGN, ASME Paper No. 67-DE-58, 1967.

Schlegel, Ronald G., King, Robert J., and Mull, Harold R., GEAR NOISE, Machine Design, February 27, 1964.

APPENDIX I

NOISE AND VIBRATION MEASUREMENTS

A series of noise and vibration measurements was made on three CH-47 helicopters operating in both cruise and hover flight conditions. Measurements were made in two CH-47A aircraft, numbers 12408 and 58012 (transmission serial numbers A7-170 and A7-284 respectively) and one CH-47B aircraft, number 619109 (transmission serial number A7-528). The actual engine speed and horsepower conditions during these measurements are shown in Table 13.

In this appendix, the instrumentation used in making the noise and vibration measurements and the procedures for its calibration are described. The results obtained, including both raw and reduced data, are presented. A discussion of the final results may be found in the main body of the report.

DESCRIPTION OF INSTRUMENTATION AND CALIBRATION PROCEDURES

The instrumentation used to obtain and analyze sound and vibration data is shown in Figure 62. The types and model numbers of the various components are as follows:

Accelerometers - Bruel & Kjaer (B & K) 4313
Microphone - B & K 4133 - 1/2-inch condenser microphone with B & K type battery-powered cathode follower
Switch - Kistler 562 - 8-position
Sound Level Meter (SLM) - B & K 2203
Frequency Analyzers - B & K 2107 narrow band; B & K 1612-1/3 octave and octave band pass
Microphone Amplifier - B & K 2603
Level Recorder - B & K 2305
Tape Recorder - Nagra III

The accelerometers have a mounted resonant frequency of 45 kHz, indicating an error of less than 1 db for an operating frequency range to 15 kHz. The condenser microphore has a flat frequency response over the range from 20 to 20,000 Hz. The sound level meter, which was used as the indicating amplifier, has an operating frequency range of from 10 to 20,000 Hz. The Nagra III recorders have a frequency range of from 30 to 15,000 Hz, flat within 1.5 db.

The equipment for readout and recording the accelerometer and microphone outputs was installed at the front of the helicopter cargo compartment opposite the door. The leads to accelerometers mounted on and around the forward rotor transmission were passed through the passageway between the cargo and pilot's compartments. The installation of the readout and record equipment in the helicopter is shown in Figure 63.

One-third-octave band and narrow-band frequency spectrum analyses were made from the recorded signals. The selectivity characteristics of the one-third-octave and narrow-band analyzers are illustrated in Figure 64. The band width of the filters is determined by the ratio of the frequencies at the filter 3-db down points. For the one-third-octave filter, this ratio is two-thirds; for the narrow-band filter, it is 6 percent of the center frequency. However, all of the "energy" under the filter curve is reflected in the filter output, even that part which is beyond the 3-db down points. During recording, the signals were monitored by earphones from the tape, on the sound level meter display and on the recorder VU meter.

The arrangements for calibration of the sound and vibration measurement systems were as follows:

1. Initial calibration of accelerometers - the accelerometers, leads, selector switch, and sound level meter were assembled in the same arrangement as that subsequently used for measurements on the helicopters. Each of the accelerometers was mounted in turn on an electromagnetic vibration exciter along with a reference calibration accelerometer. The reference accelerometer was connected to a Fluke 873A differential voltmeter using only the lead supplied with the accelerometer. The vibration exciter was adjusted for about 1-g peak acceleration at 100 and at 1,000 Hz, and readings were taken on both the differential voltmeter and the sound level meter (including both the meter reading and the recorder jack output). The calibration constant (in mv/g) of each of the measurement accelerometers with its leads, and including the selector switch, was obtained using the reference accelerometer and differential voltmeter as the standard. The differential voltmeter had recently been calibrated and was in use as a laboratory standard.

2. Calibration of the sound measuring system - a B & K type 4220 pistonphone was used for absolute calibration of the sound measuring system. When mounted properly on the microphone, the pistonphone produces a pure tone sound pressure of 124 db (re 2×10^{-4} μ bar) $\pm$ 0.2 db at 250 Hz. This signal was used to calibrate the sound level meter and was recorded on the tape recorder prior to each series of measurements in order to provide a calibration signal for setting up the analysis and level recording equipment.

SOUND PRESSURE LEVEL MEASUREMENTS

The microphone locations for sound pressure level (SPL) measurements are shown on a cabin layout schematic in Figure 65. In all cases, the microphone was positioned at about head level for a standing person except in the pilot's compartment. There, the microphone was positioned above the pilot's head in the normal seated position.

Overall SPL levels (linear response) for each measurement position and for all three aircraft are given in Table 15.

One-third-octave frequency analyses of the SPL measurements are given in Tables 16, 17, and 18 for cruise operation and in Tables 19, 20, and 21 for hover operation. The results of the narrow-band analysis of the measurements are given in Tables 22, 23, and 24 for cruise operation and in Tables 25, 26, and 27 for hover operation. The center frequencies at which there are identifiable peaks or maxima, in the SPL spectrum, are listed with the amplitudes of SPL at those frequencies.

VIBRATION MEASUREMENTS

The locations of the accelerometers on the gearbox and its support structure are shown in Figures 66 and 67. In addition, a fourth accelerometer, not visible in these figures, was mounted vertically on the inside of the transmission support structure directly below the accelerometer shown in Figure 67.

The accelerometers were cemented (Barcobond epoxy adhesive) to small aluminum blocks (5/8-inch square by 3/16-inch thick) which were in turn cemented to the gearbox or structure surface after removing the paint and thoroughly cleaning the surface with abrasive paper and solvent. The surfaces of the blocks were ground flat, except for the one used at the ring gear housing location which was shaped to fit the housing contour.

The accelerometer numbers, their locations, and their calibrations are as follows:

Accelerometer	Number	Location	Reference
1	195113	Ring Gear	78.1 db = 1g at 1 kHz
2	117539	Sump	78.75 db = 1g at 1 kHz
3	134202	Support Arm	78.0 db = 1g at 1 kHz
4	133877	Structure	77.75 db = 1g at 1 kHz

Overall levels of vibration (linear response) are tabulated in Table 28. For these readings, the instrumentation was set for linear response from 20 to 20,000 Hz. The results of one-third-octave frequency analysis for all of the vibration measurement points, with the exception of the sump accelerometer location on aircraft 12409, are shown in Tables 29, 30 and 31.

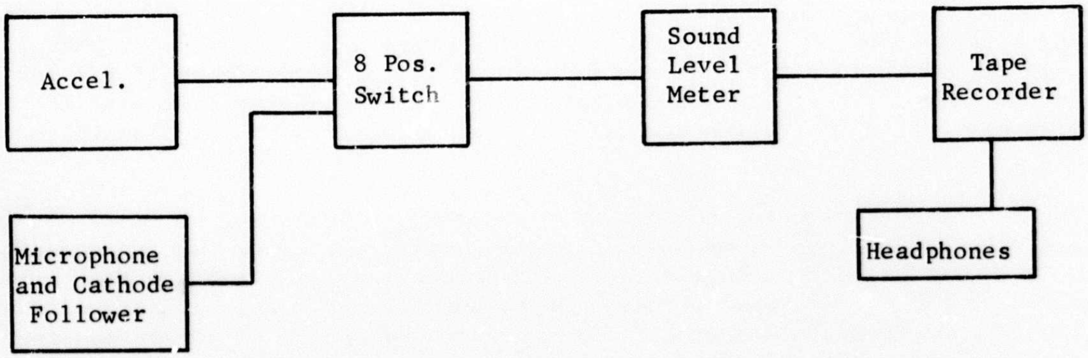

(a) Recording Instrumentation

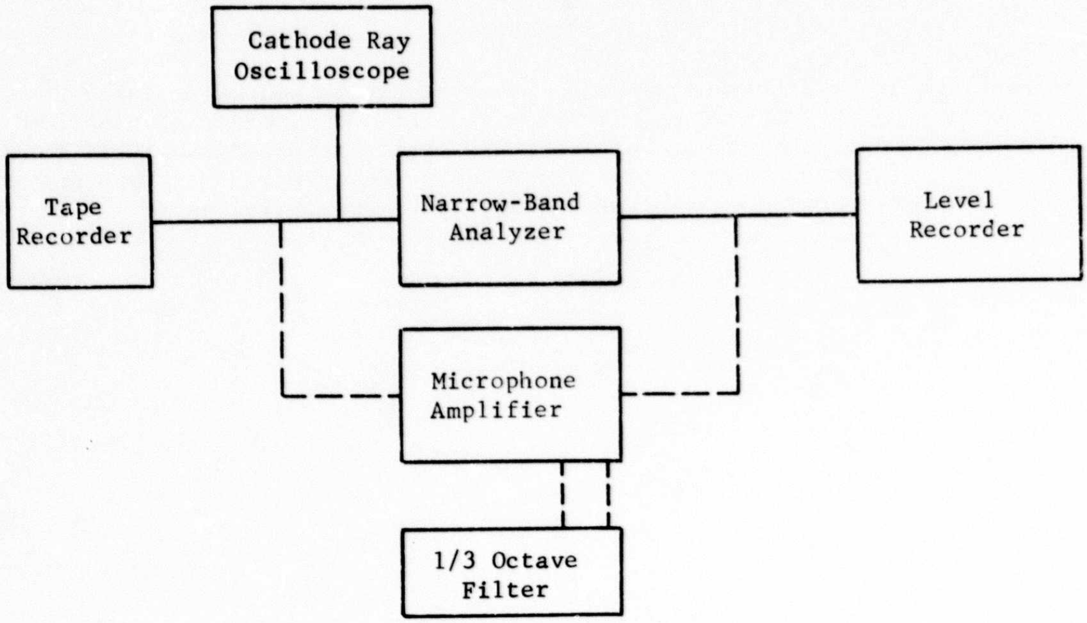

(b) Frequency Spectrum Analysis Instrumentation

Figure 62. Instrumentation Arrangements for Recording and Analyzing Sound and Vibration Data.

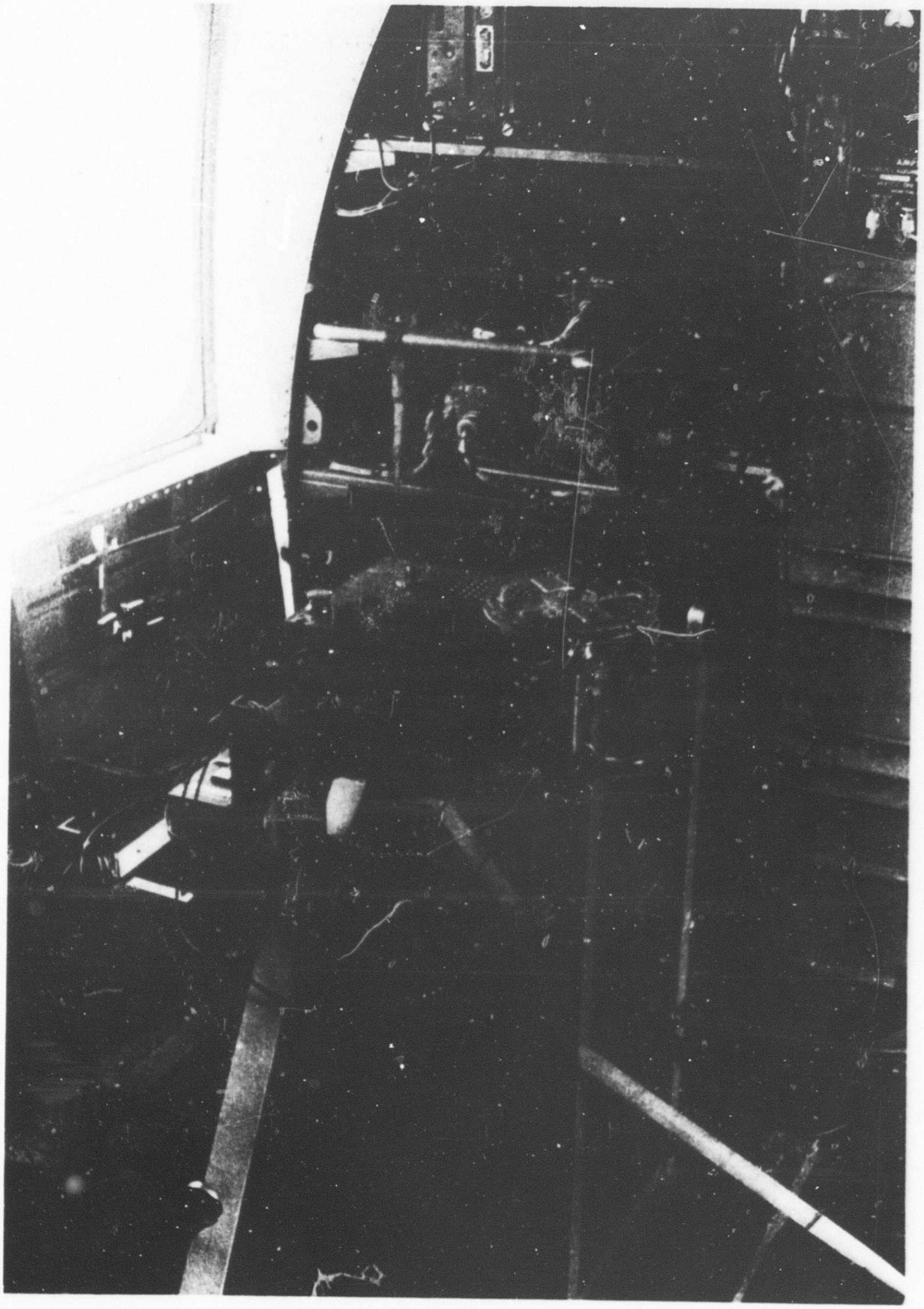

Figure 63. Installation of Readout and Recording Equipment in Helicopter.

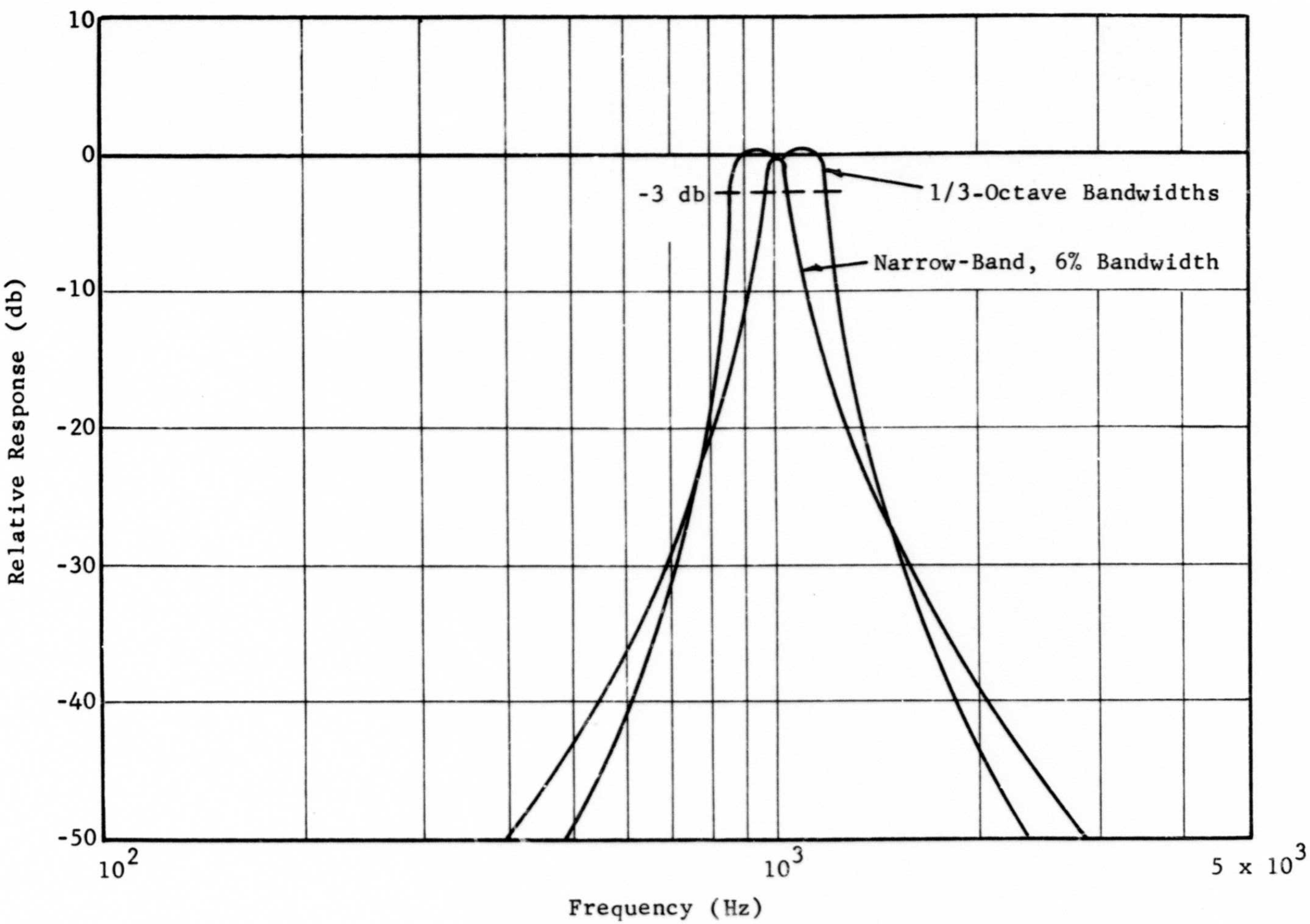

Figure 64. Typical Filter Frequency Selectivity Characteristics.

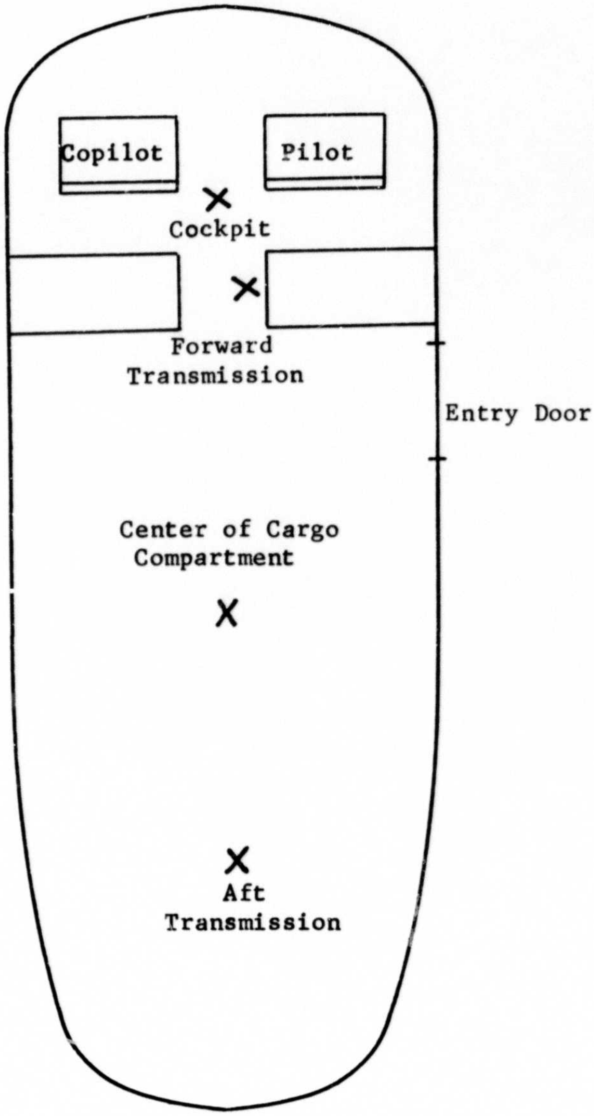

Figure 65. Microphone Locations for Sound Pressure Level Measurements.

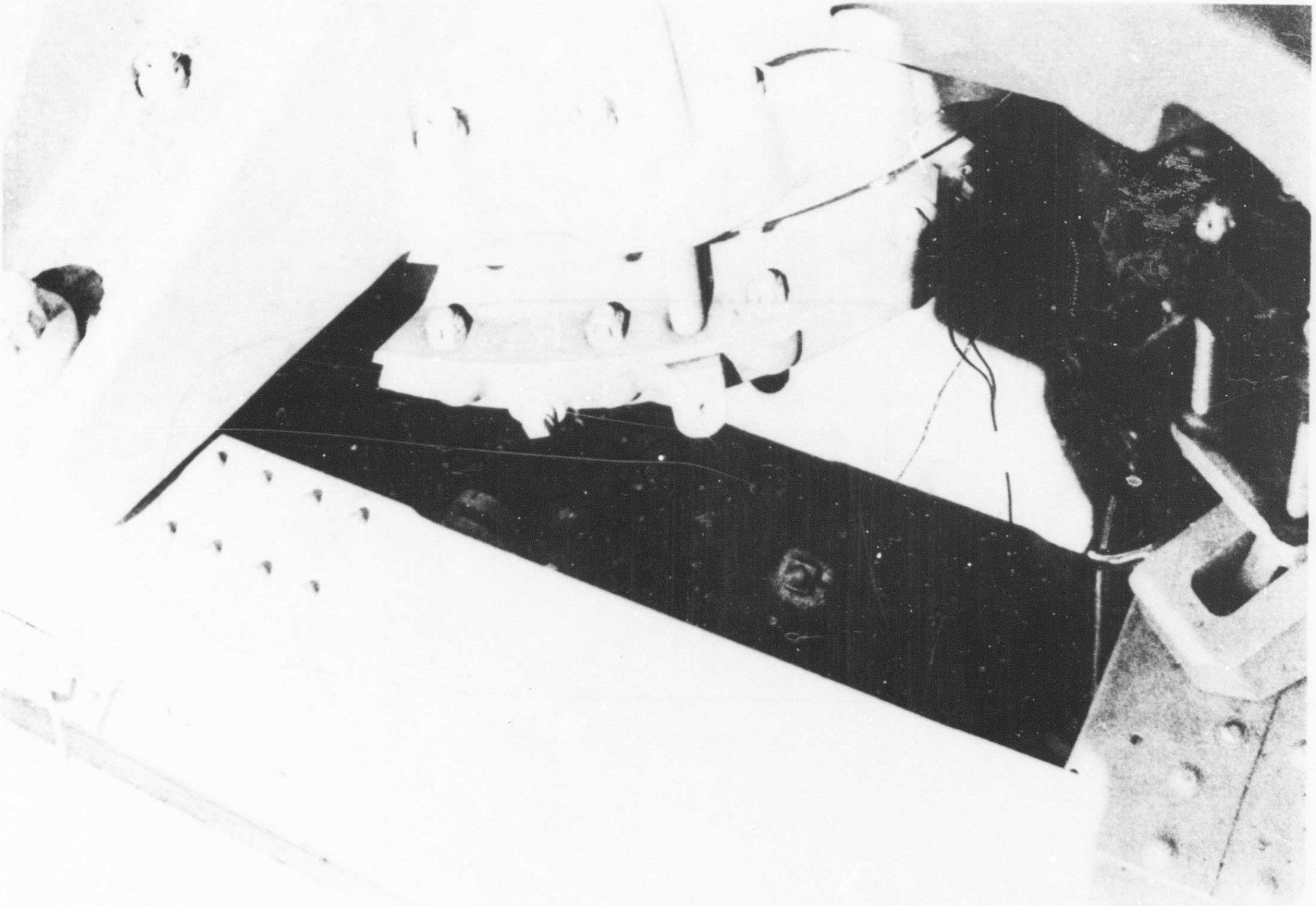

Figure 66. Mounting Locations of Sump and Ring Gear Accelerometers.

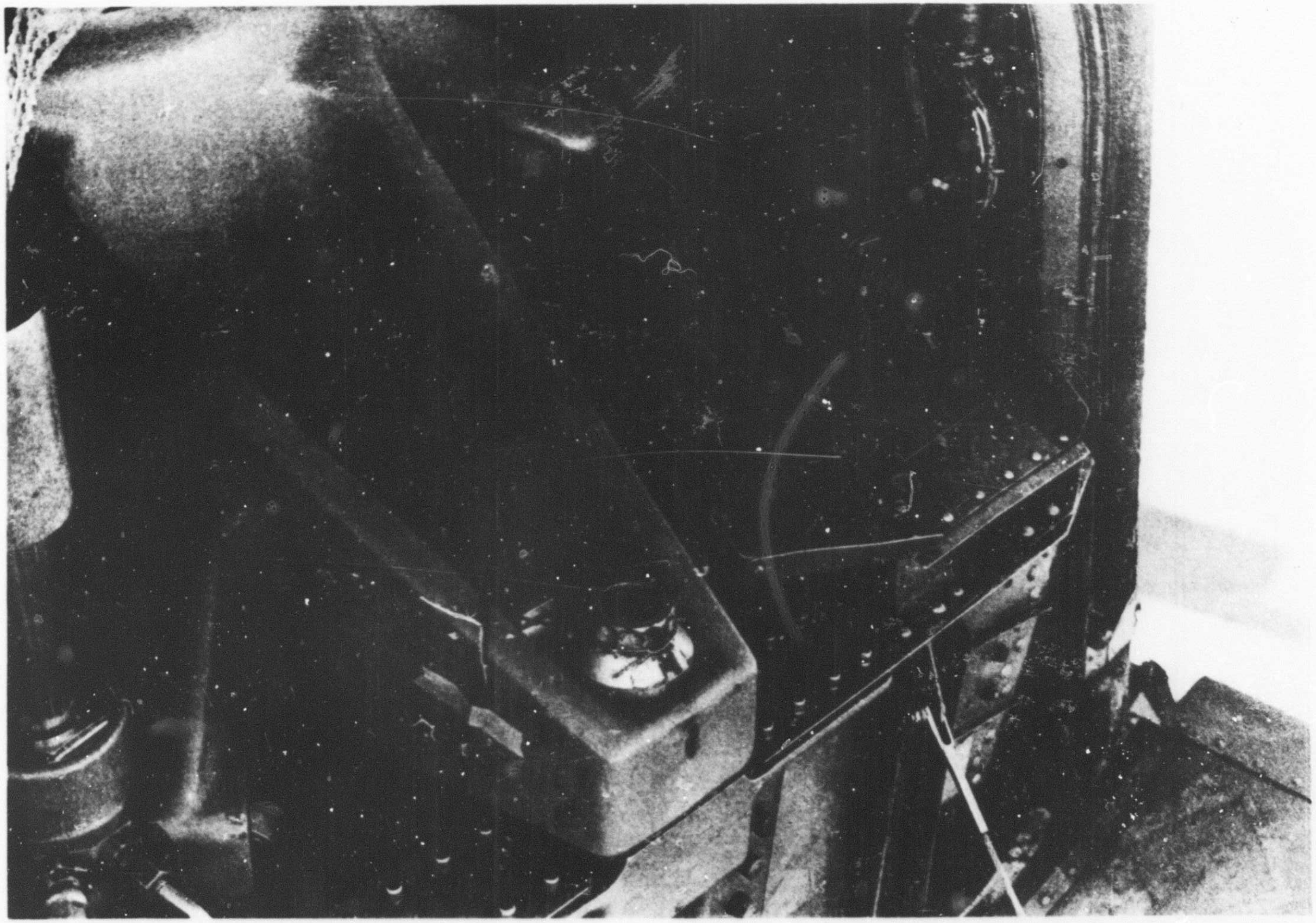

Figure 67. Mounting Locations of Transmission Support Arm Accelerometers.

TABLE 15. OVERALL SOUND PRESSURE LEVELS

(db, rms, re 0.0002 microbar)

Aircraft No.	Beneath Forward Rotor Transmission	Above Pilots' Heads	Cargo Compartment Center	Cargo Compartment Rear
Cruise Condition				
12409	124.5	118.5	113.0	118.0
619109	121.5	115.5	109.0	
58012	125.0	114.5	109.0	
Hover Condition				
12409	124.5	116.0	110.0	
619109	122.0	120.5	112.0	
58012	126.0	114.5	108.0	

TABLE 16. ONE-THIRD-OCTAVE FREQUENCY ANALYSIS OF SPL MEASUREMENTS IN CH-47A AIRCRAFT
Cruise Operation, Aircraft No. 12409 (db re 0.0002 microbar)

Center Frequency (Hz)	Beneath Forward Rotor Transmission	Above Pilots' Heads	Cargo Compartment	
			Center	Rear
25	113	114	114.7	119
315	99	100.5	106.5	104
40	99.5	96.5	105	110
50	104.5	100	107.5	114.5
63	107	103.5	107	110.5
80	.104.5	105.5	100.5	107
100	103.5	105.5	99	105.5
125	109.5	106.5	102	103
160	107.5	104	101.5	103
200	103.5	102.5	103.5	108.5
250	104	101	99	106
315	100.5	100	99	100
400	104	100.5	97	101.5
500	106	97	94	98.5
630	106	98.5	94.5	99
800	106.5	99	99.5	101
1000	105.5	95.5	95	99.5
1250	113.5	105	96	103.5
1600	116.5	107.5	99.5	107
2000	106	97	92.5	102
2500	107	99	92	100.5
3150	117.5	112.5	98	104.5
4000	113	104.5	90.5	100
5000	107.5	97	89	98.5
6300	107.5	98	88.5	99
8000	103.5	94	88	96.5
10000	98.5	90.5	87.5	93.5
12500	93	88.5	87.5	89.5
16000	89	88	87	88

TABLE 17. ONE-THIRD-OCTAVE FREQUENCY ANALYSIS OF SPL MEASUREMENTS IN CH-47A AIRCRAFT
Cruise Operation, Aircraft No. 58012 (db re 0.0002 microbar)

Center Frequency (Hz)	Beneath Forward Rotor Transmission	Above Pilots' Heads	Cargo Compartment Center
200	105	98	95
250	101	98	95.5
315	102.5	95.5	93.5
400	103	93	91
500	101	91.5	89.5
630	110	96.5	91
800	106.5	95	94
1000	103	94.5	90.5
1250	112	100	94
1600	119	104	99.5
2000	106.5	95	99.5
2500	110	97.5	92
3150	120.5	108.5	95.5
4000	115	102	93
5000	111	95.5	88
6300	107.5	93	88
8000	105	90.5	84
10000	101.5	87	79.5
12500	98	82.5	76.5
16000	90.5	77.5	76

TABLE 18. ONE-THIRD-OCTAVE FREQUENCY ANALYSIS OF SPL MEASUREMENTS IN CH-47B AIRCRAFT
Cruise Operation, Aircraft No. 619109 (db re 0.0002 microbar)

Center Frequency (Hz)	Beneath Forward Rotor Transmission	Above Pilots' Heads	Cargo Compartment Center
20	85.5	85.5	85.5
25	112.5	111	95
315	102.5	101	100
40	97	103.5	96.5
50	97.5	102	95.5
63	104.5	99	99
80	105	101.5	97.5
100	99	101.5	96.5
125	103	98.5	94
160	107	97.5	93
200	104.5	95	94.5
250	100	91.5	91.5
315	103.5	94	91
400	102	95	93
500	98.5	92.5	91.5
630	99.5	92.5	96
800	105.5	95	100
1000	103.5	93.5	92
1250	116	101.5	92.5
1600	118.5	100.5	92.5
2000	106.5	92	93.5
2500	110	95.5	93
3150	114	100.5	93
4000	107	94.5	91
5000	103	91	87.5
6300	99.5	90	87.5
8000	95.5	88	87
10000	94.5	86.5	86.5
12500	92	86	86
16000	86	86	86

TABLE 19. ONE-THIRD-OCTAVE FREQUENCY ANALYSIS OF SPL MEASUREMENTS IN CH-47A AIRCRAFT
Hover Operation, Aircraft No. 12409 (db re 0.0002 microbar)

Center Frequency (Hz)	Beneath Forward Rotor Transmission	Above Pilots' Heads	Cargo Compartment Center
20	87.5	87.5	
25	107	110	107.5
315	101	99	103.5
40	98	99.5	96.5
50	99	97.5	99
63	99.5	99.5	97
80	103	101.5	95
100	99.5	96	100.5
125	106	100.5	102.5
160	94.5	99.5	97
200	97.5	98	98
250	97	98	98
315	97	95.5	94
400	105	100	94.5
500	109	100.5	92
630	103.5	99	96.5
800	106	100.5	106.5
1000	104.5	97.5	96.5
1250	114.5	102	97.5
1600	112.5	109	103.5
2000	105	95.5	92.5
2500	106.5	97.5	92
3150	120	107.5	97
4000	116	98.5	92
5000	106.5	96	90
6300	106.5	101	89.5
8000	102	96	88.5
10000	100	91	88
12500	92.5	89	88
16000	88.5	88	88

TABLE 20. ONE-THIRD-OCTAVE FREQUENCY ANALYSIS OF SPL MEASUREMENTS IN CH-47A AIRCRAFT
Hover Operation, Aircraft No. 58012 (db re 0.0002 microbar)

Center Frequency (Hz)	Beneath Forward Rotor Transmission	Above Pilots' Heads	Cargo Compartment Center
25	106	94.5	99.5
315	92	88.5	90.5
40	96.5	85.5	95.5
50	99	101	99
63	93.5	101.5	94
80	96	101	93.5
100	95	102	94.5
125	99.5	93.5	96.5
160	100.5	95	94.5
200	100	96.5	96.5
250	96	95	95
315	103	91	90.5
400	103.5	92	91
500	98.5	91.5	89
630	109.5	95.5	93.5
800	105	95	94
1000	103.5	94	90.5
1250	112	98.5	96
1600	116	103.5	96.5
2000	106.5	96	93.5
2500	108	97.5	93.5
3150	120	110	96
4000	117.5	103.5	92.5
5000	108	97	90
6300	106	97	90.5
8000	103	92	89
10000	100	88.5	86
12500	98.5	86.5	86
16000	89	79.5	86

TABLE 21. ONE-THIRD-OCTAVE FREQUENCY ANALYSIS OF SPL MEASUREMENTS IN CH-47B AIRCRAFT
Hover Operation, Aircraft No. 619109 (db re 0.0002 microbar)

Center Frequency (Hz)	Beneath Forward Rotor Transmission	Above Pilots' Heads	Cargo Compartment Center
20	84.5		85.5
25	101	113	97.5
315	98.5	116	95.5
40	91.5	107	94.5
50	97	107	100.5
63	106	108.5	97.5
80	97	106	94
100	95	104.5	98
125	97	107	99
160	97.5	103.5	92
200	94.5	99	94
250	94.5	96	92.5
315	100	101	93.5
400	100	101	92
500	95.5	98	93
630	98	101	97.5
800	103	103.5	98
1000	100.5	102.5	92
1250	116.5	112.5	97
1600	115	111.5	101
2000	106	102	93.5
2500	110	105	94
3150	115.5	112.5	94.5
4000	107	105.5	92.5
5000	102.5	101	90
6300	101.5	98	90.5
8000	97	92.5	89
10000	93	90	86
12500	91	87.5	86
16000	86.5	85	86

TABLE 22. NARROW-BAND FREQUENCY ANALYSIS OF SPL MEASUREMENTS IN CH-47A AIRCRAFT
Cruise Operation, Aircraft No. 12409 (db re 0.0002 microbar)

Beneath Forward Rotor Transmission		Above Pilots' Heads		Center of Cargo Compartment	
Freq. (Hz)	SPL	Freq. (Hz)	SPL	Freq. (Hz)	SPL
23.5	108	24	98.5	23.5	100
27	93.5	31.8	83	31.5	86
33.1	91.5	48	82	36	89
50	94	69	83	46	84.5
60	101	84	88	60	86.5
84	96	94	87	66	85
120	98	126	85	84	84
155	97.5	144	89	121	86
202	92.5	190	83	162	78
245	91	240	82.5	205	86
410	91	360	78	249	77
570	97	410	82	315	75
840	95	560	76	420	74
1250	105.5	825	80	620	76
1450	101	1250	80	830	78
1560	103	1480	87.5	920	81
2050	95	1560	86	1220	74
2990	104	3020	85	1480	79
3450	109	3560	91	1600	80
3560	111	4450	78	2100	70
3620	107	5400	79	2950	71
3680	105	6600	77	3450	76
4400	98.5	6800	80	3650	76
6800	97	7200	76	4600	68.5
8500	88.5	8585	78 } No Peak	6400	67.5
10500	88	10236	78 } No Peak	6800	65
		13176	78 } No Peak	8400	64
				10236	No Peak
				13176	No Peak

TABLE 23. NARROW-BAND FREQUENCY ANALYSIS OF SPL MEASUREMENTS IN CH-47A AIRCRAFT

Cruise Operation, Aircraft No. 58012 (db re 0.0002 microbar)

Beneath Forward Rotor Transmission		Above Pilots' Heads		Center of Cargo Compartment	
Freq. (Hz)	SPL	Freq. (Hz)	SPL	Freq. (Hz)	SPL
209	102.5	205	98	215	93.5
230	102	260	96	235	94.5
265	98	295	94	280	94
320	97	319	94	320	90.5
350	105	365	92.5	410	92
400	101	415	93	700	91.5
500	98	600	91	860	93
670	110	640	92.5	1140	90
730	107	680	93	1250	91
800	105	790	92	1480	94
1150	107	890	91	1550	98.5
1210	110	1210	96	2150	91
1560	122	1440	106	2610	88.5
2020	103	1950	107	2950	93
2850	112	2020	92	3500	93.5
3000	110	3100	104	3620	90
3400	125	3450	109	3850	89
3420	110	4500	97	5000	86.5
4400	109	6800	89	6400	90
5000	105	1500	88	6600	87.5
6400	103.5	10400	86	6900	85
6800	103	11900	83	8450	81
7900	102				
10500	99				
12000	98				

TABLE 24. NARROW-BAND FREQUENCY ANALYSIS OF SPL MEASUREMENTS IN CH-47B AIRCRAFT

Cruise Operation, Aircraft No. 619109 (db re 0.0002 microbar)

Beneath Rotor Transmission		Above Pilots' Heads		Center of Cargo Compartment	
Freq. (Hz)	SPL	Freq. (Hz)	SPL	Freq. (Hz)	SPL
22.5	113.5	200	93	215	92.5
33	102	220	97.5	225	88
34.5	106	235	96	255	88
203	99	255	98	291	88
235	99	360	95	330	87
255	96	460	92	395	92
335	100.5	540	89.5	440	90
350	102	680	89.5	610	96.5
410	100	800	93.5	640	95
650	96	990	92	660	90.5
810	104	1220	92	770	90.5
1000	103	1420	103	795	90
1190	105	2000	89	840	92
1450	120	2150	88.5	980	87
2020	100.5	2800	98.5	1190	93
2250	100	2950	99.5	1390	98
3300	111	4100	92	1650	91
4300	102	6300	87	2000	91.5
5800	98	6700	86	2450	89.5
6500	98	8500	87	2900	95
7000	96			3400	99.5
8100	93			4400	87.5
10200	92			6600	84
10700	90			8400	84
12500	89			14200	78

TABLE 25. NARROW-BAND FREQUENCY ANALYSIS OF SPL MEASUREMENTS IN CH-47A AIRCRAFT
Hover Operation, Aircraft No. 12409 (db re 0.0002 microbar)

Beneath Forward Rotor Transmission		Above Pilots' Heads		Center of Cargo Compartment	
Freq. (Hz)	SPL	Freq. (Hz)	SPL	Freq. (Hz)	SPL
23	108	23.5	101	24	99
27	100.5	25.5	103.5	25	92
36	105.5	37	92.5	31.5	83
46	102	40	82	36	92
60	103	49	90.5	47	94
70	104	64	83.5	60	89.5
83	103.5	83	95	69	84
120	108	120	93	105	90
162	95	158	87	120	91
208	96.5	215	89.5	179	87
249	97	250	85	205	885.
315	95	310	84	242	88
410	106.5	410	90	308	80
570	110	550	93.5	415	85.5
685	104	830	90	470	80
830	104	1230	92	635	79.5
1280	110	1580	95.5	820	83.5
1510	109.5	2030	86.5	865	90
1580	120	3100	95	1260	83
2100	102	3500	103.5	1485	88
2950	109.5	4350	87	1540	92
3500	114.5	6700	83	3000	82
4400	106	7000	86	3500	88
6600	102	8500	No Peak	4600	79
6900	104	10236	No Peak	6700	75
8100	95	11850	90	6800	74.5
10700	95	12000	87		

TABLE 26. NARROW-BAND FREQUENCY ANALYSIS OF SPL MEASUREMENTS IN CH-47A AIRCRAFT
Hover Operation, Aircraft No. 58012 (db re 0.0002 microbar)

Beneath Forward Rotor Transmission		Above Pilots' Heads		Center of Cargo Compartment	
Freq. (Hz)	SPL	Freq. (Hz)	SPL	Freq. (Hz)	SPL
22.5	101	23.5	110	22	100
27	102.5	24.5	103	25	98
46	99	31	91	31	82
69	103.5	41	93	40	83
81	93.5	50	94	47	100.5
120	97	64	94	63	88
161	100	68	102.5	72	95
215	97	80	100	80	88
312	96	125	94	119	86
360	100	165	89	140	94
400	100	210	92	205	94
520	98	254	92.5	270	96
690	111	310	92	310	88
812	98	410	91	410	90
1200	108	520	89	620	88
1480	118	825	90	800	89
1550	114	1200	98	860	96
3000	116	1500	105.5	1220	93
2400	122	2450	103	1510	99
3500	125	3100	105	2150	95
4500	111	3500	111	3000	94
6580	103.5	3850	102.5	3400	94
8585	98	4500	97	4500	87
10400	98	6600	91	6600	81
12203	102	6800	92	6800	82.5
13200	94	8500	86	8400	78
		10500	86	10236	Off Graph
		13000	Off Graph		

TABLE 27. NARROW-BAND FREQUENCY ANALYSIS OF SPL MEASUREMENTS IN CH-47B AIRCRAFT
Hover Operation, Aircraft No. 619109 (db re 0.0002 microbar)

Beneath Forward Rotor Transmission		Above Pilots' Heads		Center of Cargo Compartment	
Freq.(Hz)	SPL	Freq.(Hz)	SPL	Freq.(Hz)	SPL
23	106	22.5	107.5	22.5	100
26.5	93	32	100	25.5	95
33.5	97.5	34	105	31	99
43	88	46	102	45	99
46	95	56	100.5	63	97
60	105	71	98	80	94.5
68	104	78	103.5	200	92
91	96.5	100	96.5	400	90
124	96	123	97	590	98
155	96	159	88.5	800	92
225	93.5	200	86.5	1230	93
255	94.5	250	83	1480	98.5
405	95	350	92	2000	90.5
590	95	410	89.5	2950	95
640	97	540	89	3500	96
795	101	650	89.5	4350	90
1230	106	812	91	6700	86
1420	121	1200	96		
1580	112	1470	104		
2950	111	2000	89		
3000	110.5	2967	98		
4400	104	3300	102.5		
6700	100.5	4450	91		
6820	98	6600	84.5		
8650	94	6900	83		
10200	89.5	8600	79		
13000	89	10200	76		
		13100	75		

TABLE 28. MEASURED VIBRATION LEVELS DURING CRUISE OPERATION ON THREE CH-47 HELICOPTERS

Accelerometer Location	Acceleration (db)		
	Aircraft No. 12409	Aircraft No. 58012	Aircraft No. 619109
Ring Gear (78.1 db = 1g at 1 kHz)	111.5	112.5	120.5
Sump (78.75 db = 1g at 1 kHz)	No Measurement	123.5	124.0
Support Arm (78.0 db = 1g at 1 kHz)	101.0	100.5	120.0
Structure (77.75 db = 1g at 1 kHz)	100.0	100.5	119.5

TABLE 29. TABULATED ONE-THIRD-OCTAVE FREQUENCY ANALYSIS OF IN-FLIGHT VIBRATION MEASUREMENTS FOR CH-47A HELICOPTER, CRUISE OPERATION, AIRCRAFT NO. 12409

Band Midpoint Freq. (Hz)	Acceleration (db) (Referenced to respective accelerometer thresholds)			
	1	2	3	4
	Ring Gear	Sump	Support Arm	Structure
200	75.5		65.5	64.5
250	76		66	65
315	76.5		66	65
400	82.5		72.5	74.5
500	79		73	69
630	81		73.5	81.5
800	82		79.5	88
1000	84.5		78.5	79.5
1250	94.5		91.5	94
1600	99		91.5	95.5
2000	93		78.5	83.5
2500	96		82	84
3150	107		95	90.5
4000	104.5		90.5	83.5
5000	103		89.5	83.5
6400	104		96	87
8000	102		91	81
10000	99		88.5	79
12500	99.5		87	72.5
16000	94		84.5	65.5

TABLE 30. TABULATED ONE-THIRD-OCTAVE FREQUENCY ANALYSIS OF IN-FLIGHT VIBRATION MEASUREMENTS FOR CH-47A HELICOPTER, CRUISE OPERATION, AIRCRAFT NO. 58012

Band Midpoint Freq. (Hz)	Acceleration (db) (Referenced to respective accelerometer thresholds)			
	1	2	3	4
	Ring Gear	Sump	Support Arm	Structure
200	80	84	66	64
250	88.5	84	66.5	64.5
315	80.5	84	67	67
400	81.5	85	69	84
500	81.5	84	68.5	75
630	86.5	84	78	78
800	84.5	84.5	76	79
1000	85.5	86	77.5	84
1250	92	91.5	89.5	95
1600	102	92.5	91.5	95.5
2000	91	89.5	77.5	88.5
2500	96.5	100.5	83.5	87.5
3150	106.5	121	91.5	90.5
4000	103.5	112	91.5	85
5000	105	104.5	91.5	85.5
6400	105.5	102	95	83
8000	102.5	100.5	92	85
10000	100	103.5	90.5	87.5
12500	106	103.5	91.5	87
16000	95.5	95.5	87	72.5

TABLE 31. TABULATED ONE-THIRD-OCTAVE FREQUENCY ANALYSIS OF IN-FLIGHT VIBRATION MEASUREMENTS FOR CH-47B, CRUISE OPERATION, AIRCRAFT NO. 619109

Band Midpoint Freq. (Hz)	Acceleration (db) (Referenced to respective accelerometer thresholds)			
	1	2	3	4
	Ring Gear	Sump	Support Arm	Structure
200	85.5	83.5	84.5	86.5
250	85.5	83.5	84.5	86.5
315	86.5	83.5	85	84
400	88.5	84	88.5	88.5
500	89	84	87.5	93
630	88.5	84	92	113.5
800	92.5	85	95.5	116.5
1000	93	86.5	96.5	94.5
1250	104.5	95.5	114.5	102
1600	113	99.5	114	107.5
2000	100	89	97	97
2500	108	103	105.5	102.5
3150	114	123.5	111	108
4000	113	111.5	108.5	102
5000	112	107.5	107.5	100.5
6400	112	105	110.5	100
8000	109	101	106.5	99
10000	108	102	106	100
12500	111.5	103.5	107.5	100.5
16000	104.5	95	104	89.5

APPENDIX II

TRANSMISSION CASING STRUCTURAL RESPONSE

INTRODUCTION

In the acoustic analysis of the CH-47 rotor transmission, noise predictions were based in part upon the use of two empirical factors, one representing the conversion of mechanical vibration energy to acoustic energy, and the second representing the "amplifier" characteristics of the transmission casing and its surroundings. In this situation, it is imperative that an assessment be made of the tendencies, if any, of the transmission casing to act nonuniformly as an amplifier at any frequencies within the range of interest (200-1000 Hz) due to peculiar resonances of the transmission itself. Any such tendencies will result in distorted predicted noise spectra unless they are properly accounted for in the analysis. In this study, which was directed toward this accounting, the general vibratory behavior of the casing was examined. No detailed study was made of individual resonances and their resulting mode shapes.

VIBRATION TESTS

A Vertol CH-47 forward rotor transmission (Serial No. A7-4) was utilized for this study of casing structural response. The purpose of the tests was to subject the transmission to externally imposed constant force level vibrations over a frequency range of 200-1000 Hz while recording the maximum acceleration levels of the structure at predetermined locations. The instrumentation utilized in the tests is shown in Figure 68. An MB model 1500 shaker was used as the excitation source and a force gage mounted on the shaker was calibrated to provide a constant input force. The transmission and shaker were suspended from cables as shown in Figures 69 and 70. Aluminum blocks were bonded to the transmission casing with an epoxy adhesive for attachment of the shaker push-rod and accelerometers.

Three different locations were used for exciting the transmission: the input bearing housing, the ring gear housing and the output bearing housing. Five crystal-type accelerometers, located as follows, recorded transmission vibration levels:

1. Output shaft bearing housing (normal to shaft output center line).
2. Ring gear housing (normal to output shaft center line).
3. Support arm (parallel to output shaft center line).
4. Tower casing (left side normal to casing).
5. Input vibration block (location varied with location of shaker).

At each excitation location of the shaker, the vibrational frequency was varied from 200 to 10,000 Hz and the maximum amplitude and its corresponding frequency at each accelerometer location were recorded. In addition, while exciting the transmission at the input shaft bearing location (left side), the sound pressure level on the right side at the sump area was recorded over the excitation frequency range. This was accomplished with the microphone oriented both perpendicular and parallel to the lower case sump wall.

In addition, a separate set of tests was conducted with the shaker located at the input bearing. Hand-held probes were applied to a large number of points on the transmission casing with constant-force, constant-vibrational frequency excitation to determine the location of the maximum acceleration. The frequencies utilized were the computed gear meshing frequencies. The following results were obtained:

Drive Frequency (Hz)	Vibration Amplitude (db)	
406	60 Sump:	Right Side-Center
812	60 Sump:	Bottom Near Drain Valve
1220	70 Sump:	Left Side-Center Between
1482	70 Sump:	Bottom Between Valve and Drain
2962	80 Sump:	Halfway Up Right Side, 2 in. from rear
3412	80 Sump:	Bottom Right Rear Near Drain Valve
4446	80 Rib:	Left Side Lower Housing
4446	80 Sump:	Front Wall Near Top
4446	80 Sump:	Bottom Near Drain Valve
6588	60 Sump:	Front Wall Near Top
8585	60 Sump:	Right Side Center, 3 in. from back

STRUCTURAL RESPONSE MEASUREMENTS

Maximum accelerometer measurements and their associated frequencies are presented in Table 32 for excitation at the input bearing, in Table 33 for excitation at the ring gear housing, and in Table 34 for excitation at the output bearing housing. Plots of these results are shown in Figures 71, 72, and 73.

Plots of vibration response at the drive block for various excitation locations are shown in Figure 74 (acceleration) and in Figure 75 (displacement). Response of the lower casing with excitation in various locations is presented in Figure 76.

Before the plotted results are discussed, the format of these curves will be explained. Although they appear very similar to third-octave plots of noise and vibration measurements, there are basic differences. Each measurement was made with excitation at a single, discrete frequency. Hence, the response recorded is for that frequency only, and, unlike the third-octave measurements, does not show the combined effect with response at other frequencies, adjacent or otherwise. The line segments connecting the recorded points merely show that the connected points came from the same accelerometer. The individual frequencies used for measurement were those at which local resonances occurred.

Figures 71, 72, and 73 compare the casing response at the drive point to the response at the other accelerometer locations. The measurements at these non-driving-point locations all show certain common characteristics. The response plots follow the response at the driving points, but at levels of 15 to 30 db lower. The shapes of the response curves are very similar to the higher response curves.

Figure 74 compares the response just alongside the excitation for the three different driving points. Although the driving points are widely separated on the gearbox, and the casing construction at each point is quite different, the three sets of results show strong similarities. In general, they all start from 3000 Hz and then drop off slightly until the highest frequency measure, 10,000 cycles, is reached. The nearly matching response curves would seem to indicate that despite apparent case construction differences, there is an overriding similarity throughout the casing as far as dynamic response is concerned.

There are no isolated frequencies at which all the curves show a common maximum response. For example, at 4400 Hz the ring gear response is at its highest level but the response at the input bearing is about 4 db below its highest and the response at the output bearing is about 8 db below its highest. If all three locations were excited simultaneously, as might be expected in the operating gearbox, it is quite likely that the composite response at each of the frequencies would be less variable than the individual responses are shown to be. The overall effect of casing resonance at the drive points therefore appears to be fairly uniform, at least in the frequency range above 2000 Hz. This range, incidentally, includes those frequencies previously demonstrated to have the major gear noise components.

Examination of Figures 71, 72, and 73 tends to reinforce the conclusion stated after study of Figure 74 that a composite response with excitation at all locations has no isolated resonance, and that the many individual resonances tend to combine to give a more or less uniform response at frequencies above 2000 cycles. The relationship between the response at the nondriving locations to that at the drive points leads to some additional conclusions. Although the excitation force is applied in a fairly restricted area, its effect is felt throughout the casing. The response at the other locations may be 20 or 30 db lower than that at the drive point, but this reduction may be more than offset by the larger surfaces involved. Another conclusion derives from the similarity in the response of the base, in its variation from frequency to frequency, to that of the portion of the structure where the driving force is applied. This similarity suggests that it is the resonance in the drive point structure, rather than in the connecting structure or the base itself, which determines the general character of the overall response of the gearbox casing.

Figure 75, in which the acceleration readings of Figure 74 have been converted to amplitudes, tends to confirm the foregoing conclusion that no isolated overall casing resonance exists in the frequency range of interest.

Figure 76 shows that the acceleration response as measured on the lower casing pickup point is relatively insensitive to the location of the drive force up to about 3000 Hz, with increasingly larger differences between recorded values between 3000 and 10,000 Hz.

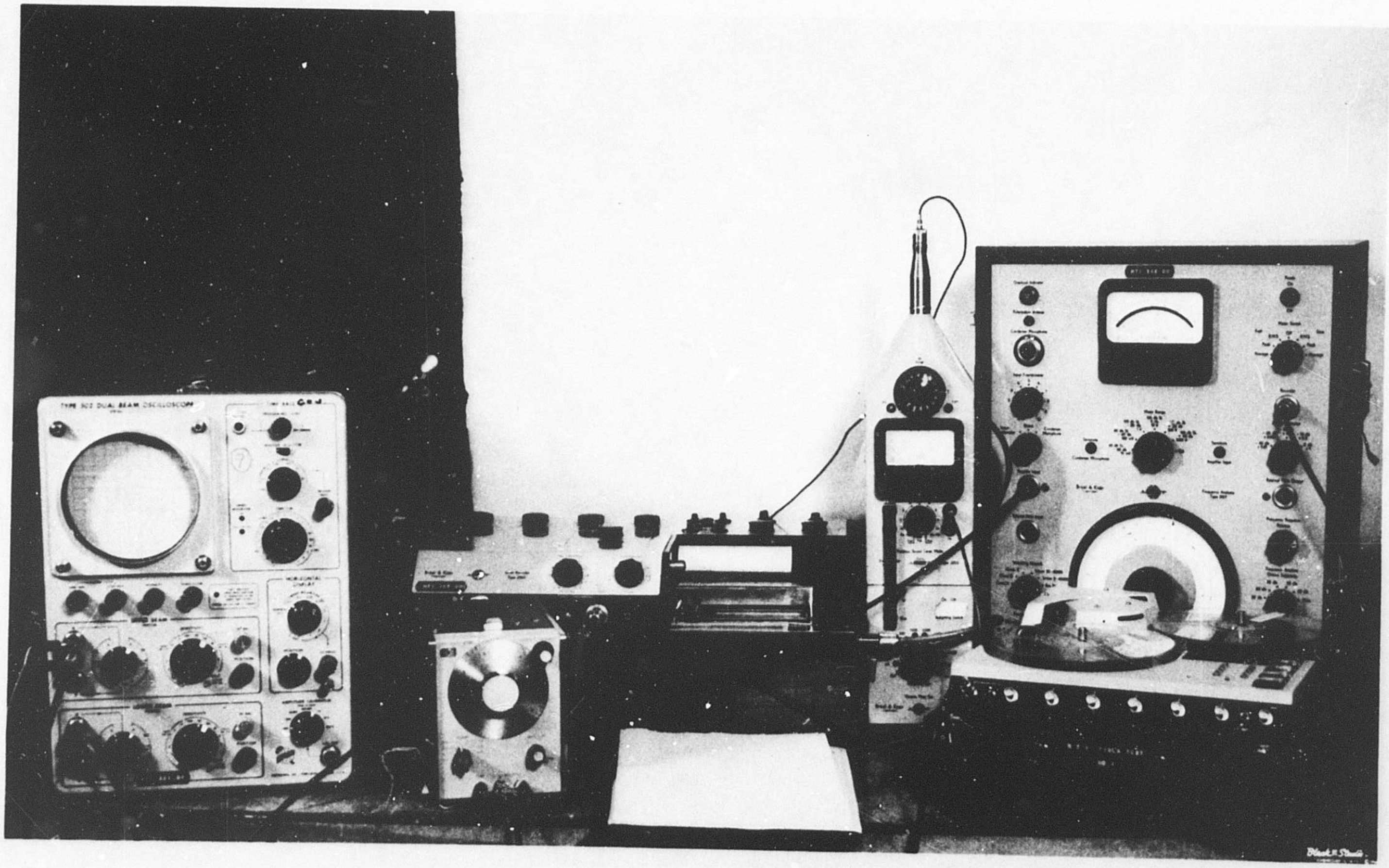

Figure 68. Instrumentation for Transmission Casing Resonance Study.

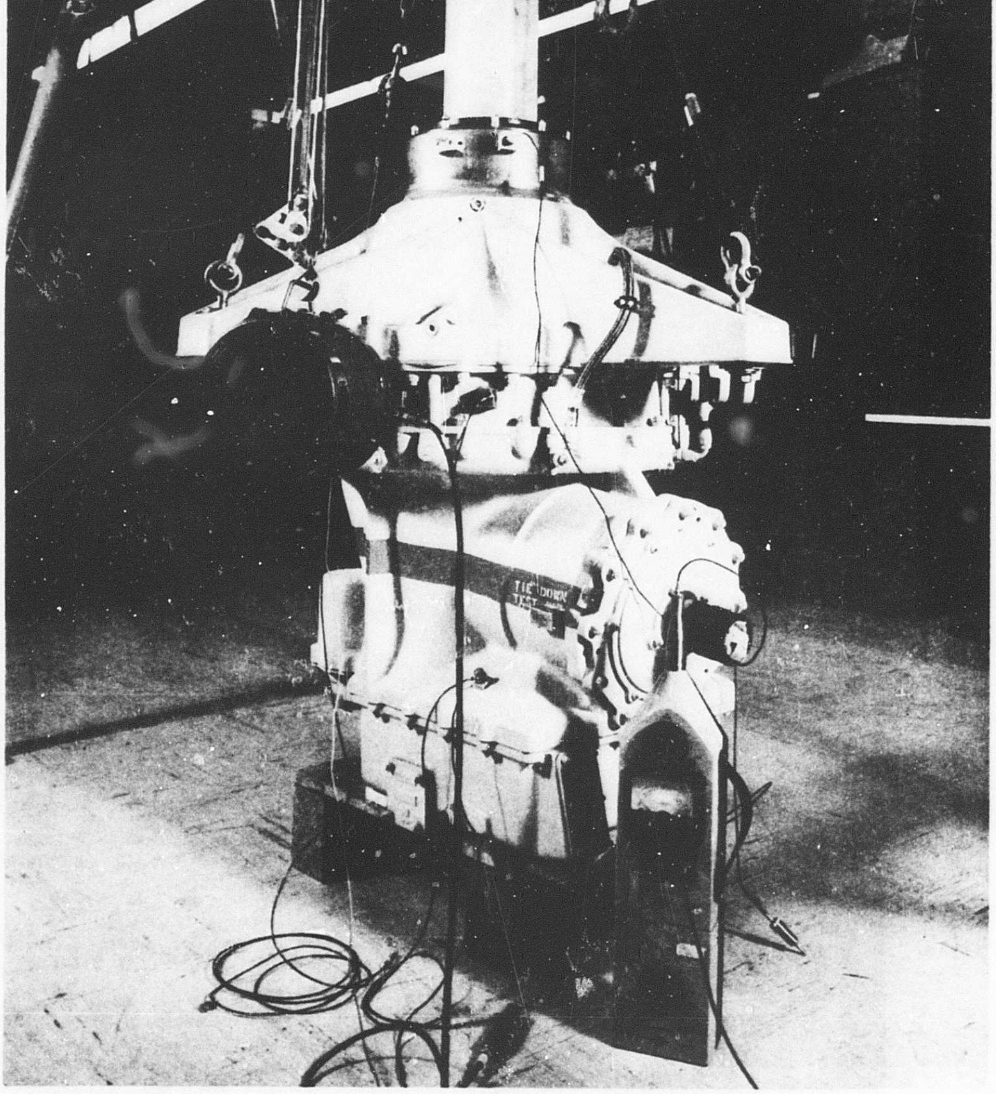

Figure 69. Experimental Setup for CH-47 Transmission Casing Resonance Study.

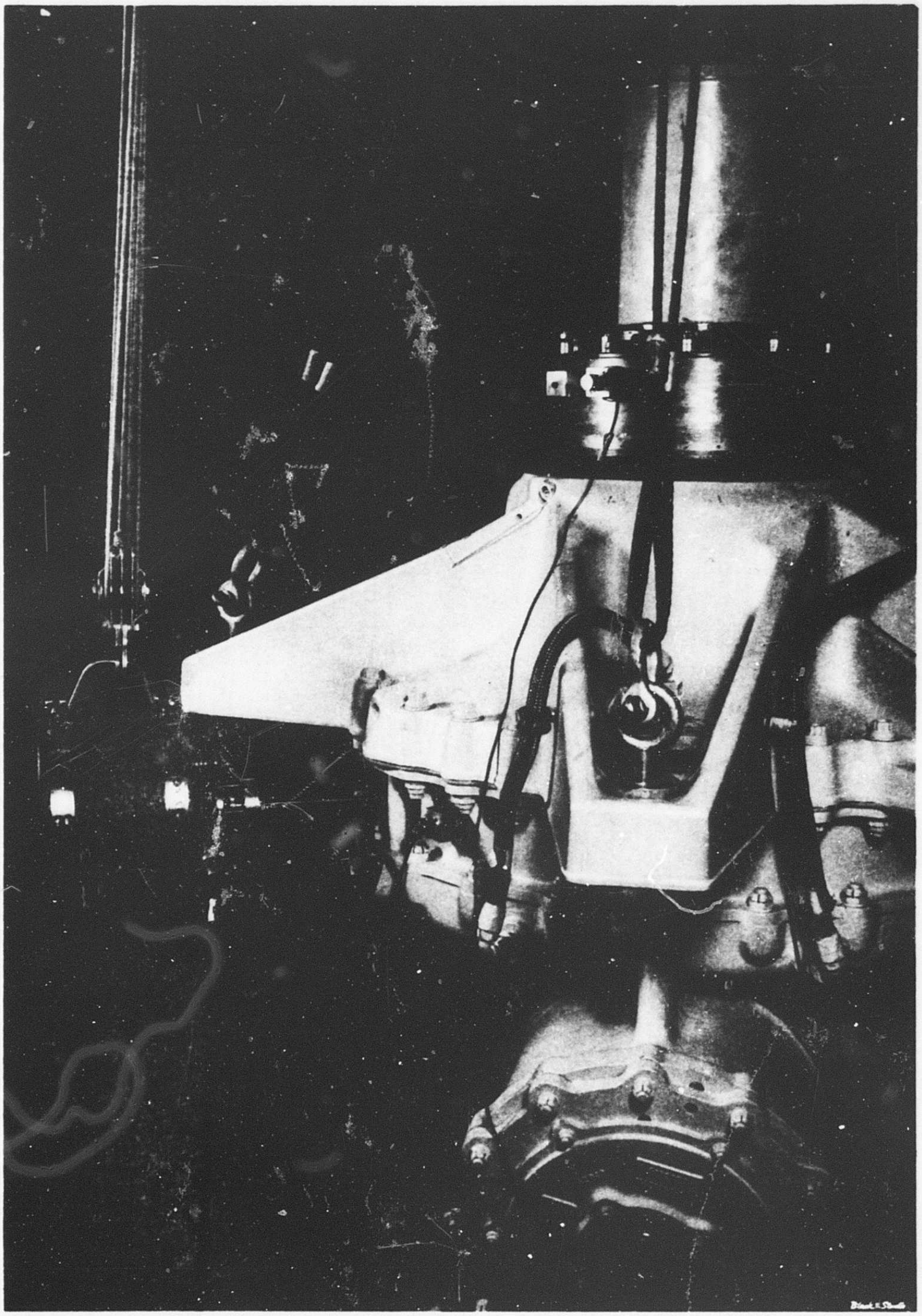

Figure 70. Experimental Setup - Detail of Shaker Connection.

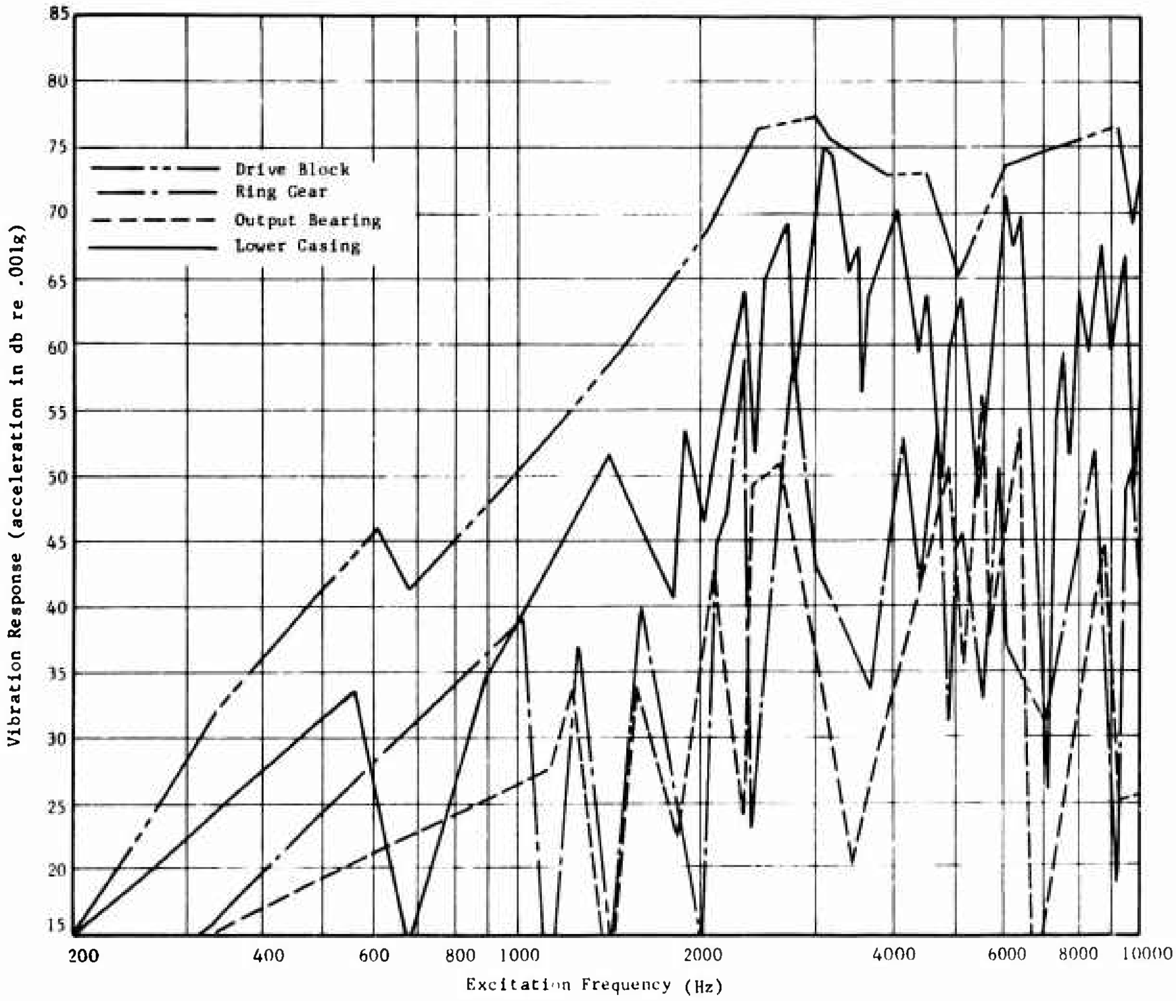

Figure 71. Casing Resonance Vibration at Various Locations - Excitation at Input Bearing Housing = 3.95 Lb.

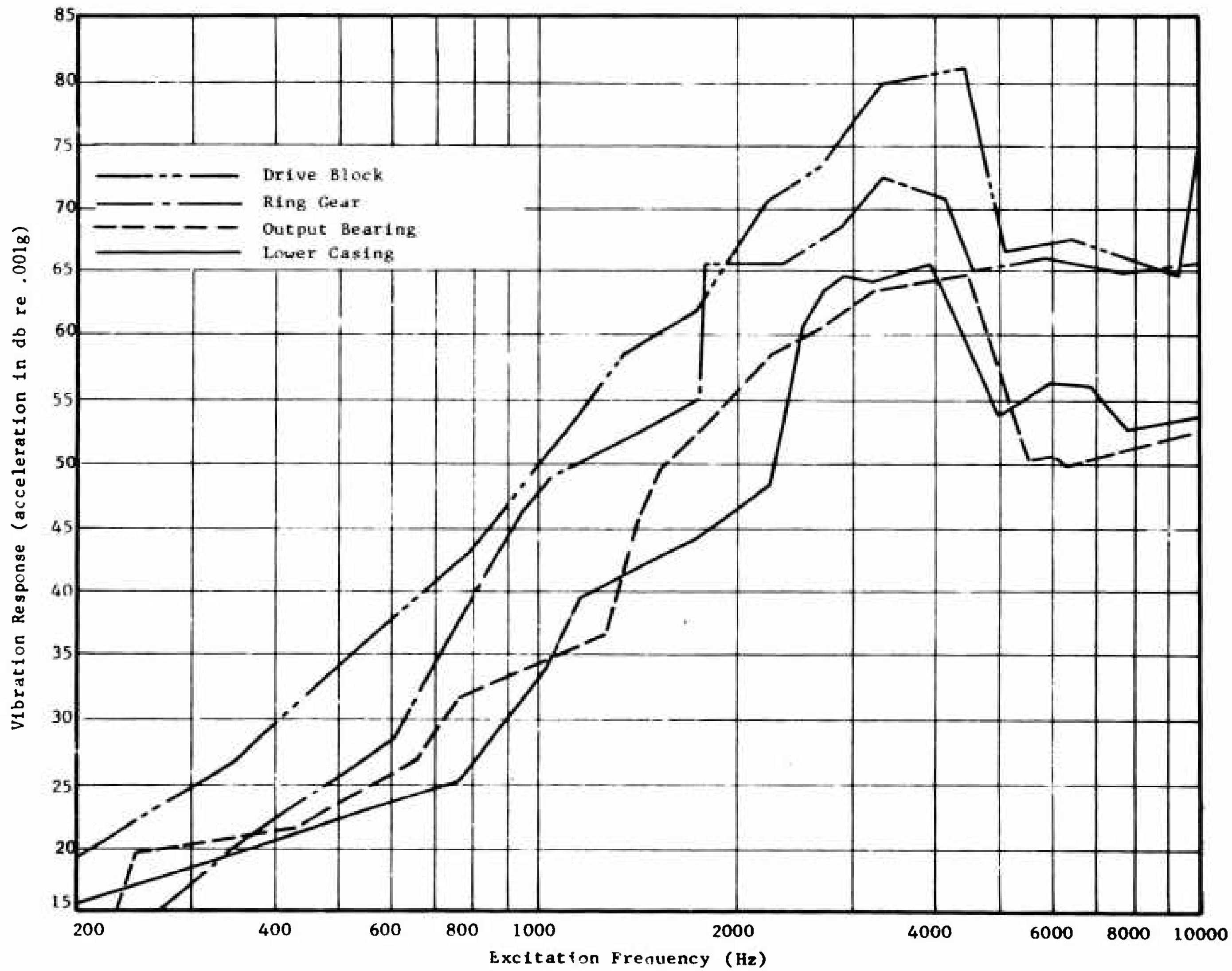

Figure 72. Casing Resonance Vibration at Various Locations - Excitation at Ring Gear = 3.95 Lb.

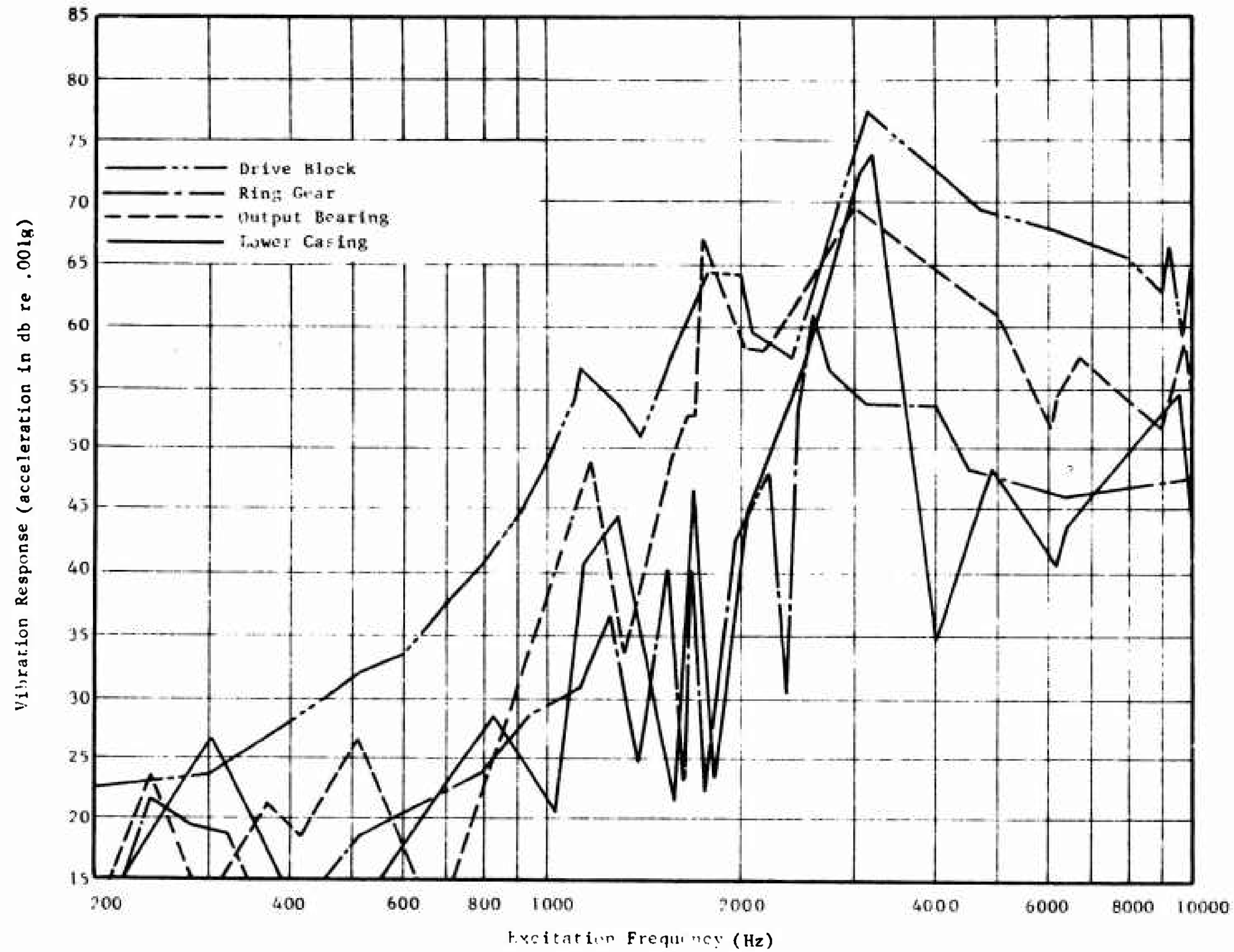

Figure 73. Casing Resonance Vibration at Various Locations - Excitation at Output Bearing.

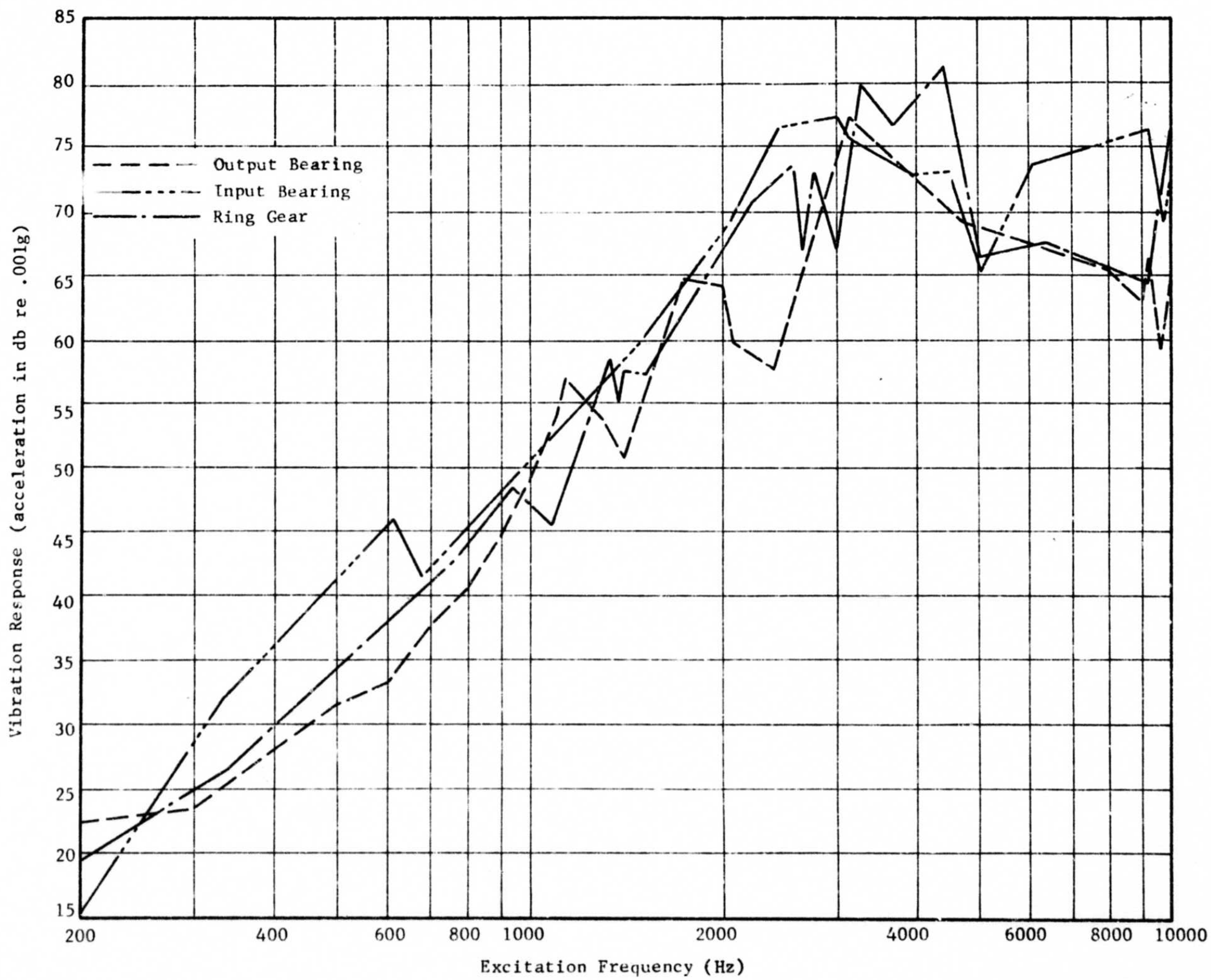

Figure 74. Casing Resonance Excitation at Various Locations - Pickup at Drive Block.

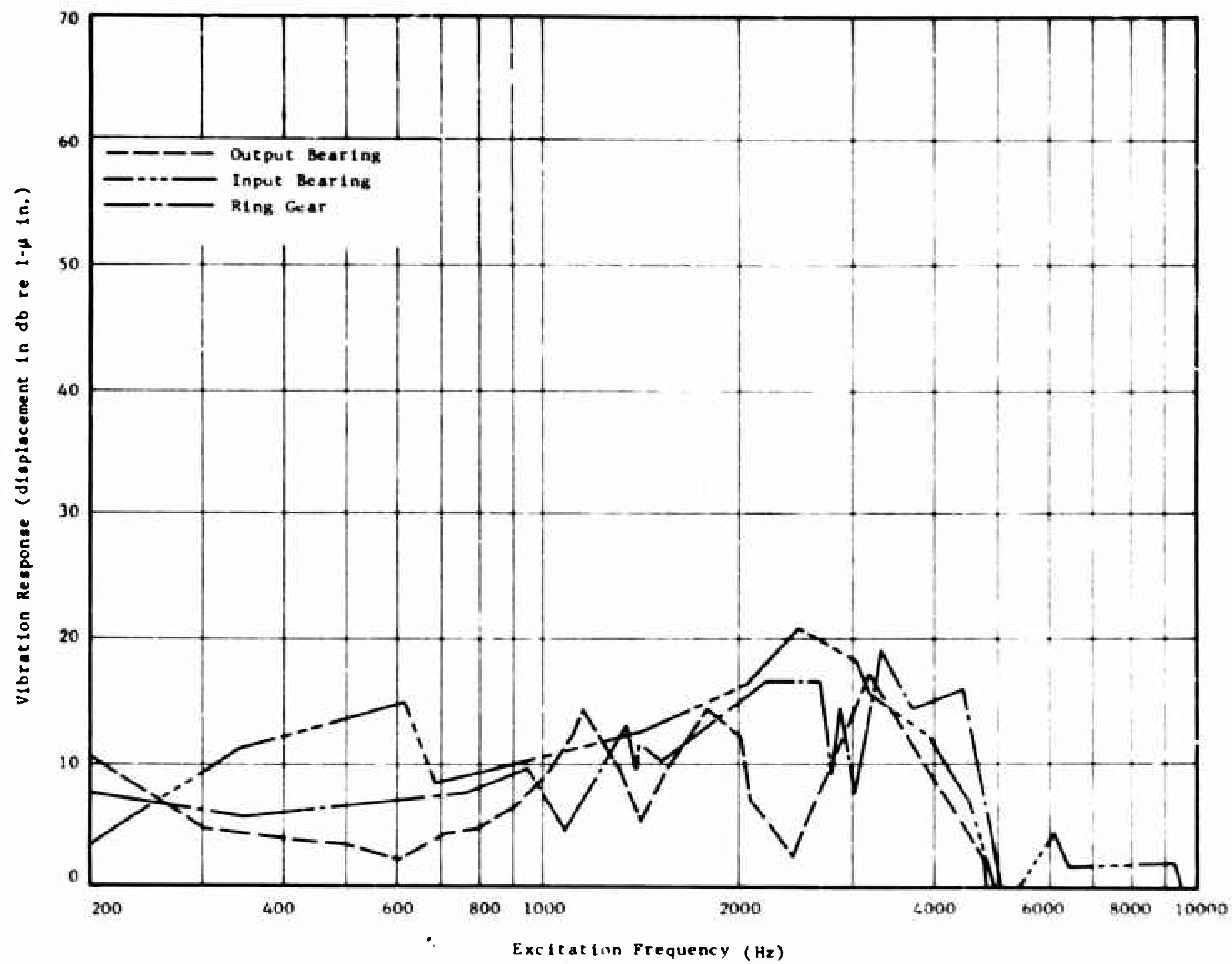

Figure 75. Casing Resonance Excitation at Various Locations - Pickup at Drive Block.

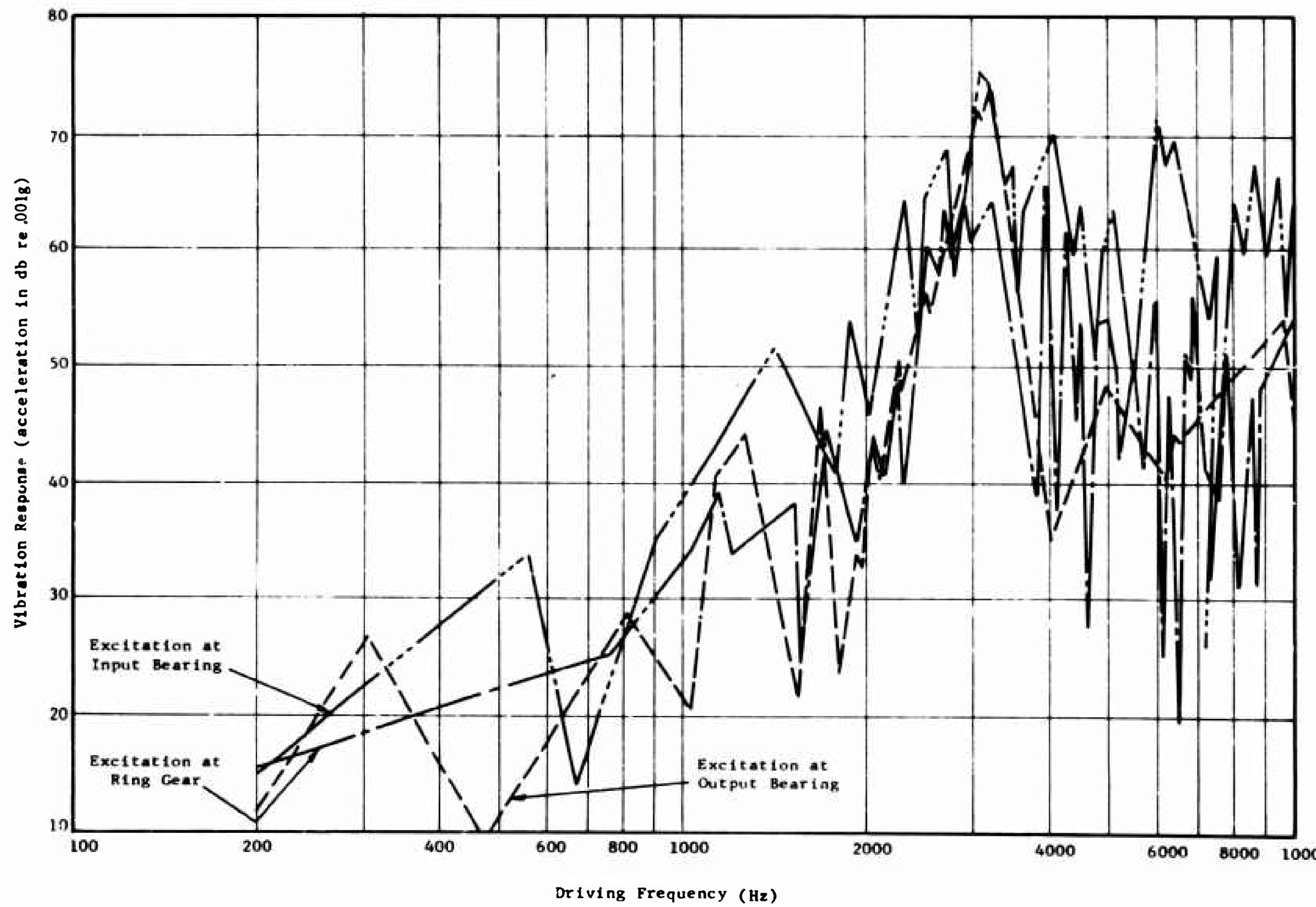

Figure 76. Lower Casing Acceleration Versus Frequency of Excitation With Excitation Location as Indicated.

TABLE 32. MEASURED CASING RESPONSE
Excitation Applied to Input Bearing Housing
Acceleration in db (re 0.001g)

Drive Block		Ring Gear		Output Bearing		Mount. Arm		Lower Casing	
Freq (Hz)	Accel (db)	Freq (Hz)	Accel (db)	Freq (Hz)	Accel (db)	Freq (Hz)	Accel (db)	Freq (Hz)	Accel (db)
200	15.2	200	6.2	200	1.12	333	28.4	200	15.2
335	32.0	333	16.0	380	16.6	435	9.40	356	25.6
610	46.0	950	37.8	1140	27.8	670	29.6	560	33.6
680	41.3	1020	39.8	1230	33.6	1050	39.0	680	14.0
1490	59.7	1120	6.20	1435	9.90	1115	33.8	900	34.8
2040	69.0	1260	37.0	1570	33.8	1230	38.7	1418	51.6
2430	76.5	1415	13.0	1830	22.4	1450	6.45	1800	40.8
3000	77.4	1630	39.6	2100	43.0	1950	2.40	1880	53.8
3150	75.8	2050	14.0	2320	24.2	2400	46.4	2020	46.4
3900	73.0	2120	45.0	2400	49.0	2550	18.0	2340	64.1
4500	73.1	2200	47.0	2680	50.9	2650	42.5	2430	52.2
5050	65.2	2320	58.9	3450	20.5	2720	23.2	2500	64.5
6050	73.5	2400	23.0	4900	50.9	2850	42.0	2720	69.1
6400	74.2	2800	59.6	5200	35.6	2950	25.5	2800	57.3
9250	76.5	3000	43.0	5550	56.0	3300	41.0	3090	75.2
9750	69.1	3700	33.8	5700	37.8	3500	25.0	3200	74.4
10000	73.3	4150	52.6	6400	53.5	4050	46.8	3375	65.6
		4400	41.8	7300	6.5	4200	11.9	3500	67.5
		4680	54.0	8800	44.8	4660	44.3	3560	56.6
		4900	31.4	9300	25.2	4800	29.7	3630	63.4
		5000	44.6	10000	25.9	5000	43.2	4050	70.3
		5160	45.6			5200	30.8	4350	59.4
		5600	33.0			5350	41.4	4500	63.9
		5900	50.4			5700	43.7	4750	50.0
		6100	37.2			6200	44.9	4900	59.6
		7100	31.0			6400	20.3	5100	63.8
		8500	52.5			8800	41.8	5500	48.1
		9200	19.0			10000	33.2	6040	71.3
		9500	49.0					6200	67.5
		9700	50.8					6420	69.8
		10000	40.8					7200	26.0
								7350	54.2
								7500	59.6
								7700	51.4
								8000	64.1
								8300	59.6
								8700	67.7
								9000	59.6

TABLE 32 - Continued									
Drive Block		Ring Gear		Output Bearing		Mount. Arm		Lower Casing	
Freq (Hz)	Accel (db)	Freq (Hz)	Accel (db)	Freq (Hz)	Accel (db)	Freq (Hz)	Accel (db)	Freq (Hz)	Accel (db)
								9500 9800 10000	66.8 49.2 59.0

TABLE 33. MEASURED CASING RESPONSE
Excitation Applied to Ring Gear Housing
Acceleration in db (re 0.001g)

Drive Block		Ring Gear		Output Bearing		Mount. Arm		Lower Casing	
Freq (Hz)	Accel (db)	Freq (Hz)	Accel (db)	Freq (Hz)	Accel (db)	Freq (Hz)	Accel (db)	Freq (Hz)	Accel (db)
200	19.4	200	9.4	200	3.2	200	6.9	200	15.6
340	26.5	245	12.9	244	19.6	347	25.6	760	25.1
760	42.8	345	20.0	425	21.4	510	14.6	1030	34.0
940	48.6	600	28.4	520	20.0	680	34.3	1150	39.5
1080	45.7	940	46.4	755	31.6	760	37.5	1200	33.7
1340	58.3	1050	49.2	950	33.4	920	31.4	1540	39.4
1370	55.0	1180	15.6	1000	33.0	1030	43.0	1650	24.6
1400	57.5	1340	45.6	1200	36.5	1080	37.9	1710	44.4
1515	57.3	1600	48.3	1400	46.0	1140	45.0	1940	34.8
2200	70.5	1710	44.6	1520	49.6	1590	24.0	2070	44.1
2660	73.5	1780	65.7	1670	48.2	1775	40.0	2130	40.8
2760	67.0	2320	65.7	1800	49.6	2080	29.4	2240	48.6
2880	73.0	2880	68.4	1900	52.9	2290	53.7	2290	40.0
3000	67.0	3300	72.6	2230	58.3	2400	45.0	2500	60.4
3300	79.9	4100	70.9	2500	47.2	2670	55.6	2610	57.6
3700	76.8	4400	54.7	2680	60.2	2800	48.1	2700	63.4
4400	81.2	5000	58.4	2900	49.6	2900	51.8	2790	59.5
5050	66.4	5800	66.0	3000	60.9	3140	44.8	2900	64.6
6400	67.5	6200	59.5	3200	63.2	3300	61.0	2970	60.6
9200	64.5	7200	51.1	3850	51.8	3500	52.5	3210	64.1
10000	75.9	7600	64.8	4050	59.4	3700	63.6	3800	39.0
		8000	54.5	4450	64.5	4400	32.2	3910	65.3
		10000	65.6	4900	53.1	5500	53.5	3970	62.5
				5000	25.6	6200	52.6	4000	64.1
				5500	50.1	6900	35.0	4130	37.7
				6000	50.6	7200	52.0	4250	61.7
				6250	50.0	8200	35.0	4400	45.2
				6600	44.5	8700	50.0	4450	53.9
				7600	39.0	9200	27.6	4620	27.2
				10000	52.9	9500	49.7	4730	53.5
						9700	35.0	4970	54.0
						10000	48.7	5130	49.6
								5200	43.1
								5500	50.7
								5650	41.3
								5920	56.4
								6100	25.1
								6250	48.7
								6500	19.6
								6600	51.3
								6750	48.6

TABLE 33 - Continued

Drive Block		Ring Gear		Output Bearing		Mount.Arm		Lower Casing	
Freq (Hz)	Accel (db)	Freq (Hz)	Accel (db)	Freq (Hz)	Accel (db)	Freq (Hz)	Accel (db)	Freq (Hz)	Accel (db)
								6800	56.1
								7180	41.3
								7520	38.7
								7610	40.2
								7750	53.0
								8100	31.0
								8550	47.7
								8700	31.1
								8750	48.0
								10000	54.1

TABLE 34. MEASURED CASING RESPONSE
Excitation Applied to Output Bearing Housing
Acceleration in db (re 0.001g)

Drive Block		Ring Gear		Output Bearing		Mount. Arm		Lower Casing	
Freq (Hz)	Accel (db)	Freq (Hz)	Accel (db)	Freq (Hz)	Accel (db)	Freq (Hz)	Accel (db)	Freq (Hz)	Accel (db)
200	22.3	200	8.9	200	8.25	200	11.0	200	11.8
300	23.4	243	21.5	242	23.5	242	22.2	303	26.7
400	28.0	280	19.5	295	13.1	287	15.6	485	8.8
500	31.6	320	18.8	370	21.0	350	29.0	825	28.6
600	33.2	405	7.0	415	18.8	405	21.6	1030	20.4
700	37.8	510	18.4	510	26.6	535	30.9	1140	40.4
800	40.8	775	23.8	665	13.0	758	35.7	1270	44.2
900	44.4	940	28.8	1165	49.0	900	26.3	1560	21.3
1000	49.0	1120	31.0	1325	33.6	1135	47.9	1680	46.6
1100	54.0	1250	36.6	1650	52.7	1230	40.2	1810	23.4
1137	56.8	1380	24.6	1700	52.7	1380	23.8	1925	33.5
1300	53.6	1540	40.1	1750	67.0	1480	37.6	2030	44.4
1400	51.0	1630	23.2	1900	61.9	1610	15.9	2260	50.4
1520	56.4	1680	40.1	2030	58.3	1720	36.8	2500	56.6
1775	64.4	1760	22.2	2160	58.1	1870	27.6	3060	72.2
2000	64.2	1860	33.0	2280	59.3	2280	52.4	3200	73.8
2070	59.6	1950	42.4	3000	69.7	2520	48.2	4000	34.6
2400	57.7	2200	48.2	5000	61.0	2700	57.1	4900	48.3
3150	77.2	2350	30.8	6050	51.8	2850	46.5	6150	40.7
4750	69.2	2440	53.0	6200	54.7	3920	38.7	6400	43.6
		2600	61.2	6700	57.6	5000	32.1	9600	54.3
6200	67.6	2780	56.6	9000	51.6	6000	42.2	10000	44.8
8000	65.5	3150	53.8	9750	58.6	7800	11.9		
9000	63.0	4000	53.7	10000	55.0	9000	37.0		
9250	66.2	4500	48.2			9500	51.8		
9700	59.2	6400	46.0			10000	33.8		
10000	65.0	10000	47.5						

APPENDIX III

CALCULATION OF EXCITATION OF FORWARD ROTOR TRANSMISSION SPIRAL BEVEL GEAR MESH

SUMMARY AND EXPLANATION OF ANALYSIS

This analysis is based on the assumption that the spiral bevel gear torsional excitation approximates a rectangular wave in form, as shown in Figure 77, in which the instantaneous lag of the driven gear behind its position for true conjugate action is plotted versus the fraction of gear rotation over a single tooth mesh cycle.

The start of the single tooth mesh cycle is taken at the position when the tooth section of midface width is in contact at its pitch point.

From the Fourier analysis of this wave, omitting consideration of phase, coefficients may be derived as follows:

$$A_o = b_1 - h(b_1 - b_2) \tag{1}$$

$$A_1 = \frac{2}{\pi}(b_1 - b_2)\sin h\pi \tag{2}$$

$$A_2 = \frac{1}{\pi}(b_1 - b_2)\sin 2h\pi \tag{3}$$

(A_o here signifies the mean value which is half of the values given in the output of the gear excitation computer program GEARO.)

It is further assumed that this form of excitation results only from deflection of the gear teeth, without any significant influence from gear geometry, whether in tooth profile or tooth spiral angle. When this is the case, the displacements may be replaced by the products of load and compliance, both taken as effective tangent to the pitch circle in the plane of rotation, as follows:

$$b_1 = W_R \times q_{R1} \tag{4}$$

$$b_2 = W_R \times q_{R2} \tag{5}$$

Here, the subscripts differentiate between the effective compliances with one or two pairs of teeth transferring load.

Equation (1) may then be written in the form

$$A_o = W_R \left[q_{R1} - h(q_{R1} - q_{R2}) \right] \tag{6}$$

This may be used to find the mean compliance required for the dynamic studies as follows:

$$q_{1-2} = \frac{A_o}{W_R} = q_{R1} - h(q_{R1} - q_{R2}) \qquad (7)$$

Equations (2) and (3) become

$$A_1 = \frac{2}{\pi} W_R (q_{R1} - q_{R2}) \sin h\pi \qquad (8)$$

$$A_2 = \frac{1}{\pi} W_R (q_{R1} - q_{R2}) \sin 2h\pi \qquad (9)$$

To use equations (7), (8), and (9), it is necessary to assign values to h, q_{R1} and q_{R2}.

The value of h may be determined by assuming that the modified contact ratio "m", as evaluated by Gleason in its spiral bevel gear design procedure, is an adequate estimate of the duration of load transfer time for a single pair of teeth. For m between 1 and 2,

$$h = m - 1 \qquad (10)$$

The value of q_{R1} may be determined by selecting a value of combined compliance along the line of action for a pair of "equivalent spur gears". These spur gears will be equivalent to the spiral bevel gears only in the sense that their physical proportions, those likely to influence deflection under load, approximate the mean proportions of the actual spiral bevel gear teeth. The value of combined compliance may be taken from those generated by the gear excitation computer program when applied to the equivalent spur gears. The particular value to be used is the minimum value of those for the various points of contact along the involute profile. This minimum value will not usually be found at the pitch point unless the mating teeth are fully identical. (The procedure for converting the spiral bevel gears to equivalent spur gears is presented in Table 35.)

The value selected, (q_{12}) min, must be adjusted from its value along the line of action to a value for the plane of rotation.

$$q_{R1} = \frac{(q_{12})\text{min}}{\cos^2 \psi \; \cos^2 \phi} \qquad (11)$$

where ψ = Spiral angle
ϕ = Normal pressure angle

The second compliance, q_{R2}, will not necessarily be one-half q_{R1} even though two pairs of teeth share the load in place of one. Rather, it will be somewhat larger, since when two pairs of spur teeth are sharing load, the points of contact are removed from the point of minimum compliance. A similar situation occurs in spiral bevel gears. When two pairs of teeth are sharing load, the areas of contact will be near the ends of the gear rather than at the more rigid center. Because of this, a better estimate of the compliance when two pairs are transferring load is

$$q_{R2} = 0.7q_{R1} \tag{12}$$

With this relationship, equations (7), (8), and (9) become

$$q_{1-2} = q_{R1}(1-0.3h) \tag{13}$$

$$A_1 = \frac{2}{\pi}W_R q_{R1}(0.3) \sin h\pi \tag{14}$$

$$A_2 = \frac{1}{\pi}W_R q_{R1}(0.3) \sin 2h\pi \tag{15}$$

Equations (14) and (15) show that A_1 can go to zero if h = 0 or 1 and that A_2 can go to zero if h = 0, 0.5, or 1. This is due to the special form of the rectangular wave for these values of h. For h = 0 or 1, the wave becomes a straight line, and hence has no sinusoidal components. For h = 0.5, the greater symmetry achieved restricts the components to the odd harmonics only. In these cases the assumption of the rectangular wave shape departs too much from the actual excitation condition. To meet this limitation and thus avoid zero component values when some excitation level is present in the spiral bevel gear set, a minimum value for the sine term of 0.2 is used. This implies that adjusting the spiral bevel gear design to change the contact ratio will affect the excitation levels, but only to a point, and that beyond this point, present design and/or manufacturing technology is not sufficient to reduce the excitation further.

The restriction on the sine terms may be expressed as follows:

$$\sin h\pi \geq 0.2 \tag{16}$$

$$\sin 2h\pi \geq 0.2 \tag{17}$$

SAMPLE CALCULATION FOR FORWARD ROTOR TRANSMISSION SPIRAL BEVEL GEARS

Data Required

m - modified contact ratio

$(q_{12})min$ - minimum combined compliance along line of action for equivalent spur gears

Ψ - spiral angle

ϕ - normal pressure angle

W_R - total load transmitted at mean pitch circle in plane of rotation

Data and Source

m = 1.936 from Table 36, calculation of modified contact ratio.

$(q_{12})min$ = $.114 \times 10^{-6}$ in./lb from computer program GEARO (Appendix IV of Reference 1). Computations of gear tooth meshing errors for CH-47 forward rotor transmission spiral bevel gear cases.

Calculation Point on Driving Gear	QJ1ABC (microin./lb) Driving Gear Pitch-Line Compliance	Calculation Point on Driven Gear	QJ2ABC(micro in./lb) Driven Gear Pitch-Line Compliance	Sum of QJ1ABC &QJ2ABC (micro-in./lb)
0 (pitch point)	.0171	0 (pitch point)	.0552	.0723
6	.0266	-6	.0363	.0629
7	.0286	-7	.0337	.0623
8	.0307	-8	.0313	.0620 (min)
9	.0330	-9	.0291	.0621
10	.0354	-10	.0270	.0624

Q_{JD} for 300C (cruise) = $.0521 \times 10^{-6}$ in./lb
300H (hover) = .0505
Mean Value = .0516

$(q_{12})min = (QJ1ABC + QJ2ABC)min + Q_{JD}$

$(q_{12})min = .0620 + .0516 = .1136$ microin./lb

$\Psi = 25^\circ$ from Table 36

$\phi = 22.5^\circ$

$\cos \Psi = .90631$ $\quad \cos^2 \Psi = .8214$

$\cos \phi = .0239$ $\quad \cos^2 \phi = .8436$

W_R = 2760 lb for cruise condition
= 3764 lb for hover condition

From table of static tooth forces transmitted by drive system gears

Calculations

From equation(10):

$$h = m - 1 = 1.936 - 1.0 = 0.936$$

From equation (11):

$$q_{R1} = \frac{(q_{12})\min}{\cos^2 \psi \cos^2 \phi} = \frac{.114}{.821 \times .844} = .164 \text{ microin./lb}$$

From equation (13) mean mesh compliance:

$$q_{1-2} = q_{R1} (1 - 0.3h)$$

$$q_{1-2} = .164(1-0.3 \times .936) = .164 \times .719 = .118 \text{ microin./lb}$$

Calculation of excitation components:

Fundamental

For cruise condition:
Equation (14): $A_1 = \frac{2}{\pi} W_R q_{R1} (0.3) \sin h\pi$

$$A_{1C} = \frac{2}{\pi} \times 2760 \times .164 \times 0.3 \times \sin(.936 \times \pi)$$

$$= .638 \times 2760 \times .0492 \times \sin(168.7^{\circ})$$

$$= .0314 \times 2760 \times 0.196$$

By equation (16), however, $\sin h\pi \geq 0.2$.

$$A_{1C} = .0314 \times 2760 \times 0.2 = .00628 \times 2760 = 17.3 \text{ microin.}$$

For the hover condition:

$$A_{1H} = .00628 \times 3764$$

$$A_{1H} = 23.6 \text{ microin.}$$

Second Harmonic

For cruise condition:

From equation (15): $A_2 = \frac{1}{\pi} W_R q_{R1} (0.3) \sin 2h$

$$A_{2C} = \frac{1}{\pi} \times 2760 \times .164 \frac{\mu in.}{lb} \times 0.3 \sin (2 \times .936 \times \pi)$$

$$= .0157 \times 2760 \times \sin 22.6^{o}$$

$$= .0157 \times 2760 \times .384$$

$$= 16.6 \text{ microin.}$$

For hover condition:

$$A_{2H} = .00604 \times 3764$$

$$A_{2H} = 22.8 \text{ microin.}$$

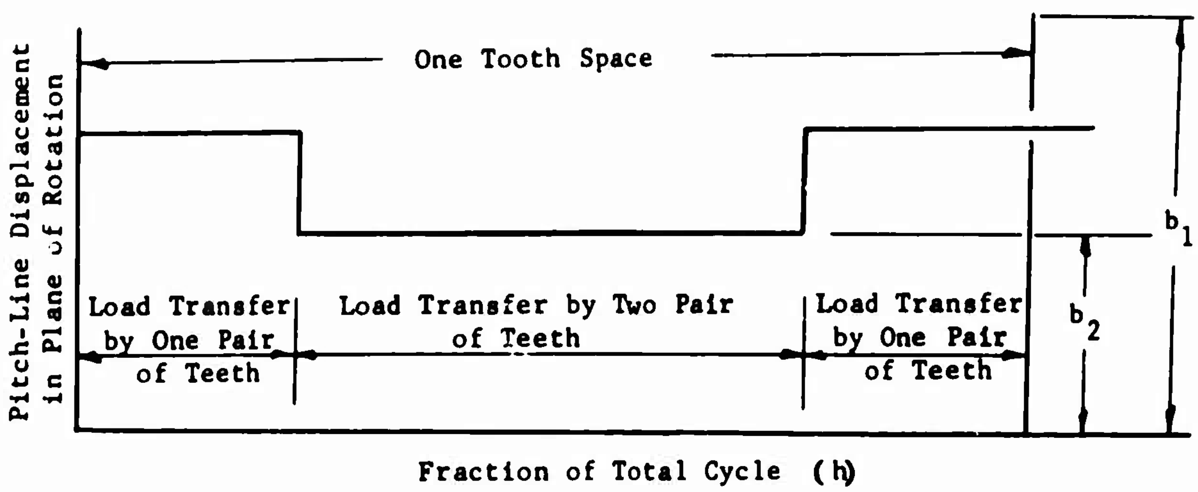

Figure 77. Tooth Load Variation During Meshing of One Pair of Teeth With Contact Ratio Between 1 and 2.

TABLE 35. CONVERSION OF SPIRAL BEVEL GEARS INTO EQUIVALENT SPUR GEARS FOR CH-47 FORWARD ROTOR TRANSMISSION

SYMBOL	DEFINITION	UNITS	PINION [114D1044(12)] SPIRAL BEVEL	PINION HELICAL	PINION SPUR	GEAR [114D1053(13)] SPIRAL BEVEL	GEAR HELICAL	GEAR SPUR
N	NUMBER OF TEETH OF SPIRAL BEVEL	—	29			51		
γ	PITCH CONE ANGLE OF SPIRAL BEVEL	DEGREES	31° 39'			67° 21'		
	COS γ	—	.85127			.38510		
	SIN γ	—	.52473			.92287		
ψ	SPIRAL ANGLE OF SPIRAL BEVEL = HELIX ANGLE OF EQUIVALENT HELICAL	DEGREES	25°	25°		25°	25°	
	COS ψ	—	.90631	.90631		.90631	.90631	
	$COS^2 \psi$	—	.82140	.82140		.82140	.82140	
	$COS^3 \psi$	—	.74444	.74444		.74444	.74444	
N_V	NUMBER OF TEETH OF EQUIVALENT HELICAL = N/COS γ	—		34.0655			132.4331	
N_S	NUMBER OF TEETH OF EQUIVALENT SPUR = $N_V/COS^3 \psi$	—			45.7623			177.9058
F	FACE WIDTH OF SPIRAL BEVEL	INCHES	2.188			2.188		
F_V	FACE WIDTH OF EQUIVALENT HELICAL = F	INCHES		2.188			2.188	
F_S	FACE WIDTH OF EQUIVALENT SPUR = F_V/COS ψ	INCHES			2.4142			2.4142
R	PITCH RADIUS OF SPIRAL BEVEL AT LARGE END	INCHES	3.775			6.639		
R_M	MEAN PITCH RADIUS OF SPIRAL BEVEL = R − (F/2) SIN γ	INCHES	3.2010			5.6294		
R_V	PITCH RADIUS OF EQUIVALENT HELICAL = R_M/COS γ	INCHES		3.7601			14.6180	
R_S	PITCH RADIUS OF EQUIVALENT SPUR = $R_V/COS^2 \psi$	INCHES			4.5776			17.7964
α	RATIO OF RADII OF SPIRAL BEVEL = R_M/R	—	.8479			.8479		
a	ADDENDUM OF SPIRAL BEVEL AT LARGE END	INCHES	.297			.146		
a_v	ADDENDUM OF EQUIVALENT HELICAL = α a	INCHES		.2518			.1237	
a_s	ADDENDUM OF EQUIVALENT SPUR = a_v	INCHES			.2518			.1237
R_{OV}	OUTER RADIUS OF EQUIVALENT HELICAL = $R_V + a_v$	INCHES		4.0119			14.7417	
R_{OS}	OUTER RADIUS OF EQUIVALENT SPUR = $R_S + a_s$	INCHES			4.8294			17.9201
b	DEDENDUM OF SPIRAL BEVEL AT LARGE END	INCHES	.195			.346		
b_v	DEDENDUM OF EQUIVALENT HELICAL = α b	INCHES		.1653			.2933	
b_s	DEDENDUM OF EQUIVALENT SPUR = b_v	INCHES			.1653			.2933
R_{RV}	ROOT RADIUS OF EQUIVALENT HELICAL = $R_V - b_v$	INCHES		3.5948			14.3247	
R_{RS}	ROOT RADIUS OF EQUIVALENT SPUR = $R_S - b_s$	INCHES			4.4123			17.5031
d	WORKING DEPTH OF SPIRAL BEVEL AT LARGE END	INCHES	.443			.443		
d_M	MEAN WORKING DEPTH OF SPIRAL BEVEL = α d	INCHES	.3756			.3756		
d_V	WORKING DEPTH OF EQUIVALENT HELICAL = d_M	INCHES		.3756			.3756	
d_S	WORKING DEPTH OF EQUIVALENT SPUR = d_V	INCHES			.3756			.3756
$TIFR_V$	TRUE INVOLUTE FORM RADIUS OF EQUIVALENT HELICAL = $R_{OV} - d_V$	INCHES		3.6363			14.3661	
$TIFR_S$	TRUE INVOLUTE FORM RADIUS OF EQUIVALENT SPUR = $R_{OS} - d_S$	INCHES			4.4538			17.5445
T	CIRCULAR TOOTH THICKNESS OF SPIRAL BEVEL AT LARGE END	INCHES	.506			.312		
T_M	MEAN CIRCULAR TOOTH THICKNESS OF SPIRAL BEVEL = α T COS ψ	INCHES	.3888			.2397		
T_V	CIRCULAR TOOTH THICKNESS OF EQUIVALENT HELICAL = T_M			.3888			.2397	
T_S	CIRCULAR TOOTH THICKNESS OF EQUIVALENT SPUR = T_V	INCHES			.3888			.2397
C_V	RADIAL CLEARANCE OF EQUIVALENT HELICAL = $TIFR_V - R_{RV}$	INCHES		.0415			.0414	
C_S	RADIAL CLEARANCE OF EQUIVALENT SPUR = $TIFR_S - R_{RS}$	INCHES			.0415			.0414
r_V	TOOTH FILLET RADIUS OF EQUIVALENT HELICAL = (.75)C_V	INCHES		.0311			.0310	
r_S	TOOTH FILLET RADIUS OF EQUIVALENT SPUR = (.75)C_S	INCHES			.0311			.0310

TABLE 36. CALCULATION OF MODIFIED CONTACT RATIO FOR CH-47 FORWARD ROTOR TRANSMISSION SPIRAL BEVEL GEARS

SYMBOL	DEFINITION	UNITS	PINION [114D1044(12)]	GEAR [114D1053(13)]
A_o	OUTER CONE DISTANCE	INCHES	7.194	7.194
a_o	LARGE END ADDENDUM	INCHES	.297	.146
D	LARGE END PITCH DIAMETER	INCHES	7.550	13.278
F'	FACE WIDTH	INCHES	2.188	2.188
P_d	LARGE END DIAMETRAL PITCH	—	3.841	3.841
Γ	PITCH ANGLE	DEGREES	$31^\circ 39'$	$67^\circ 21'$
Γ_o	FACE ANGLE	DEGREES	$34^\circ 44'$	$69^\circ 13'$
ϕ	NORMAL PRESSURE ANGLE	DEGREES	$22^\circ 30'$	$22^\circ 30'$
ψ	MEAN SPIRAL ANGLE	DEGREES	$25^\circ 00'$	$25^\circ 00'$
A	MEAN CONE DISTANCE $= A_o - (0.5)F'$	INCHES	6.100	6.100
α	ADDENDUM ANGLE $= \Gamma_o - \Gamma$	DEGREES	$3^\circ 5'$	$1^\circ 52'$
a	MEAN ADDENDUM $= a_o - (0.5)F'(\tan\alpha)$	INCHES	.238	.110
P	LARGE END TRANSVERSE CIRCULAR PITCH $= \pi/P_d$	—	.818	.818
P_n	MEAN NORMAL CIRCULAR PITCH $= (A/A_o)P(\cos\psi)$	—	.629	.629
P_2	FACTOR $= P_n/(\cos\phi)(\cos^2\psi + \tan^2\phi)$	—	.685	.685
R	MEAN TRANSVERSE PITCH RADIUS $= (D/2\cos\Gamma)(A/A_o)$	INCHES	3.760	14.618
R_N	MEAN NORMAL PITCH RADIUS $= R/\cos^2\psi$	INCHES	4.578	17.796
R_{bN}	MEAN NORMAL BASE RADIUS $= R_N(\cos\phi)$	INCHES	4.229	16.442
R_{oN}	MEAN NORMAL OUTSIDE RADIUS $= R_N + a$	INCHES	4.816	17.907
$\Delta\rho$	PROPORTIONAL LENGTH OF ACTION $= \sqrt{R_{oN}^2 - R_{bN}^2} - R_N\sin\phi$	INCHES	.551	.283
Z_N	LENGTH OF ACTION IN MEAN NORMAL SECTION $= \Delta\rho_P + \Delta\rho_G$	INCHES	.835	.835
K_2	FACTOR $= F'/A_o[2 - (F'/A_o)/2(1 - F'/A_o)]$	—	.371	.371
M_P	TRANSVERSE CONTACT RATIO $= Z_N/P_2$	—	1.219	1.219
M_F	FACE CONTACT RATIO $= [(K_2\tan\psi - K_2^3/3\tan^3\psi)A_oP_d]/J$	—	1.505	1.505
M_o	MODIFIED CONTACT RATIO $= \sqrt{M_P^2 + M_F^2}$	—	1.936	1.936

APPENDIX IV

GEAR TOOTH FORCE ANALYSIS

INTRODUCTION

Any geared system transmitting power is subject to torsional vibration because it contains the necessary elements of rotational inertia, torsional elasticity, and a source of excitation. The inertia may be present in concentrated form, as in the body of a gear, or it may be distributed as in the sections of connecting shafting. Similarly, the elasticity may be concentrated in a coupling or in the flexibility of gear teeth, or it may be distributed in the shaft sections. As in any other torsionally vibrating system, the excitation may come from externally applied pulsating torques, such as that from a driving motor or turbine, or from some fluctuating resistance to the steady rotation. However, in geared systems there is also a displacement form of excitation which comes from the imperfect transfer of motion in the meshing gears. This excitation requires the meshing gears to undergo dynamic changes in relative motion. This changing of relative motion can be achieved only if there exist dynamic forces acting between the teeth to impose the necessary accelerations. These dynamic forces, generated in response to the gear displacement excitation, can subject the gear teeth to greater loads than those required for the steady transmission of power. These high tooth loads are an important factor in the generation of noise in the transmission system.

A detailed analysis of these gear tooth forces is contained in Appendix V of Reference 1. The data required by that analysis to describe the torsionally vibrating system can be in the form of physical dimensions taken directly from design drawings. At the same time, however, the analysis will also accept system data in the form of concentrated inertia or concentrated compliances.

Several features make the analysis sufficiently versatile to deal with a wide range of gear system designs. First, the analysis has provision for branches in the vibrating system. Second, it not only treats multiple cases of the simple gear set in which one gear drives another, but it can also treat multiple cases of one type of planetary gear set (the sun gear driving, the ring gear restrained, and the planet carrier transmitting the vibration to the balance of the system). Third, it includes the effects of externally applied damping such as might be developed at the bearings. The analysis presents the resulting dynamic gear tooth forces in a form which gives their phase relationships as well as their magnitudes.

As a result of the present study, several improvements have been added to the gear tooth force computer program contained in Reference 1. The revisions were made necessary primarily because of the increased complexity of the CH-47 drive train, compared to that of the UH-1D. The changes took the form of new logic for treating branches and provision for giving the increase in precision required in systems with a great many stations. In addition, the program was expanded to treat the effects of damping between system stations.

LIMITATIONS AND ASSUMPTIONS

The limitations in the gear systems treated and the major assumptions which form a basis for the revised analysis are listed below:

1. Excitation is introduced into the system only at the gear meshing points and only in the form of sinusoidal displacements. These displacements constitute differences in pitch-line motion of the mating teeth from the two gears and are introduced in series with any elastic compliances of the teeth themselves.

2. The system is considered linear; that is, all compliances and damping coefficients are assumed to be constant. The varying gear tooth stiffness is represented as a constant mean stiffness, while the effect of the variability under a steady load is assumed to have been incorporated in the calculation of the displacement excitation. The linear system also requires that the dynamic tooth force amplitude be smaller than the static force, so that no separation takes place at a gear mesh.

3. The members of the system are assumed to be compliant only in the torsional mode, with full rigidity in the lateral direction. Thus, the interaction between torsional and lateral modes, often present in the gear system, is not considered in this analysis.

4. The only gearing stages treated are:

   a. the simple gear set (driver and driven gears)

   b. the planetary gear set with the sun gear driving, the ring gear elasticity restrained, and the planet carrier as the driven member

5. The system may have simple branches.

6. The overall system has no rigid, torsional restraints at its end or at any other point; neither does it have any externally applied dynamic forces other than those applied at a damping or elastic constraint and due to its own dynamic angular motion. (Rigid restraints, however, may be simulated by introducing very large concentrated inertias at the points of interest.)

7. Damping may be applied between system stations and ground, as well as between adjacent points within the system. In the latter case, the damping may be the only element between the stations, or it may appear in parallel with a concentrated compliance. There is no provision, however, for damping within a planetary set or at the gear mesh in any gear set.

8. In the planetary gear set,

   a. all planets are equally spaced.

   b. all excitations from planet to planet are the same in magnitude but differ in phase relation, according to the planet frequency and rotational speeds.

   c. all radial forces on the sun or ring are fully balanced, the sun and ring are rigidly supported in the radial direction, or any other set of conditions exists which eliminates lateral modes of vibration.

DESCRIPTION OF ANALYSIS

The analysis of the improved program is essentially the same as that described in Appendix V of Reference 1. The one change involves a revision to the description of the branch treatment on p. 220 of that reference.

When a station with a branch is encountered, there is an additional element in the calculation. In one step, a unit angular motion is tentatively assumed for the free end of the branch and the same kind of station-to-station calculation is made until the branching station is reached and a value for motion at this station is calculated. The other step is identical except that zero angular motion is tentatively assumed for the free end of the branch. This normally gives a different value for the branching station motion. These two values are then compared to the value of motion at the same station as found in the main system calculation. From this comparison, actually one of interpolation (or extrapolation), the value of the branch free-end motion is found which correctly matches the branch to the main system. Using this value, the branch is retraced yielding all branch motions and torques including the torque applied by the branch at the branching station. This is then combined with the torque applied by the prior part of the main system, and the calculations for the main system are carried forward.

DERIVATION OF ANALYTICAL RELATIONSHIPS

There is only one change in the analytical relationships derived in Appendix V of Reference 1. This is the addition of the between-station damping term in the Holzer Analysis. The symbol added is C_n''. This quantity is the concentrated torsional damping coefficient acting between station n and station n + 1, either along or in parallel with a concentrated torsional compliance with no distributed mass.

Adding this compliance requires revisions in the equations written for the system with no distributed mass, starting with equation (169) in Reference 1.

As seen in Figure 78, the torque transmitted between stations divides between the elastic member and the damping member, while the torque is the same at both ends.

$$T'_n = \left[\frac{\theta_{(n+1)} - \theta_n}{Q''_n}\right] + j\omega \left[\theta_{(n+1)} - \theta_n\right] C''_n \qquad (18)$$

$$T_{n+1} = T'_n \qquad (19)$$

The first of these equations may be simplified to

$$T'_n = \left[\frac{1}{Q''_n} + j\omega C''_n\right] \left[\theta_{(n+1)} - \theta_n\right] \qquad (20)$$

Solved for $\theta_{(n+1)}$, this becomes

$$\theta_{(n+1)} = \theta_n + T'_n \left[\frac{Q''_n}{1 + j\omega C'_n Q''_n}\right] \qquad (21)$$

With the aid of complex algebra, this revised equation may be combined with the remaining equations, and the improved analysis is complete.

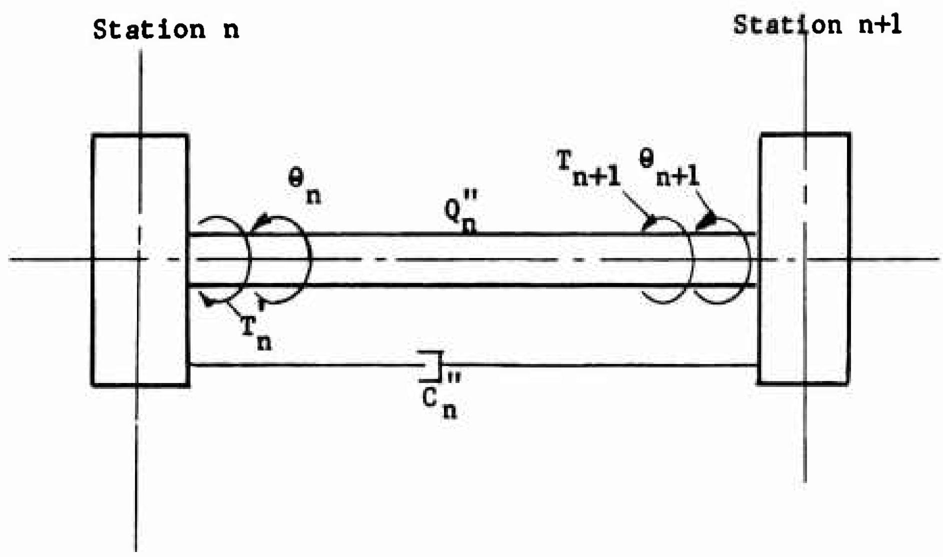

Figure 78. General Portion of the Torsional System Showing Concentrated Damping C''_n and Compliance Q''_n Between Stations.

INPUT VARIABLES, FORMAT AND INSTRUCTIONS

Card 1. Title. Format (72H). This card precedes each set of input data.

a. Printing instructions, column 1
For printer to skip a line, use 0
For printer to go to next sheet, use 1

b. Title, columns 2-72

Card 2. Control Integers. Format (13I5, 10X, I5)

a. NS — Total number of stations. ($NS \leq 200$)
Instructions for selection of stations given in earlier section.
Place last digit of this number in column 5.

b. NB — Number of stations with external constraints, in the form of elastic restraint or damping, both with respect to ground. ($NB \leq NS$)
Place last digit of this number in column 10.

c. NBR — Number of branches, not including main system. ($NBR \leq 20$)
Place last digit of this number in column 15.

d. NMPG — Total number of cases of gear excitation. A change in either station number, frequency, or magnitude of either excitation component constitutes a separate case. In the planetary stations, one pair of sun and ring excitations at the same frequency constitutes one case. Individual solutions are found for each case. When there are multiple excitations at the same frequency at different points in the system, other than in the planetary stages, the solutions for the individual excitations must be combined outside of the program.
Place last digit of this number in column 20.

e. INP — Identification as to whether this control card represents the last complete set of input data being submitted.
If more sets of input data follow, use 0.
If this is the last set, use 1.
Place this digit in column 25.

f. NSRG Number of simple gear sets. ($0<NSRG\leq20$)
Each set consists of two gears. If an idler is used between two gears, the combination must be represented by two simple gear sets, where the idler is replaced by two connected gears with no compliance between them and with a total inertia equal to that of the idler. Where one gear drives two or more gears, each leading off to separate branches, a similar conversion must be made. If one gear drives through multiple gears back into the main system, in a so-called star arrangement, the only treatment possible in this program is to combine the multiple intermediate gears into one composite gear, assuming that the excitations, if any, are torsionally synchronous. Place the last digit of this number in column 30.

g. NPLG Number of planetary gear stages. ($NPLG\leq2$)
Place this digit in column 35.

Card 3. Rotor Material Properties. Format (5X, 2E12.4)

a. GM Shear modulus of elasticity, lb-in^2. May be zero only if all values of RJ in the rotor data are zero. Use columns 6-17.

b. DENST Weight density, lb/in^3. May be zero only if all values of RL in the rotor data are zero. Use columns 18-29.

Cards 4-1 to 4-NS. Rotor Data. Format (I5, 6E12.4)

a. NSTA Station number at or after which the rotor data applies. These must be given in numerical sequence with no omissions.
Place the last digit of this number in column 5.

b. RIP Polar moment of inertia concentrated at station NSTA, lb-in^2. This includes any inertia in the system which is not to be calculated by the program from dimensional data. At the stations for simple gear sets, list the inertias of both members in the rotor data. All planetary inertias are included only in the separate planetary data cards. The station which immediately follows the planetary may have a separate inertia value specified. Use columns 6-17.

c. RL Length of uniform cylindrical shaft section between this station and the adjoining higher numbered station, in. At the station for the first member of a simple gear set and at the station for a

planetary gear stage, use 0.0 or 1.0.
Use columns 18-29.

d. DST Outer diameter for stiffness calculation of the cylindrical shaft section, in. This diameter measures the section which transmits torque. If the actual shaft section is reduced as by a keyway, a diameter which approximates the reduced section should be used. At the station for the first member of a simple gear set and at the station for a planetary gear stage, use 0.0. At the terminating station, use 0.0.
Use columns 30-41.

e. DMS Outer diameter for mass calculation of the cylindrical shaft section, in. This diameter measures the section which contributes inertia. It may include any assembled sleeves or hubs which extend the full distance and rotate with the shaft. Use 0.0 for the special stations as described under DST.
Use columns 42-53.

f. DIN Inner diameter for both stiffness and mass calculation of the shaft section, in. If the shaft section is solid, use 0.0. Use 0.0 for the special stations as described under DST.
Use columns 54-65.

g. CCOM Concentrated compliance acting between this station and the adjoining higher numbered station, rad/in.-lb. This compliance is separate from that calculated by the program from the dimensional data, and can be used only when there is no such dimensional data between the same two stations. Any value listed as a concentrated compliance will enter into the computations only if RL = 0 for the same station. Use 0.0 for the special stations as described under DST. Concentrated compliances associated with any of the gears are included only in the special data cards for the particular type of gear stage.
Use columns 66-77.

Cards 5-1 to 5-NB. External Constraints. Format (I5, 3E12.4)

a. LB Station number at which the constraints are acting. These must be given in numerical sequence.
Place last digit of this number in column 5.

b. BK External torsional elastic restraint acting at the station, expressed as a torsional stiffness, in.-lb/rad. In an actual system which has steady

rotation, the stiffness must be 0 if the restraint is to ground. If in such a rotating system the restraint is to an "infinite" but rotating mass, the stiffness may have any finite value.
Use columns 6-17.

c. BCB Coefficient of the external damping constraint acting at the station, in.-lb-sec/rad.
Use columns 18-29.

d. DMP Coefficient of interstation damping, in.-lb-sec/rad.
Use columns 30-41.

Cards 6-1 to 6-NSRG. Simple Gear Set Data. Format (I5, 4E12.4)
(At least one card must be submitted)

a. LS Station number at which the first, or lower numbered, member of the gear set is located. (The second member of the gear set is understood to be at the station LS + 1, except if it serves as a common station to a branch. In this case, the second member has the number which completed the branch.) The simple gear set station numbers must be given in numerical sequence.
Place the last digit of this number in column 5.

b. RP Pitch radius of the first member of the gear set, at station LS, in.
Use columns 6-17.

c. RG Pitch radius of the second member of the gear set, in.
Use columns 18-29.

d. SG Combined linear compliance of the two gears, tangential to their pitch circles, in./lb.
Use columns 30-41.

Cards 7-1-A, B, C to 7-NPLGA, B, C. Planetary Gear Stage Data.

(These cards are omitted if NPLG = 0. When they are included they must appear in sets of three, and each set must be arranged in the order given.)

<u>First card of set - A. Planetary Geometry</u>. Format (I5, 3E12.4)

a. LEC Station number at the start of the planetary stage. This location of the station is at the connecting point to the sun gear, but the station does not include the sun gear. The sun gear and other planetary components, including the planet carrier, lie between this station and the one following it. Place the last digit of this number in column 5.

b. PN — Number of planet gears in the planetary stage. Use columns 6-17. Do not omit decimal point.

c. RS — Pitch radius of the sun gear, in. Use columns 18-29.

d. RW — Pitch radius of the planet gear, in. The pitch radius of the ring gear will be calculated within the program by adding twice the planet radius to the sun radius. Use columns 30-41.

Second card of set - B. Planetary Inertias. Format (I5, 5E12.4)

a. IPL — Station number of the planetary state, the same as LEC. Place the last digit of this number in column 5.

b. PMS — Weight of one planet gear, lb. This includes all components which rotate with the planet, everything between bearing surface and gear teeth. One-half the weight of any rolling elements in the bearing should be included. Use columns 6-17.

c. PSP — Moment of inertia of the sun gear, lb-in^2. This includes all components between the point of connection to the outside system and the gear teeth. Use columns 18-29.

d. PIP — Moment of inertia of each planet gear, lb-in^2. This includes all components used in computing the weight PMS. Use columns 30-41.

e. PRP — Moment of inertia of the ring gear, lb-in^2. This includes all components between the gear teeth and the point of elastic connection to ground. If the connection to ground is rigid, with zero compliance, any finite inertia may be used for the ring gear. Use columns 42-53.

f. PCP — Moment of inertia of the planet carrier, lb-in^2. This includes all components between the bearing surfaces in the planet gears and the point of connection to the outside system. Use columns 54-65.

Third card of set - C. Planetary Compliances. Format (I5, 5E12.4)

a. IPL Station number of the planetary stage, a repetition of the value in the previous card.
Place the last digit of this number in column 5.

b. SS Combined linear compliance of each sun-planet gear mesh, tangential to their pitch circles, in.-lb. If the sun gear construction is such that there is a significant compliance between the hub and the rim, the starting connection point to the sun gear should be redefined as located at the rim. The hub would then be associated with the outside system as a separate station with the structural compliance of the sun gear as a connecting concentrated compliance. In this case, the mesh compliance still appears under SS, but the sun gear inertia under PSP would be limited to that of the rim construction.
Use columns 6-17.

c. SR Combined linear compliance of each planet-ring gear mesh, tangential to their pitch circles, in.-lb.
Use columns 18-29.

d. SW Linear compliance of the planet support in the planet carrier, tangential to the path of planet centers, in./lb. This compliance is the combination of the compliance of the planet bearing and the compliance of any portion of the carrier which will deflect with the individual planet. If the carrier construction is such that there is a compliance between a hub and a rim-type member which supports all the planets collectively, this structural compliance may be combined with the others to give a total planet carrier compliance. Alternatively, the system may be changed so that the end of the planetary stage, that is, its connection to the external system, is taken at the rim-type member. In this case, the hub becomes associated with the outside system as a separate concentrated compliance between the station at the close of the planetary stage and the new station for the hub. With this change, the compliance used under SW is the combination of only the first two compliances mentioned above, namely, those associated with the individual planet.
Use columns 30-41.

e. Blank columns 42-53 are not read in this main computer program. The auxiliary program used in conjunction with this main program will take the same input planetary data on the same cards except for one item for which this field has been reserved.

f. ST — Angular compliance of the support between the ring and ground, rad/in.-lb. If the ring is rigidly connected to ground, set this compliance equal to zero. Use columns 54-65.

Cards 8-1 to 8-BR. Branch Data. Format (3I5)
These cards are omitted if BR = 0

a. LBR — Number of the far end station of the branch. Place the last digit of this number in column 5.

b. LBS — Number of the common station of the branch at which it is connected to the main system. Place the last digit of this number in column 10.

Cards 9-1 to 9-NMPG. Gear Excitation Data. Format (I5, 6E12.4, I3)

a. IT — Station number which identifies the gears at which the excitation is introduced. For simple gear sets, the number of the first member is used, as for LS in card 6. For planetary gear stages, the station number at the start of the planetary is used, as for LEC in card 7-A.
Place the last digit of this number in column 5.

b. FFQ (TE1) — Frequency of the excitation, Hz.
(TE1 is used for temporary storage.)
Use columns 6-17.

c. AXY or AXY1 — The real or cosine component of the linear excitation in the simple gear set (AXY) or in the sun-planet mesh of the planetary gear stage (AXY1), in. This excitation is introduced at the gear mesh tangential to the pitch circles.
(TE2 is used for temporary storage.)
Use columns 18-29.

d. BXY or BXY1 (TE3) — The imaginary or sine component of the linear excitation described above, in.
Use columns 30-41.

e. AXY2 (TE4) — The real or cosine component of the linear excitation in the planet-ring mesh of the planetary gear stage, in. This excitation is introduced at the gear mesh tangential to the pitch circles. On a card with excitation for a simple gear set, this field is left blank. (TE4 is used for temporary storage.)
Use columns 42-53.

f. BXY2 (TE5) The imaginary or sine component of the linear excitation described just above, in.
Use columns 54-65.

OUTPUT VARIABLES AND EXPLANATIONS

Tabulation of Input Data

Title - as in input card 1.
Control Numbers - NS, NB, NBR, NMPG, INP, NSRG, NPLG, as in input card 2.

Rotor Material Properties - GM, DENST, as in input card 3.
Rotor Data - NSTA, RIP, RL, DST, DMS, DIN, CCOM, as in input card 4.
External Constraint Data - LB, BK, BCB, as in input card 5.
Simple Gear Set Data - LS, RP, RG, SG, as in input card 6.
Planetary Gear Stage Data - LEC, PN, RS, RW; IPL, PMS, PSP, PID, PRP, PCP; IPL, SS, SR, SW, Blank, ST } all as in input card 7

Branch Data - LBR, LBS, as in input card 8.

Excitation Data - IT, FFO, AXY, or AXY1, BXY or BXY1, AXY2, BXY2, as in input card 9. Each set of excitation data is given separately followed by its own calculated response.

Calculated Data

Computed response at each simple gear set - LS, TTFR, TTFE
where:
- LS - Station number identifying the simple gear set.
- TTFR - Real or cosine component of the dynamic tangential tooth force developed at the gear mesh, lb.
- TTFE - Imaginary or sine component of the same force, lb.

Computed response at each planetary gear stage - LEC, C1, C2, C3, C4
where:
- LEC - Station number identifying the planetary gear stage.
- C1 - Real component of the dynamic tangential tooth force developed at the sun-planet gear mesh, lb.
- C2 - Imaginary component of the same force, lb.
- C3 - Real components of the dynamic tangential tooth force developed at the planet ring gear mesh, lb.
- C4 - Imaginary component of the same force, lb.

PROGRAM LISTING OF SOURCE DECK

This program is written in FORTRAN II - Extended and may be compiled with FORTRAN IV. In the source deck listing which follows, the READ and WRITE statements are written with the variable NR = 5 to specify the standard reading unit and the variable NW = 6 to specify the standard writing unit. To recompile the program for any nonstandard computer, introduce the required unit numbers making the necessary changes on the cards as noted in the listing.

In addition to the controlling portion of this torsional response program, named TORRP, there are other subroutines. One, named PLNST, treats the planetary stage. Another, named MATIN, performs the matrix inversion that solves the simultaneous equations of the PLNST subroutine. Another, named BLOOP, applies to the branch treatment. The others, named CDIV, CDIV2, PANGF, AMPF, CAD, CSUB and CMPY, perform arithmetic operations.

```
      PROGRAM TORRP(INPUT,OUTPUT,TAPE5=INPUT,TAPE6=OUTPUT)
      DIMENSION AXY(20),HXY(20) ,LEX(20)
      DIMENSION HXAT(2),TEMPS(2),LMC(20),LTW(20),LHST(20)
      COMMON TBR(2,2),THE(2,2),TPH(2,2),TPE(2,2),TFSPH(2,2),TFSPE(2,2),
     1 TFPHR(2,2),TFPHE(2,2),TTPCH(2,2),TTPCE(2,2),TTGHR(2,2),TTGRE(2,2)
      COMMON RIP(200),DST(200),DMS(200),DIN(200),BCH(50),LB(50),DDI(200)
     1,BK(50),LEC(2),RS(2),RW(2),PIP(2),PMS(2),PN(2),SS(2),SW(2),SR(2),
     2 ST(2),LBR(20),LBS(20),CCOM(200),AXY1,AXY2,BAY1,BAY2,TLH(200),
     3 TLE(200),THR(200),THE(200),THH(200),TRE(200),THR1(200)
      COMMON A(7,7),H(7,2),LS(20),RP(20),RG(20),SG(20),THR2(200),
     1 TRE1(200),THE1(200),TLE1(200),THE2(200),TTFH(20),TTFE(20),
     2 PSP(2),THR1(200),TLR1(200),THR2(200),TLR2(200),THE2(200),
     3 TLE2(200),RL(200),PCP(2),PHP(2)   ,DMP(50)
      COMMON I1, K4,L4,MDIAG,FRQ2,ANGP,ANGE,TOR,TOE  ,J,NS  ,MI,NW,NR,NPLG
      COMMON  K1,K2,K3,K9,L1,L2,L3,L9,LG(10),IBRAN
C    NR REFERS TO INPUT UNIT
C   NW REFERS TO OUTPUT UNIT
      NR=5
      NW=6
      MDIAG=0
      MDTW=0
      NTW=0
      MUSG=0
      IEXP=0
  200 READ(NR,100)
      READ(NR,101)NS,NB,NBR,NMPG,INP,NSHG,NPLG
      IOP=0
      FFQ=0.0
      CXY=0.
      DAY=0.
      MPOL = -1
      IF (MDIAG -2) 3021,3020,3021
 3020 MPOL = 0
      GO TO 3025
 3021 IF(MDIAG +2) 3025,3022,3025
 3022 MPOL = 1
 3025 READ (NR,102)GM,DENST
      WRITE(NW,100)
      WRITE(NW,103)
      WRITE(NW,106)NS,NB,NBR,NMPG,INP,NSHG,NPLG
 2022 WRITE(NW,135) GM,DENST
      DENST=DENST/386.089                                          20
      IF(IEXP) 2023,2024,2025
 2023 IEXP=-IEXP
      AINT=1./10.**IEXP
      GO TO 2026
 2024 AINT=1.
      GO TO 2026
 2025 AINT=10.**IEXP
 2026 WRITE(NW,107)
```

```
      DO 201 J=1,NS                                                     23
      READ(NR,190)NSTA,RIP(J),RL(J),DST(J),DMS(J),DIN(J),CCOM(J)
      IF(NSTA-J) 2000,2001,2000
 2000 WRITE(NW,191)
 2001 WRITE(NW,108)NSTA,RIP(J),RL(J),DST(J),DMS(J),DIN(J),CCOM(J)
  201 RIP(J)=RIP(J)/386.069                                             26
      LEX(1) = NS+2
      LH(1)=NS+2                                                        27
      LEC(1)=NS+2                                                       28
      LOUT =0
      LF=0
      KL=0
      LI=0
      LHR(1)=NS+2
      LHS(1)=NS+2                                                       30
      LS(1) =NS+2
      LG(1)=NS+2
      LFT=0
      KLT=0
      LIT=0
      LTW(1)=NS+2
      IF(NB) 2031,2031,203
  203 WRITE(NW,109)
      DO 204 J=1,NB                                                     34
      READ(NR,190)LB(J),BR(J),BCB(J),DMP(J)
  204 WRITE(NW,108)LB(J),BR(J),BCB(J),DMP(J)
 2031 IF(NSHG)206,206,2032
 2032 WRITE(NW,112)
      WRITE(NW,113)
      DO 205 I=1,NSHG
      READ(NR,190)LS(I),HP(I),HG(I),SG(I)
  205 WRITE(NW,108)LS(I),HP(I),HG(I),SG(I)
  206 IF(NPLG)210,210,209
  209 WRITE(NW,114)
      DO 212 J=1,NPLG
      READ (NR,190) LEC(J),PR(J),RS(J),RW(J)
      WRITE(NW,127)
      WRITE (NW,108) LEC(J),PR(J),RS(J),RW(J)
      READ (NR,190) IPL,PMS(J),PSP(J),PIP(J),PRP(J),PCP(J)
      WRITE (NW,128)
      WRITE (NW,130) IPL,PMS(J),PSP(J),PIP(J),PRP(J),PCP(J)
      READ (NR,130) IPL,SS(J),SR(J),SW(J),ST(J)
      WRITE (NW,129)
      WRITE (NW,131) IPL,SS(J),SR(J),SW(J),ST(J)
      PSP(J) =PSP(J)/386.069
      PCP(J)=PCP(J)/386.069                                             65
      PRP(J)=PRP(J)/386.069                                             66
      PIP(J)=PIP(J)/386.069                                             67
  212 PMS(J)=PMS(J)/386.069                                             68
  210 IF(NWH) 2130,2130,214
```

```
  214 WRITE(NW,118)
      DO 215 J=1,NBR
      READ(NR,101) LBR(J),LBS(J),LMC(J)
  215 WRITE(NW,119) LBR(J),LBS(J)
 2130 KS=NS-1
      DO 216 J=1,KS
      C1=RL(J)
      C2=DST(J)
      IF(C1) 217,216,217
  217 IF(C2) 218,216,218
  218 C5=DIN(J)*DIN(J)
      C4=C5*C5
      C6=DMS(J)*DMS(J)
      C8=0.09817477*(C2**4-C4)
      C3=C8*GM
      C4=0.09817477*DENST*(C6*C6-C4)
      DDT(J)=C1/C3
      DMS(J) = C1*SQRT(C4/C3)
      DIN(J) = SQRT(C3*C4)
  216 CONTINUE
      DO 501 IERR =1,NMPG
      FFO=0.0
      AXY1=0.0
      BXY1=0.0
      AXY2=0.0
      BXY2=0.0
      MAX =1
      IEX = 1
 4009 READ (NR,190) IT,TE1,TE2,TE3,TE4,TE5,TE6,NEX
      FFO=TE1
      CXY=TE2
      DXY=TE3
      IF (NEX) 2013,4010,4010
 4010 IF(IEX-1) 4012,4011,4012
 4011 MAX = NEX
 4012 DO 2011 I=1,NSRG
      IF(IT-LS(I)) 2011,2010,2011
 2010 AXY(IEX) = TE2
      BXY(IEX) = TE3
      LEX(IEX) = IT
      WRITE (NW,194)
      WRITE(NW,108)IT,TE1,TE2,TE3
      IEX = IEX +1
      IF (IEX- MAX) 4009,4009,2020
 2011 CONTINUE
      IF(NPLG) 3019,3019,2013
 2013 DO 2017 I=1,NPLG
      IF(IT-LEC(I)) 2017,2014,2017
 2014 WRITE(NW,195)
      AXY1=TE2
```

```
      BXY1=TE3
      AXY2=TE4
      BXY2=TE5
      WRITE(NW,108)IT,TE1,TE2,TE3,TE4,TE5
      GO TO 2020
 2017 CONTINUE
 3019 WRITE(NW,192)
      IF(INP) 506,200,506
 2020 FRQ=6.2831853*FFQ
      IF(FRQ) 501,501,599
  599 FRQ2=FRQ*FRQ
      NEX=1
      ISEP=0
 5020 BRAT(1)=1.0
      BRAT(2)=0.0
      IBRAT=0
      IBRAN=0
      M1=1
  502 ANGR=0.0
      IF(IOP) 5021,5022,5021
 5021 ANGR=AINT
 5022 ANGE=0.0
      ANGE=0.0
      TOR=0.0
      TOE=0.0
      A13R=0.0
      A13E=0.0
      K1=1
      K2=1
      K4=1
      K5=NS+2
      K9=1
      L1=LBR(1)
      L2=LB(1)
      K3=1
      L3=LS(1)
      L4 =LEC(1)
      L9=LG(1)
      GO TO (227,228),M1
  227 ANGR=AINT
  228 J=1
      IF(NTW) 2275,2270,2270
 2270 LFT=LTW(1)
      LIT=1
      RLT=1
 2275 IF(NWR) 2280,2280,2279
 2279 LF=LWR(1)
      LOUT=LWC(1)
      IF(LOUT) 2277,2278,2278
 2277 LOUT=-LOUT
```

```
2278 LI=1
     KL=1
2280 IF(IOP) 2282,2281,2282
2281 IF(J-LF) 249,2300,249
2300 CALL  HLOOP(LHH,LBS,LMC,LI,KL,LF,NBH,LIT,KLT,LFT)
     GO TO 249
2282 IF(J-LI) 231,230,231                                        135
 230 IF(M1-1) 232,232,234                                        136
 234 IBRAN=1
 232 TLIR=TOR                                                    137
     ALIR=ANGR                                                   138
     TLIE=TOE                                                    139
     ALIE=ANGE                                                   140
 562 ANGR=AINT
     ANGE=0.                                                     162
     TOR=0.                                                      163
     TOE=0.                                                      164
     A13R=0.                                                     165
     A13E=0.                                                     166
 235 KS=LBS(K1)                                                  167
     K6=LI                                                       168
     K1=K1+1                                                     169
     IF(NHH-K1) 237,236,236                                      170
 236 LI=LHR(K1)
     GO TO 249
 237 LI=NS+2
     GO TO 249
 231 IF(J-KS) 249,248,249
 248 AA1 =(ANGR*ANGR+ANGE*ANGE)
     IBRAN=0
     AA2=DSQRT(AA1)
     AA5 =ALIR*ANGR +ALIE*ANGE
     AA3 =(ALIR*ALIR +ALIE*ALIE)
     AA4=DSQRT(AA3)
     IF (AA2-1.0E-7*AA4) 242,241,241
 241 AA8 =AA5/AA1
     AAE = (ANGR*ALIE- ANGE*ALIR) /AA1
     TE1 = TOR
     TE2 = TLIR
     TE3 = TOE
     TE4 = TLIE
     ANGR= ALIR
     ANGE = ALIE
     [illegible]
     [illegible]
     IF(M1-2) 2420,2410,2420
2410 IF(IBMAT) 2411,2420,2411
2411 IF(IBMAT-2) 2420,2412,2420
2412 BMAT(1)=AA8
     BMAT(2)=AAE
```

```
2413 IBRAT=1
     GO TO 2420
 242 AAR = AA5/ AA3
     AAE = ( AL1R*ANGE- AL1E*ANGR) / AA3
     TE1 = TL1R
     TE2 = TQR
     TE3 =TL1E
     TE4 = TQE
     K7=1
     K8=K6-1
     IF (M1-2) 2420,2440,2420
2440 IF(IBRAT) 2441,2420,2441
2441 IF(IBRAT-1) 2413,2412,2413
2420 TQR = AAR* TE1 -AAE* TE3 +TE2
     TQE = AAE *TE1 + AAR*TE3 + TE4
 243 DO 244 L=K7,K8
     C1 = TLR(L)
     C2 = TLE(L)
     C3 = THR(L)
     C4 = THE(L)
     C5 = TRR(L)
     C6 = TRE(L)
     TLR(L) = AAR*C1-AAE*C2
     THR(L) = AAR*C3-AAE*C4
     TRR(L) = AAR*C5-AAE*C6
     TLE(L) = AAE*C1+ AAR* C2
     THE(L) = AAE*C3+ AAR* C4
 244 TRE(L) = AAE*C5+ AAR* C6
 249 THE(J)=ANGE
     TLE(J)=TQE
     THR(J)=ANGR
     TLR(J)=TQR
     CD=0.0
     IF(J-L2) 284,283,284
 283 C1=BK(K2)
     CD=DMP(K2)
     C2=BCB(K2)
     K2=K2+1
     IF(NB-K2) 261,260,260
 260 L2=LB(K2)
     GO TO 285
 261 L2=NS+2
     GO TO 285
 284 C1=0.0
     C2=0.0
 285 C1=C1-FRQ2*RIP(J)
     C2=FRQ*C2
     TQE=TQE+C1*ANGE   +C2*ANGR
     TQR=TQR+C1*ANGR-C2*ANGE
     IF(J-LOUT) 2853,2850,2853
```

```
2850 J1=LBR(KL-1)
     TQR=TQR-TLR(J1)
     TQE=TQE-TLE(J1)
     IF(KL-NBR) 2851,2851,2852
2851 LOUT=LMC(KL)
     IF(LOUT) 2848,2853,2853
2848 LOUT=-LOUT
     GO TO 2853
2852 LOUT=NS+2
2853 TRE(J)=TQE
     TRR(J)=TQR
     IF(J-NS) 286,287,287
 287 IF(M1-1) 401,401,402
 286 IF(J-L3) 288,289,288
 289 C1=RP(K3)
     C2=RG(K3)
     A11=-C1/C2
     A22=1.0/A11
     A21=0.0
     A12=-SG(K3)/(C1*C2)
     K3=K3+1
     IF(K3-NSRG) 1019,1019,1020
1019 L3=LS(K3)
     GO TO 1021
1020 L3=NS+2
1021 IF (M1-1) 351,351,251
 251 IF (LEX(NEX) - J) 351,2899,351
2899 IF(M1-2) 290,2900,2900
2900 IF(IBRAN) 2901,2910,2901
2901 IF(IBRAT) 2902,2903,2902
2902 WRITE(NW,136)
     ISEP=1
     GO TO 351
2903 IBRAT=2
     GO TO 290
2910 IF(IBRAT) 2912,2911,2912
2911 IBRAT=1
     GO TO 290
2912 IF(BRAT(1)-1.0) 2902,2913,2902
2913 IF(BRAT(2)) 2902,290,2902
 290 A13R=-AXY(NEX)/C2
     A13E=-BXY(NEX)/C2
     IF (NEX-MAX) 5000,351,351
5000 NEX = NEX+1
     GO TO 351
 288 IF(J-L4) 255,254,255
 254 IF(MDIAG+1) 1092,1092,1095
1092 IF (K4-1) 1095,1096,1095
1096 IF (M1-1) 1093,1093,1094
1093 WRITE (NW,181)
```

```
      GO TO 1095
 1094 WRITE (NW,182)
 1095 CALL PLNST
      GO TO 503
  255 C1=RL(J)
      IF(C1) 257,256,257
  256 A11=1.0
      A12 =CCOM(J)
      IF(CD) 3001,3000,3001
 3000 A21=0.0
      A22=1.0
      GO TO 351
 3001 TEMP=1.0+(FRQ*CD*A12)**2
      TEMP1=FRQ*CD*A12**2
      ANGR=ANGR+(A12*TQR+TEMP1*TQE)/TEMP
      ANGE=ANGE+(A12*TQE-TEMP1*TQR)/TEMP
      GO TO 503
  257 C3=FRQ*DMS(J)
      IF(C3-0.0003) 258,258,259
  258 C4=C3*C3
      A11=1.0-0.5*C4
      A22=A11
      A12=DDT(J)
      A21=-C3*DIN(J) *FRQ
      GO TO 351
  259 A11=DCOS(C3)
      A22=A11
      C5=DIN(J)*FRQ
      C4=DSIN(C3)
      A12=C4/C5
      A21=-C4*C5
  351 C1=ANGE
      ANGE=A11*ANGE+A12*TQE+A13 E
      TQE=A21*C1   +A22*TQE
      C1=ANGR
      ANGR=A11*ANGR+A12*TQR+A13R
      TQR=A21*C1   +A22*TQR
      A13R=0.0
      A13E=0.0
  503 J=J+1
      IF(J-NS) 2280,2280,401
  401 IF(MDIAG+1) 410,410,411
  410 IF (NPLG) 1090,1090,1091
 1090 WRITE(NW,181)
 1091 WRITE(NW,126)
      WRITE(NW,701)
  411 DO 403 J=1,NS
      TRR1(J)=TRR(J)
      THR1(J)=THR(J)
      TLR1(J)=TLR(J)
```

```
      TRE1(J)=TRE(J)
      THE1(J)=THE(J)
      TLE1(J)=TLE(J)
      IF(MDIAG+1) 1030,1030,403
 1030 WRITE(NW,108)J,THR1(J),THE1(J),TLR1(J),TLE1(J),TRR1(J),TRE1(J)
  403 CONTINUE
      M1=M1+1
      GO TO 502
  402 IRAT=1
      IF(BRAT(1)-1.0) 4132,4130,4132
 4130 IF(BRAT(2)) 4132,4133,4132
 4132 IRAT=2
 4133 IF(MDIAG+1) 412,412,413
  412 IF(NPLG) 414,414,415
  414 WRITE(NW,182)
  415 WRITE(NW,126)
      WRITE(NW,701)
  413 DO 404 J=1,NS
      IF(IRAT-2) 4040,4041,4040
 4040 TLR2(J)=TLR(J)
      THE2(J)=THE(J)
      TLE2(J)=TLE(J)
      TRR2(J)=TRR(J)
      TRE2(J)=TRE(J)
      THR2(J)=THR(J)
      GO TO 4045
 4041 TEMPS(1)=TLR(J)
      TEMPS(2)=TLE(J)
      CALL CDIV(TEMPS,BRAT,TEMPS)
      TLR2(J)=TEMPS(1)
      TLE2(J)=TEMPS(2)
      TEMPS(1)=THR(J)
      TEMPS(2)=THE(J)
      CALL CDIV(TEMPS,BRAT,TEMPS)
      THR2(J)=TEMPS(1)
      THE2(J)=TEMPS(2)
      TEMPS(1)=TRR(J)
      TEMPS(2)=TRE(J)
      CALL CDIV(TEMPS,BRAT,TEMPS)
      TRR2(J)=TEMPS(1)
      TRE2(J) =TEMPS(2)
 4045 IF(MDIAG+1) 1040,1040,404
 1040 WRITE(NW,108)J,THR2(J),THE2(J),TLR2(J),TLE2(J),TRR2(J),TRE2(J)
  404 CONTINUE
      IF(IRAT-2) 4050,4046,4050
 4046 IF(NPLG) 4050,4050,4047
 4047 DO 4048 KK=1,NPLG
      CALL CDIV2(TBR,TBE,BRAT,KK,MDIAG)
      CALL CDIV2(TPR,TPE,BRAT,KK,MDIAG)
      CALL CDIV2(TFSPR,TFSPE,BRAT,KK,MDIAG)
```

```
      CALL CDIV2(TFPRR,TFPRE,BRAT,KK,MDIAG)
      CALL CDIV2(TTPCR,TTPCE,BRAT,KK,MDIAG)
 4048 CALL CDIV2(TTGRR,TTGRE,BRAT,KK,MDIAG)
 4050 C1=TRR2(NS)
      C2=TRE2(NS)
      C3=TRR1(NS)
      C4=TRE1(NS)
      C5=C4/C3
      C6=C3+C4*C5
      Q1R=-(C1+C5*C2)/C6
      Q1E=(C1*C5-C2)/C6
      IF (MDIAG-2) 1049,1051,1049
 1049 IF(MDIAG) 1050,1051,1050
 1050 WRITE(NW,183)
      WRITE(NW,126)
      WRITE(NW,701)
 1051 L=1
      DO 407 J=1,NS
      C1=THR1(J)*Q1R+THR2(J) -Q1E*THE1(J)
      C2=THR1(J)*Q1E+THE2(J)+Q1R*THE1(J)
      C3=TLR1(J)*Q1R+TLR2(J) -Q1E*TLE1(J)
      C4=TLR1(J)*Q1E+TLE2(J)+TLE1(J)*Q1R
      C5    =TRR1(J)*Q1R-Q1E*TRE1(J)+TRR2(J)
      C6    =TRR1(J)*Q1E+Q1R*TRE1(J)+TRE2(J)
      NGS =LS(L)
      IF(J-NGS) 1054,1100,1054
 1100 TTFR(L) =C5/RP(L)
      TTFE(L) =C6/RP(L)
      L =L+1
 1054 IF(MDIAG) 1055,407,1055
 1055 IF(MPOL) 1056,1057,1056
 1056 WRITE(NW,108)J,C1,C2,C3,C4,C5,C6
      IF(MPOL) 407,1057,1057
 1057 THR1(J)=AMPF(C1,C2)
      THE1(J)=PANGF(C1,C2)
      TLR1(J)=AMPF(C3,C4)
      TLE1(J)=PANGF(C3,C4)
      TLR2(J)=AMPF(C5,C6)
      TLE2(J)=PANGF(C5,C6)
  407 CONTINUE
C TEST FOR POLAR FORM OPTION
      IF(MPOL) 1195,1058,1058
 1058 WRITE(NW,126)
      WRITE(NW,123)
      DO 1059 J=1,NS
 1059 WRITE(NW,108)J,THR1(J),THE1(J),TLR1(J),TLE1(J),TLR2(J),TLE2(J)
 1195 IF(NPLG) 1201,1201,1196
 1196 IF(MDIAG) 1199,1201,1199
 1199 DO 1200 J=1,NPLG
      C7 =PN(J) *RS(J)
```

```
      C8 =( RS(J) +2. *RW(J))*PN(J)
      C1 =TBR(1,J)*Q1R+TBR(2,J)-Q1E*TBE(1,J)
      C2 =TBR(1,J)*Q1E+TBE(2,J)+Q1R*TBE(1,J)
      C3 =C7*(TFSPR(1,J)*Q1R+TFSPR(2,J)-Q1E*TFSPE(1,J))
      C4 =C7*(TFSPR(1,J)*Q1E+TFSPE(2,J)+Q1R*TFSPE(1,J))
      C5 =TTPCR(1,J)*Q1R+TTPCR(2,J)-Q1E*TTPCE(1,J)
      C6 =TTPCR(1,J)*Q1E+TTPCE(2,J)+Q1R*TTPCE(1,J)
      IF(MPOL) 1060,1061,1060
 1060 WRITE(NW,700)
      WRITE(NW,701)LEC(J),C1,C2,C3,C4,C5,C6
      IF(MPOL) 1062,1061,1061
 1061 WRITE(NW,700)
      JP=1
 1062 TE1=AMPF(C1,C2)
      TE2=PANGF(C1,C2)
      TE3=AMPF(C3,C4)
      TE4=PANGF(C3,C4)
      TE5=AMPF(C5,C6)
      TE6=PANGF(C5,C6)
      WRITE(NW,123)
      WRITE(NW,108)LEC(J),TE1,TE2,TE3,TE4,TE5,TE6
      GO TO (1063,1200),JP
 1063 C1=TPR(1,J)*Q1R+TPR(2,J)-Q1E*TPE(1,J)
      C2 =TPR(1,J)*Q1E+TPE(2,J)+Q1R*TPE(1,J)
      C3 =C8*(TFPRR(1,J)*Q1R+TFPRR(2,J)-Q1E*TFPRE(1,J))
      C4 =C8*(TFPRR(1,J)*Q1E+TFPRE(2,J)+Q1R*TFPRE(1,J))
      C5 =TTGRR(1,J)*Q1R+TTGRR(2,J)-Q1E*TTGRE(1,J)
      C6 =TTGRR(1,J)*Q1E+TTGRE(2,J)+Q1R*TTGRE(1,J)
      IF(MPOL) 1064,1065,1064
 1064 WRITE(NW,702)
      WRITE(NW,701)LEC(J),C1,C2,C3,C4,C5,C6
      IF(MPOL) 1200,1065,1065
 1065 JP=2
      WRITE(NW,702)
      GO TO 1062
 1200 CONTINUE
 1201 IF(NSRG) 1207,1207,1202
 1202 IF(MPOL) 1203,1205,1203
 1203 WRITE(NW,180)
      DO 1070 J=1,NSRG
 1070 WRITE (NW,108) LS(J),TTFR(J),TTFE(J)
      IF(MPOL) 1207,1205,1205
 1205 WRITE(NW,124)
      DO 1206 J=1,NSRG
      C1=AMPF(TTFR(J),TTFE(J))
      C2=PANGF(TTFR(J),TTFE(J))
 1206 WRITE(NW,108)LS(J),C1,C2
 1207 IF(NPLG) 1219,1219,1079
 1079 IF(MPOL) 1210,1215,1210
 1210 WRITE(NW,122)
```

```
1215 DO 1080 J=1,NPLG
     TE1=TFSPR(1,J)
     TE2=TFSPR(2,J)
     TE3=TFSPE(1,J)
     TE4=TFSPE(2,J)
     C1=TE1*Q1R+TE2-TE3*Q1E
     C2=TE1*Q1E+TE4+TE3*Q1R
1076 TE1=TFPRR(1,J)
     TE2=TFPRR(2,J)
     TE3=TFPRE(1,J)
     TE4=TFPRE(2,J)
     C3=TE1*Q1R+TE2-TE3*Q1E
     C4=TE1*Q1E+TE4+TE3*Q1R
     IF(MPOL) 1216,1077,1216
1077 THR1(J)=AMPF(C1,C2)
     THE1(J)=PANGF(C1,C2)
     TLR1(J)=AMPF(C3,C4)
     TLE1(J)=PANGF(C3,C4)
     GO TO 1080
1216 WRITE(NW,108)LEC(J),C1,C2,C3,C4
1080 CONTINUE
     IF(MPOL) 1219,1217,1217
1217 WRITE(NW,125)
     DO 1218 J=1,NPLG
1218 WRITE(NW,108)THR1(J),THE1(J),TLR1(J),TLE1(J)
1219 IF(NEX-MAX) 5007,501,501
5007 IF(ISEP-1) 5009,5008,5009
5008 ISEP=2
     GO TO 5020
5009 NEX=NEX+1
     IF(NEX-MAX) 5020,501,501
 501 CONTINUE
5010 IF(INP) 506,200,506
 506 CALL EXIT
 100 FORMAT(72H1
    :                                    )
 101 FORMAT(9I5,5X,3I5,10X,I5)
 102 FORMAT(5X,6E12.4)
 103 FORMAT(82H0 TORSIONAL RESPONSE OF THE SYSTEM WITH GEARS,EPICYCLIC
    1GEARS AND BRANCHES  PN408 )
 105 FORMAT(8X,6E12.5)
 106 FORMAT(1H0,1X,8HSTATIONS,1X,12HBRG+EXT.CON.,2X,8HBRANCHES,1X,
    19HNO.OF FRQ,2X,8HINP SETS,2X,8HSR GEARS,2X,8HPL GEARS/
    2        I7,6X,I5,2X,5I10)
 107 FORMAT(/5X,10HROTOR DATA//4X,3HSTA,1X,12H  MOM.INERT.,3X,
    16HLENGTH,4X,10HSTIFFN.DIA,3X,8HMASS DIA,3X,9HINNER DIA,2X,
    212HCONC. COMPL./4X3HNO.2X,9HLBS-IN**2,7X,2HIN,10X,2HIN,10X,2HIN,
    310X,2HIN,6X, 9HRAD/IN-LB)
 108 FORMAT(I7,1X,6E12.5)
 109 FORMAT(/1H1,7X,46HEXTERNAL TORSIONAL CONSTRAINT AND DAMPING DATA//
```

```
   1 4X,3HSTA,2X, 9HSTIFFNESS,2X,24HDAMPING- (LB-IN-SEC/RAD)/
   2 4X,3HNO.,1X,11H(LB-IN/RAD),2X,9HTO GROUND,2X,12HTO NEXT STA.)
112 FORMAT(/1H1,9X,26HSINGLE REDUCTION GEAR DATA)
113 FORMAT(/4X,3HSTA,3X,20HGEAR SET RADII (IN.),2X,
   1 31HCOMBINED TANGENTIAL COMPLIANCES//9X,10HFIRST GEAR,2X
   2 ,11HSECOND GEAR,3X,7H(IN/LB))
114 FORMAT (/15X,18HPLANETARY SET DATA)
118 FORMAT(/5X,17HBRANCHES           /6X,7HFAR END,5X,6HCOMMON)
119 FORMAT(6X,3(I5,5X))
120 FORMAT ( 1H0,5X,11HFREQUENCY =,E14.6,2X,3HCPS)
121 FORMAT(/1H1)
122 FORMAT(/ 8X,40HCOMPUTED RESPONSE AT PLANETARY GEAR SETS//
   1 10X,43HTANGENTIAL TOOTH FORCE AT EACH PLANET (LBS)/
   2 4X,3HSTA,8X,10HSUN-PLANET,13X,11HRING-PLANET/
   3 4X,3HNO.,5X,4HREAL,6X,9HIMAGINARY,5X,4HREAL,6X,9HIMAGINARY)
123 FORMAT(9X,9HAMPLITUDE,1X,13HPHASE-ANG,DEG,1X,9HAMPLITUDE,1X,
   1 13HPHASE-ANG,DEG,1X,9HAMPLITUDE,1X,13HPHASE-ANG,DEG)
124 FORMAT(/8X,36HCOMPUTED RESPONSE AT SIMPLE GEAR SET/
   1/ 4X,3HSTA,2X,28HTANGENTIAL TOOTH FORCE (LBS)/  9X,9HAMPLITUDE,
   2 1X ,13HPHASE-ANG,DEG)
125 FORMAT(/ 8X,40HCOMPUTED RESPONSE AT PLANETARY GEAR SETS//
   1 10X,43HTANGENTIAL TOOTH FORCE AT EACH PLANET (LBS)/
   2 4X, 3HSTA,8X,10HSUN-PLANET,13X,11HRING-PLANET/ 4X,3HNO.,2X,
   3 9HAMPLITUDE,1X,13HPHASE-ANG,DEG,1X,9HAMPLITUDE,1X,
   4 13HPHASE-ANG,DEG)
126 FORMAT(/ 4X,3HSTA,4X,19HANGULAR DISP.(RAD.)  ,5X, 8HTORQUE-1,2X,
   1 8H(IN-LBS),6X, 8HTORQUE-2,2X,8H(IN-LBS))
127 FORMAT(/4X,3HSTA,4X,6HNO. OF,8X,3HSUN,7X,6HPLANET/
   14X,3HNO.,3X,7HPLANETS,4X,10HRADIUS(IN),2X,10HRADIUS(IN))
128 FORMAT(/4X,3HSTA,2X,10HWEIGHT(LB),4X,41HPOLAR MASS MOMENTS OF INER
   1TIA (LBS-IN**2)/ 4X,3HNO.,4X,6HPLANET,8X,3HSUN,7X,6HPLANET,7X,
   24HRING,7X,7HCARRIER)
129 FORMAT(/4X,3HSTA,6X,26HCOMPLIANCE- LINEAR(IN./LB),16X,
   1 15HCOM-ANG(RAD/LB)/ 4X,3HNO.,2X,10HSUN-PLANET,2X,11HPLANET-RING,
   2 1X,10HPLAN.-CAR.,14X,11HRING-GROUND)
130 FORMAT (I5,3E12.4,12X,E12.4)
131 FORMAT(I7,1X,3E12.4,12X,E12.4)
132 FORMAT(/5X,13HBRANCH OPTION,I5)
135 FORMAT(/9X,10HSHEAR MOD.,2X,11HWT. DENSITY/9X, 9HLBS/IN**2 ,3X,
   1 9HLBS/IN**3/8X,2E12.5)
136 FORMAT(/5X,35HADDED EXCITATION TREATED SEPARATELY)
180 FORMAT (/8X,36HCOMPUTED RESPONSE AT SIMPLE GEAR SET/
   1/4X,3HSTA,2X,28HTANGENTIAL TOOTH FORCE (LBS)/12X,4HREAL,6X,
   2 9HIMAGINARY)
181 FORMAT(12H0DIAGNOSTICS/5X,53HFIRST PASS- UNIT AMPLITUDE AT STATION
   1 1-NO EXCITATION)
182 FORMAT(12H0DIAGNOSTICS/5X,57HSECOND PASS- ZERO AMPLITUDE AT STATIO
   1N 1- WITH EXCITATION)
183 FORMAT(42H0OUTPUT- COMPUTED RESPONSE AT ALL STATIONS/
   110X,63H(TORQUE-1- GOING INTO STATION, TORQUE-2- COMING OUT OF STAT
```

```
   2ION))
184 FORMAT(8X,6HTFSPR1,6X,6HTFSPR2,6X,6HTFSPE1,6X,6HTFSPE2,9X,3HQIR,
   19X,3HQIE)
185 FORMAT(8X,6HTFPRR1,6X,6HTFPRR2,6X,6HTFPRE1,6X,6HTFPRE2)
190 FORMAT (I5,6E12.4,I3)
191 FORMAT(36HOSTATION NO. INCORRECT OR OUT OF ORDER)
192 FORMAT( 37HOSTATION NO. FOR GEAR ERROR INCORRECT)
194 FORMAT(1H1,14X,46HSINGLE REDUCTION GEAR- LINEAR EXCITATION (IN.)/
   14X,3HSTA,2X,9HFREQUENCY,6X,4HREAL,6X,9HIMAGINARY)
195 FORMAT(1H1,14X,39HPLANETARY GEAR- LINEAR EXCITATION (IN.)/
   14X,3HSTA,2X,9HFREQUENCY,9X, 8HSUN GEAR,17X, 9HRING GEAR/
   224X,4HREAL,6X,9HIMAGINARY,5X,4HREAL,6X 9HIMAGINARY)
700 FORMAT(/4X,3HSTA,1X,24HANG. DISP.-PLANET CENTER,1X,
   1 22HTOT. TORQUE SUN-PLANET,2X,23HTOT TORQUE PLAN-CARRIER)
701 FORMAT( 4X,3HNO.,5X,4HREAL,6X,9HIMAGINARY,5X,4HREAL,6X,9HIMAGINARY
   15X,4HREAL,6X,9HIMAGINARY /I7,,X,6E12.5)
702 FORMAT(/ 4X,3HSTA,2X,22HANG. DISP.-PLANET BODY,2X,
   1 23HTOT. TORQUE PLANET-RING,2X,22HTOT. TORQUE GRND.-RING)
    END
```

Subroutine PLNST

```
    SUBROUTINE PLNST
    COMMON TBR(2,2),TBE(2,2),TPR(2,2),TPE(2,2),TFSPR(2,2),TFSPE(2,2),
   1 TFPRR(2,2),TFPRE(2,2),TTPCR(2,2),TTPCE(2,2),TTGRR(2,2),TTGRE(2,2)
    COMMON RIP(200),DST(200),DMS(200),DIN(200),BCB(50),LB(50),DDI(200)
   1,BK(50),LEC(2),RS(2),RW(2),PIP(2),PMS(2),PN(2),SS(2),SW(2),SR(2),
   2 ST(2),LBR(20),LBS(20),CCOM(200),AXY1,AXY2,BXY1,BXY2,TLR(200),
   3 TLE(200),THR(200),THE(200),TRR(200),TRE(200),TRR1(200)
    COMMON A(7,7),B(7,2),LS(20),RP(20),RG(20),SG(20),TRR2(200),
   1 TRE1(200),THE1(200),TLE1(200),TRE2(200),TTFR(20),TTFE(20),
   2 PSP(2),THR1(200),TLR1(200),THR2(200),TLR2(200),THE2(200),
   3 TLE2(200),RL(200),PCP(2),PRP(2)   ,DMP(50)
    COMMON IT, K4,L4,MDIAG,FRQ2,ANGR,ANGE,TQR,TQE ,J,NS ,M1,NW,NR,NPLG
    COMMON  K1,K2,K3,K9,L1,L2,L3,L9,LG(10),IBRAN
    C1=RS(K4)+RW(K4)
    C2=C1+RW(K4)
    FLNL=PN(K4)
    A(1,1)=RW(K4)
    A(1,2)=0.
    A(1,3)= FRQ2*PIP(K4)
    A(1,4)=0.
    A(1,5)=0.
```

```
A(1,6)=0.
A(1,7)=0.
A(2,1)=1.0
A(2,2)=-1.0
A(2,3)=0.
A(2,4)=-FRQ2*PMS(K4)*C1
A(2,5)=0.
A(2,6)=0.
A(2,7)=0.
A(3,1)=0.
A(3,2)=C1
A(3,3)=0.
A(3,4)=0.
A(3,5)=-1.0
A(3,6)=0.
A(3,7)=-FRQ2*PCP(K4)
A(4,1)=C2
A(4,2)=0.
A(4,3)=0.
A(4,4)=0.
A(4,5)=0.
A(4,6)=FRQ2*PRP(K4)*ST(K4)-1.0
A(4,7)=0.
A(5,1)=0.
A(5,2)=SW(K4)
A(5,3)=0.
A(5,4)=C1
A(5,5)=0.
A(5,6)=0.
A(5,7)=-(FLNL)*C1
A(6,1)=0.
A(6,2)=0.
A(6,3)=-RW(K4)
A(6,4)=-C1
A(6,5)=0.
A(6,6)=0.
A(6,7)=0.
A(7,1)=SR(K4)
A(7,2)=0.
A(7,3)= RW(K4)
A(7,4) =-C1
A(7,5)=0.
A(7,6)=FLNL*C2*ST(K4)
A(7,7)=0.
C3 =PSP(K4)*FRQ2
FSR=(TLR(J)-C3*THR(J))/RS(K4)
FSI=(TLE(J)-C3*THE(J))/RS(K4)
B(1,1)=RW(K4)*FSR
B(1,2)=RW(K4)*FSI
B(2,1)=-FSR
```

```
      B(2,2)=-FSI
      B(3,1)=0.
      B(3,2)=0.
      B(4,1)=0.
      B(4,2)=0.
      B(5,1)=0.
      B(5,2)=0.
      IF(M1-1) 440,440,441
  441 IF(L4-IT) 440,443,440
  440 EE1=0.
      EE2=0.
      EE3=0.
      EE4=0.
      GO TO 442
  443 EE1 =AXY1*FLNL
      EE2=BXY1*FLNL
      EE3=AXY2*FLNL
      EE4 =BXY2*FLNL
  442 B(6,1)=-RS(K4)*FLNL*THR(J)+EE1-SS(K4)*FSR
      B(6,2)=-RS(K4)*FLNL*THE(J)+EE2-SS(K4)*FSI
      B(7,1) =EE3
      B(7,2) =EE4
      CALL MATIN (A,7,B,2,CF9,IDD)
      TQR=B(5,1)
      EER=B(6,1)
      ANGR=B(7,1)
      TQE=B(5,2)
      EEI=B(6,2)
      ANGE=B(7,2)
      TFPRR(M1,K4)=B(1,1)/FLNL
      TFPRE(M1,K4)=B(1,2)/FLNL
      TTPCR(M1,K4)=C1*B(2,1)
      TTPCE(M1,K4)=C1*B(2,2)
C TTPCR= TOTAL TORQUE, PLANET-CARRIER, REAL
C TTPCE= TOTAL TORQUE, PLANET-CARRIER, IMAGINARY
      TPR(M1,K4)=B(3,1) /FLNL
      TPE(M1,K4)=B(3,2) /FLNL
      TBR(M1,K4)=B(4,1) /FLNL
      TBE(M1,K4)=B(4,2) /FLNL
      TTGRR(M1,K4)=EER
      TTGRE(M1,K4)=EEI
      TFSPR(M1,K4)=FSR/FLNL
      TFSPE(M1,K4)=FSI/FLNL
      C3=RS(K4)*FSR
      C4=PS(K4)*FSI
      C5=C2*B(1,1)
      C6=C2*B(1,2)
C TEST DIAGNOSTIC
      IF(MDIAG) 600,608,608
  600 IF(K4-1) 621,620,621
```

```
620 WRITE(NW,703)
621 WRITE(NW,700)
    WRITE(NW,701)L4,TBR(M1,K4),TBE(M1,K4),C3,C4,TTPCR(M1,K4),
   1 TTPCE(M1,K4)
    WRITE(NW,702)
    WRITE(NW,701)L4,TPR(M1,K4),TPE(M1,K4),C5,C6,TTGRR(M1,K4),
   1 TTGRE(M1,K4)
608 K4=K4+1
    IF(K4-NPLG) 332,332,333
332 L4=LEC(K4)
    RETURN
333 L4=NS+2
    RETURN
700 FORMAT(/4X,3HSTA,1X,24HANG. DISP.-PLANET CENTER,1X,
   1 22HTOT. TORQUE SUN-PLANET,2X,23HTOT TORQUE PLAN-CARRIER)
701 FORMAT( 4X,3HNO.,5X,4HREAL,6X,9HIMAGINARY,5X,4HREAL,6X,9HIMAGINARY
   15X,4HREAL,6X,9HIMAGINARY /I7,1X,6E12.5)
702 FORMAT(/ 4X,3HSTA,2X,22HANG. DISP.-PLANET BODY,2X,
   1 23HTOT. TORQUE PLANET-RING,2X,22HTOT. TORQUE GRND.-RING)
703 FORMAT(/15X,              66HALL TORQUES GIVEN IN INCH-LB, AND ANGUL
   1AR DISPLACEMENTS IN RADIANS)
705 FORMAT(12X,4HREAL,6X,9HIMAGINARY,5X,4HREAL,6X,9HIMAGINARY,5X,
   14HREAL,6X,9HIMAGINARY)
    END
```

Subroutine MATIN

```
      SUBROUTINE MATIN(A,N1,B,M1,DETER,ID)
      DIMENSION A(7,7),B(7,2),INDEX(7,3)
C
C     GENERAL FORM OF DIMENSION STATEMENT
C
      EQUIVALENCE (IROW,JROW), (ICOLU ,JCOLU ), (AMAX, T, SWAP)
C
C     INITIALIZATION
C
      M=M1
      N=N1
   10 DETER =1.0
   15 DO 20 J=1,N
   20 INDEX(J,3) = 0
   30 DO 550 I=1,N
C
C     SEARCH FOR PIVOT ELEMENT
```

```
C
   40 AMAX=0.0
   45 DO 105 J=1,N
      IF(INDEX(J,3)-1) 60, 105, 60
   60 DO 100 K=1,N
      IF(INDEX(K,3)-1) 80, 100, 715
   80 IF (      AMAX -ABS (A(J,K))) 85, 100, 100
   85 IROW=J
   90 ICOLU =K
      AMAX=ABS (A(J,K))
  100 CONTINUE
  105 CONTINUE
      INDEX(ICOLU ,3) = INDEX(ICOLU ,3) +1
  260 INDEX(I,1)=IROW
  270 INDEX(I,2)=ICOLU
C
C     INTERCHANGE ROWS TO PUT PIVOT ELEMENT ON DIAGONAL
C
  130 IF (IROW-ICOLU ) 140, 310, 140
  140 DETER =-DETER
  150 DO 200 L=1,N
  160 SWAP=A(IROW,L)
  170 A(IROW,L)=A(ICOLU ,L)
  200 A(ICOLU ,L)=SWAP
      IF(M) 310, 310, 210
  210 DO 250 L=1, M
  220 SWAP=B(IROW,L)
  230 B(IROW,L)=B(ICOLU ,L)
  250 B(ICOLU ,L)=SWAP
C
C     DIVIDE PIVOT ROW BY PIVOT ELEMENT
C
  310 PIVOT   =A(ICOLU ,ICOLU )
      DETER =DETER *PIVOT
  330 A(ICOLU ,ICOLU )=1.0
  340 DO 350 L=1,N
  350 A(ICOLU ,L)=A(ICOLU ,L)/PIVOT
  355 IF(M) 380, 380, 360
  360 DO 370 L=1,M
  370 B(ICOLU ,L)=B(ICOLU ,L)/PIVOT
C
C     REDUCE NON-PIVOT ROWS
C
  380 DO 550 L1=1,N
  390 IF(L1-ICOLU ) 400, 550, 400
  400 T=A(L1,ICOLU )
  420 A(L1,ICOLU )=0.0
      IF(T)430,550,430
  430 DO 450 L=1,N
  450 A(L1,L)=A(L1,L)-A(ICOLU ,L)*T
```

```
  455 IF(M) 550, 550, 460                                          0067
  460 DO 500 L=1,M                                                 0068
  500 B(L1,L)=B(L1,L)-B(ICOLU ,L)*T                                0069
  550 CONTINUE                                                     0070
C                                                                  0071
C     INTERCHANGE COLUMNS                                          0072
C                                                                  0073
  600 DO 710 I=1,N                                                 0074
  610 L=N+1-I                                                      0075
  620 IF (INDEX(L,1)-INDEX(L,2)) 630, 710, 630                     0076
  630 JROW=INDEX(L,1)                                              0077
  640 JCOLU =INDEX(L,2)                                            0078
  650 DO 705 K=1,N                                                 0079
  660 SWAP=A(K,JROW)                                               0080
  670 A(K,JROW)=A(K,JCOLU )                                        0081
  700 A(K,JCOLU )=SWAP                                             0082
  705 CONTINUE                                                     0083
  710 CONTINUE                                                     0084
      DO 730 K = 1,N                                               0085
      IF(INDEX(K,3) -1) 715,720,715                                0086
  720 CONTINUE                                                     0089
  730 CONTINUE                                                     0090
      ID=1                                                         0091
  740 RETURN                                                       0092
  715 ID =2                                                        0087
      WRITE(6,760)
  760 FORMAT (5X,18HMATRIX IS SINGULAR)
      GO TO 740                                                    0088
      END                                                          0093
```

Subroutine BLOOP

```
      SUBROUTINE BLOOP(LFE,LOC,LMC,LI,KL,LF,NBR,LIT,KLT,LFT)
      DIMENSION LT1(2),LT2(2),LT3(2),LT4(2),LT9(2),KT1(2),KT2(2),KT3(2)
     1, KT4(2),KT9(2),MLIT(2),MKLT(2),MLFT(2)
      DIMENSION LFE(20),LOC(20),LMC(20),TC(2),OC(2),TCT(2),OCT(2),TCZ(2)
     1,OCZ(2),TMZ(2),OMZ(2),TM1(2),TBCZ(2),OM(2),TBM(2),TF(2),OM1(2),
     2TCTH(2),CCTH(2),TEMP1(2),TEMP2(2),OF(2)
      COMMON TBR(2,2),TBE(2,2),TPR(2,2),TPE(2,2),TFSPR(2,2),TFSPE(2,2),
     1 TFPRR(2,2),TFPRE(2,2),TTPCR(2,2),TTPCE(2,2),TTGRR(2,2),TTGRE(2,2)
      COMMON RIP(200),DST(200),DMS(200),DIN(200),BCB(50),LB(50),DOT(200)
     1,BK(50),LEC(2),RS(2),RW(2),PIP(2),PMS(2),PN(2),SS(2),SW(2),SR(2),
     2 ST(2),LBR(20),LBS(20),CCOM(200),AXY1,AXY2,BXY1,BXY2,TLR(200),
     3 TLE(200),THR(200),THE(200),TRR(200),TRE(200),TRR1(200)
      COMMON A(7,7),B(7,2),LS(20),RP(20),RG(20),SG(20),TRR2(200),
     1 TRE1(200),THE1(200),TLE1(200),TRE2(200),TTFR(20),TTFE(20),
     2 PSP(2),THR1(200),TLR1(200),THR2(200),TLR2(200),THE2(200),
     3 TLE2(200),RL(200),PCP(2),PRP(2)   ,DMP(50)
      COMMON II, K4,L4,MDIAG,FRU2,ANGR,ANGE,TOR,TOE  ,J,NS  ,M1,NW,NR,NPLG
      COMMON  K1,K2,K3,K9,L1,L2,L3,L9,LG(10),IBRAN
      IF(LI-1)2,1,2
    1 II=1
      ID=0
      IF(LMC(KL)) 5,4,4
    5 ID=1
      LMC(KL)=-LMC(KL)
      GO TO 4
    2 IF(LI-4) 9,3,9
    3 II=2
    4 LT1(II)=L1
      LT2(II)=L2
      LT3(II)=L3
      LT4(II)=L4
      LT9(II)=L9
      KT1(II)=K1
      KT2(II)=K2
      KT3(II)=K3
      KT4(II)=K4
      KT9(II)=K9
      MLIT(II)=LIT
      MKLT(II)=KLT
      MLFT(II)=LFT
    9 GO TO (10,20,30,40,50,60,70,71),LI
   10 DO 11 II=1,2
        TC(II)=0.0
      OC(II)=0.0
      TCT(II)=0.0
      OCT(II)=0.0
      TCZ(II)=0.0
      OCZ(II)=0.0
      TMZ(II)=0.0
      OMZ(II)=0.0
```

```
      TM1(II)=0.0
      OM1(II)=0.0
      TBCZ(II)=0.0
   11 OM(II)=0.0
      TBM(II)=0.0
      TF(II)=0.0
      TCTH(II)=0.0
      OCTH(II)=0.0
      OF(II)=0.0
      TC(1)=TQR
      TC(2)=TQE
      OC(1)=ANGR
      OC(2)=ANGE
      ANGR=0.0
      ANGE=0.0
      TQR=0.0
      TQE=0.0
      LF=LOC(KL)
      GO TO 90
   20 TCZ(1)=TQR
      TCZ(2)=TQE
      OCZ(1)=ANGR
      OCZ(2)=ANGE
      ANGR=1.
      ANGE=0.
      TQR=0.
      TQE=0.
      GO TO 97
   30 TCTH(1)=TQR
      TCTH(2)=TQE
      OCTH(1)=ANGR
      OCTH(2)=ANGE
      IF(LMC(KL)) 31,35,31
   31 ANGR=0.0
      ANGE=0.0
      TQR=1.0
      TQE=0.0
      GO TO 97
   35 TF(1)=0.0
      TF(2)=0.0
      GO TO 45
   40 IF(LMC(KL)) 400,55,400
  400 TCT(1)=TQR
      TCT(2)=TQE
      OCT(1)=ANGR
      OCT(2)=ANGE
      OF(1)=0.0
      OF(2)=0.0
   41 CALL CSUB(OCTH,OCZ,TEMP1)
      CALL CMPY(TEMP1,OF,TEMP1)
```

```
      CALL CSUB(OC,OCZ,TEMP2)
      CALL CSUB(TEMP2,TEMP1,TEMP1)
      CALL CSUB(OCT,OCZ,TEMP2)
      CALL CDIV(TEMP1,TEMP2,TF)
      IF(LI-6) 42,44,42
   42 CALL CSUB(TCTH,TCZ,TEMP1)
      CALL CMPY(TEMP1,OF,TEMP1)
      CALL CSUB(TCT,TCZ,TEMP2)
      CALL CMPY(TF,TEMP2,TEMP2)
      CALL CADD(TEMP1,TEMP2,TEMP1)
      CALL CADD(TEMP1,TCZ,TBCZ)
      CALL CADD(TBCZ,TC,TEMP1)
      ANGR=OC(1)
      ANGE=OC(2)
      LF=LMC(KL)
      TQR=TEMP1(1)
      TQE=TEMP1(2)
      GO TO (90,90,90,80,98,97,90),LI
   44 ANGR=OF(1)
      ANGE=OF(2)
      TQR=TF(1)
      TQE=TF(2)
      J=LFE(KL)
      LF=LOC(KL)
      J1=LF
      J2=LMC(KL)
      II=1
      GO TO 99
   45 CALL CSUB(OCTH,OCZ,TEMP1)
      CALL CSUB(OC,OCZ,TEMP2)
      CALL CDIV(TEMP2,TEMP1,OF)
      ANGR=OF(1)
      ANGE=OF(2)
      TQR=TF(1)
      TQE=TF(2)
      GO TO 97
   50 TMZ(1)=TQR
      TMZ(2)=TQE
      OMZ(1)=ANGR
      OMZ(2)=ANGE
      OF(1)=1.0
      OF(2)=0.0
      GO TO 41
   55 CALL CSUB(TCTH,TCZ,TEMP1)
      CALL CMPY(TEMP1,OF,TEMP1)
      CALL CADD(TEMP1,TCZ,TBM)
      CALL CADD(TC,TBM,TEMP2)
      TQR=TEMP2(1)
      TQE=TEMP2(2)
      GO TO 71
```

```
60  TM1(1)=TQR
    TM1(2)=TQE
    OM1(1)=ANGR
    OM1(2)=ANGE
    TEMP1(1)=1.0-OM1(1)
    TEMP1(2)=OM1(2)
    CALL CADD(TEMP1,OMZ,TEMP1)
    CALL CDIV(OMZ,TEMP1,OF)
    GO TO 41
70  TEMP1(1)=TQR
    TEMP1(2)=TQE
    CALL CADD(TEMP1,TC,TEMP1)
    TQR=TEMP1(1)
    TQE=TEMP1(2)
    GO TO 85
71  KL=KL+1
    IF(KL-NBR) 72,72,73
72  LF=LFE(KL)
    LI=1
    GO TO 74
73  LF=NS+2
    LI=0
74  IF(ID) 75,92,75
75  J3=KL-1
    IF(LMC(J3)) 77,76,77
76  J2=LOC(J3)
    GO TO 78
77  J2=LMC(J3)
78  J1=LFE(J3)
    LMC(J3)=-LMC(J3)
    DO 79 IO=J1,J2
79  WRITE(NW,108) IO,THR(IO),THE(IO),TLR(IO),TLE(IO),TRR(IO),TRE(IO)
    GO TO 91
80  J1=LFE(KL)
    J2=LOC(KL)
    GO TO 990
85  LF=LMC(KL)
    GO TO 80
90  LI=LI+1
    IF(ID) 91,92,91
91  WRITE(NW,100)
    WRITE(NW,101) (TC(II),OC(II),TCT(II),OCT(II),TCZ(II),OCZ(II),
   1II=1,2)
    WRITE(NW,102)
    WRITE(NW,101)(TMZ(II),OMZ(II),TM1(II),OM1(II),TBCZ(II),OM(II),
   1II=1,2)
    WRITE(NW,103)
    WRITE(NW,101)(TBM(II),TF(II),TCTM(II),OCTM(II),OF(II),II=1,2)
92  RETURN
97  J=LFE(KL)
```

```
      J2=LOC(KL)
      J1=J
      LF=J2
      II=1
      GO TO 99
   98 J2=LMC(KL)
      J=LOC(KL)
      J1=J
      LF=J2
      II=2
   99 L1=LT1(II)
      L2=LT2(II)
      L3=LT3(II)
      L4=LT4(II)
      L9=LT9(II)
      K1=KT1(II)
      K2=KT2(II)
      K3=KT3(II)
      K4=KT4(II)
      K9=KT9(II)
      LIT=MLIT(II)
      KLT=MKLT(II)
      LFT=MLFT(II)
  990 IF(TD) 90,90,992
  992 WRITE(NW,126)
      WRITE(NW,701)
      DO 991 IO=J1,J2
  991 WRITE(NW,108) IO,THR(IO),THE(IO),TLR(IO),TLE(IO),TRR(IO),TRE(IO)
      GO TO 90
  108 FORMAT(I7,1X,6E12.5)
  126 FORMAT(/ 4X,3HSTA,4X,19HANGULAR DISP.(RAD.)  ,5X, 8HTORQUE-1,2X,
     1 8H(IN-LBS),6X, 8HTORQUE-2,2X,8H(IN-LBS))
  701 FORMAT( 4X,3HNO.,5X,4HREAL,6X,9HIMAGINARY,5X,4HREAL,6X,9HIMAGINARY
     15X,4HREAL,6X,9HIMAGINARY /I7,1X,6E12.5)
  100 FORMAT(/14X,3HT-C,9X,3HO-C,7X,5HT-C,T,3X,9HTHETA-C,T,4X,
     1 5HT-C,O,3X,9HTHETA-C,O)
  101 FORMAT(5X,6E12.5)
  102 FORMAT(/12X,5HT-M,0,3X,9HTHETA-M,0,9X,5HT-M,1,3X,9HTHETA-M,1,
     19X,3HTBC,5X,7HTHETA-M)
  103 FORMAT(/14X,3HTBM,9X,3HT-F,3X,9HT-C,THETA,1X,11HTHETA-C,TM.,
     15X,7HTHETA-F)
      END
```

Subroutine CDIV

```
      SUBROUTINE CDIV(A,B,C)
      DIMENSION A(2),B(2),C(2)
      IF(B(2)) 10,5,10
    5 IF(B(1)) 7,6,7
    6 WRITE(6,101)
      GO TO 14
    7 C7=A(1)/B(1)
      C8=A(2)/B(1)
      GO TO 15
   10 IF(B(1)) 12,11,12
   11 C7=A(2)/B(2)
      C8= -A(1)/B(2)
      GO TO 15
   12 C5=B(2)/B(1)
      C6=B(1)+B(2)*C5
      C7   =(A(1)+C5*A(2))/C6
      C8  =(A(2)-A(1)*C5)/C6
      GO TO 15
   14 WRITE(6,100) (A(I),B(I),I=1,2),C7,C8
   15 C(1) =C7
      C(2)=C8
      RETURN
  100 FORMAT(5X,15HDIAGNOSTIC-CDIV/6E13.5)
  101 FORMAT(5X,/24HCOMPLEX DIVISION BY ZERO)
      END
```

Subroutine CDIV2

```
      SUBROUTINE CDIV2(A,B,C,K,M)
      DIMENSION A(2,2),B(2,2),C(2),TK(2)
      TK(1)=A(2,K)
      TK(2)=B(2,K)
      IF(M-5) 10,5,10
    5 WRITE(6,100) TK(1),TK(2),C(1),C(2)
   10 CALL CDIV(TK,C,TK)
      A(2,K)=TK(1)
      B(2,K)=TK(2)
      IF(M-5) 20,15,20
   15 WRITE(6,101) TK(1),TK(2)
   20 RETURN
  100 FORMAT(/14X,3HPFR,9X,3HPFE,7X,5HBRATR,7X,5HBRATE/5X,4E12.5)
  101 FORMAT(/10X,7HRATIO-R,5X,7HRATIO-E/5X,2E12.5)
      END
```

Function PANGF

```
      FUNCTION PANGF(A,B)
      IF (A) 30,50,30
   30 IF (B) 31,60,31
   31 THET = ATAN(B/A)*57.29577951
      PANGF = THET
      IF (A) 32,32,35
   32 PANGF = THET + 180.0
   33 RETURN
   35 IF (B) 36,33,33
   36 PANGF = THET + 360.0
       GO TO 33
   50 IF (B) 51,52,53
   51 PANGF = 270.0
      GO TO 33
   52 PANGF = 0.0
      GO TO 33
   53 PANGF = 90.0
      GO TO 33
   60 IF (A) 61,52,52
   61 PANGF = 180.0
      GO TO 33
      END
```

Function AMPF

```
FUNCTION AMPF(A,B)
C=B/A
AMPF = ABS(A)*SQRT(1.0+C*C)
END
```

Subroutine CADD

```
SUBROUTINE CADD(A,B,C)
DIMENSION A(2),B(2),C(2)
C(1)=A(1)+B(1)
C(2)=A(2)+B(2)
RETURN
END
```

Subroutine CSUB

```
SUBROUTINE CSUB(A,B,C)
DIMENSION A(2),B(2),C(2)
C(1)=A(1)-B(1)
C(2)=A(2)-B(2)
RETURN
END
```

Subroutine CMPY

```
SUBROUTINE CMPY(A,B,C)
DIMENSION A(2),B(2),C(2)
C1=A(1)*B(1)-A(2)*B(2)
C2=A(1)*B(2)+A(2)*B(1)
C(1)=C1
C(2)=C2
RETURN
END
```

APPENDIX V

NOISE LEVEL CALCULATIONS

INTRODUCTION

The noise in the immediate environment of an enclosed gear system originates in the dynamic forces which act on the internal components. The actual mechanism connecting these forces and the noise is very complex. It includes the transmission of the forces through the rotating elements, through the bearings, and into the casing which encloses the system. In the course of this transmission, the forces are subject to amplification or attenuation, according to the dynamic response of the components along which they travel. The casing itself responds to the forces applied at different points by vibrating in many modes, each different in amplitude and phase relationship. The means of support of the casing acts to modify this response. Sound waves radiated by each vibrating portion of the casing reinforce and interfere with each other, according to their phase relationship and wave lengths and the geometry of the casing. Noise levels in the immediate environment of the gearbox are directly influenced by all these variables.

The sheer complexity of these many mechanical and acoustical effects prohibits at this time a complete and detailed analysis relating noise levels around an actual gearbox to the vibration forces developed inside the box. Therefore, an analysis useful for predicting noise levels must, of necessity, employ empirical elements. The analysis contained in Reference 1, which forms the basis for the computer program reported herein, is of this semiempirical character. The empiricism results from one underlying assumption, the validity of which is substantiated by the effectiveness of the analysis in predicting results later obtained by measurement, as demonstrated in the referenced report. In one such case, an analysis using the same assumption has also been shown to give confirmed results when applied to a marine gear application (Reference 4).

DESCRIPTION OF COMPUTER PROGRAM

Calculation of Sound Pressure Level at Each Excitation Frequency

At each of a total of N_f values of the excitation frequency, "f", the following is calculated:

$$\left[K_L = (4.94 \times 10^4)\ (\alpha\beta f) \sum_{j=1}^{N_j} (r_{cj} e_j F_j) \right] / r^2 \qquad (22)$$

In this equation,

α = energy conversion factor

β = gear housing geometry and environment factor

f = excitation frequency (Hz)

N_j = number of equal-frequency sets of excitation and force data

n_e = number of excitations at frequency f

e = gear pitch-line excitation amplitude (microinches)

F = dynamic response force amplitude (lb)

r = radial distance to center of sound radiation surface (ft)

Excitation frequencies and corresponding calculated values of K_L are stored as intermediate values. Then, for each value of K_L, the sound pressure level is calculated using the following equation:

$$L = 4.343 \log_e K_L \text{ (db)} \quad (23)$$

Calculation of Sound Pressure Level by Third-Octave Band Widths

The third-octave band width calculations are performed in two steps as follows:

1. For third-octave midband frequency f_n (Hz), the ratio shown in the following equation is calculated:

$$\rho = \frac{(f)_k}{f_n} \quad (24)$$

where $(f)_k$ is the excitation frequency. For each value of f_n, there will be as many ratios as excitation frequencies for which a value of K_L has been calculated.

2. For each ratio ρ, the filter attenuation factor (FAF) is calculated by subroutine TBFAF, whose arguments are ρ, $(f)_k$, f_n, and FAF.

Here, the quantities $(f)_k$ and f_n are provided since different filter characteristics may be used for different frequency ranges. This more general option was not employed in the present work. The filter attenuation factor is calculated using the following assumptions:

(a) For $\rho \geq 2$ or $\leq .5$, FAF is equal to zero.

(b) For $\rho < 1$, the reciprocal of ρ is found before application of the following equations, since the values of FAF are symmetrical on either side of $\rho = 1$.

Equations Used for Calculation of the Filter Attenuation Factor

The value of N may be calculated by the following expression:

$$N = \left[\log_e(\rho) \right] / .693 \tag{25}$$

Using the calculated value of N, the value of A_N may be determined:

Values of N	Expression for A_N
$N \leq .125$	0.0
$.125 < N \leq .1666667$	72N-9
$.1666667 < N \leq .25$	120N-17
$.25 < N \leq .5$	68N-4
$.5 < N \leq .75$	50N-5
$.75 < N < 1$	30N+20

(26)

When A_N has been calculated,

$$FAF = 1/(10^{A_N/10}) \tag{27}$$

For each band midpoint frequency, the following calculation may then be made:

$$L = 4.343 \log_e \left[\sum_{j=1}^{N_f} (K_L)_j (FAF)_j \right] \tag{28}$$

Calculation of Sound Pressure Level by Full-Octave Band Widths

The full-octave band width calculations are performed in two steps as follows:

1. For each full octave midband frequency f_n' (Hz), the ratio shown in the following equation is calculated:

$$\rho' = \frac{(f)_k}{f_n'} \tag{29}$$

where $(f)_k$ = excitation frequency (Hz).

For each value of k_n' there will be as many ratios as excitation frequencies for which a value of K_L has been calculated.

2. For each ratio the filter attenuation factor (FAF') is calculated by subroutine TBLL, whose arguments are ρ', $(f)_k$, f'_n, and FAF'.

The quantities $(f)_k$ and f_n' are again provided since different filter characteristics may apply over different frequency ranges. This option was not used in the present work.

The filter attenuation factor is calculated using the following assumption:

(a) For $\rho' \geq 4$ or $\leq .25$, FAF' is equal to zero.

(b) For $\rho' < 1$, the reciprocal of ρ' is found before application of the following equations, since the values of FAF' are symmetrical on either side of $\rho' = 1$.

Equations Used for Calculation of the Filter Attenuation Factor

The value of N' may be calculated by the following expression:

$$N' = \left[\log_e(\rho') \right] /.693 \tag{30}$$

Using the calculated value of N', the value of A_n' may be determined

Values of N'	Expression for A'_n
$N' < .45$	0.0
$.45 < N' \leq .5$	$80N' - 36$
$.5 < N' \leq .65$	$83.33333N' - 37.66667$ (31)
$.65 < N' \leq .9$	$54N' - 18.6$
$.9 < N' \leq 1$	$37.14285714N' - 3.4285714$
$1.25 < N' \leq 2$	$27.33333N' - 8.33333$

When A_n' has been calculated,

$$FAF' = 1/(10^{A_n'/10}) \tag{32}$$

For each full octave midband frequency, the following calculation may then be made:

$$L = 4.343 \log_e \left[\sum_{j=1}^{N_f} (K_L)_m (FAF')_j \right] \tag{33}$$

Calculation of Overall Sound Pressure Level

All filter attenuation factors = 1

$$L = 4.343 \log_e \left[\sum_{j=1}^{N_f} (K_L)_j \right] \qquad (34)$$

INPUT VARIABLES, FORMAT, AND INSTRUCTIONS

Card 1 Control Numbers. Format (14I5)

(a) NF Total number of excitation frequencies (card 3) ($0 \leq 100$) Place the last digit of this number in column 5.

(b) NSC Number of subcases using the same set of band midpoint frequencies and full-octave band frequencies.

Place the last digit of this number in column 10.

(c) INP Input indicator
"1" indicates additional sets of input data follow,
"0" indicates this is the last complete set of input data.

Place the last digit of this number in column 15.

(d) IOP Option indicator

IOP Value	Calculated Sound Pressure Level Output Desired
1	at each frequency
2	at each frequency and by third-octave band widths
3	at each frequency and by full-octave band widths
4	at each frequency by third-octave band widths and by full-octave band widths
5	overall
6	at each frequency by third-octave band widths by full-octave band widths, and overall

Place the last digit of this number in column 20.

Card 2 Title, Format (72H). This card precedes each set of excitation frequency cards.

(a) Printing Instructions, column 1
"0" indicates printer should skip a line
"1" indicates printer should skip to next page

(b) Title, columns 2-72.

Card 3. Excitation Frequency Cards (a total of NF cards required). Format (I5, 7E10.4).

(a) INCF — Index for combining frequencies
"1" indicates no combination of frequencies is desired, although 2 frequencies may have the same value.
"0" indicates combination of frequencies is desired, if the frequencies have the same numerical value.

Place the last digit of this number in column 5.

(b) EXFR — Excitation frequency (Hz)

Use columns 6-15.

(c) AMPL — Excitation amplitude (microinches)

Use columns 16-25.

(d) FORCE — Response force, F (lb)

Use columns 25-35.

(e) ANE — Number of excitation points, W_e

Use columns 36-45.

(f) ALPHA — Energy conversion factor, α

Use columns 46-55.

(g) BETA — Geometrical and environmental factor, β

Use columns 56-65.

Card 4. Format (E10.4)

RADIS — Radial distance to center of sound radiating sphere surface (ft)

Use columns 1-10.

Card 5 Format (2E10.4)

(a) FL — Initial third octave band midpoint frequency (Hz)

Use columns 1-10.

(b) FLAST — Last third octave band midpoint frequency (Hz)

Use columns 11-20.

NOTE:

If either F1 or FLAST or both are not equal to the values given in the list of midband frequencies contained within the program, then either F1 is set equal to the nearest midband frequency which is less than F1, or FLAST is set equal to the nearest midband frequency which is greater than FLAST, or both.

Card 5 is necessary only for the first set of cards, beginning with card 3 when IOP is set equal to 2, 4,or 6 on card 2.

Card 6. Format (2E10.4)

(a) FFL1 First full-octave band midpoint frequency (Hz)

Use columns 1-10.

(b) FFKAS Last full-octave band midpoint frequency (Hz)

Use columns 11-20.

If either FFL1 or FFLAS or both are not equal to values given in the list of full-octave midband frequencies contained within the program, then either FFL1 is set equal to the nearest midband frequency which is less than FFL1, or FFLAS is set equal to the nearest midband frequency which is greater than FFLAS, or both. Card 6 is necessary only for the first set of cards beginning with card 3 when IOP is set equal to 3, 4, or 5 on card 2.

The input data cards continue with sets of cards 3 and 4 until NSC sets of cards have been provided.

The next complete input case must include cards 1, 2, 3, and 4 and cards 5 and 6 as required.

OUTPUT VARIABLES AND EXPLANATIONS

Input Data

Same as in input cards 1 to 4.

Calculated Data

Depending upon the value of IOP selected, the output may contain calculated values of sound pressure level at each input frequency, at each requested third-octave midband frequency, and at each requested full-octave midband frequency, as well as the overall sound pressure level.

PROGRAM LISTING OF SOURCE DECK

This program is written in FORTRAN II - Extended and may be compiled with FORTRAN IV. In the source listing which follows, the READ and WRITE statements use the variables NR = 5 and NW = 6 to specify the reading and writing units, respectively. To compile on a nonstandard computer, introduce the required unit numbers by changing the cards as noted in the listing.

In addition to the main program, there are two subroutines. The first, named TBFAF, calculates the filter attenuation factor in the third-octave band width noise calculation. The second subroutine performs the same function in the full-octave band width noise calculation.

Gear Noise Calculations

```
      PROGRAM PN429(INPUT,OUTPUT,TAPE5=INPUT,TAPE6=OUTPUT)
      DIMENSION BMPF(33),FULL(11)
      COMMON NF,MPF,INP,INCF(100),NR,NW
      COMMON EXFR(100),AMPL(100),FORCE(100),ALPHA(100),BETA(100),
     1 OFREQ(100),EKL(100),ANE(100),RADIS
      DATA BMPF/25.,31.5,40.,50.,63.,80.,100.,125.,160.,200.,250.,315.,
     1 400.,500.,630.,800.,1000.,1250.,1600.,2000.,2500.,3150.,4000.,
     2 5000.,6300.,8000.,10000.,12500., 16000.,20000.,25000.,31500.,
     3 40000./
      DATA FULL/31.5,63.,125.,250.,500. ,1000.,2000.,4000.,8000.,
     1 16000.,31500./
C PN429  GEAR NOISE CALCULATION
C NF= NO. OF EXCITATION FREQUENCIES
C MPF= NO. OF BAND-MID-POINT FREQUENCIES
C INP= INPUT INDICATOR, 0 INDICATES NO MORE INPUT, 1 INDICATES MORE INPUT
C INCF= INDEX FOR COMBINING FREQUENCIES OF THE SAME VALUE
C EXFR(I)= EXCITATION FREQUENCY(HZ)
C AMPL(I)= EXCITATION AMPLITUDE(MICRO-INCHES)
C FORCE(I)= RESPONSE FORCE(LBS)
C ALPHA(I)= ENERGY CONVERGENCE FACTOR
C BETA(I)= ENERGY CONVERGENCE FACTOR
C RADIS = RADIAL DISTANCE TO CENTER OF SOUND RADIATING SURFACE (FT)
C BMPF(I)=BAND MID-POINT FREQUENCIES
C NB = NO OF 3RD OCTAVE BANDS, STARTING WITH F1
C F1 = INITIAL FREQ. FOR 3RD OCTAVE BANDS
C NBFL= NO. OF FULL BANDS, STARTING WITH FFL1
C FFL1= INITIAL FREQ. FOR FULL OCTAVE BANDS
C FULL(I)= FULL OCTAVE BAND WIDTH FREQUENCIES
      NR=5
      NW=6
    2 READ(NR,101) NF,NSC,INP,IOP
C NF= NO. OF EXCITATION FREQUENCIES IN EACH SUB-CASE
C INP= 0 INDICATES NO MORE BAND MID-POINT FREQUENCIES TO BE READ IN.
C NSC= NO. OF SUB-CASES FOR THE SAME BAND MID-POINT FREQUENCY
C IOP= OPTION ON CALCULATED SOUND PRESSURE LEVEL
C    1=NONE, 2=1/3 OCTIV., 3=FULL, 4=1/3+FULL, 5=OVERALL, 6=1/3+FULL+OVERALL
      WRITE(NW,103)
      WRITE (NW,113)
      WRITE (NW,104) NF,NSC,INP,IOP
      DO 300 INSC=1,NSC
      READ(NR,100)
      WRITE (NW,131)
      WRITE(NW,100)
      WRITE(NW,107)
      DO 5 I=1,NF
      READ(NR,108)INCF(I),EXFR(I),AMPL(I),FORCE(I),ANE(I),ALPHA(I),
```

```
  1 BETA(I)
    IF (INCF(I)) 3,4,3
  3 WRITE(NW,109)INCF(I),EXFR(I),AMPL(I),FORCE(I),ANE(I),ALPHA(I),
  1 BETA(I)
    GO TO 5
  4 WRITE (NW,130) EXFR(I),AMPL(I),FORCE(I),ANE(I),ALPHA(I),BETA(I)
  5 CONTINUE
    READ(NR,102)RADIS
    WRITE(NW,118)RADIS
    WRITE (NW,129)
    WRITE(NW,110)
    SUM=0.0
    EXFR(NF+1)=0.0
    J=1
    DO 30 I=1,NF
    SUM=SUM+ANE(I)*AMPL(I)*FORCE(I)
    IF (INCF(I))  20,16,20
 16 IF (EXFR(I)-EXFR(I+1)) 20,30,20
 20 PROD=4.94E4*ALPHA(I)*BETA(I)*EXFR(I)*SUM/RADIS/RADIS
    IF (PROD) 21,21,22
 21 WRITE(NW,116)
    ELL= 0.0
    GO TO 300
 22 ELL=4.342944819*ALOG(PROD)
    EKL(J)=PROD
    OFREQ(J)=EXFR(I)
    WRITE (NW,112) OFREQ(J),ELL
    MAXFR = J
    J=J+1
    SUM=0.0
 30 CONTINUE
    GO TO (300,31,60,31,200,31),IOP
 31 IF(INSC-1) 414,32,414
 32 READ (NR,102) F1,FLAST
    CALL SSWTCH(2,MS)
    GO TO (401,33),MS
401 WRITE(NW,105)
    WRITE (NW,106) (BMPF(I),I=1,33)
 33   WRITE (NW,114) F1,FLAST
    ISTAR = 2
    DO 35 J=1,33
    N=J
    IF (BMPF(J)-F1) 35,37,36
 35 CONTINUE
C BAND MID-POINT FREQUENCY GREATER THAN F1
 36 N=N-1
    IF (N) 409,409,37
 37 IF (N-33) 39,38,39
 38 WRITE(NW,115)
409 N=1
 39 DO 410 J=N,33
    MAXNB= J
```

```
      IF (BMPF(J) -FLAST) 410,414,411
  410 CONTINUE
      GO TO 412
  411 MAXNB=MAXNB+1
  412 IF (MAXNB-33) 414,413,413
  413 WRITE (NW,115)
      MAXNB= 33
  414 WRITE (NW,131)
      WRITE(NW,125)
      WRITE (NW,117)
      DO 55 J=N,MAXNB
      SUM=0.0
      BFR=BMPF(J)
      DO 45 K=1,MAXFR
      FR=OFREQ(K)
      RATIO=FR/BFR
C TEST RATIO GREATER THAN 2
      IF(RATIO-2.0) 40,40,45
C TEST RATIO LESS THAN .5
   40 IF(RATIO-.5) 45,41,41
   41 CALL TBFAF(FR,BFR,RATIO,FAF)
      SUM=FAF*EKL(K)+SUM
   45 CONTINUE
C TEST FAF*KL=0.0 OR NEGATIVE
   46 IF(SUM) 47,47,48
CORRECTION FOR LOG(0.0)
   47 WRITE(NW,119)BFR
      ISTAR=1
      GO TO 55
   48 ELLEN=4.342944819*ALOG(SUM)
   50 WRITE(NW,112)BFR,ELLEN
   55 CONTINUE
      GO TO (56,57),ISTAR
   56 WRITE(NW,120)
   57 GO TO (300,300,60,60,200,60),IOP
C OPTIONS 3,4 AND 6- FULL OCTAVE BAND WIDTHS
   60 IF(INSC-1) 424,61,424
   61 READ (NR,102) FFL1,FFLAS
      CALL SSWITCH(2,MS)
      GO TO (62,65),MS
   62 WRITE(NW,121)
      WRITE(NW,106)(FULL(I),I=1,11)
   65 WRITE (NW,122) FFL1,FFLAS
      ISTAR=2
      DO 70 J=1,33
      M=J
      IF(FULL(J)-FFL1) 70,73,72
   70 CONTINUE
   72 M= M-1
      IF (M) 415,415,73
   73 IF (M-11) 79,78,78
  415 M=1
   78 WRITE (NW,115)
   79 DO 420 J=M,11
      MAXFL =J
      IF (FULL(J)-FFLAS)420,424,421
  420 CONTINUE
```

```
      GO TO 422
  421 MAXFL=MAXFL+1
  422 IF (MAXFL-11) 424,423,424
  423 WRITE (NW,115)
      MAXFL=11
  424 WRITE (NW,131)
      WRITE(NW,123)
      WRITE (NW,117)
      DO 90 J=M,MAXFL
      SUM=0.0
      RFULL=FULL(J)
      DO 85 K=1,MAXFR
      FR=OFREQ(K)
      RATIO=FR/RFULL
C TEST RATIO GREATER THAN 4
      IF(RATIO-4.0) 80,80,85
C TEST RATIO LESS THAN .25
   80 IF(RATIO-.25) 85,81,81
   81 CALL TBLL(FR,RFULL,RATIO,FAL)
      SUM=FAL*EKL(K)+SUM
   85 CONTINUE
C TEST FILTER ATTENUATION FACTOR* KL  ZERO OR NEGATIVE
   86 IF(SUM) 87,87,88
   87 WRITE(NW,124)RFULL
      ISTAR=1
      GO TO 90
   88 ELLEN=4.342944819*ALOG(SUM)
      WRITE(NW,112)RFULL,ELLEN
   90 CONTINUE
      GO TO (91,92),ISTAR
   91 WRITE(NW,126)
   92 GO TO (300,300,300,300,200,200),IOP
  200 SUM=EKL(1)
      DO 210 I=2,MAXFR
  210 SUM=SUM+EKL(I)
      ELL=4.342944819*ALOG(SUM)
      CALL SSWTCH(2,MS)
      GO TO (211,212),MS
  211 WRITE(NW,127)(EKL(I),I=1,MAXFR)
  212 WRITE(NW,128)ELL
  300 CONTINUE
      IF(INP) 2,305,2
  305 CALL EXIT
  100 FORMAT(72H
     1                  )
  101 FORMAT (14I5)
  102 FORMAT(8E10.4)
  103 FORMAT(/1H1,25X,29HGEAR NOISE CALCULATION, PN429)
  104 FORMAT(/9X,15HNO. EXCITATIONS,2X, 6HNO. OF,6X,
     15HINPUT,5X,6HOUTPUT/ 9X,13HEACH SUB-CASE,3X,9HSUB-CASES,3X,
     2 9HINDICATOR,2X,6HOPTION/13X,I5,8X,I5,5X,I5,5X,I5)
  105 FORMAT(/25X,26HBAND MID-POINT FREQUENCIES/ )
  106 FORMAT (5X,8F9.1)
```

```
107 FORMAT(/5X,5HINDEX,1X,10HEXCITATION,2X,10HEXCITATION,3X,8HRESPONSE
   1,4X,6HNUMBER,6X,6HENERGY,7X,8HGEOM.    /
   2 12X,9HFREQUENCY,3X,9HAMPLITUDE,4X,5HFORCE,8X,2HOF,5X,10HCONVERSIO
   3N,5X, 11HENVIR.      /14X,4H(HZ),4X,11H(MICRO-IN.),4X,5H(LBS),
   44X,11HEXCITATIONS,3X,6HFACTOR,6X,6HFACTOR/)
108 FORMAT(I5,7E10.4)
109 FORMAT (5X,I3,4F12.3,2F12.5)
110 FORMAT(/15X,49HCALCULATED SOUND PRESSURE LEVEL AT EACH FREQUENCY/
   110X,25HEXCITATION FREQUENCY (HZ),5X,25HSOUND PRESSURE LEVEL (DB))
111 FORMAT(/5X,42HINDEX FOR COMBINING FREQUENCIES INCORRECT.)
112 FORMAT(15X,F12.1,19X,F12.5)
113 FORMAT (//30X,10HINPUT DATA/)
114 FORMAT (/5X,50HTHIRD OCTAVE BANDS, WITH MID-BAND FREQUENCIES FROM,
   1 F10.3,3H TO,F10.3,3H HZ)
115 FORMAT(/5X,45HNO. OF BANDS REQUESTED GREATER THAN GIVEN NO.)
116 FORMAT(/5X,69HINSUFFICIENT INPUT DATA- ARGUMENT FOR LOGARITHM IS
   1ZERO OR NEGATIVE.)
117 FORMAT (/11X,24HMID-BAND FREQUENCY (HZ),5X,25HSOUND PRESSURE LEVEL
   1 (DB))
118 FORMAT(/5X,57HRADIAL DISTANCE TO CENTER OF SOUND RADIATING SURFACE
   1-(FT),F12.5)
119 FORMAT (15X,F12.1,24X,1H*)
120 FORMAT(  5X,34H* NO EXCITATION WITHIN ONE OCTAVE.)
121 FORMAT(/5X,23HFULL OCTAVE BAND WIDTHS)
122 FORMAT ( /5X,49HFULL OCTAVE BANDS, WITH MID-BAND FREQUENCIES FROM,
   1 F10.3,3H TO,F10.3,3H HZ)
123 FORMAT(10X,58HCALCULATED SOUND PRESSURE LEVEL BY FULL OCTAVE BAND
   1WIDTHS)
124 FORMAT (15X,F12.1,24X,2H**)
125 FORMAT(10X,59HCALCULATED SOUND PRESSURE LEVEL BY THIRD OCTAVE BAND
   1 WIDTHS)
126 FORMAT(/5X,36H** NO EXCITATION WITHIN TWO OCTAVES.)
127 FORMAT(/5X, 9HKL VALUES/  (8E13.5))
128 FORMAT(/5X,73HCALCULATED OVERALL SOUND PRESSURE LEVEL (FROM THE IN
   1PUT NOISE COMPONENTS)/35X,F12.5,3H DB)
129 FORMAT (/1H1,30X,11HOUTPUT DATA/)
130 FORMAT (8X,4F12.3,2F12.5)
131 FORMAT (10X)
    END
```

Subroutine TBFAF

```
      SUBROUTINE TBFAF(FR,BFR,RATIO,FAF)
      DIMENSION A(5),AL(5),CN(6)
      COMMON NF,MPF,INP,INCF(100),NR,NW
      COMMON EXFR(100),AMPL(100),FORCE(100),ALPHA(100),BETA(100),
     1 OFREQ(100),EKL(100),ANE(100),RADIS
      DATA A/72.0,120.0,68.0,50.0,30.0/
      DATA AL/-9.0,-17.0,-4.0,5.0,20.0/
      DATA CN/.125,.1666667,.25,.5,.75,1.0/
CALCULATION OF FAF FACTOR-FILTER ATTENUATION FACTOR
C TEST RATIO FOR NEGATIVE VALUE
C THE ARGUMENT IDENTIFIES THE BAND AND COMPONENT FREQUENCIES, BUT IS IGNORED
C BECAUSE THE SAME FILTER CHARACTERISTIC IS USED FOR ALL BANDS
      IF(RATIO) 5,10,10
    5 WRITE(NW,100)FR,BFR,RATIO
      RATIO=-RATIO
   10 FRAT=RATIO
      IF(FRAT-1.0) 11,12,12
   11 FRAT=1.0/FRAT
   12 ENN=ALOG (FRAT)/.6931471806
      DO 20 J=1,6
      JS=J-1
      IF (ENN-CN(J)) 21,21,20
   20 CONTINUE
   21 IF(JS) 22,22,24
   22 FAF=1.0
   23 RETURN
   24 AY=A(JS)*ENN+AL(JS)
      EXP=ABS(AY)/10.0
      FAF=1.0/10.0**EXP
      CALL SSWTCH(2,MS)
      GO TO (30,23),MS
   30 WRITE(NW,101)FR,BFR,RATIO,ENN,A(JS),AL(JS),EXP,FAF
      RETURN
  100 FORMAT(/5X,18HCHECK INPUT VALUES/ 5X,61HRATIO OF COMPONENT AND BAN
     1D MIDPOINT FREQUENCIES IS NEGATIVE./  5X,11HCOMP. FREQ.,2X,
     110HBAND FREQ.,6X,5HRATIO/ 5X,3E12.5)
  101 FORMAT(/5X,11HCOMP. FREQ.,2X,10HBAND FREQ.,6X,5HRATIO,10X,1HN,10X,
     12HC1,10X,2HC2, 7X, 8HEXPONENT, 7X,3HFAF/ 5X,8E12.5)
      END
```

Subroutine TBLL

```
      SUBROUTINE TBLL(FR,RFULL,RATIO,FAL)
      DIMENSION B(5),BL(5),BN(6)
      COMMON NF,MPF,INP,INCF(100),NR,NW
      COMMON EXFR(100),AMPL(100),FORCE(100),ALPHA(100),BETA(100),
     1 OFREQ(100),EKL(100),ANE(100),RADIS
      DATA BL/-36.0,-37.666667,-18.6,-3.4285714,8.8333333/
      DATA B/80.0,83.333333,54.0,37.14285714,27.3333333/
      DATA BN/.45,.5,.65,.9,1.25,2.0/
C THE ARGUMENT IDENTIFIES THE BAND AND COMPONENT FREQUENCIES, BUT IS IGNORED
C BECAUSE THE SAME FILTER CHARACTERISTIC IS USED FOR ALL BANDS
      IF(RATIO) 5,10,10
    5 WRITE(NW,100)FR,RFULL,RATIO
      RATIO=-RATIO
   10 FRAT=RATIO
      IF(FRAT-1.0) 11,12,12
   11 FRAT=1.0/FRAT
   12 ENN=ALOG(FRAT)/.6931471806
      DO 20 J=1,6
      JS=J-1
      IF (ENN-BN(J)) 21,21,20
   20 CONTINUE
   21 IF(JS) 22,22,24
   22 FAL=1.0
      GO TO 25
   24 AY=B(JS)*ENN+BL(JS)
      EXP=ABS(AY)/10.0
      TEXP=10.0**EXP
      FAL=1.0/10.0**EXP
   25 CALL SSWTCH (2,MS)
      GO TO (30,31),MS
   30 WRITE (NW,101) FR,RFULL,RATIO,ENN,B(JS),BL(JS),EXP,FAL,TEXP
   31 RETURN
  100 FORMAT(/5X,18HCHECK INPUT VALUES/ 5X,61HRATIO OF COMPONENT AND BAN
     1D MIDPOINT FREQUENCIES IS NEGATIVE./  5X,11HCOMP. FREQ.,2X,
     110HBAND FREQ.,6X,5HRATIO/ 5X,3E12.5)
  101 FORMAT(/5X,11HCOMP. FREQ.,2X,10HBAND FREQ.,6X,5HRATIO,10X,1HN,10X,
     12HC1,10X,2HC2,7X,8HEXPONENT,7X,3HFAF,7X,7H10**EXP/5X,9E12.5)
      END
```

Unclassified
Security Classification

DOCUMENT CONTROL DATA - R & D

(Security classification of title, body of abstract and indexing annotation must be entered when the overall report is classified)

1. ORIGINATING ACTIVITY (Corporate author) Mechanical Technology Incorporated, Latham, New York	2a. REPORT SECURITY CLASSIFICATION Unclassified; 2b. GROUP
3. REPORT TITLE: PROGRAM FOR HELICOPTER GEARBOX NOISE PREDICTION AND REDUCTION	
4. DESCRIPTIVE NOTES (Type of report and inclusive dates): Final Technical Report	
5. AUTHOR(S) (First name, middle initial, last name): Robert A. Badgley; Irving Laskin	
6. REPORT DATE: March 1970	7a. TOTAL NO. OF PAGES: 234; 7b. NO. OF REFS: 12
8a. CONTRACT OR GRANT NO. DAAJ02-68-C-0070; b. PROJECT NO.; c. Task 1G162203D14414; d.	9a. ORIGINATOR'S REPORT NUMBER(S): USAAVLABS Technical Report 70-12; 9b. OTHER REPORT NO(S) (Any other numbers that may be assigned this report): MTI - 70TR 8
10. DISTRIBUTION STATEMENT: This document is subject to special export controls, and each transmittal to foreign governments or foreign nationals may be made only with prior approval of U. S. Army Aviation Materiel Laboratories, Fort Eustis, Virginia 23604.	
11. SUPPLEMENTARY NOTES	12. SPONSORING MILITARY ACTIVITY: U.S. Army Aviation Materiel Laboratories, Fort Eustis, Virginia 23604

13. ABSTRACT A method of computing helicopter gearbox noise from design and operating data is verified by a comparison of calculated and measured gearbox noise spectra. Measurements on CH-47 helicopters are used to provide experimental data.

Positive identification of the source and mechanism of gearbox noise energy has been made. The most objectional noise originates in the meshing action of the gear teeth. The gear tooth deflection, together with tooth profile variations due to manufacturing errors, excites torsional vibrations in the helicopter power train. Each gear mesh produces noise components at frequencies corresponding to the tooth meshing rates and their higher harmonics. This gear-induced vibration is transmitted to the gearbox casing and thence to the aircraft structure. Results indicate that the CH-47 gearbox mounts transmit a significantly higher level of vibration to the aircraft structure than do the UH-1D mounts.

Calculations on the CH-47 gearbox indicate that spur gear tooth profile variations can be used to reduce gearbox noise levels, but manufacturing tolerances do not yet appear to be low enough for application of this principle. Studies further indicate that variations in planet carrier torsional compliance will result in only modest changes in noise level over the range of compliance studied.

DD FORM 1 NOV 65 1473 REPLACES DD FORM 1473, 1 JAN 64, WHICH IS OBSOLETE FOR ARMY USE.

Unclassified
Security Classification

14. KEY WORDS	LINK A		LINK B		LINK C	
	ROLE	WT	ROLE	WT	ROLE	WT
Helicopters						
Noise Measurements						
Vibration Measurements						
Gearbox Noise Calculation						
Gearbox						
Noise						
Vibration						
Structural Resonance						
Design for Noise Reduction						
Gear						
Torsional Vibrations						
Dynamic Tooth Forces						
Bevel Gear						
Equivalent Spur Gear						
Spur Gear						
Tooth Profile Variations						
Tooth Deflection						
Planetary Gearing						
Vibrations						
Planet Carrier Torsional Compliance						
Noise						
Measurement						
Prediction						